Improvement of Single Pion Production
for T2K experiment simulation tools

Monireh Kabirnezhad

Supervisor: **prof. Jan Sobczyk**

Co-supervisors: **Dr Pawel Przewlocki**

National Center for Nuclear Research

This dissertation is submitted for the degree of
Doctor of Philosophy

January 2020

Acknowledgements

Having the theoretical background, I found it so challenging to start your Ph.D. project with an experimental group and to join a successful collaboration. Luckily I met wonderful people who have guided me with their wisdom, shared their knowledge and helped me to have a unique experience.

First of all, I would like to thanks, My supervisor, Prof. Ewa Rondio, who has patiently supported me in every aspect of my work. Apart from the challenging project, working in experimental high energy physics with an Iranian passport, you face several visa issue. Only a wise person with a great soul, standing on your side can give you enough strength to continue. I am also extremely grateful for the support of Dr. Pawel Przewlocky, without whom I might still be struggling with programming. Also thanks to the rest of Warsaw neutrino group who has offered help and care to me.

I have received invaluable advice from Prof. Jan Sobczyk over the last few months. His detailed review of draft chapters improved the description of my work and ensured the veracity of every piece of the calculation, and for this, I would like to thank him. I am also thankful to Dr. Jakub Zmuda and Dr. Krzysztof Graczyk for useful discussions on the initial stage of work, Dr. Raul Gonzalez Jimenezand who validated my result, and Prof. Juan Nieves for valuable comments on my work.

I am glad to be a member of T2K experiment and working with excellent researchers. I would like to thank T2K collaborators who have offered important advice along the way, but I am particularly grateful to Prof. Kevin McFarland who has supported my work loudly and publicly, where I gained encouragement and inspiration for the rest of my career. Working with Clarence Wret was a great time with his unique humor and enthusiast. I would like to thanks him for sharing his knowledge with me generously. Also thanks to Dr. Daniel Cherdack whose advice was very helpful to make important decisions, and Dr. Callum Wilkinson who has kindly discussed with me during the collaboration meeting.

Finally, I would like to thank my friends and family for the continuous support they have given me through the years, and for being with me during hard times.

Abstract

Neutrino-nucleon interactions that produce a single pion in the final-state are of critical importance to accelerator based neutrino experiments. These Single Pion Production (SPP) channels make up the largest fraction of the inclusive neutrino-nucleus cross section in the $1 - 3$ GeV range, a region covered by most accelerator based neutrino beams.

Models of SPP cross section processes are required to accurately predict the number and topology of observed charged-current (CC) neutrino interactions, and to estimate the dominant source of neutral-current (NC) backgrounds, where a charged (neutral) pion is confused for a final-state muon (electron). These experiments make use of nuclear targets, however, the foundation of neutrino-nucleus interaction models are neutrino-nucleon reaction processes like the one described in this paper.

This work represents an extension of the single pion production model proposed by D.Rein [9]. The model consists of resonant pion production and nonresonant background contributions coming from three Born diagrams in the helicity basis. The new work includes lepton mass effects, and nonresonance interaction is described by five diagrams as it is proposed in [10]. The main challenge of the recent work is to calculate them in helicity basis in order to study the interference effect of resonance and non-resonance interactions. The interference contribution has a visible effects on cross-section especially on pion angular distributions.

The resonant interaction is Rein-Sehgal model [7] with one exception on the sign of resonances. We choose different signs for few resonances, to get the best description of data.

The full model has very good agreement with all available data and it is implemented in NEUT to be used for the future T2K analysis.

Table of contents

List of figures

List of tables

Chapter 1

Introduction

The three neutrino flavors, ν_e, ν_μ and ν_τ, in the Standard Model are massless. They are all experimentally observed and the number of neutrino species was already predicted from the Z^0 decay width, long before the last (ν_τ) neutrino was detected by DONUT experiment at Fermilab in 2000 [82].

The discovery of neutrino oscillation at Super-Kamiokande (1998) [79] in Japan and then at SNO (2001) [80] experiment in Canada (2015 Nobel prize awarded to this discovery), was an evidence of new physics beyond the Standard Model, as it demonstrates that neutrinos have mass.

In the three-neutrino mixing model, the neutrino flavour eigenstate $|\nu_\alpha\rangle$, where $\alpha = e, \mu, \tau$, is a linear superposition of the mass eigenstates $|\nu_j\rangle$, where $j = 1, 2, 3$. The mixing matrix in the leptonic sector is called PMNS matrix, where relates the neutrino mass eigenstate to the flavour eigenstates.

$$|\nu_\alpha\rangle = U_{\alpha j}^* |\nu_j\rangle, \tag{1.1}$$

where U is Pontecorvo-Maki-Nakagawa-Sakata (PMNS) mixing matrix, which is a unitary matrix. Applying this unitarity constraint allows us to parametrise the matrix in terms of three mixing angles ($\theta_{12}, \theta_{23}, \theta_{13}$) and a CP violating phase, δ_{cp}. We assume neutrinos are Dirac particles meaning they are not their own antiparticles. If neutrinos are Majorana particles, then U should be multiplied by diag $\left(e^{i\alpha_1}, \quad e^{i\alpha_2}, \quad 1 \right)$ where α_1 and α_2 are Majorana phase factors. The Majorana phases do not affect neutrino oscillations so can be neglected in this discussion.

The $|\nu_j\rangle$ are the Hamiltonian's eigenstates with eigenvalue $E_j = \sqrt{p^2 + m_j^2}$, propagating in

time as plane waves:

$$|\nu_j(t)\rangle = e^{-iE_jt}|\nu_j\rangle, \tag{1.2}$$

Thus the evolution in time of the flavour eigenstates is:

$$|\nu_\alpha(t)\rangle = \sum_{\beta=e,\mu,\tau}\left(\sum_{j=1}^{3} U_{\alpha j}^* e^{-iE_jt} U_{\beta j}\right)|\nu_\beta\rangle. \tag{1.3}$$

Therefore a neutrino created in a flavour eigenstate, ν_α, along with the corresponding lepton of flavour α, can later be measured to have different flavour. The probability is:

$$P_{\nu_\alpha \to \nu_\beta} = |\langle \nu_\beta|\nu_\alpha(t)\rangle|^2 = \sum_{k=1}^{3}\sum_{j=1}^{3} U_{\alpha k}^* U_{\beta k} U_{\alpha j} U_{\beta j}^* e^{-i(E_k-E_j)t}. \tag{1.4}$$

Depending on whether the neutrino flavour in the final state is similar to the one in the initial state or not, the neutrino oscillation measurements have two disappearance ($\nu_\alpha \to \nu_\alpha$) and appearance ($\nu_\alpha \to \nu_\beta$) modes. In the relativistic limit (where $t \approx L$) and for light neutrino masses we have:

$$
\begin{aligned}
E = &\ \sqrt{P^2+m^2} \approx p + \frac{m^2}{2p} \approx p + \frac{m^2}{2E}, \\
\implies &\ e^{-i(E_k-E_j)t} = e^{-im_j^2 L/2E},
\end{aligned}
\tag{1.5}
$$

therefore:

$$P_{\nu_\alpha \to \nu_\beta} = \sum_{k=1}^{3}\sum_{j=1}^{3} U_{\alpha k}^* U_{\beta k} U_{\alpha j} U_{\beta j}^* \exp\left(-i\frac{\Delta m_{kj}^2 L}{2E}\right). \tag{1.6}$$

where $\Delta m_{kj}^2 = m_k^2 - m_j^2$. Equation 1.6 clearly shows that the oscillation probability depends on the mixing matrix, mass-squared differences, the traveled distance, L, and the neutrino energy E.

Measuring all the oscillation parameters at the same time can be very difficult, however the mass splittings differ by several orders of magnitude, $\Delta m_{21}^2 \ll |\Delta m_{31}^2| \simeq |\Delta m_{32}^2|$, so the three-neutrino case can often be factorised to two-neutrino cases. Atmospheric and beam experiments can determine the magnitude of Δm_{32}^2 and θ_{23}. Solar and reactor measurements can determine Δm_{21}^2 and θ_{12}. Finally, and most recently, beam and reactor experiments have determined the magnitude of θ_{13} and found it to be nonzero.

Table 1.1 summarises the most up-to-date measurements of all of the neutrino oscillation parameters. This is all we know from the measurements of the neutrino oscillation

Table 1.1 The best-fit values and 3σ allowed ranges of the 3-neutrino oscillation parameters for normal (inverted), derived from a global fit of the current neutrino oscillation data (from [78]). Note that the mass ordering is known for Δm^2_{21} and $\Delta m^2 = m^2_3 - (m^2_2 + m^2_1)/2 \simeq \Delta m^2_{32} \simeq \Delta m^2_{31}$.

Parameters	best-fit	3σ
$\Delta m^2_{21}[10^{-5}eV^2]$	7.37	$6.93 - 7.97$
$\Delta m^2[10^{-3}eV^2]$	2.50 (2.46)	$2.37 - 2.63$ (2.33 − 2.60)
$\sin^2\theta_{12}$	0.297	$0.250 - 0.354$
$\sin^2\theta_{23}, \Delta m^2 > 0$	0.437	$0.379 - 0.616$
$\sin^2\theta_{23}, \Delta m^2 < 0$	0.569	$0.383 - 0.637$
$\sin^2\theta_{13}, \Delta m^2 > 0$	0.0214	$0.0185 - 0.0246$
$\sin^2\theta_{13}, \Delta m^2 < 0$	0.0218	$0.0186 - 0.0248$

experiments, however there are still few fundamental questions need to be addressed, such as:

- There are currently no measurements of δ_{CP}, although some hints to its value exist. Does the behavior of neutrinos violate CP? What is a value of δ_{CP} in neutrino oscillations?

- Atmospheric and beam experiments can only determine the magnitude of Δm^2_{32}. What is the sign of Δm^2_{32}? In other words is the hierarchy of neutrino masses normal or inverted?

where the future improvements in the precision measurements of currently running and future neutrino experiments can lead us to the answer.

Neutrino oscillation experiments measure the charged-current and neutral-current event rates in their detectors, which can generically be expressed as

$$R = \Phi \times \sigma \times \varepsilon \times P(\nu_\alpha \to \nu_\beta), \qquad (1.7)$$

where R is the event rate, Φ is the neutrino flux, σ is the neutrino cross section and ε is the detector efficiency. It is obvious from this equation that in order to measure the neutrino oscillation probability $P(\nu_\alpha \to \nu_\beta)$, the neutrino flux and cross section must be known with a good precision.

To perform oscillation analyses, experiments use Monte Carlo simulations to make predictions. This will involve a simulation of the interactions in the detector which usually requires

an interaction simulation followed by a detector simulation. All oscillation experiments rely on interaction generators to perform oscillation measurements, so the measurements can have some dependence on the model used.

Many neutrino experiments such as T2K, take advantage of a two-detectors configuration to constrain uncertainties in neutrino flux and neutrino cross sections. The main goal of cross-section programs at T2K near detector is to understand the neutrino interaction cross-sections and to validate models, in order to increase the precision in measurements. There has also been experiments dedicated to the cross-section measurements and problem of neutrino interactions such as MINERνA [71].

The oscillation probability depends directly on the neutrino energy, however, the neutrino energy cannot be measured directly. In experiments such as T2K, the two-body kinematics involved in a pure charged-current quasi-elastic (CCQE) event (detected in the near detector) allows an approximate reconstruction of the neutrino energy using only the final state lepton kinematics[1].

Single Pion Production (SPP) is the main background for CCQE interaction largely due to the missing of pion in the detector. This background is predicted directly from simulation and rely on SPP model. Here are two examples that the pion misidentification can effect on the T2K measurements.

1. $\pi^{\pm}$ can misidentified with $\mu^{\pm}$, because they have similar mass and charge. This can change the event rate of ν_{μ} in the disappearance ($\nu_{\mu} \to \nu_{\mu}$) mode, and as explained before, it can also change the neutrino energy reconstruction.

2. π^0 and $e^{\pm}$ can produce similar rings in Cherenkov detector. This is very important in the appearance ($\nu_{\mu} \to \nu_e$) mode of the T2K measurements[2].

Therefore having a good model that can predict the production rate of single pions is crucial for T2K and other neutrino experiments.

Recent cross-section measurements of single pion production show significant discrepancies with models in the low energy region and the lack of an accurate model can be a reason for the discrepancies. Implementing a new model that has better agreements with data can reduce systematic uncertainties in neutrino oscillation measurements which are necessary to achieve the main goal of neutrino experiments such as the determination of leptonic CP

---

[1]CCQE cross-section is the dominant process in T2K. It will be introduced in chapter 2.

[2]This will be discussed later with Super-Kamiokande detector, in subsection 7.1.3.

phase and neutrino mass hierarchy.

Pions can be produced either by the decay of nucleon resonances or directly by nonresonant interaction. The main concern in theoretical discussions of the single pion production is the description of nonresonant background model and its interference with resonant interactions that is sometimes missing in neutrino MC generators. From the above-mentioned reasons, developing neutrino MC generators is very important for precision neutrino oscillation measurements.

The main motivation of this thesis is developing a model for single pion production in neutrino-nucleon interaction, suitable for neutrino MC generators to address the described needs of neutrino experiments.

1.1   Structure of this thesis

All neutrino experiments rely on Monte Carlo neutrino interaction generators. Neutrino generators implement all interaction models to simulate the neutrino cross-section in the detector medium. The T2K near detectors highlights the importance of having accurate neutrino interaction models in neutrino Monte Carlo generators. A general description of neutrino interactions and models currently used by neutrino generators such as NEUT and GENIE, the official neutrino Monte Carlo generators will be given in chapter 2.

The neutrino-nucleon single pion production model is a part of the cross-section models in NEUT and GENIE. The current single pion production model in NEUT and GENIE is missing a reliable model for nonresonant interaction. An accurate model for single pion production should include resonant and non-resonant interactions, calculated in a common framework in order to include the interference effects. The single pion production model proposed in this work consist of resonant and nonresonant interactions based on helicity amplitudes. Therefore a general formalism is needed to add the two interactions coherently. This will be introduced in chapter 3, and the general cross-section computation in terms of helicity amplitudes will be given at the end of this chapter.

The main discussion in chapter 3 is about the helicity amplitudes calculation for resonant and nonresonant interactions. We will also discuss about the isospin coefficients which is very important to calculate the charged and neutral current single pion production channels (given in Equation 3.1 - 3.4). Knowing the helicity amplitudes with their relative isospin

coefficients for all channels it is straightforward to calculate the single pion cross-section as it will be discussed at the end of this chapter.

A very important step for a new model is to validate it with the available data in order to see how reliable it is. To show the predictions of the proposed model, it is implemented in cross-section calculation code which is capable of predicting the differential cross-section for all single pion production channels. In chapter 5 the model predictions will be compared with the bubble chamber data on the light nucleus. This data is also used to adjust the free parameters in the resonant interaction.

The new model we will propose in this thesis is for neutrino-nucleon interaction. In order to compare it with the recent cross-section measurements on nuclear target one need to include the nuclear effects. The nominal nuclear models are already implemented in the T2K neutrino generators. Chapter 6, provides all information about the current single pion production model in the NEUT and GENIE. Then we describe the new model implementation in the NEUT. We also show the validation plots and NEUT prediction with the current and new model on free nucleon and nucleus.

Finally in chapter 7 we will show the NEUT comparison before and after the model implementation, with single pion production data from T2K, MINERνA and MiniBooNE on various targets.

Chapter 2

Neutrino Scattering

Neutrino can only interact via the weak interaction. In charged-current interaction mediated by W exchange, the neutrino turns into a charged lepton, while no charge is transferred in neutral-current interaction via a Z boson. In neutrino-nucleus scattering, depends of energy, a neutrino can interact with a nucleus as a whole, an individual nucleon, or with quarks inside nucleon.

In reality, describing neutrino-nucleus interaction can be very difficult especially at the intermediate neutrino energy (which is the region of interest for accelerator neutrino experiments), because nucleus is a complicated environment. A complete neutrino-nucleus interaction model involves a number of ingredients:

1. A nuclear model, describing the initial state of nucleons within the nucleus.

2. A cross-section model.

3. A model relating the products of the initial interaction to the outgoing final state particles.

Items 1 and 2 are initial state interaction and item 3 is Final State Interaction (FSI).

The current cross-section measurements have been made on nuclear targets and in the intermediate range of energy (few GeV). Therefore Monte Carlo neutrino interaction generators should include all required models in order to simulate the neutrino interactions in detectors[1]. A review of generator and theoretical model predictions is given in [20].

In this work, we will talk about the interaction models in two Monte Carlo (MC) neutrino interaction generators: NEUT [56], the official generator of the Super-Kamiokande and T2K collaborations; and GENIE [57], which is widely used by neutrino experiments.

---

[1]in recent years there has been development for more generic generators to be used by few neutrino experiments, like GENIE.

This chapter is devoted to neutrino interaction, and the relevant models which are used in the NEUT and GENIE.

2.1   Neutrino interaction model

The bubble chamber in old experiments (see chapter 5) were usually filled with light nucleus like hydrogen or deuterium, which is a very good target to investigate the models. The existing bubble chamber data is still being used for the validation of the cross-section models. In this section, we start with cross-section models for neutrino scattering from nucleon, parton and nucleus. Then we will discuss about the nuclear effects i.e. nuclear model and the final state interaction.

2.1.1   Cross-section model

One way of classifying neutrino-nucleon interactions can be based on the type of final state particles appearing. In Figure 2.1 if particle X is a single nucleon it is called elastic or quasi-elastic scattering. If X is a pair of $N\pi$ hadrons, it is called single pion production. In Deep Inelastic Scattering (DIS) where a neutrino interacts with quarks, a nucleon can be with any other particles (including single pion) in the final state.

 Figure 2.2 shows the contribution of neutrino interaction in different range of energy, where
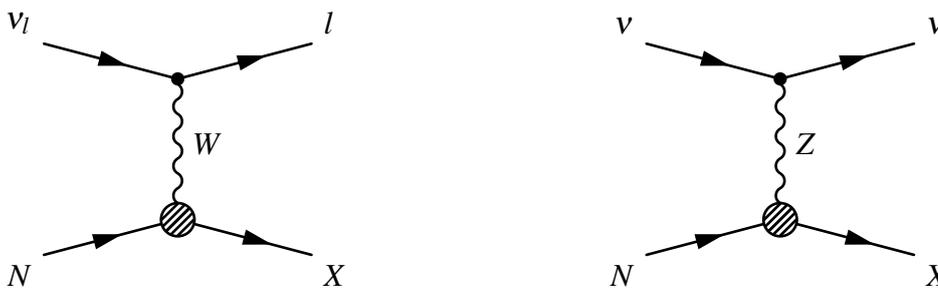
Fig. 2.1 Neutrino-nucleon interaction via W boson in the charged current interaction (left) and neutral-current interaction by a Z boson exchange (right). X can be a single particle or more than one particles in different types of neutrino interaction.

quasi-elastic and single pion production contribute to the low energy and the DIS is dominant at high energy. The modeling of transition region between pion production and DIS can be particularly difficult at the intermediate energy where there is the possibility for overlap between the models.

Elastic and Quasi-elastic Scattering

Elastic scattering off a nucleon is a process without charge exchange (neutral current):

$$\nu_l + p \rightarrow \nu_l + p \qquad\qquad \bar{\nu}_l + p \rightarrow \bar{\nu}_l + p$$
$$\nu_l + n \rightarrow \nu_l + n \qquad\qquad \bar{\nu}_l + n \rightarrow \bar{\nu}_l + n \tag{2.1}$$

while charged current quasi-elastic (CCQE) scattering is an interaction with charged lepton in the final state:

$$\nu_l + n \rightarrow l^- + p \qquad\qquad \bar{\nu}_l + p \rightarrow l^+ + n \tag{2.2}$$

The CCQE interaction is dominant at $E_\nu \sim 1\,\text{GeV}$ (see Figure 2.2). Cross-section models for CCQE and NCEL can be found in References [23, 24]

Single pion production on nucleon (SPP)

Single pion production has significant contribution at energy of few-GeV (see Figure 2.2). It is the simplest inelastic neutrino scattering off a nucleon that produce a lepton and a pair of $N\pi$ hadrons in the final state. Single pion in neutrino-nucleon scattering can be produced directly or via decay of resonances.

In resonant interaction, single pion mainly produce via decay of Δ resonance. $\Delta = \begin{pmatrix} \Delta^{++} & \Delta^+ & \Delta^0 & \Delta^- \end{pmatrix}$ produce in CC and NC (anti-) neutrino interaction:

$$\nu_l + p \rightarrow l^- + \Delta^{++} \qquad\qquad \bar{\nu}_l + p \rightarrow l^+ + \Delta^0$$
$$\nu_l + n \rightarrow l^- + \Delta^+ \qquad\qquad \bar{\nu}_l + n \rightarrow l^+ + \Delta^-$$

$$\nu_l + p \rightarrow \nu_l + \Delta^+ \qquad\qquad \bar{\nu}_l + p \rightarrow \bar{\nu}_l + \Delta^+$$
$$\nu_l + n \rightarrow \nu_l + \Delta^0 \qquad\qquad \bar{\nu}_l + n \rightarrow \bar{\nu}_l + \Delta^0, \tag{2.3}$$

then it decays into final states containing a pion and a nucleon[2].

Similarly $N\pi$ pair can be produced directly via nonresonant interaction. Therefore we call both reactions as single pion production which is going to be discussed later. All single pion production channels are given in Eq. 3.1 - 3.4.

Several models have been proposed (since 70s) in the literature concerning single pion production. Most of them include only Δ resonance and nonresonant interaction, but they

---

[2]Δ is the lightest resonance, but several other heavier resonances can also contribute.

differ in the coupling, form-factor, etc. The most complete unitarized model[3] in the Δ region is Sato-Lee model [4]. In terms of nonresonant interaction, Adler model [8] uses the three Born diagram based on linear sigma model [11] and HNV model [10] use the five Feynman diagram based on non-linear σ-model. These diagrams have nucleon and pion propagators, however, in Reference [3] there are more diagrams with other mesons like ρ or ω propagators. There are other models that include higher $I = \frac{1}{2}$ resonances. In particular a model by Fogli-Nardulli [2] include three more resonances (S_{11}, P_{11}, D_{13}) to extend the πN invariant mass region (up to $W = 1.6$ GeV) in the model.

A model for nonresonant interaction is usually a set of Feynman diagrams with defined couplings, but it is sometimes missing in the single pion production models. For instance the Rein-Sehgal model [7] includes 18 resonances up to $W = 2$ GeV, but there is no model for nonresonant interaction instead they introduce extra ad hoc helicity amplitudes for nonresonant background with $I = \frac{1}{2}$. Later a model by Rein [9] includes three Born diagrams to the Rein-Sehgal model.

Both GENIE and NEUT use the Rein-Sehgal model [7] for single pion production. Detailed information about the RS model can be found in chapter 4, and the model implementation in NEUT and GENIE will be discussed in section 6.1.

Deep Inelastic Scattering (DIS)

At high energy neutrino can interact with individual partons within the nucleon, thus breaking apart the nucleon and generally producing a jet of hadrons. At high energy the cross-section is dominant by deep inelastic scattering (see Figure 2.2), and it is well defined in this region. On the other hand for lower energies of a few GeV, other reactions especially single pion production contribute, therefore it is more difficult to describe it in this region.

For relatively high invariant mass events, both NEUT and GENIE rely on the PYTHIA program [30] to model the reaction of the incoming W(Z) boson on partons inside the nucleon. Figure 2.2 shows the cross-section measurements for the three types of interactions that CCQE and single pion production contribute to the low energy and the main contribution at high energy comes from DIS.

The DIS model in NEUT[4] is based on parton distribution from References [25, 26] up to $W < 2$ GeV and PYTHIA for $W > 2$ GeV. In the actual calculation to obtain the cross-section in NEUT, the probability function of pion multiplicity is used, which is a function of W and gives the probability to generate more than one pion, in the small W region ($W < 2$ GeV). Therefore, single pions in this region only come from the single pion

---

[3]Unitarized model will be discussed in section 4.3.
[4]This paragraph is taken from Reference [56].
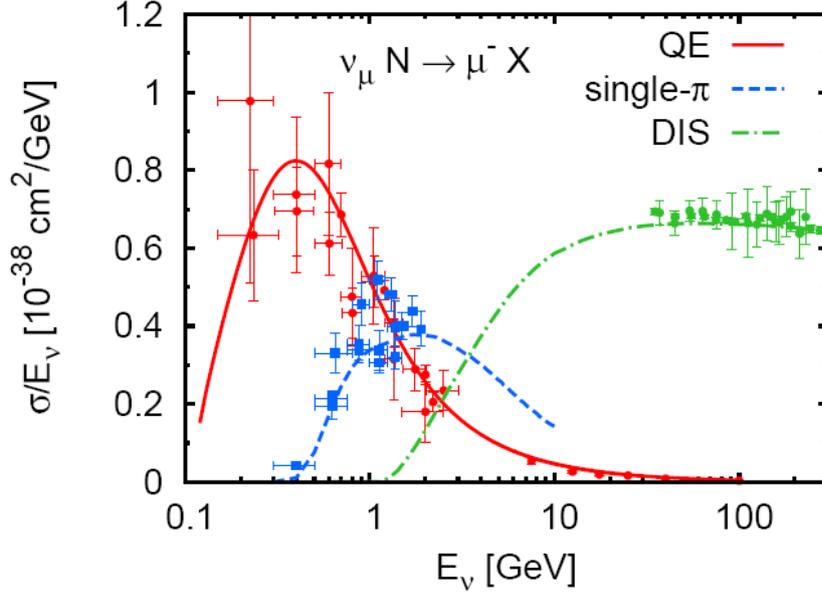
Fig. 2.2 Total neutrino cross-sections (per nucleon) for $\nu_\mu N \to \mu X$ divided by E_ν (as a function of the neutrino energy), for quasi-elastic scattering, single-π production and deep-inelastic scattering (DIS) compared to data. Figure is from Reference [22].

production in section 2.1.1. NEUT also use the experimental result to have consistency between these two regions.

Coherent pion production

At low energy neutrino can also scatter from the nucleus as a whole, such that the nucleus is left in its ground state after the interaction with a produced single pion. In CC and NC coherent (anti-) neutrino interactions a single pion can be produced:

$$\nu_l + A \to \nu_l + A + \pi^0 \qquad\qquad \bar{\nu}_l + A \to \bar{\nu}_l + A + \pi^0$$
$$\nu_l + A \to l^- + A + \pi^+ \qquad\qquad \bar{\nu}_l + A \to l^+ + A + \pi^- \qquad (2.4)$$

Both NEUT and GENIE simulate coherent scattering with the Rein-Sehgal coherent model [31] with improvement in from Reference [32].

2.1.2   Nuclear models

If a neutrino interacts with a bound nucleon inside the nucleus, we must take into account the nuclear model to describe the initial an final states of nucleons within the nucleus. The impulse approximation, where the neutrino interaction is with a single nucleon, separated

from the rest of nucleus, is assumed in neutrino MC generators. The simplest nuclear model which use the impulse approximation, describes the nucleus by a Fermi gas model. One assumes the ground state to be a Fermi sea of protons and neutrons filled up completely to a certain Fermi level defined by Fermi momentum, which has a flat distribution in momentum space [27]. The Fermi gas model, based on this assumptions, is called global Fermi gas. The alternative way to describe the nucleus in the Fermi gas picture is to use local density approximation [27], which is called local Fermi gas. In this approach nuclear matter density is described by the distribution $\rho(r)$. The local Fermi momentum is assumed to depend on $\rho(r)$ (where r is a distance from the center of the nucleus) for proton and neutron:

$$
\begin{aligned}
p_F^{(p)}(r) &= \hbar \left(3\pi^2 \rho(r) \frac{Z}{A} \right)^{1/3} \\
p_F^{(n)}(r) &= \hbar \left(3\pi^2 \rho(r) \frac{A-Z}{A} \right)^{1/3}
\end{aligned}
\tag{2.5}
$$

In the case of constant density ($\rho(r) = A(\frac{4}{3}\pi R^3)^{-1}$) you can find the Fermi momentum for global Fermi gas model.

Since all states are filled up to the Fermi momentum, outgoing nucleons with a momentum less than the Fermi momentum are Pauli blocked. The Pauli blocking is different between global and local Fermi gas, since the Fermi momentum depends on $\rho(r)$.

The Fermi gas model is still used in many analyses, However, it is well known from the electron scattering data, that a sophisticated model called spectral function [28], provides a more realistic description of the momentum and energy distributions of initial nucleons within a nucleus than the Fermi gas models.

2.1.3   Final state interaction (FSI)

Initially produced hadrons can interact with themselves and with other nucleons in targets on their way out of the nuclear target. Therefore the initially produced hadrons can be different than the outgoing particles being detected at the end. Final state interactions of pions are essential in the analysis of neutrino data:

1. **Pion absorption: Initially produced pion can be absorbed, for instance via $NN\pi \rightarrow NN$.**

2. **Charge exchange: Pion can also exchange its charge, for instance; $\pi^+ N \rightarrow \pi^0 p$.**

3. **Pion production: Pion can be created for instance from inelastic nucleon-nucleon collisions in the medium; $NN \rightarrow NN\pi$.**

Final state interactions of pions are essential in the analysis of neutrino data. There is a significant contribution coming from single pion production (see Figure 2.2). If the pion is absorbed in the nuclear matter, the event is misidentified from CCQE which is very important in the oscillation analysis. To estimate this background, it is necessary to have a good theoretical model for both, pion production in the primary vertex and FSI.

Cascade models are used by both NEUT [56, 29] and GENIE [57, 58], but implementations are slightly different for different kinds of hadrons.

Chapter 3

Neutrino-Induced Single Pion Production

Single pions in neutrino-nucleon interactions are dominantly produced through resonance decay but they also can be produced directly via non-resonant interactions (see Fig. 3.1).

There are three channels for Charged Current (CC) neutrino-nucleon and similarly for
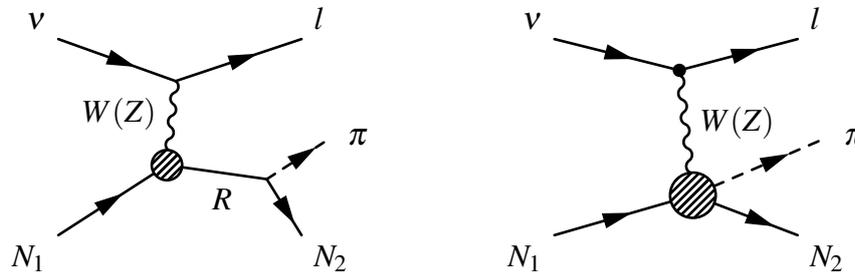
Fig. 3.1 Single pion production through resonance decay (left) and non-resonant interaction (right)

antineutrino-nucleon interactions with single pion production at final states:

$$
\begin{aligned}
\nu_\mu + p &\to \mu p \pi^+ \,, \\
\nu_\mu + n &\to \mu p \pi^0 \,, \\
\nu_\mu + n &\to \mu n \pi^+ \,,
\end{aligned}
\qquad (3.1)
$$

$$
\begin{aligned}
\bar{\nu}_\mu + n &\to \mu^+ n \pi^- \\
\bar{\nu}_\mu + p &\to \mu^+ n \pi^0 \\
\bar{\nu}_\mu + p &\to \mu^+ p \pi^-
\end{aligned}
\qquad (3.2)
$$

and four channels for NC neutrino-nucleon and antineutrino-nucleon interactions :

$$\nu + p \rightarrow \quad \nu p \pi^0 \,,$$
$$\nu + p \rightarrow \quad \nu n \pi^+ \,,$$
$$\nu + n \rightarrow \quad \nu n \pi^0 \,,$$
$$\nu + n \rightarrow \quad \nu p \pi^- \,, \qquad (3.3)$$

$$\bar{\nu} + p \rightarrow \quad \bar{\nu} p \pi^0$$
$$\bar{\nu} + p \rightarrow \quad \bar{\nu} n \pi^+$$
$$\bar{\nu} + n \rightarrow \quad \bar{\nu} n \pi^0$$
$$\bar{\nu} + n \rightarrow \quad \bar{\nu} p \pi^-. \qquad (3.4)$$

In this chapter we introduce helicity amplitudes, the amplitudes for different helicities of incident and outgoing particles, for SPP interactions. The helicity amplitudes of the individual resonances were given in [5, 6] for the first time, and the idea has been extended by Rein and Sehgal [7] to all resonances up to $W = 2GeV$. The helicity amplitudes of non-resonant interaction were introduced in [8] and [9] and this chapter is based on this idea, but unlike [8] and [9], the lepton mass is not neglected in this thesis.

Main goal in this chapter is to define a suitable framework in section 3.1 for both resonant and non-resonant interactions and calculate a general form for helicity amplitudes (subsection 3.1.3). Finally, the description of cross-section in terms of helicity amplitudes will be presented in section 3.2. In this section two alternative cross section will be presented in terms of pion angle and angular momentum (subsection 3.2.1).

3.1   General Formalism

Single pion production in neutrino-nucleon interactions can be generally defined as:

$$\nu(k_1) + N(p_1) \longrightarrow l(k_2) N(p_2) \pi(q), \qquad (3.5)$$

where l is a charged lepton in the CC interactions, or neutrino in the NC interaction. The particle's momenta for single pion production are shown in Figure 3.2 where k_1 and k_2 are the lepton four-momenta for incoming neutrino and outgoing leptons. p_1 and p_2 are the nucleon four-momenta and q is the pion four-momentum. $\mathbf{k} = \mathbf{k}_1 - \mathbf{k}_2$ is momentum transfer, and $Q^2 = -k^2 = -(k_1 - k_2)^2$

The transition amplitude for a charged current reaction is

$$\mathcal{M}_{CC}(\nu N \rightarrow l N' \pi) = \frac{G_F}{\sqrt{2}} \cos\theta_C \, \varepsilon_{CC}^{\rho} \, \langle N'\pi| \, J_\rho \, |N \, \rangle \qquad (3.6)$$

where θ_C is Cabibbo angle and ε^ρ is lepton charged current

$$\varepsilon_{CC}^{\rho} = \bar{u}_l(k_2) \gamma^\rho (1 - \gamma_5) u_\nu(k_1). \qquad (3.7)$$
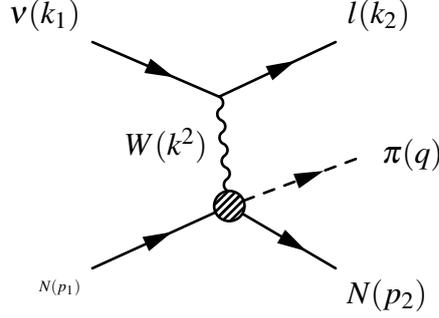
Fig. 3.2 Single pion production off nucleons
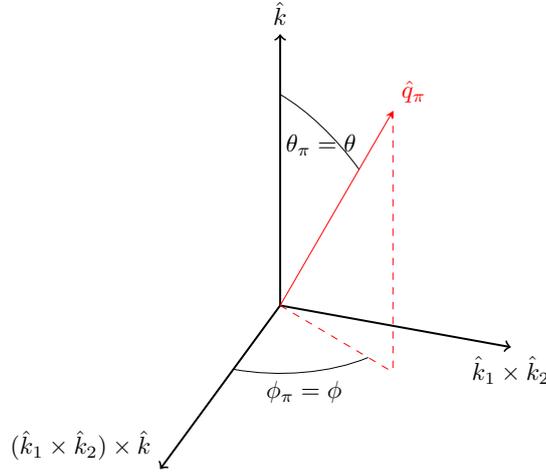
Fig. 3.3 Isobaric frame; the πN center of mass frame

For neutral-current (NC) the transition amplitude and the lepton current are the following:

$$\mathcal{M}_{NC}(\nu N \to \nu N' \pi) = \frac{G_F}{\sqrt{2}} \, \varepsilon_{NC}^{\rho} \, \langle \, N' \pi | \, J_{\rho} \, | N \, \rangle$$

$$\varepsilon_{NC}^{\rho} = \frac{1}{2} \bar{u}_{\nu}(k_2) \gamma^{\rho} (1 - \gamma_5) u_{\nu}(k_1). \tag{3.8}$$

The hadron current has different form in CC and NC interactions but in either case they can be decomposed to vector and axial vector parts $J_{\rho} = J_{\rho}^{V} - J_{\rho}^{A}$.

It is suitable to calculate the single pion production in the nucleon-pion rest frame that was proposed by Adler [8] and is called isobaric or Adler frame. The definition of the frame is shown in Figure 3.3, where lepton momentum transfer is along $\hat{z}$ axis. The angle between momentum transfer ($\hat{z}$ direction) and the pion direction is pion polar angle (θ), and ϕ is the pion azimuthal angle. The four-momentum of particles in the SPP has the following definition in the isobaric

frame:
$$
\begin{aligned}
k_1 &= (k_{01}, \mathbf{k}_1), & k_2 &= (k_{02}, \mathbf{k}_2), \\
p_1 &= (p_{01}, \mathbf{p}_1), & p_2 &= (p_{02}, \mathbf{p}_2), \\
q &= (q_0, \mathbf{q}),
\end{aligned}
\tag{3.9}
$$

where k_{01} and k_{02} are the energy of leptons, p_{01} and p_{02} are the energy of nucleons and q_0 is pion's energy in the isobaric frame. We denote by m_l, m_π and M, the lepton, pion and nucleon masses respectively. most of the calculation in this work is done in the rest frame of the final pion and nucleon (Figure 3.3), define by

$$
\mathbf{q} + \mathbf{p}_2 = \mathbf{k} + \mathbf{p}_1 = 0,
\tag{3.10}
$$

however a few times we use lab frame with a subscript "L" for particle's Energy and momentum.

Using Equation 3.10 we can define:

$$
\begin{aligned}
q_0 &= \frac{W^2 + m_\pi^2 - M^2}{2W}, & k_0 &= \frac{W^2 - M^2 + k^2}{2W} \\
p_{01} &= \frac{W^2 + M^2 - k^2}{2W}, & p_{02} &= \frac{W^2 + M^2 - m_\pi^2}{2W},
\end{aligned}
\tag{3.11}
$$

where $W^2 = (p_2 + q)^2 = (p_1 + k)^2$.

3.1.1 Lepton currents

The outgoing charged lepton in CC interactions is massive, therefore $k_{02} \neq \mathbf{k}_2$ in the general case, but we can set the lepton mass to zero when outgoing lepton is neutrino in the NC interactions.

Massive lepton can have both right-handed and left-handed helicities, therefore the lepton current can be defined as:

$$
\varepsilon_\lambda^\rho = \bar{u}_{l_\lambda}(k_2)\gamma^\rho(1 - \gamma_5)u_{\nu_L}(k_1),
\tag{3.12}
$$

where $\lambda = -(+)$ stands for left(right)- handed helicity. The lepton current's components can be represented by two-dimensional Pauli matrices and spinors, if we substitute Dirac matrices and Dirac spinors in terms of Pauli matrices and spinors according to our notation

(see Appendix A):

$$\varepsilon_\lambda^0 = N_1 N_2^* \, \chi_{(s_2,\lambda)}^\dagger \left(1 - \frac{\boldsymbol{\sigma}.\mathbf{k}_2}{k_{02}+m_l} \right) \left(1 - \frac{\boldsymbol{\sigma}.\mathbf{k}_1}{k_{01}} \right) \chi_{s_1} \tag{3.13}$$

$$\varepsilon_\lambda^j = N_1 N_2^* \, \chi_{(s_2,\lambda)}^\dagger \left(1 - \frac{\boldsymbol{\sigma}.\mathbf{k}_2}{k_{02}+m_l} \right) (-\sigma^j) \left(1 - \frac{\boldsymbol{\sigma}.\mathbf{k}_1}{k_{01}} \right) \chi_{s_1}. \tag{3.14}$$

The lepton current's components can be further calculated in the isobaric frame (Figure 3.3) by knowing the lepton's Pauli spinors in the isobaric frame given in Appendix B. Detailed calculation can be found in Appendix C, however we summarize the lepton current's components in the isobaric frame:

$$
\begin{aligned}
\varepsilon_\lambda^0 &= 2\lambda A_\lambda \sqrt{1 - \lambda \cos\delta} \\
\varepsilon_\lambda^1 &= 2\lambda A_\lambda \frac{k_{01} - \lambda |\mathbf{K_2}|}{|\mathbf{k}|} \sqrt{1 + \lambda \cos\delta} \\
\varepsilon_\lambda^2 &= 2i A_\lambda \sqrt{1 + \lambda \cos\delta} \\
\varepsilon_\lambda^3 &= 2\lambda A_\lambda \frac{k_{01} + \lambda |\mathbf{K_2}|}{|\mathbf{k}|} \sqrt{1 - \lambda \cos\delta},
\end{aligned}
\tag{3.15}
$$

where δ is the angle between neutrino and charged lepton in $N\pi$ rest frame, and

$$A_\pm = \sqrt{k_{01}(k_{02} \mp |\mathbf{k}_2|)}. \tag{3.16}$$

The lepton current ε^ρ can be interpreted as the intermediate gauge boson's polarization vector. In the isobaric frame where momentum transfer is in the $\hat{z}$ direction we have:

$$\varepsilon_\lambda^\rho = C_{L_\lambda} e_L^\rho + C_{R_\lambda} e_R^\rho + C_\lambda e_\lambda^\rho. \tag{3.17}$$

where $\mathbf{e}_L$ and $\mathbf{e}_R$ are transverse polarizations perpendicular to momentum transfer, and $\mathbf{e}_\lambda$s are along $\mathbf{z}$ direction in the isobaric system.

If we neglect the lepton mass, we can only have the left-handed current and $k_\rho \varepsilon^\rho = 0$, therefore the number of independent polarizations will be reduced to three:

$$\varepsilon_-^\rho = C_{L_-} e_L^\rho + C_{R_-} e_R^\rho + C_- e_-^\rho. \tag{3.18}$$

Transverse polarizations are unit vectors and have the following forms in the plane perpendicular to the $\hat{z}$ axis:

$$
\begin{aligned}
e_L^\rho &= \frac{1}{\sqrt{2}} \begin{pmatrix} 0 & 1 & -i & 0 \end{pmatrix} \\
e_R^\rho &= \frac{1}{\sqrt{2}} \begin{pmatrix} 0 & -1 & -i & 0 \end{pmatrix},
\end{aligned}
\tag{3.19}
$$

and

$$
\begin{aligned}
C_{L_\lambda} &= e_L^{\rho^*}(\varepsilon_\lambda)_\rho = \frac{1}{\sqrt{2}}\left(\varepsilon_\lambda^1 + i\varepsilon_\lambda^2\right) \\
C_{R_\lambda} &= e_R^{\rho^*}(\varepsilon_\lambda)_\rho = -\frac{1}{\sqrt{2}}\left(\varepsilon_\lambda^1 - i\varepsilon_\lambda^2\right).
\end{aligned}
\tag{3.20}
$$

e_λ should be a unit vector along $\hat{z}$. We can start with a general form:

$$
\begin{aligned}
e_-^\rho &= \frac{1}{\sqrt{|\alpha_-^2 - \beta_-^2|}}\begin{pmatrix} \alpha_- & 0 & 0 & \beta_- \end{pmatrix} \\
e_+^\rho &= \frac{1}{\sqrt{|\alpha_+^2 - \beta_+^2|}}\begin{pmatrix} \alpha_+ & 0 & 0 & \beta_+ \end{pmatrix}.
\end{aligned}
\tag{3.21}
$$

To calculate $\alpha_\mp$, $\beta_\mp$ and $C_\mp$, we need to calculate $\varepsilon^\rho k_\rho$:

$$
\begin{aligned}
\varepsilon_-^\rho k_\rho &= \varepsilon_-^0 k_0 - \varepsilon_-^3 |k| \\
\varepsilon_+^\rho k_\rho &= \varepsilon_+^0 k_0 - \varepsilon_+^3 |k|
\end{aligned}
$$
nonumber (3.22)

$$
\begin{aligned}
\varepsilon_-^\rho k_\rho &= C_- e_-^\rho k_\rho = \frac{C_-}{\sqrt{|\alpha_-^2 - \beta_-^2|}}(\alpha_- k_0 - \beta_- |k|) \\
\varepsilon_+^\rho k_\rho &= C_+ e_+^\rho k_\rho = \frac{C_+}{\sqrt{|\alpha_+^2 - \beta_+^2|}}(\alpha_+ k_0 - \beta_+ |k|).
\end{aligned}
\tag{3.23}
$$

Equating Equation 3.22) with 3.23, we can extract:

$$
\begin{aligned}
\alpha_- &= \varepsilon_-^0 \\
\beta_- &= \varepsilon_-^3
\end{aligned}
\qquad
\begin{aligned}
\alpha_+ &= \varepsilon_+^0 \\
\beta_+ &= \varepsilon_+^3
\end{aligned}
\tag{3.24}
$$

Therefore:

$$
\begin{aligned}
e_\lambda^\rho &= \frac{1}{\sqrt{|(\varepsilon_\lambda^0)^2 - (\varepsilon_\lambda^3)^2|}}\begin{pmatrix} \varepsilon_\lambda^0 & 0 & 0 & \varepsilon_\lambda^3 \end{pmatrix}. \\
C_\lambda &= \sqrt{(\varepsilon_\lambda^0)^2 - (\varepsilon_\lambda^3)^2}.
\end{aligned}
\tag{3.25}
$$

Unlike transverse polarization, $e_\pm$ depend on lepton current's helicity, therefore for right handed lepton and only $e_- \to e_+$. To summarize there are four independent polarizations i.e. e_L, e_R and $e_\pm$ in the general case. Later we will use λ_k as four different gauge boson's helicities.

3.1.2 Hadron Currents

Hadronic currents can be be decomposed to vector and axial vector parts

$$\langle\, N\pi|\, J^\rho \,|N\,\rangle = \langle\, N\pi|\, J_V^\rho - J_A^\rho \,|N\,\rangle \tag{3.26}$$

We can further decompose the vector and axial vector parts such as:

$$
\begin{aligned}
J_V^\rho e_\rho^{\lambda_k} &= \sum_{k=1}^{6} V_k(s,t,u)\, \bar{u}_N(p_2) O^{\lambda_k}(V_k) u_N(p_1) \\
J_A^\rho e_\rho^{\lambda_k} &= \sum_{k=1}^{8} A_k(s,t,u)\, \bar{u}_N(p_2) O^{\lambda_k}(A_k) u_N(p_1),
\end{aligned}
\tag{3.27}
$$

where λ_k is gauge boson's polarization, and it stands for e_L, e_R and $e_\pm$.
Dirac equation allows us to have 16 independent Lorentz invariants $O(V_k)$ and $O(A_k)$, but vector current conservation will reduce the number of $O(V_k)$ to six. They are represented in [8], and you can also find them in Table 3.1. Invariant amplitudes V_k and A_k can be calculated once the interactions and diagrams are defined. They are generally a function of the following invariant (Mandelstam) variables:

$$
\begin{aligned}
s &= (p_2+q)^2 = (p_1+k)^2 = W^2, \\
t &= (k-q)^2 \ \ \text{and} \ \ u = (q-p_1)^2.
\end{aligned}
\tag{3.28}
$$

Using the representations of Dirac matrices and spinors in terms of two dimensional Pauli matrices and spinors given in Appendix A, we can rewrite the right hand side of Equation 3.27 in terms of 2×2 matrices Σ_k and Λ_k:

$$
\begin{aligned}
J_V^\rho e_\rho^{\lambda_k} &= \sum_{k=1}^{6} \mathscr{F}_k(s,t,u)\, \chi_2^* \, \Sigma_k^{\lambda_k} \, \chi_1 \\
J_A^\rho e_\rho^{\lambda_k} &= \sum_{k=1}^{8} \mathscr{G}_k(s,t,u)\, \chi_2^* \, \Lambda_k^{\lambda_k} \, \chi_1
\end{aligned}
\tag{3.29}
$$

where χ_1 (χ_2) is the Pauli spinor of the incident (outgoing) nucleon given in Appendix A, and Σ_k and Λ_k are given in Table 3.2.
$\mathscr{F}_k^{\lambda_k}$ and $\mathscr{G}_k^{\lambda_k}$ can be found by equating the right hand sides of Equation 3.27 and Equation 3.29 for both vector and axial parts, but first we need to derive $O^{\lambda_k}(V_k)$ and $O^{\lambda_k}(A_k)$ in terms of 2×2 Pauli matrices. Here we show the final result, but the derivation for $O^{\lambda_k}(A_1)$

Table 3.1 Lorentz Invariants

Vector invariants	Axial vector Invariants
$O^{\lambda_k}(V_1) = \frac{1}{2}\gamma_5\left[(\gamma e^{\lambda_k})(\gamma k) - (\gamma k)(\gamma e^{\lambda_k})\right]$	
$O^{\lambda_k}(V_2) = -2\gamma_5\left[(Pe^{\lambda_k})(qk) - (Pk)(qe^{\lambda_k})\right]$	$O^{\lambda_k}(A_1) = \frac{1}{2}[(\gamma q)(\gamma e^{\lambda_k}) - (\gamma e^{\lambda_k})(\gamma q)]$
$O^{\lambda_k}(V_3) = \gamma_5\left[(\gamma e^{\lambda_k})(qk) - (\gamma k)(qe^{\lambda_k})\right]$	$O^{\lambda_k}(A_2) = 2(e^{\lambda_k}P)$
$O^{\lambda_k}(V_4) = 2\gamma_5\left[(\gamma e^{\lambda_k})(Pk) - (\gamma k)(Pe^{\lambda_k})\right]$	$O^{\lambda_k}(A_3) = (e^{\lambda_k}q)$
$\qquad\qquad - M\gamma_5\left[(\gamma e^{\lambda_k})(\gamma k) - (\gamma k)(\gamma e^{\lambda_k})\right]$	$O^{\lambda_k}(A_4) = M\gamma e^{\lambda_k}$
$O^{\lambda_k}(V_5) = -\gamma_5\left[(ke^{\lambda_k})(qk) - k^2(qe^{\lambda_k})\right]$	$O^{\lambda_k}(A_5) = -2(\gamma k)(e^{\lambda_k}P)$
$O^{\lambda_k}(V_6) = \gamma_5\left[(ke^{\lambda_k})(\gamma k) - k^2(\gamma e^{\lambda_k})\right]$	$O^{\lambda_k}(A_6) = -(\gamma k)(e^{\lambda_k}q)$
	$O^{\lambda_k}(A_7) = (e^{\lambda_k}k)$
	$O^{\lambda_k}(A_8) = -(\gamma k)(e^{\lambda_k}k)$

$P = 1/2(p_1 + p_2)$ and $ek = \varepsilon^0 k_0 - \boldsymbol{\varepsilon}.\mathbf{k}$. e^{λ_k} can be e_L, e_R and $e_{\pm}$.

can be found in Appendix D.

$$O^{\lambda_k}(V_1) = \mathbb{1}_4\left[(\boldsymbol{\sigma}e^{\lambda_k})k_0 - (\boldsymbol{\sigma}\mathbf{k})e_0^{\lambda_k}\right] - \gamma_5\left[(\boldsymbol{\sigma}e^{\lambda_k})(\boldsymbol{\sigma}\mathbf{k}) - e^{\lambda_k}.\mathbf{k}\right]$$

$$O^{\lambda_k}(V_2) = -\gamma_5\left[(p_1+p_2)e(qk) - (p_1+p_2)k(qe^{\lambda_k})\right]$$

$$O^{\lambda_k}(V_3) = \left[k_0(\mathbf{q}e^{\lambda_k}) - e_0^{\lambda_k}(\mathbf{q}\mathbf{k})\right]\begin{pmatrix} 0 & -\mathbb{1}_2 \\ \mathbb{1}_2 & 0 \end{pmatrix} + \left[(qe^{\lambda_k})(\boldsymbol{\sigma}\mathbf{k}) - (qk)(\boldsymbol{\sigma}e^{\lambda_k})\right]\begin{pmatrix} -\mathbb{1}_2 & 0 \\ 0 & \mathbb{1}_2 \end{pmatrix}$$

$$O^{\lambda_k}(V_4) = \left[k_0(\mathbf{p_1}+\mathbf{p_2}).e^{\lambda_k} - e_0^{\lambda_k}(\mathbf{p_1}-\mathbf{p_2}).\mathbf{k}\right]\begin{pmatrix} 0 & -\mathbb{1}_2 \\ \mathbb{1}_2 & 0 \end{pmatrix} \tag{3.30}$$

$$+ \left[(p_1+p_2)e(\boldsymbol{\sigma}\mathbf{k}) - (p_1+p_2)k(\boldsymbol{\sigma}e^{\lambda_k})\right]\begin{pmatrix} -\mathbb{1}_2 & 0 \\ 0 & \mathbb{1}_2 \end{pmatrix} - 2MO(V_1)$$

$$O^{\lambda_k}(V_5) = \left[k^2(e^{\lambda_k}q) - (e^{\lambda_k}k)(qk)\right]\begin{pmatrix} 0 & \mathbb{1}_2 \\ \mathbb{1}_2 & 0 \end{pmatrix}$$

$$O^{\lambda_k}(V_6) = \gamma_5\begin{pmatrix} (e^{\lambda_k}k)k_0 - k^2 e_0^{\lambda_k} & (e^{\lambda_k}k)(\mathbf{k}.\boldsymbol{\sigma}) - k^2(e^{\lambda_k}.\boldsymbol{\sigma}) \\ k^2(\mathbf{e}^{\lambda_k}.\boldsymbol{\sigma}) - (e^{\lambda_k}k)(\mathbf{k}.\boldsymbol{\sigma}) & k^2 e_0 - (e^{\lambda_k}k)k_0 \end{pmatrix}$$

$$= \begin{pmatrix} k^2(\mathbf{e}^{\lambda_k}.\boldsymbol{\sigma}) - (e^{\lambda_k}k)(\mathbf{k}.\boldsymbol{\sigma}) & k^2 e_0 - (e^{\lambda_k}k)k_0 \\ (e^{\lambda_k}k)k_0 - k^2 e_0^{\lambda_k} & (e^{\lambda_k}k)(\mathbf{k}.\boldsymbol{\sigma}) - k^2(\mathbf{e}^{\lambda_k}.\boldsymbol{\sigma}) \end{pmatrix} \tag{3.31}$$

Table 3.2 Isobaric frame amplitudes.

Vector	Axial vector
$\Sigma_1^{\lambda_k} = \boldsymbol{\sigma}e^{\lambda_k} - (\boldsymbol{\sigma}\hat{\mathbf{k}})(\hat{\mathbf{k}}e^{\lambda_k})$ $\Sigma_2^{\lambda_k} = -i(\boldsymbol{\sigma}\hat{\mathbf{q}})\boldsymbol{\sigma}.(\hat{\mathbf{k}} \times e^{\lambda_k})$ $\Sigma_3^{\lambda_k} = (\boldsymbol{\sigma}\hat{\mathbf{k}})(\hat{\mathbf{q}}e^{\lambda_k} - (\hat{\mathbf{q}}\hat{\mathbf{k}})(\hat{\mathbf{k}}e^{\lambda_k}))$ $\Sigma_4^{\lambda_k} = (\boldsymbol{\sigma}\hat{\mathbf{q}})(\hat{\mathbf{q}}e^{\lambda_k} - (\hat{\mathbf{q}}\hat{\mathbf{k}})(\hat{\mathbf{k}}e^{\lambda_k}))$ $\Sigma_5^{\lambda_k} = (\boldsymbol{\sigma}\hat{\mathbf{k}})\hat{\mathbf{k}}.(k_0 e^{\lambda_k} - e_0^{\lambda_k}\mathbf{k})$ $\Sigma_6^{\lambda_k} = (\boldsymbol{\sigma}\hat{\mathbf{q}})\hat{\mathbf{k}}.(k_0 e^{\lambda_k} - e_0^{\lambda_k}\mathbf{k})$	$\Lambda_1^{\lambda_k} = -\boldsymbol{\sigma}\hat{\mathbf{q}}(\boldsymbol{\sigma}e^{\lambda_k} - (\boldsymbol{\sigma}\hat{\mathbf{k}})(\hat{\mathbf{k}}e^{\lambda_k}))$ $\Lambda_2^{\lambda_k} = i\boldsymbol{\sigma}.(\hat{\mathbf{k}} \times e^{\lambda_k})$ $\Lambda_3^{\lambda_k} = -(\boldsymbol{\sigma}\hat{\mathbf{q}})(\boldsymbol{\sigma}\hat{\mathbf{k}})(\hat{\mathbf{q}}e^{\lambda_k} - (\hat{\mathbf{q}}\hat{\mathbf{k}})(\hat{\mathbf{k}}e^{\lambda_k}))$ $\Lambda_4^{\lambda_k} = -(\hat{\mathbf{q}}e^{\lambda_k} - (\hat{\mathbf{q}}\hat{\mathbf{k}})(\hat{\mathbf{k}}e^{\lambda_k}))$ $\Lambda_5^{\lambda_k} = -(\boldsymbol{\sigma}\hat{\mathbf{q}})(\boldsymbol{\sigma}\hat{\mathbf{k}})(\hat{\mathbf{k}}e^{\lambda_k})\dfrac{|\mathbf{k}|}{k_0}$ $\Lambda_6^{\lambda_k} = -(\hat{\mathbf{k}}e^{\lambda_k})\dfrac{|\mathbf{k}|}{k_0}$ $\Lambda_7^{\lambda_k} = -(\boldsymbol{\sigma}\hat{\mathbf{q}})(\boldsymbol{\sigma}\hat{\mathbf{k}})(e^{\lambda_k}k)/k_0$ $\Lambda_8^{\lambda_k} = -(e^{\lambda_k}k)/k_0$

$\mathbf{A}\boldsymbol{\sigma} = A^i\sigma_i = A^1\sigma_1 + A^2\sigma_2 + A^3\sigma_3$

$$O^{\lambda_k}(A_1) = \left[(\boldsymbol{\sigma}\mathbf{q})e_0^{\lambda_k} - (\boldsymbol{\sigma}e^{\lambda_k})q^0\right]\begin{pmatrix} 0 & \mathbb{1}_2 \\ \mathbb{1}_2 & 0 \end{pmatrix} + \left[e^{\lambda_k}\mathbf{q} - (\boldsymbol{\sigma}\mathbf{q})(\boldsymbol{\sigma}e^{\lambda_k})\right]\mathbb{1}_4$$

$$O^{\lambda_k}(A_2) = (e^{\lambda_k}p_1) + (e^{\lambda_k}p_2) = e_0^{\lambda_k}(p_{01} + p_{02}) - e^{\lambda_k}.(\mathbf{p}_1 + \mathbf{p}_2)$$

$$O^{\lambda_k}(A_3) = (e^{\lambda_k}q)\mathbb{1}_4$$

$$O^{\lambda_k}(A_4) = M\begin{pmatrix} e_0^{\lambda_k}\mathbb{1}_2 & -\boldsymbol{\sigma}.\mathbf{e}^{\lambda_k} \\ \boldsymbol{\sigma}.e^{\lambda_k} & -e_0^{\lambda_k}\mathbb{1}_2 \end{pmatrix}$$

$$O^{\lambda_k}(A_5) = -(e_0^{\lambda_k}(p_{01} + p_{02}) - e^{\lambda_k}.(\mathbf{p}_1 + \mathbf{p}_2))\begin{pmatrix} k_0\mathbb{1}_2 & -\boldsymbol{\sigma}.\mathbf{k} \\ \boldsymbol{\sigma}.\mathbf{k} & -k_0\mathbb{1}_2 \end{pmatrix}$$

$$O^{\lambda_k}(A_6) = -(e_0^{\lambda_k}q^0 - e^{\lambda_k}.\mathbf{q})\begin{pmatrix} k_0\mathbb{1}_2 & -\boldsymbol{\sigma}.\mathbf{k} \\ \boldsymbol{\sigma}.\mathbf{k} & -k_0\mathbb{1}_2 \end{pmatrix}$$

$$O^{\lambda_k}(A_7) = e_0^{\lambda_k}q^0 - e^{\lambda_k}.\mathbf{q}$$

$$O^{\lambda_k}(A_8) = -(e^{\lambda_k}k)\begin{pmatrix} k_0\mathbb{1}_2 & -\boldsymbol{\sigma}.\mathbf{k} \\ \boldsymbol{\sigma}.\mathbf{k} & -k_0\mathbb{1}_2 \end{pmatrix} \tag{3.32}$$

where e^{λ_k} can be e_L, e_R and $e_\pm$.

Appendix A shows the relation between Dirac spinors (matrices) and Pauli spinors (matrices). In Appendix D we show the detailed calculation for $O^{\lambda_k}(A_1)$ and $\mathscr{G}_k^{\lambda_k}$s that are related to $O^{\lambda_k}(A_1)$.

3.1.3 Helicity amplitudes

Helicity amplitude can be defined with three indices: incident nucleon helicity (λ_1), outgoing nucleon helicity (λ_2) and gauge boson's polarization (λ_1), while pion is spinless. From Equation 3.12 Equation 3.6 for left and right handed lepton we have:

$$
\begin{aligned}
\mathscr{M}_{CC}(\nu N \to l_\lambda N' \pi) &= \frac{G_F}{\sqrt{2}} \cos\theta_C \langle N'\pi | \, \varepsilon_\lambda^\rho J_\rho \, | N \rangle \\
&= \frac{G_F}{\sqrt{2}} \cos\theta_C \langle N'\pi | \, C_{L_\lambda} e_L^\rho J_\rho + C_{R_\lambda} e_R^\rho J_\rho + C_\lambda e_\lambda^\rho J_\rho | N \rangle.
\end{aligned}
\tag{3.33}
$$

Using Equation 3.33, we can define the helicity amplitudes for vector and axial currents:

$$
\begin{aligned}
\tilde{F}_{\lambda_2,\lambda_1}^{\lambda_k} &= \langle N\pi | \, e_{\lambda_k}^\rho V_\rho \, | N \rangle \\
\tilde{G}_{\lambda_2,\lambda_1}^{\lambda_k} &= \langle N\pi | \, e_{\lambda_k}^\rho A_\rho \, | N \rangle
\end{aligned}
\tag{3.34}
$$

where

$$
V = \frac{1}{2M} J^V \ , \qquad A = \frac{1}{2M} J^A,
\tag{3.35}
$$

which is defined in [7] and is going to be useful in the next chapter.

For instance we can calculate $\tilde{F}_{\frac{1}{2}\frac{1}{2}}^{e_R}$ for $\lambda_1 = \lambda_2 = 1/2$ and $\mathbf{e}_R$. From Equation 3.19 and Figure 3.3 we have:

$$
\begin{aligned}
\mathbf{e}_R &= \frac{1}{\sqrt{2}} \begin{pmatrix} -1 & -i & 0 \end{pmatrix} \\
\hat{k} &= \hat{z} \Rightarrow \hat{k}.\mathbf{e}_R = 0 \\
\hat{q} &= (\sin\theta\cos\phi)\hat{x} + (\sin\theta\sin\phi)\hat{y} + cos\theta\hat{z},
\end{aligned}
\tag{3.36}
$$

then from Table 3.2 we can calculate all Σ_k like:

$$
\begin{aligned}
\Sigma_1 &= \boldsymbol{\sigma}.\mathbf{e}_R - \sigma_3(\hat{z}.\mathbf{e}_R) = -\frac{2}{\sqrt{2}} \begin{pmatrix} 0 & 1 \\ 0 & 0 \end{pmatrix} \\
\Sigma_2 &= -i(\boldsymbol{\sigma}.\hat{q})\boldsymbol{\sigma}.(\hat{z} \times \mathbf{e}_R) = \sqrt{2} \begin{pmatrix} 0 & \cos\theta \\ 0 & \sin\theta e^{i\phi} \end{pmatrix} \\
\Sigma_3 &= \sigma_3(-\frac{1}{\sqrt{2}}\sin\theta(\cos\phi + i\sin\phi) = -\frac{1}{\sqrt{2}}\sin\theta e^{i\phi} \begin{pmatrix} 1 & 0 \\ 0 & -1 \end{pmatrix} \\
\Sigma_4 &= -\frac{1}{\sqrt{2}}\sin\theta e^{i\phi} \begin{pmatrix} \cos\theta & \sin\theta e^{-i\phi} \\ \sin\theta e^{i\phi} & -\cos\theta \end{pmatrix}
\end{aligned}
\tag{3.37}
$$

and $\Sigma_5 = \Sigma_6 = 0$. Therefore:

$$\sum_{k=1}^{6} \mathscr{F}_k \, \Sigma_k = \mathscr{F}_1 \Sigma_1 + \mathscr{F}_2 \Sigma_2 + \mathscr{F}_3 \Sigma_3 + \mathscr{F}_4 \Sigma_4$$

$$= \frac{1}{\sqrt{2}} \begin{pmatrix} -(\mathscr{F}_3 \sin\theta + \mathscr{F}_4 \sin\theta \cos\theta)e^{i\phi} & -2\mathscr{F}_1 + 2\mathscr{F}_2 \cos\theta - \mathscr{F}_4 \sin^2\theta \\ -\mathscr{F}_4 \sin^2\theta \, e^{2i\phi} & (2\mathscr{F}_2 \sin\theta + \mathscr{F}_3 \sin\theta + \mathscr{F}_4 \sin\theta \cos\theta)e^{i\phi} \end{pmatrix}.$$

$$(3.38)$$

Knowing nucleon's spinors $\chi_1 = \chi_2 = |\uparrow\rangle$ from Appendix B, and from Equation 3.29, Equation 3.34 and Equation 3.38, we can find the helicity amplitude for the defined polarizations:

$$\tilde{F}^{e_R}_{\frac{1}{2}\frac{1}{2}} = \chi_2^{\dagger}(\uparrow) \left(\sum_{k=1}^{6} \mathscr{F}_k \, \Sigma_k \right) \chi_1(\uparrow)$$

$$= -\sqrt{2} \Big[\sin\frac{\theta}{2}(\mathscr{F}_1 + \mathscr{F}_2) + \frac{1}{2}\sin\theta \cos\frac{\theta}{2}(\mathscr{F}_3 + \mathscr{F}_4) \Big].$$

$$(3.39)$$

Similarly for e_L we can also calculate $\tilde{F}^{e_L}_{\frac{1}{2}\frac{1}{2}}$:

$$\mathbf{e}_L = \frac{1}{\sqrt{2}} \begin{pmatrix} 1 & -i & 0 \end{pmatrix}$$

$$\hat{k}.\mathbf{e}_L = 0, \qquad \boldsymbol{\sigma}.(\hat{\mathbf{k}} \times \mathbf{e}_L) = \begin{pmatrix} 0 & 0 \\ \sqrt{2}i & 0 \end{pmatrix},$$

$$(3.40)$$

$$\Sigma_1 = \boldsymbol{\sigma}.\mathbf{e}_L - \sigma_3(\hat{z}.\mathbf{e}_L) = -\sqrt{2} \begin{pmatrix} 0 & 0 \\ 1 & 0 \end{pmatrix}$$

$$\Sigma_2 = -i(\boldsymbol{\sigma}.\hat{q})\boldsymbol{\sigma}.(\hat{z} \times \mathbf{e}_L) = \sqrt{2} \begin{pmatrix} \sin\theta e^{-i\phi} & 0 \\ -\cos\theta & 0 \end{pmatrix}$$

$$\Sigma_3 = \sigma_3(\frac{1}{\sqrt{2}}\sin\theta(\cos\phi - i\sin\phi)) = \frac{1}{\sqrt{2}}\sin\theta e^{-i\phi} \begin{pmatrix} 1 & 0 \\ 0 & -1 \end{pmatrix}$$

$$\Sigma_4 = \frac{1}{\sqrt{2}}\sin\theta e^{-i\phi} \begin{pmatrix} \cos\theta & \sin\theta e^{-i\phi} \\ \sin\theta e^{i\phi} & -\cos\theta \end{pmatrix}$$

$$(3.41)$$

and $\Sigma_5 = \Sigma_6 = 0$. Therefore:

$$
\sum_{k=1}^{6} \mathscr{F}_k \Sigma_k = \mathscr{F}_1 \Sigma_1 + \mathscr{F}_2 \Sigma_2 + \mathscr{F}_3 \Sigma_3 + \mathscr{F}_4 \Sigma_4
$$

$$
= \frac{1}{\sqrt{2}} \begin{pmatrix} (2\mathscr{F}_2 + \mathscr{F}_3 + \mathscr{F}_4 \cos\theta)\sin\theta e^{-i\phi} & \mathscr{F}_4 \sin^2\theta e^{-2i\phi} \\ 2\mathscr{F}_1 - 2\cos\theta\, \mathscr{F}_2 + \sin^2\theta\, \mathscr{F}_4 & -(\mathscr{F}_3 + \cos\theta\, \mathscr{F}_4)\sin\theta e^{-i\phi} \end{pmatrix}.
$$

(3.42)

and

$$
\tilde{F}_{\frac{1}{2}\frac{1}{2}}^{e_L} = \chi_2^{\dagger}(\uparrow)\left(\sum_{k=1}^{6} \mathscr{F}_k \Sigma_k\right)\chi_1(\uparrow) = \frac{1}{\sqrt{2}}\sin\theta\cos\frac{\theta}{2}(\mathscr{F}_3 + \mathscr{F}_4)e^{-2i\phi}.
$$

(3.43)

Equation 3.39 and all helicity amplitudes for transverse polarization ($\tilde{F}_{\lambda_2,\lambda_1}^{(e_{L(R)})}$ and $\tilde{G}_{\lambda_2,\lambda_1}^{(e_{L(R)})}$) are the same (with [9]) when you neglect lepton mass ($m_l = 0$), but it is not the case for $\tilde{F}_{\lambda_2,\lambda_1}^{(e_{\pm})}$ and $\tilde{G}_{\lambda_2,\lambda_1}^{(e_{\pm})}$. To show this we also calculate $\tilde{F}_{\frac{1}{2}\frac{1}{2}}^{e_-}$. For e_-:

$$
\mathbf{e}_- = \frac{\varepsilon_L^3}{C_-}\begin{pmatrix} 0 & 0 & 1 \end{pmatrix}, \qquad e_-^0 = \frac{\varepsilon_L^0}{C_-}
$$

$$
\hat{\mathbf{k}}.\mathbf{e} = \frac{\varepsilon_L^3}{C_-}, \qquad \boldsymbol{\sigma}.\mathbf{e} = \sigma_3 \frac{\varepsilon_L^3}{C_-}.
$$

(3.44)

$\Sigma_1 = \Sigma_2 = \Sigma_3 = \Sigma_4 = 0$ in this case and

$$
\Sigma_5 = \sigma_3\left(\frac{k_0 \varepsilon_L^3}{C_-} - |\mathbf{k}|\frac{\varepsilon_L^0}{C_-}\right) = \frac{1}{C_-}\left(k_0 \varepsilon_L^3 - |\mathbf{k}|\varepsilon_L^0\right)\begin{pmatrix} 1 & 0 \\ 0 & -1 \end{pmatrix}
$$

$$
\Sigma_6 = \frac{1}{C_-}\left(k_0 \varepsilon_L^3 - |\mathbf{k}|\varepsilon_L^0\right)\begin{pmatrix} \cos\theta & \sin\theta e^{-i\phi} \\ \sin\theta e^{i\phi} & -\cos\theta \end{pmatrix}.
$$

(3.45)

Therefore:

$$
\sum_{k=1}^{6} \mathscr{F}_k \Sigma_k = \frac{1}{C_-}\left(k_0 \varepsilon_L^3 - |\mathbf{k}|\varepsilon_L^0\right)\begin{pmatrix} \mathscr{F}_5 + \mathscr{F}_6 \cos\theta & \mathscr{F}_6 \sin\theta e^{-i\phi} \\ \mathscr{F}_6 \sin\theta e^{i\phi} & -(\mathscr{F}_5 + \mathscr{F}_6 \cos\theta) \end{pmatrix}.
$$

(3.46)

Knowing nucleon's spinors $\chi_1 = \chi_2 = |\uparrow\rangle$ from Appendix B, and from Eqs. 3.29, we can find the helicity amplitude for the defined polarizations:

$$
\begin{aligned}
\tilde{F}^{e_-}_{\frac{1}{2}\frac{1}{2}} &= \chi_2^\dagger(\uparrow)\left(\sum_{k=1}^{6} \mathscr{F}_k\,\Sigma_k\right)\chi_1(\uparrow) \\
&= \frac{k_0\varepsilon_L^3 - |\mathbf{k}|\varepsilon_L^0}{\sqrt{|(\varepsilon_L^0)^2 - (\varepsilon_L^3)^2|}}\,[\mathscr{F}_5 + \mathscr{F}_6]\cos\frac{\theta}{2}e^{-i\phi}.
\end{aligned}
\tag{3.47}
$$

if $m_l \to 0$ then $\varepsilon_L^0 \to |\mathbf{k}|$, $\varepsilon_L^3 \to k_0$, and $C_- \to \sqrt{-k^2}$ and Equation 3.47 becomes

$$
\tilde{F}^{e_-}_{\frac{1}{2}\frac{1}{2}}(m_l \to 0) = -\sqrt{-k^2}\,[\mathscr{F}_5 + \mathscr{F}_6]\cos\frac{\theta}{2}e^{-i\phi},
\tag{3.48}
$$

as it is defined in [9].

For each vector and axial currents we can define $2 \times 2 \times 4 = 16$ helicity amplitudes $\tilde{F}^{(\lambda_k)}_{\lambda_2,\lambda_1}$, and $\tilde{G}^{(\lambda_k)}_{\lambda_2,\lambda_1}$. The final result for all helicity amplitudes are summarized in Equation 3.49 - 3.56.

$$
\begin{aligned}
\tilde{F}^{e_L}_{\frac{1}{2}\frac{1}{2}} &= \frac{1}{\sqrt{2}}e^{-2i\phi}\sin\theta\cos\frac{\theta}{2}(\mathscr{F}_3 + \mathscr{F}_4) \\
\tilde{F}^{e_L}_{\frac{-1}{2}\frac{1}{2}} &= -\frac{1}{\sqrt{2}}e^{-i\phi}\sin\theta\sin\frac{\theta}{2}(\mathscr{F}_3 - \mathscr{F}_4) \\
\tilde{F}^{e_L}_{\frac{1}{2}\frac{-1}{2}} &= \sqrt{2}e^{-i\phi}\left[\cos\frac{\theta}{2}(\mathscr{F}_1 - \mathscr{F}_2) - \frac{1}{2}\sin\theta\sin\frac{\theta}{2}(\mathscr{F}_3 - \mathscr{F}_4)\right] \\
\tilde{F}^{e_L}_{\frac{-1}{2}\frac{-1}{2}} &= -\sqrt{2}\left[\sin\frac{\theta}{2}(\mathscr{F}_1 + \mathscr{F}_2) + \frac{1}{2}\sin\theta\cos\frac{\theta}{2}(\mathscr{F}_3 + \mathscr{F}_4)\right]
\end{aligned}
\tag{3.49}
$$

$$
\begin{aligned}
\tilde{F}^{e_R}_{\frac{1}{2}\frac{1}{2}} &= -\sqrt{2}\left[\sin\theta/2(\mathscr{F}_1 + \mathscr{F}_2) + \frac{1}{2}\sin\theta\cos\frac{\theta}{2}(\mathscr{F}_3 + \mathscr{F}_4)\right] \\
\tilde{F}^{e_R}_{\frac{-1}{2}\frac{1}{2}} &= -\sqrt{2}e^{i\phi}\left[\cos\theta/2(\mathscr{F}_1 - \mathscr{F}_2) - \frac{1}{2}\sin\theta\sin\frac{\theta}{2}(\mathscr{F}_3 - \mathscr{F}_4)\right] \\
\tilde{F}^{e_R}_{\frac{1}{2}-\frac{1}{2}} &= \frac{1}{\sqrt{2}}e^{i\phi}\sin\theta\sin\frac{\theta}{2}(\mathscr{F}_3 - \mathscr{F}_4) \\
\tilde{F}^{e_R}_{-\frac{1}{2}-\frac{1}{2}} &= \frac{1}{\sqrt{2}}e^{2i\phi}\sin\theta\cos\frac{\theta}{2}(\mathscr{F}_3 + \mathscr{F}_4)
\end{aligned}
\tag{3.50}
$$

$$\tilde{F}^{e_-}_{\frac{1}{2}\frac{1}{2}} = e^{-i\phi}\cos\frac{\theta}{2}\frac{1}{C_-}(k_0\varepsilon_L^0 - |\mathbf{k}|\varepsilon_L^3)(\mathscr{F}_5 + \mathscr{F}_6)$$

$$\tilde{F}^{e_-}_{-\frac{1}{2}\frac{1}{2}} = -\sin\frac{\theta}{2}\frac{1}{C_-}(k_0\varepsilon_L^0 - |\mathbf{k}|\varepsilon_L^3)(\mathscr{F}_5 - \mathscr{F}_6)$$

$$\tilde{F}^{e_-}_{\frac{1}{2}-\frac{1}{2}} = -\sin\frac{\theta}{2}\frac{1}{C_-}(k_0\varepsilon_L^0 - |\mathbf{k}|\varepsilon_L^3)(\mathscr{F}_5 - \mathscr{F}_6)$$

$$\tilde{F}^{e_-}_{-\frac{1}{2}-\frac{1}{2}} = -e^{i\phi}\cos\frac{\theta}{2}\frac{1}{C_-}(k_0\varepsilon_L^0 - |\mathbf{k}|\varepsilon_L^3)(\mathscr{F}_5 + \mathscr{F}_6) \qquad (3.51)$$

$$\tilde{F}^{e_+}_{\frac{1}{2}\frac{1}{2}} = e^{-i\phi}\cos\frac{\theta}{2}\frac{1}{C_+}(k_0\varepsilon_R^0 - |\mathbf{k}|\varepsilon_R^3)(\mathscr{F}_5 + \mathscr{F}_6)$$

$$\tilde{F}^{e_+}_{-\frac{1}{2}\frac{1}{2}} = -\sin\frac{\theta}{2}\frac{1}{C_+}(k_0\varepsilon_R^0 - |\mathbf{k}|\varepsilon_R^3)(\mathscr{F}_5 - \mathscr{F}_6)$$

$$\tilde{F}^{e_+}_{\frac{1}{2}-\frac{1}{2}} = -\sin\frac{\theta}{2}\frac{1}{C_+}(k_0\varepsilon_R^0 - |\mathbf{k}|\varepsilon_R^3)(\mathscr{F}_5 - \mathscr{F}_6)$$

$$\tilde{F}^{e_+}_{-\frac{1}{2}-\frac{1}{2}} = -e^{i\phi}\cos\frac{\theta}{2}\frac{1}{C_+}(k_0\varepsilon_R^0 - |\mathbf{k}|\varepsilon_R^3)(\mathscr{F}_5 + \mathscr{F}_6) \qquad (3.52)$$

$$\tilde{G}^{e_L}_{\frac{1}{2}\frac{1}{2}} = \frac{1}{\sqrt{2}}e^{-2i\phi}\sin\theta\cos\frac{\theta}{2}(\mathscr{G}_3 + \mathscr{G}_4)$$

$$\tilde{G}^{e_L}_{-\frac{1}{2}\frac{1}{2}} = \frac{1}{\sqrt{2}}e^{-i\phi}\sin\theta\sin\frac{\theta}{2}(\mathscr{G}_3 - \mathscr{G}_4)$$

$$\tilde{G}^{e_L}_{\frac{1}{2}-\frac{1}{2}} = \sqrt{2}e^{i\phi}\left[\cos\frac{\theta}{2}(\mathscr{G}_1 - \mathscr{G}_2) - \frac{1}{2}\sin\theta\sin\frac{\theta}{2}(\mathscr{G}_3 - \mathscr{G}_4)\right]$$

$$\tilde{G}^{e_L}_{-\frac{1}{2}-\frac{1}{2}} = \sqrt{2}\left[\sin\frac{\theta}{2}(\mathscr{G}_1 + \mathscr{G}_2) + \frac{1}{2}\sin\theta\cos\frac{\theta}{2}(\mathscr{G}_3 + \mathscr{G}_4)\right] \qquad (3.53)$$

$$\tilde{G}^{e_R}_{\frac{1}{2}\frac{1}{2}} = -\sqrt{2}\left[\sin\theta/2(\mathscr{G}_1 + \mathscr{G}_2) + \frac{1}{2}\sin\theta\cos\frac{\theta}{2}(\mathscr{G}_3 + \mathscr{G}_4)\right]$$

$$\tilde{G}^{e_R}_{-\frac{1}{2}\frac{1}{2}} = \sqrt{2}e^{i\phi}\left[\cos\theta/2(\mathscr{G}_1 - \mathscr{G}_2) - \frac{1}{2}\sin\theta\sin\frac{\theta}{2}(\mathscr{G}_3 - \mathscr{G}_4)\right]$$

$$\tilde{G}^{e_R}_{\frac{1}{2}-\frac{1}{2}} = \frac{1}{\sqrt{2}}e^{i\phi}\sin\theta\sin\frac{\theta}{2}(\mathscr{G}_3 - \mathscr{G}_4)$$

$$\tilde{G}^{e_R}_{-\frac{1}{2}-\frac{1}{2}} = -\frac{1}{\sqrt{2}}e^{2i\phi}\sin\theta\cos\frac{\theta}{2}(\mathscr{G}_3 + \mathscr{G}_4) \qquad (3.54)$$

$$\tilde{G}^{e_-}_{\frac{1}{2}\frac{1}{2}} = e^{-i\phi}\cos\frac{\theta}{2}\frac{1}{C_-k_0}\left[|\mathbf{k}|\varepsilon_L^3(\mathscr{G}_5+\mathscr{G}_6)+(k_0\varepsilon_L^0-|\mathbf{k}|\varepsilon_L^3)(\mathscr{G}_7+\mathscr{G}_8)\right]$$

$$\tilde{G}^{e_-}_{-\frac{1}{2}\frac{1}{2}} = \sin\frac{\theta}{2}\frac{1}{C_-k_0}\left[|\mathbf{k}|\varepsilon_L^3(\mathscr{G}_5-\mathscr{G}_6)+(k_0\varepsilon_L^0-|\mathbf{k}|\varepsilon_L^3)(\mathscr{G}_7-\mathscr{G}_8)\right]$$

$$\tilde{G}^{e_-}_{\frac{1}{2}-\frac{1}{2}} = -\sin\frac{\theta}{2}\frac{1}{C_-k_0}\left[|\mathbf{k}|\varepsilon_L^3(\mathscr{G}_5-\mathscr{G}_6)+(k_0\varepsilon_L^0-|\mathbf{k}|\varepsilon_L^3)(\mathscr{G}_7-\mathscr{G}_8)\right]$$

$$\tilde{G}^{e_-}_{-\frac{1}{2}-\frac{1}{2}} = e^{i\phi}\cos\frac{\theta}{2}\frac{1}{C_-k_0}\left[|\mathbf{k}|\varepsilon_L^3(\mathscr{G}_5+\mathscr{G}_6)+(k_0\varepsilon_L^0-|\mathbf{k}|\varepsilon_L^3)(\mathscr{G}_7+\mathscr{G}_8)\right] \tag{3.55}$$

$$\tilde{G}^{e_+}_{\frac{1}{2}\frac{1}{2}} = e^{-i\phi}\cos\frac{\theta}{2}\frac{1}{C_+k_0}\left[|\mathbf{k}|\varepsilon_R^3(\mathscr{G}_5+\mathscr{G}_6)+(k_0\varepsilon_R^0-|\mathbf{k}|\varepsilon_R^3)(\mathscr{G}_7+\mathscr{G}_8)\right]$$

$$\tilde{G}^{e_+}_{-\frac{1}{2}\frac{1}{2}} = \sin\frac{\theta}{2}\frac{1}{C_+k_0}\left[|\mathbf{k}|\varepsilon_R^3(\mathscr{G}_5-\mathscr{G}_6)+(k_0\varepsilon_R^0-|\mathbf{k}|\varepsilon_R^3)(\mathscr{G}_7-\mathscr{G}_8)\right]$$

$$\tilde{G}^{e_+}_{\frac{1}{2}-\frac{1}{2}} = -\sin\frac{\theta}{2}\frac{1}{C_+k_0}\left[|\mathbf{k}|\varepsilon_R^3(\mathscr{G}_5-\mathscr{G}_6)+(k_0\varepsilon_R^0-|\mathbf{k}|\varepsilon_R^3)(\mathscr{G}_7-\mathscr{G}_8)\right]$$

$$\tilde{G}^{e_+}_{-\frac{1}{2}-\frac{1}{2}} = e^{i\phi}\cos\frac{\theta}{2}\frac{1}{C_+k_0}\left[|\mathbf{k}|\varepsilon_R^3(\mathscr{G}_5+\mathscr{G}_6)+(k_0\varepsilon_R^0-|\mathbf{k}|\varepsilon_R^3)(\mathscr{G}_7+\mathscr{G}_8)\right] \tag{3.56}$$

3.2   Cross Section

A detailed derivation of the cross-section for single pion production can be found in Appendix E. The final result is a differential cross-section as a function of E, Q^2, W, θ and ϕ:

$$\frac{d\sigma(\nu N \to lN\pi)}{dQ^2 dW d\Omega_\pi} = \frac{1}{(2\pi)^4}\frac{1}{(4ME_\nu)^2}\frac{|\mathbf{q}|}{4}|\mathscr{M}|^2, \tag{3.57}$$

where $\mathscr{M}$ is the transition amplitude and it has been given in Equation 3.6 and Equation 3.8. For unpolarized spinors:

$$|\mathscr{M}|^2 = \frac{G_F^2}{2}\cos^2\theta_C\frac{1}{2}\sum_{spin}\left\{[\varepsilon_L^\beta\langle N\pi|J_\beta|N\rangle]^*[\varepsilon_L^\alpha\langle N\pi|J_\alpha|N\rangle]\right.$$

$$\left. +[\varepsilon_R^\beta\langle N\pi|J_\beta|N\rangle]^*[\varepsilon_R^\alpha\langle N\pi|J_\alpha|N\rangle]\right\}. \tag{3.58}$$

In both [7] and [9] the lepton current is multiplied by a factor and the cross-section (Equation 3.57) is divided by same factor:

$$\varepsilon^\alpha \to -\frac{1}{\sqrt{2}}\frac{1}{\sqrt{-k^2}}\frac{|k_L|}{2E_\nu}\varepsilon^\alpha. \tag{3.59}$$

Therefore the differential cross section formula for single pion production can be found by using Equation 3.33- 3.34, and from Equation 3.57- 3.59 we have:

$$\frac{d\sigma(\nu N \to lN\pi)}{dk^2 dW d\Omega_\pi} = \frac{G_F^2}{2} \frac{1}{(2\pi)^4} \frac{|\mathbf{q}|}{4} \frac{-k^2}{(k^L)^2} \sum_{\lambda_2,\lambda_1} \Bigg\{$$

$$\left| C_{L_-}(\tilde{F}^{e_L}_{\lambda_2\lambda_1}(\theta,\phi) - \tilde{G}^{e_L}_{\lambda_2\lambda_1}(\theta,\phi)) + C_{R_-}(\tilde{F}^{e_R}_{\lambda_2\lambda_1}(\theta,\phi) - \tilde{G}^{e_R}_{\lambda_2\lambda_1}(\theta,\phi)) + C_-(\tilde{F}^{e_-}_{\lambda_2\lambda_1}(\theta,\phi) - \tilde{G}^{e_-}_{\lambda_2\lambda_1}(\theta,\phi)) \right|^2$$

$$+ \left| C_{L_+}(\tilde{F}^{e_L}_{\lambda_2\lambda_1}(\theta,\phi) - \tilde{G}^{e_L}_{\lambda_2\lambda_1}(\theta,\phi)) + C_{R_+}(\tilde{F}^{e_R}_{\lambda_2\lambda_1}(\theta,\phi) - \tilde{G}^{e_R}_{\lambda_2\lambda_1}(\theta,\phi)) + C_+(\tilde{F}^{e_+}_{\lambda_2\lambda_1}(\theta,\phi) - \tilde{G}^{e_+}_{\lambda_2\lambda_1}(\theta,\phi)) \right|^2 \Bigg\}.$$

$$(3.60)$$

For anti-neutrino interactions, one needs to swap $C_{L_\pm}$ with $C_{R_\pm}$. We can expand Equation 3.60:

$$\frac{d\sigma(\nu N \to lN\pi)}{dk^2 dW d\Omega_\pi} = \frac{G_F^2}{2} \frac{1}{(2\pi)^4} \frac{|\mathbf{q}|}{4} \frac{-k^2}{(k^L)^2} \sum_{\lambda_2,\lambda_1} \Bigg\{$$

$$|C_L|^2 |\tilde{F}^{e_L}_{\lambda_2\lambda_1}(\theta,\phi) - \tilde{G}^{e_L}_{\lambda_2\lambda_1}(\theta,\phi)|^2 + |C_R|^2 |\tilde{F}^{e_R}_{\lambda_2\lambda_1}(\theta,\phi) - \tilde{G}^{e_R}_{\lambda_2\lambda_1}(\theta,\phi)|^2$$

$$+ |C_-|^2 |\tilde{F}^{e_-}_{\lambda_2\lambda_1}(\theta,\phi) - \tilde{G}^{e_-}_{\lambda_2\lambda_1}(\theta,\phi)|^2 + |C_+|^2 |\tilde{F}^{e_+}_{\lambda_2\lambda_1}(\theta,\phi) - \tilde{G}^{e_+}_{\lambda_2\lambda_1}(\theta,\phi)|^2$$

$$+ C_{L_-}^* C_- \, (\tilde{F}^{e_L}_{\lambda_2\lambda_1}(\theta,\phi) - \tilde{G}^{e_L}_{\lambda_2\lambda_1}(\theta,\phi))^* (\tilde{F}^{e_-}_{\lambda_2\lambda_1}(\theta,\phi) - \tilde{G}^{e_-}_{\lambda_2\lambda_1}(\theta,\phi)) + c.c.$$

$$+ C_{R_-}^* C_- \, (\tilde{F}^{e_R}_{\lambda_2\lambda_1}(\theta,\phi) - \tilde{G}^{e_R}_{\lambda_2\lambda_1}(\theta,\phi))^* (\tilde{F}^{e_-}_{\lambda_2\lambda_1}(\theta,\phi) - \tilde{G}^{e_-}_{\lambda_2\lambda_1}(\theta,\phi)) + c.c.$$

$$+ C_{L_+}^* C_- \, (\tilde{F}^{e_L}_{\lambda_2\lambda_1}(\theta,\phi) - \tilde{G}^{e_L}_{\lambda_2\lambda_1}(\theta,\phi))^* (\tilde{F}^{e_-}_{\lambda_2\lambda_1}(\theta,\phi) - \tilde{G}^{e_-}_{\lambda_2\lambda_1}(\theta,\phi)) + c.c.$$

$$+ C_{R_+}^* C_- \, (\tilde{F}^{e_R}_{\lambda_2\lambda_1}(\theta,\phi) - \tilde{G}^{e_R}_{\lambda_2\lambda_1}(\theta,\phi))^* (\tilde{F}^{e_-}_{\lambda_2\lambda_1}(\theta,\phi) - \tilde{G}^{e_-}_{\lambda_2\lambda_1}(\theta,\phi)) + c.c.$$

$$+ (C_{L_-}^* C_{R_-} + C_{L_+}^* C_{R_+})(\tilde{F}^{e_L}_{\lambda_2\lambda_1}(\theta,\phi) - \tilde{G}^{e_L}_{\lambda_2\lambda_1}(\theta,\phi))^* (\tilde{F}^{e_R}_{\lambda_2\lambda_1}(\theta,\phi) - \tilde{G}^{e_R}_{\lambda_2\lambda_1}(\theta,\phi)) + c.c. \Bigg\}$$

$$(3.61)$$

where

$$|C_L|^2 = |C_{L_-}|^2 + |C_{L_+}|^2 \quad , \qquad |C_R|^2 = |C_{R_-}|^2 + |C_{R_+}|^2, \qquad (3.62)$$

and $c.c.$ is complex-conjugate.

The helicity amplitudes in Equation 3.49- 3.56 have a very simple dependance to the ϕ angle,

i.e. a phase. Therefore we can separate the ϕ dependence of helicity amplitudes by using:

$$(\tilde{F}^{e_L}_{\lambda_2\lambda_1}(\theta,\phi) - \tilde{G}^{e_L}_{\lambda_2\lambda_1}(\theta,\phi))^*(\tilde{F}^{e_R}_{\lambda_2\lambda_1}(\theta,\phi) - \tilde{G}^{e_R}_{\lambda_2\lambda_1}(\theta,\phi)) =$$
$$e^{2i\phi}(\tilde{F}^{e_L}_{\lambda_2\lambda_1}(\theta) - \tilde{G}^{e_L}_{\lambda_2\lambda_1}(\theta))^*(\tilde{F}^{e_R}_{\lambda_2\lambda_1}(\theta) - \tilde{G}^{e_R}_{\lambda_2\lambda_1}(\theta))$$
$$(\tilde{F}^{e_L}_{\lambda_2\lambda_1}(\theta,\phi) - \tilde{G}^{e_L}_{\lambda_2\lambda_1}(\theta,\phi))^*(\tilde{F}^{e_\pm}_{\lambda_2\lambda_1}(\theta,\phi) - \tilde{G}^{e_\pm}_{\lambda_2\lambda_1}(\theta,\phi)) =$$
$$e^{i\phi}(\tilde{F}^{e_L}_{\lambda_2\lambda_1}(\theta) - \tilde{G}^{e_L}_{\lambda_2\lambda_1}(\theta))^*(\tilde{F}^{e_\pm}_{\lambda_2\lambda_1}(\theta) - \tilde{G}^{e_\pm}_{\lambda_2\lambda_1}(\theta))$$
$$(\tilde{F}^{e_R}_{\lambda_2\lambda_1}(\theta,\phi) - \tilde{G}^{e_R}_{\lambda_2\lambda_1}(\theta,\phi))^*(\tilde{F}^{e_\pm}_{\lambda_2\lambda_1}(\theta,\phi) - \tilde{G}^{e_\pm}_{\lambda_2\lambda_1}(\theta,\phi)) =$$
$$e^{-i\phi}(\tilde{F}^{e_R}_{\lambda_2\lambda_1}(\theta) - \tilde{G}^{e_R}_{\lambda_2\lambda_1}(\theta))^*(\tilde{F}^{e_\pm}_{\lambda_2\lambda_1}(\theta) - \tilde{G}^{e_\pm}_{\lambda_2\lambda_1}(\theta)) \qquad (3.63)$$

Therefore Equation 3.61 will be

$$\frac{d\sigma(\nu N \to lN\pi)}{dk^2 dW d\Omega_\pi} = \frac{G_F^2}{2}\frac{1}{(2\pi)^4}\frac{|\mathbf{q}|}{4}\frac{-k^2}{(k^L)^2}\sum_{\lambda_2,\lambda_1}\Bigg\{$$

$$|C_L|^2|\tilde{F}^{e_L}_{\lambda_2\lambda_1}(\theta) - \tilde{G}^{e_L}_{\lambda_2\lambda_1}(\theta)|^2 + |C_R|^2|\tilde{F}^{e_R}_{\lambda_2\lambda_1}(\theta) - \tilde{G}^{e_R}_{\lambda_2\lambda_1}(\theta)|^2$$
$$+ \ |C_-|^2 \ |\tilde{F}^{e_-}_{\lambda_2\lambda_1}(\theta) - \tilde{G}^{e_-}_{\lambda_2\lambda_1}(\theta)|^2 + |C_+|^2 \ |\tilde{F}^{e_+}_{\lambda_2\lambda_1}(\theta) - \tilde{G}^{e_+}_{\lambda_2\lambda_1}(\theta)|^2$$

$$+2\cos\phi\Big\{ \quad C_{L_-}C_- \ \mathrm{Re}\left[(\tilde{F}^{e_L}_{\lambda_2\lambda_1}(\theta) - \tilde{G}^{e_L}_{\lambda_2\lambda_1}(\theta))^*(\tilde{F}^{e_-}_{\lambda_2\lambda_1}(\theta) - \tilde{G}^{e_-}_{\lambda_2\lambda_1}(\theta))\right]$$
$$+ \ C_{R_-}C_- \ \mathrm{Re}\left[(\tilde{F}^{e_R}_{\lambda_2\lambda_1}(\theta) - \tilde{G}^{e_R}_{\lambda_2\lambda_1}(\theta))^*(\tilde{F}^{e_-}_{\lambda_2\lambda_1}(\theta) - \tilde{G}^{e_-}_{\lambda_2\lambda_1}(\theta))\right]$$
$$+ \ C_{L_+}C_+ \ \mathrm{Re}\left[(\tilde{F}^{e_L}_{\lambda_2\lambda_1}(\theta) - \tilde{G}^{e_L}_{\lambda_2\lambda_1}(\theta))^*(\tilde{F}^{e_+}_{\lambda_2\lambda_1}(\theta) - \tilde{G}^{e_+}_{\lambda_2\lambda_1}(\theta))\right]$$
$$+ \ C_{R_+}C_+ \ \mathrm{Re}\left[(\tilde{F}^{e_R}_{\lambda_2\lambda_1}(\theta) - \tilde{G}^{e_R}_{\lambda_2\lambda_1}(\theta))^*(\tilde{F}^{e_+}_{\lambda_2\lambda_1}(\theta) - \tilde{G}^{e_+}_{\lambda_2\lambda_1}(\theta))\right]\Big\}$$

$$+2\sin\phi\Big\{ \ - \ C_{L_-}C_- \ \mathrm{Im}\left[(\tilde{F}^{e_L}_{\lambda_2\lambda_1}(\theta) - \tilde{G}^{e_L}_{\lambda_2\lambda_1}(\theta))^*(\tilde{F}^{e_-}_{\lambda_2\lambda_1}(\theta) - \tilde{G}^{e_-}_{\lambda_2\lambda_1}(\theta))\right]$$
$$+ \ C_{R_-}C_- \ \mathrm{Im}\left[(\tilde{F}^{e_R}_{\lambda_2\lambda_1}(\theta) - \tilde{G}^{e_R}_{\lambda_2\lambda_1}(\theta))^*(\tilde{F}^{e_-}_{\lambda_2\lambda_1}(\theta) - \tilde{G}^{e_-}_{\lambda_2\lambda_1}(\theta))\right]$$
$$- \ C_{L_+}C_+ \ \mathrm{Im}\left[(\tilde{F}^{e_L}_{\lambda_2\lambda_1}(\theta) - \tilde{G}^{e_L}_{\lambda_2\lambda_1}(\theta))^*(\tilde{F}^{e_+}_{\lambda_2\lambda_1}(\theta) - \tilde{G}^{e_+}_{\lambda_2\lambda_1}(\theta))\right]$$
$$+ \ C_{R_+}C_+ \ \mathrm{Im}\left[(\tilde{F}^{e_R}_{\lambda_2\lambda_1}(\theta) - \tilde{G}^{e_R}_{\lambda_2\lambda_1}(\theta))^*(\tilde{F}^{e_+}_{\lambda_2\lambda_1}(\theta) - \tilde{G}^{e_+}_{\lambda_2\lambda_1}(\theta))\right]\Big\}$$

$$+2\cos2\phi\,(C^*_{L_-}C_{R_-} \ + \ C^*_{L_+}C_{R_+})\,\mathrm{Re}\left[(\tilde{F}^{e_L}_{\lambda_2\lambda_1}(\theta) - \tilde{G}^{e_L}_{\lambda_2\lambda_1}(\theta))^*(\tilde{F}^{e_R}_{\lambda_2\lambda_1}(\theta) - \tilde{G}^{e_R}_{\lambda_2\lambda_1}(\theta))\right]$$

$$-2\sin2\phi\,(C^*_{L_-}C_{R_-} \ + \ C^*_{L_+}C_{R_+})\,\mathrm{Im}\left[(\tilde{F}^{e_L}_{\lambda_2\lambda_1}(\theta) - \tilde{G}^{e_L}_{\lambda_2\lambda_1}(\theta))^*(\tilde{F}^{e_R}_{\lambda_2\lambda_1}(\theta) - \tilde{G}^{e_R}_{\lambda_2\lambda_1}(\theta))\right]\Bigg\}$$

$$(3.64)$$

3.2.1   Alternative Cross Section in terms of angular momentum

Differential cross-section in Equation 3.60 is a function of pion angles, θ and ϕ. It can be alternatively defined in terms of angular momentums, j. This is an important step to understand how to add the two different interactions coherently. In resonant interaction, pion produces indirectly via an intermediate resonance with definite angular momentum while in the nonresonant interaction a pion is produced directly.

In this section we will derive an alternative cross-section in terms of angular momenta, but first we need to have a standard form of helicity amplitudes to be eligible to do a multipole expansion. An equivalent set of standard helicity amplitudes can be defined with two indices μ and λ [15]:

$$F_{\mu\lambda}(\theta,\phi), \quad G_{\mu\lambda}(\theta,\phi) \tag{3.65}$$

where

$$
\begin{aligned}
\lambda &= \lambda_k - \lambda_1, & \lambda &= -\tfrac{3}{2}, -\tfrac{1}{2}, \tfrac{1}{2}, \tfrac{3}{2} \\
\mu &= \lambda_q - \lambda_2 = -\lambda_2, & \mu &= -\tfrac{1}{2}, \tfrac{1}{2}.
\end{aligned}
\tag{3.66}
$$

λ_k is the polarization of the gauge bosons; $\lambda_k(e_L) = -1$, $\lambda_k(e_R) = +1$ and $\lambda_k(e_{\pm}) = 0$. λ_q is helicity of pion which is zero for a scalar particle.

Standard helicity amplitudes (Equation 3.65) are related with helicity amplitudes defined in subsection 3.1.3 and Equation 3.60:

$$
\begin{aligned}
F_{\mu\lambda}(\theta,\phi) &= e^{i[\lambda_1\pi + \lambda_2(\pi+2\phi)]} \tilde{F}^{\lambda_k}_{\lambda_2,\lambda_1}(\theta,\phi), \\
G_{\mu\lambda}(\theta,\phi) &= e^{i[\lambda_1\pi + \lambda_2(\pi+2\phi)]} \tilde{G}^{\lambda_k}_{\lambda_2,\lambda_1}(\theta,\phi).
\end{aligned}
\tag{3.67}
$$

The detailed derivation can be found in Appendix F, and the explicit expression is given in Table 3.3.

Multipole Expansion

Helicity amplitudes are invariant under ordinary rotation, therefore it is always possible to expand them over angular momentums (Appendix F) [15]. First step is to define the initial (final) state in the positive direction. In the isobaric frame two initial (final) particles are back to back, then we simply need to reflect the initial (final) nucleon in the positive direction i.e. $\lambda_1(\lambda_2) \rightarrow -\lambda_1(\lambda_2)$ according to F, F.1 and F.2.

Now we show the standard helicity amplitudes (Equation 3.67) in the form of bra-ket from Appendix F. In the isobaric frame, the initial state, along $\hat{z}$, is $|0,0; \lambda_k - \lambda_1\rangle = |0,0; \lambda\rangle$,

Table 3.3 Standard Helicity Amplitudes $F_{\mu\lambda}(\theta,\phi)$, $G_{\mu\lambda}(\theta,\phi)$

Vector	Axial vector
$F_{\frac{1}{2}\frac{1}{2}} = e^{-i\phi}\tilde{F}^{eR}_{-\frac{1}{2}\frac{1}{2}}$	$G_{\frac{1}{2}\frac{1}{2}} = e^{-i\phi}\tilde{G}^{eR}_{-\frac{1}{2}\frac{1}{2}}$
$F_{\frac{1}{2}\frac{3}{2}} = -e^{-i\phi}\tilde{F}^{eR}_{-\frac{1}{2}-\frac{1}{2}}$	$G_{\frac{1}{2}\frac{3}{2}} = -e^{-i\phi}\tilde{G}^{eR}_{-\frac{1}{2}-\frac{1}{2}}$
$F_{-\frac{1}{2}\frac{1}{2}} = -e^{i\phi}\tilde{F}^{eR}_{\frac{1}{2}\frac{1}{2}}$	$G_{-\frac{1}{2}\frac{1}{2}} = -e^{i\phi}\tilde{G}^{eR}_{\frac{1}{2}\frac{1}{2}}$
$F_{-\frac{1}{2}\frac{3}{2}} = e^{i\phi}\tilde{F}^{eR}_{\frac{1}{2}-\frac{1}{2}}$	$G_{-\frac{1}{2}\frac{3}{2}} = e^{i\phi}\tilde{G}^{eR}_{\frac{1}{2}-\frac{1}{2}}$
$F_{\frac{1}{2}-\frac{3}{2}} = e^{-i\phi}\tilde{F}^{eL}_{-\frac{1}{2}\frac{1}{2}}$	$G_{\frac{1}{2}-\frac{3}{2}} = e^{-i\phi}\tilde{G}^{eL}_{-\frac{1}{2}\frac{1}{2}}$
$F_{\frac{1}{2}-\frac{1}{2}} = -e^{-i\phi}\tilde{F}^{eL}_{-\frac{1}{2}-\frac{1}{2}}$	$G_{\frac{1}{2}-\frac{1}{2}} = -e^{-i\phi}\tilde{G}^{eL}_{-\frac{1}{2}-\frac{1}{2}}$
$F_{-\frac{1}{2}-\frac{3}{2}} = -e^{i\phi}\tilde{F}^{eL}_{\frac{1}{2}\frac{1}{2}}$	$G_{-\frac{1}{2}-\frac{3}{2}} = -e^{i\phi}\tilde{G}^{eL}_{\frac{1}{2}\frac{1}{2}}$
$F_{-\frac{1}{2}-\frac{1}{2}} = e^{i\phi}\tilde{F}^{eL}_{\frac{1}{2}-\frac{1}{2}}$	$G_{-\frac{1}{2}-\frac{1}{2}} = e^{i\phi}\tilde{G}^{eL}_{\frac{1}{2}-\frac{1}{2}}$
$F^{(\pm)0}_{\frac{1}{2}\frac{1}{2}} = -e^{-i\phi}\tilde{F}^{e\pm}_{-\frac{1}{2}-\frac{1}{2}}$	$G^{(\pm)0}_{\frac{1}{2}\frac{1}{2}} = -e^{-i\phi}\tilde{G}^{e\pm}_{-\frac{1}{2}-\frac{1}{2}}$
$F^{(\pm)0}_{\frac{1}{2}-\frac{1}{2}} = e^{-i\phi}\tilde{F}^{e\pm}_{-\frac{1}{2}\frac{1}{2}}$	$G^{(\pm)0}_{\frac{1}{2}-\frac{1}{2}} = e^{-i\phi}\tilde{G}^{e\pm}_{-\frac{1}{2}\frac{1}{2}}$
$F^{(\pm)0}_{-\frac{1}{2}-\frac{1}{2}} = -e^{i\phi}\tilde{F}^{e\pm}_{\frac{1}{2}\frac{1}{2}}$	$G^{(\pm)0}_{-\frac{1}{2}-\frac{1}{2}} = -e^{i\phi}\tilde{G}^{e\pm}_{\frac{1}{2}\frac{1}{2}}$
$F^{(\pm)0}_{-\frac{1}{2}\frac{1}{2}} = e^{i\phi}\tilde{F}^{e\pm}_{\frac{1}{2}-\frac{1}{2}}$	$G^{(\pm)0}_{-\frac{1}{2}\frac{1}{2}} = e^{i\phi}\tilde{G}^{e\pm}_{\frac{1}{2}-\frac{1}{2}}$

and the final state along (θ,ϕ) is $|\theta,\phi;\lambda_q - \lambda_2\rangle = |\theta,\phi;\mu\rangle$. In fact we reduce the number of indices to two λ and μ. Therefore:

$$F_{\mu\lambda}(\theta,\phi) = \langle\theta,\phi;\mu|F|0,0;\lambda\rangle \tag{3.68}$$

$$G_{\mu\lambda}(\theta,\phi) = \langle\theta,\phi;\mu|G|0,0;\lambda\rangle \tag{3.69}$$

where F and G should be invariant under rotation and reflection. From now on we only take into the vector part, however, derivation and all steps are the same for axial helicity amplitudes. Applying section F.3) in Equation 3.68

$$F_{\mu\lambda}(\theta,\phi) = \sum_{jm}\sum_{j'm'}\langle\theta,\phi;\mu|j,m;\mu\rangle\langle j,m;\mu|F|j',m';\lambda\rangle\langle j',m';\lambda|0,0;\lambda\rangle$$

$$= \sum_{jm}\sqrt{\frac{2j+1}{4\pi}}D^{j^*}_{m,\mu}(\phi,\theta,-\phi)\langle\mu|F^j|\lambda\rangle\sqrt{\frac{2j+1}{4\pi}}\delta_{m\lambda} \tag{3.70}$$

Table 3.4 $d_{\lambda,\mu}^j$ for $j = l + \frac{1}{2}$

$$d_{\frac{1}{2}\frac{1}{2}}^j = (l+1)^{-1}\cos\frac{\theta}{2}(P'_{l+1} - P'_l)$$

$$d_{-\frac{1}{2}\frac{1}{2}}^j = (l+1)^{-1}\sin\frac{\theta}{2}(P'_{l+1} + P'_l)$$

$$d_{\frac{1}{2}\frac{3}{2}}^j = (l+1)^{-1}\sin\frac{\theta}{2}(\sqrt{\frac{l}{l+2}}P'_{l+1} + \sqrt{\frac{l+2}{l}}P'_l)$$

$$d_{-\frac{1}{2}\frac{3}{2}}^j = (l+1)^{-1}\cos\frac{\theta}{2}(-\sqrt{\frac{l}{l+2}}P'_{l+1} + \sqrt{\frac{l+2}{l}}P'_l)$$

P_l are Legendre polynomials and $P'_l = dP_l/d\cos\theta$

where $\mu = \lambda_q - \lambda_2 = -\lambda_2$ and $\lambda = \lambda_k - \lambda_1$. The following relation (given in [15]):

$$\langle \theta, \phi; \mu | j, m; \mu' \rangle = \sqrt{\frac{2J+1}{4\pi}} \delta_{\mu\mu'} D_{m,\mu}^{J^*}(\phi, \theta, -\phi)$$

$$\langle 0, 0; \mu | j, m; \mu' \rangle = \sqrt{\frac{2J+1}{4\pi}} \delta_{\mu\mu'} \delta_{m,\mu}$$

$$\langle j'm'; \lambda' | jm; \lambda \rangle = \delta_{jj'} \delta_{mm'} \delta_{\lambda\lambda'} \quad (3.71)$$

has been used in Equation 3.70, where

$$D_{m,\mu}^{J}{}^*(\phi, \theta, -\phi) = e^{-i\mu\phi} \, d_{m,\mu}^J(\theta) \, e^{im\phi} \quad (3.72)$$

As it is explained in Appendix F. $\langle \mu | F^j | \lambda \rangle$ are the helicity amplitudes for definite angular momentum j, i.e. $F_{\mu\lambda}^j$. Therefore:

$$F_{\mu\lambda}(\theta, \phi) = \sum_j F_{\mu\lambda}^j (2j+1) d_{\lambda\mu}^j(\theta) e^{i(\lambda-\mu)\phi}$$

$$G_{\mu\lambda}(\theta, \phi) = \sum_j G_{\mu\lambda}^j (2j+1) d_{\lambda\mu}^j(\theta) e^{i(\lambda-\mu)\phi}. \quad (3.73)$$

Similarly the multipole expansion for $F_{\mu\lambda}^{(\pm)0}$ and $G_{\mu\lambda}^{(\pm)0}$ can be defined where $\sqrt{\frac{2j+1}{4\pi}} d_{\lambda,\mu}^j(\theta) e^{i(\lambda-\mu)\phi}$ are mutually orthonormal functions, and $d_{\lambda,\mu}^j$ are real and given in [15], [78] and also in Table 3.4.

$$\int_0^\pi d_{\lambda,\mu}^j(\theta) d_{\lambda,\mu}^{j'}(\theta) d\cos\theta = \frac{2}{2j+1} \delta_{jj'}$$

$$\sum_j \frac{2j+1}{2} d_{\lambda,\mu}^j(\theta) d_{\lambda,\mu}^j(\theta') = \delta(\cos\theta - \cos\theta') \quad (3.74)$$

The expansion coefficients $F^j_{\mu\lambda}$ and $G^j_{\mu\lambda}$ can be found by integrating over $d^j_{\mu\lambda}(\theta)e^{-i(\lambda-\mu)\phi}d\Omega$

$$
\begin{aligned}
F^j_{\mu\lambda} &= \frac{1}{4\pi}\int F_{\mu\lambda}(\theta,\phi)d^j_{\lambda\mu}(\theta)e^{-i(\lambda-\mu)\phi}d\Omega \\
G^j_{\mu\lambda} &= \frac{1}{4\pi}\int G_{\mu\lambda}(\theta,\phi)d^j_{\lambda\mu}(\theta)e^{-i(\lambda-\mu)\phi}d\Omega,
\end{aligned}
\tag{3.75}
$$

and similarly for $F^{0j}_{\mu\lambda}$ and $G^{0j}_{\mu\lambda}$, when $\lambda_k = 0$.

The expansion coefficients refer to πN states of definite angular momentum, but not of definite parity. Parity eigenstates refer to l orbital angular momentum. Therefore we can define eigenstates with definite angular momentum and parity by adding and subtracting eigenstate with same j and different helicity of outgoing nucleon ($\mu = -\lambda_2$), i.e. we set $j = l + \frac{1}{2}$:

$$
\begin{aligned}
A^V_{l+} &= -\frac{1}{\sqrt{2}}\left(F^j_{\frac{1}{2}\frac{1}{2}}+F^j_{-\frac{1}{2}\frac{1}{2}}\right) & A^A_{l+} &= -\frac{1}{\sqrt{2}}\left(G^j_{\frac{1}{2}\frac{1}{2}}+G^j_{-\frac{1}{2}\frac{1}{2}}\right) \\
A^V_{l+1-} &= \frac{1}{\sqrt{2}}\left(F^j_{\frac{1}{2}\frac{1}{2}}-F^j_{-\frac{1}{2}\frac{1}{2}}\right) & A^A_{l+1-} &= \frac{1}{\sqrt{2}}\left(G^j_{\frac{1}{2}\frac{1}{2}}-G^j_{-\frac{1}{2}\frac{1}{2}}\right) \\[2ex]
B^V_{l+} &= \sqrt{\frac{2}{l(l+2)}}\left(F^j_{\frac{1}{2}\frac{3}{2}}+F^j_{-\frac{1}{2}\frac{3}{2}}\right) & B^A_{l+} &= \sqrt{\frac{2}{l(l+2)}}\left(G^j_{\frac{1}{2}\frac{3}{2}}+G^j_{-\frac{1}{2}\frac{3}{2}}\right) \\
B^V_{l+1-} &= -\sqrt{\frac{1}{l(l+2)}}\left(F^j_{\frac{1}{2}\frac{3}{2}}-F^j_{-\frac{1}{2}\frac{3}{2}}\right) & B^A_{l+1-} &= -\sqrt{\frac{2}{l(l+2)}}\left(G^j_{\frac{1}{2}\frac{3}{2}}-G^j_{-\frac{1}{2}\frac{3}{2}}\right) \\[2ex]
S^{(\pm)V}_{l+} &= \frac{1}{\sqrt{2}}\frac{\sqrt{-k^2}}{|k|}\left(F^{(\pm)0j}_{\frac{1}{2}\frac{1}{2}}+F^{(\pm)0j}_{-\frac{1}{2}\frac{1}{2}}\right) & S^{(\pm)A}_{l+} &= \frac{1}{\sqrt{2}}\frac{\sqrt{-k^2}}{|k|}\left(G^{(\pm)0j}_{\frac{1}{2}\frac{1}{2}}+G^{(\pm)0j}_{-\frac{1}{2}\frac{1}{2}}\right) \\
S^{(\pm)V}_{l+1-} &= \frac{1}{\sqrt{2}}\frac{\sqrt{-k^2}}{|k|}\left(F^{(\pm)0j}_{\frac{1}{2}\frac{1}{2}}-F^{(\pm)0j}_{-\frac{1}{2}\frac{1}{2}}\right) & S^{(\pm)A}_{l+1-} &= \frac{1}{\sqrt{2}}\frac{\sqrt{-k^2}}{|k|}\left(G^{(\pm)0j}_{\frac{1}{2}\frac{1}{2}}-G^{(\pm)0j}_{-\frac{1}{2}\frac{1}{2}}\right),
\end{aligned}
\tag{3.76}
$$

where the index l is the orbital angular momentum of the final pion-nucleon system and subscript $\pm$ in $l+$ and $(l+1)-$ identifies the total angular momentum j as $j = l \pm 1/2$. Now we are ready to make integration from Equation 3.64 by knowing that all terms related to ϕ angle are going to be zero after integration. Here we only show the detailed derivation

of the first term:

$$\int d\Omega \sum_{\lambda_1 \lambda_2} |C_L|^2 |\tilde{F}^{e_L}_{\lambda_2 \lambda_1} - \tilde{G}^{e_L}_{\lambda_2 \lambda_1}|^2$$

$$=|C_L|^2 \int d\Omega \Big\{ |\tilde{F}^{e_L}_{\frac{1}{2}\frac{1}{2}} - \tilde{G}^{e_L}_{\frac{1}{2}\frac{1}{2}}|^2 + |\tilde{F}^{e_L}_{-\frac{1}{2}\frac{1}{2}} - \tilde{G}^{e_L}_{-\frac{1}{2}\frac{1}{2}}|^2 + |\tilde{F}^{e_L}_{\frac{1}{2}-\frac{1}{2}} - \tilde{G}^{e_L}_{\frac{1}{2}-\frac{1}{2}}|^2 + |\tilde{F}^{e_L}_{-\frac{1}{2}-\frac{1}{2}} - \tilde{G}^{e_L}_{-\frac{1}{2}-\frac{1}{2}}|^2 \Big\}$$

$$(3.77)$$

$$=|C_L|^2 \int d\Omega \Big\{ |-F_{\frac{1}{2}\frac{3}{2}} - G_{\frac{1}{2}\frac{3}{2}}|^2 + |-F_{-\frac{1}{2}\frac{3}{2}} - G_{-\frac{1}{2}\frac{3}{2}}|^2 + |-F_{\frac{1}{2}\frac{1}{2}} - G_{\frac{1}{2}\frac{1}{2}}|^2 + |-F_{-\frac{1}{2}\frac{1}{2}} - G_{\frac{1}{2}-\frac{1}{2}}|^2 \Big\}$$

$$(3.78)$$

$$=|C_L|^2 \int d\Omega \sum_j (2j+1)^2 \Big\{ |(-F^j_{\frac{1}{2}\frac{3}{2}} - G^j_{\frac{1}{2}\frac{3}{2}}) d^j_{\frac{3}{2}\frac{1}{2}}(\theta)|^2 + |(-F^j_{-\frac{1}{2}\frac{3}{2}} - G^j_{-\frac{1}{2}\frac{3}{2}}) d^j_{\frac{3}{2}-\frac{1}{2}}(\theta)|^2$$

$$+ |(-F^j_{\frac{1}{2}\frac{1}{2}} - G^j_{\frac{1}{2}\frac{1}{2}}) d^j_{\frac{1}{2}\frac{1}{2}}(\theta)|^2 + |(-F^j_{-\frac{1}{2}\frac{1}{2}} - G^j_{\frac{1}{2}-\frac{1}{2}}) d^j_{\frac{1}{2}-\frac{1}{2}}(\theta)|^2 \Big\} \qquad (3.79)$$

$$=|C_L|^2 4\pi(2j+1) \sum_j \Big\{ |F^j_{\frac{1}{2}\frac{3}{2}} + G^j_{\frac{1}{2}\frac{3}{2}}|^2 + |F^j_{-\frac{1}{2}\frac{3}{2}} + G^j_{-\frac{1}{2}\frac{3}{2}}|^2 + |F^j_{\frac{1}{2}\frac{1}{2}} + G^j_{\frac{1}{2}\frac{1}{2}}|^2 + |F^j_{-\frac{1}{2}\frac{1}{2}} + G^j_{\frac{1}{2}-\frac{1}{2}}|^2 \Big\}$$

$$(3.80)$$

where from Equation 3.77 to Equation 3.78 we used Equation 3.67 and from Equation 3.78 to Equation 3.79 we used Equation 3.73. From Equation 3.79 to Equation 3.80 we use Equation 3.74. Using Equation 3.76, we will have:

$$=|C_L|^2 \sum_l 8\pi(l+1) \Big\{ \frac{1}{2} \big[|(A^V_{l+} - A^V_{l+1-}) + (A^A_{l+} - A^A_{l+1-})|^2 + |(A^V_{l+} + A^V_{l+1-}) + (A^A_{l+} + A^A_{l+1-})|^2 \big]$$

$$+ \frac{l(l+2)}{8} \big[|(B^V_{l+} - B^V_{l+1-}) + (B^A_{l+} - B^A_{l+1-})|^2 + |(B^V_{l+} + B^V_{l+1-}) + (B^A_{l+} + B^A_{l+1-})|^2 \big] \Big\}$$

$$=|C_L|^2 \sum_l 8\pi(l+1) \Big\{ |A^V_{l+} + A^A_{l+}|^2 + |A^V_{l+1-} + A^A_{l+1-}|^2 + \frac{l(l+2)}{4} \big[|B^V_{l+} + B^A_{l+}|^2 + |B^V_{l+1-} + B^A_{l+1-}|^2 \big] \Big\}.$$

$$(3.81)$$

We can do the same calculation for other terms, but here we show the final cross section in terms of angular momentum instead of pion angles (compare with Equation 3.64).

$$
\frac{d\sigma(\nu N \to lN\pi)}{dk^2 dW} = \frac{G_F^2}{2} \frac{1}{(2\pi)^3} |\mathbf{q}| \frac{-k^2}{(k^L)^2} \sum_l (l+1) \Bigg\{
$$

$$
|C_L|^2 \Big[|A_{l+}^V + A_{l+}^A|^2 + |A_{l+1-}^V + A_{l+1-}^A|^2 + \frac{l(l+2)}{4} \big[|(B_{l+}^V + B_{l+}^A|^2 + |B_{l+1-}^V + B_{l+1-}^A)|^2 \big] \Big]
$$

$$
+|C_R|^2 \Big[|A_{l+}^V - A_{l+}^A|^2 + |A_{l+1-}^V - A_{l+1-}^A|^2 + \frac{l(l+2)}{4} \big[|(B_{l+}^V - B_{l+}^A|^2 + |B_{l+1-}^V - B_{l+1-}^A)|^2 \big] \Big]
$$

$$
+|C_-|^2 \frac{|\mathbf{k}|^2}{(-k^2)} \Big[|S_{l+}^{(-)V} + S_{l+}^{(-)A}|^2 + |S_{l+1-}^{(-)V} + S_{l+1-}^{(-)A}|^2 + |S_{l+}^{(-)V} - S_{l+}^{(-)A}|^2 + |S_{l+1-}^{(-)V} - S_{l+1-}^{(-)A}|^2 \Big]
$$

$$
+|C_+|^2 \frac{|\mathbf{k}|^2}{(-k^2)} \Big[|S_{l+}^{(+)V} + S_{l+}^{(+)A}|^2 + |S_{l+1-}^{(+)V} + S_{l+1-}^{(+)A}|^2 + |S_{l+}^{(+)V} - S_{l+}^{(+)A}|^2 + |S_{l+1-}^{(+)V} - S_{l+1-}^{(+)A}|^2 \Big] \Bigg\}
$$

$$(3.82)$$

Chapter 4

Resonance Contributions and Nonresonant Background

In this chapter, a detailed calculation of helicity amplitudes for both resonant (section 4.1) and nonresonant (section 4.2) interactions will be given. Applying both contributions in Equation 3.60 will provide the single pion production cross-section.

4.1   Single Pion Production via Resonance decay

Rein and Sehgal (RS) model [7] describes single pion that is produced in neutrino-nucleon interaction via resonance decay. This model is based on helicity amplitudes derived in a relativistic quark model [5]. The helicity amplitudes depend on the spin projection of the initial and final particles. The quark model had been extended to neutrino interactions by Ravndal [6], and later the RS model includes resonances up to $M_R < 2 GeV$, as they are given in Table 4.1 where first column identifies resonances with their quantum numbers (l, I, j), for instance Δ resonance or $P_{33}(1232)$ is identified with $l = 1, I = 3/2$, and $j = 3/2$. The second and third columns identify the Breit-Wigner mass and the width of resonances.

The original paper [7] ignored the lepton mass while there are several papers [12–14] that include the lepton mass for the RS-model.

Resonance excitation is like a two particles interaction; $\nu(k_1)N(p_1) \to l(k_2)H(p_R)$. The general form of cross-section with N outgoing particles is given in Appendix E, where for on-shell nucleons the δ function can be integrated out. On the other hand for broad states like resonances in the final state, it can be replaced by a spectral function of the particle. In

the resonance rest frame ($p_R^2 = W^2$) we have:

$$\delta(p_R^2 - M_R^2) = \frac{1}{2M_R} \delta(W - M_R)$$

$$= \frac{1}{2M_R} \frac{1}{\pi} \lim_{\varepsilon \to 0} \frac{\varepsilon}{W^2 + \varepsilon^2}. \tag{4.1}$$

In the case of broad resonance state, $\varepsilon \to \Gamma_R/2$, therefore:

$$\delta(p_R^2 - M_R^2) \to \mathscr{A}(p_R) = \frac{1}{2M_R} \frac{1}{\pi} \frac{\Gamma_R/2}{(W - M_R)^2 + \Gamma_R^2/4} \tag{4.2}$$

with

$$\Gamma_R = \Gamma_0 (|\mathbf{q}(W)|/|\mathbf{q}(M_R)|)^{2l+1}, \tag{4.3}$$

where Γ_0 and M_R are given in Table 4.1, and l is orbital angular momentum quantum number of individual resonance.

With the help of Appendix E, we can have

$$\frac{d\sigma(\nu N \to lN)}{dQ^2 dW} = \frac{1}{2\pi} \frac{1}{(4ME_\nu)^2} W \frac{1}{2M_R} \delta(p_R^2 - M_R^2) |\mathscr{M}|^2, \tag{4.4}$$

$\mathscr{M}$ is similar to what was presented on Equation 3.58, but in RS model [7], different notation is used for hadronic current operator:

$$J_\alpha = J_\alpha^V - J_\alpha^A = 2M_R F^\alpha \tag{4.5}$$

From Equation 3.6 and similar to Equation 3.33:

$$\varepsilon_\lambda^\alpha \langle R| J_\alpha |N \rangle = 2M_R \langle R| C_{L_\lambda} e_L^\alpha F_\alpha + C_{R_\lambda} e_R^\alpha F_\alpha + C_\lambda e_\lambda^\alpha F_\alpha |N \rangle$$

$$= 2M_R \langle R| C_{L_\lambda} F_- + C_{R_\lambda} F_+ + C_\lambda F_0^{(\lambda)} |N \rangle \tag{4.6}$$

where $\lambda = -(+)$ stands for left(right) handed helicity, and $F_- = \frac{1}{\sqrt{2}}(F_x - iF_y)$ and $F_+ = -\frac{1}{\sqrt{2}}(F_x + iF_y)$.

It is important to notice that the definitions of the RS-model [7] is a little bit different than our definitions when we defined the general framework in chapter 3, therefore first we should adapt the RS-model to our definitions. For instant production amplitudes in the RS-model

[7] are given in terms of s_z:

$$f_{\pm|2s_z|} = \langle N, s_z \pm 1|F_\pm|R, s_z\rangle$$
$$f_{0\pm} = \langle N, s_z = \pm\frac{1}{2}|F_0|R, s_z = \pm\frac{1}{2}\rangle, \tag{4.7}$$

while we need to rewrite them in terms of helicity in the isobaric frame by knowing the direction of particle's momenta; $\lambda_1 = -s_{1z}$, $\lambda_2 = -s_{2z}$ and $\lambda_R = s_{R_z}$. Therefore[1]:

$$
\begin{aligned}
\langle R, \lambda_R = a|e_L^\alpha F_\alpha|N_1, \lambda_1 = -(a+1)\rangle &= \langle R, \lambda_R = a|F_-|N_1, \lambda_1 = -(a+1)\rangle \\
&= \langle N_1, \lambda_1 = -(a+1)|F_-^\dagger|R, \lambda_R = a\rangle^* \\
&= \langle N_1, \lambda_1 = -(a+1)|-F_+|R, \lambda_R = a\rangle^* \\
&= -\langle N_1, s_{1z} = a+1|F_+|R, s_{R_z} = a\rangle^* = -f_{+|2a|}^* = -f_{+|2a|}
\end{aligned}
$$

$$
\begin{aligned}
\langle R, \lambda_R = a|e_R^\alpha F_\alpha|N_1, \lambda_1 = -(a-1)\rangle &= \langle R, \lambda_R = a|F_+|N_1, \lambda_1 = -(a-1)\rangle \\
&= \langle N_1, \lambda_1 = -(a-1)|F_+^\dagger|R, \lambda_R = a\rangle^* \\
&= \langle N_1, \lambda_1 = -(a-1)|-F_-|R, \lambda_R = a\rangle^* \\
&= -\langle N_1, s_{1z} = a-1|F_-|R, s_{R_z} = a\rangle^* = -f_{-|2a|}^* = -f_{-|2a|}
\end{aligned}
$$

$$
\begin{aligned}
\langle R, \lambda_R = \pm\frac{1}{2}|e_-^\alpha F_\alpha|N_1, \lambda_1 = \mp\frac{1}{2}\rangle &= \frac{|\mathbf{k}|}{\sqrt{-k^2}}\langle R, \lambda_R = \pm\frac{1}{2}|F_0^{(-)}|N_1, \lambda_1 = \mp\frac{1}{2}\rangle \\
&= \frac{|\mathbf{k}|}{\sqrt{-k^2}}\langle N_1, \lambda_1 = \mp\frac{1}{2}|F_0^{(-)\dagger}|R, \lambda_R = \pm\frac{1}{2}\rangle^* \\
&= \frac{|\mathbf{k}|}{\sqrt{-k^2}}\langle N_1, s_{1z} = \pm\frac{1}{2}|F_0^{(-)}|R, s_{R_z} = \pm\frac{1}{2}\rangle^* \\
&= \frac{|\mathbf{k}|}{\sqrt{-k^2}}f_{0\pm}^{(-)*} = \frac{|\mathbf{k}|}{\sqrt{-k^2}}f_{0\pm}^{(-)}
\end{aligned}
$$

$$
\begin{aligned}
\langle R, \lambda_R = \pm\frac{1}{2}|e_+^\alpha F_\alpha|N_1, \lambda_1 = \mp\frac{1}{2}\rangle &= \frac{|\mathbf{k}|}{\sqrt{-k^2}}\langle R, \lambda_R = \pm\frac{1}{2}|F_0^{(+)}|N_1, \lambda_1 = \mp\frac{1}{2}\rangle \\
&= \frac{|\mathbf{k}|}{\sqrt{-k^2}}\langle N_1, \lambda_1 = \mp\frac{1}{2}|F_0^{(+)\dagger}|R, \lambda_R = \pm\frac{1}{2}\rangle^* \\
&= \frac{|\mathbf{k}|}{\sqrt{-k^2}}\langle N_1, s_{1z} = \pm\frac{1}{2}|F_0^{(+)}|R, s_{R_z} = \pm\frac{1}{2}\rangle^* \\
&= \frac{|\mathbf{k}|}{\sqrt{-k^2}}f_{0\pm}^{(+)*} = \frac{|\mathbf{k}|}{\sqrt{-k^2}}f_{0\pm}^{(+)}
\end{aligned}
$$

$$\tag{4.8}$$

---

[1]This is given in Rein paper [9]

Production amplitudes ($f_{\pm 1}(R)$ and $f_{0\pm}^{(\pm)}(R)$) depend on different helicities of nucleons and
gauge boson. They are given in [7] for massless lepton, but later they are calculated for
massive lepton in [13, 14] and you can also find them in Appendix G for all resonances.
Applying Equation 4.2 - 4.8, Equation 3.58 and Equation 3.59 into Equation 4.4 one can find
the RS cross-section:

$$
\frac{d\sigma(\nu N \to lR \to lN\pi)}{dQ^2 dW} = \frac{G_F^2}{2}\cos^2\theta_c \frac{1}{(2\pi)^3}\frac{(-k^2)}{\mathbf{k}_L^2}\frac{W^2}{M^2}\frac{\pi\Gamma_R\chi_E}{(W-M_R)^2+\Gamma_R^2/4}|C_{N\pi}^I|^2\Big\{
$$

$$
|C_{L_-}|^2\left(|f_{+1}^{CC}|^2+|f_{+3}^{CC}|^2\right)+|C_{R_-}|^2\left(|f_{-1}^{CC}|^2+|f_{-3}^{CC}|^2\right)+|C_-|^2\left(|f_{0+}^{(-)CC}|^2+|f_{0-}^{(-)CC}|^2\right)
$$

$$
+|C_{L_+}|^2\left(|f_{+1}^{CC}|^2+|f_{+3}^{CC}|^2\right)+|C_{R_+}|^2\left(|f_{-1}^{CC}|^2+|f_{-3}^{CC}|^2\right)+|C_+|^2\left(|f_{0+}^{(+)CC}|^2+|f_{0-}^{(+)CC}|^2\right)\Big\}
$$

$$
(4.9)
$$

where it is multiplied to χ_E; branching ratio for decay of individual resonance to $N\pi$
(Table 4.1).
Using Equation 3.62 we will obtain:

$$
\frac{d\sigma(\nu N \to lR \to lN\pi)}{dQ^2 dW} = \frac{G_F^2}{2}\cos^2\theta_c \frac{1}{(2\pi)^3}\frac{(-k^2)}{\mathbf{k}_L^2}\frac{W^2}{M^2}\frac{\pi\Gamma_R\chi_E}{(W-M_R)^2+\Gamma_R^2/4}|C_{N\pi}^I|^2\Big\{
$$

$$
|C_L|^2\left(|f_{+1}^{CC}|^2+|f_{+3}^{CC}|^2\right)+|C_R|^2\left(|f_{-1}^{CC}|^2+|f_{-3}^{CC}|^2\right)
$$

$$
+|C_-|^2\left(|f_{0+}^{(-)CC}|^2+|f_{0-}^{(-)CC}|^2\right)+|C_+|^2\left(|f_{0+}^{(+)CC}|^2+|f_{0-}^{(+)CC}|^2\right)\Big\}
$$

$$
(4.10)
$$

$C_{N\pi}^I$ are relevant isospin coefficients in the RS-model and they are given in Table 4.2.
Equation 4.10 is cross-section for the resonant interaction with lepton mass ($m_l \neq 0$), and the
production amplitudes are given in [13, 14], and also in Appendix G.

4.1.1 Isospin coefficients for resonant interactions

Table 4.1 shows (in the second subscript of) resonances have either isospin $1/2$ or isospin $3/2$. On the other hand from Table A.1 for CC interactions we have:

$$
\mathscr{M}(\nu p \to l^- p\pi^+) = \frac{1}{\sqrt{2}}A^{CC}_{3/2}
$$
$$
\mathscr{M}(\nu n \to l^- p\pi^0) = \frac{1}{3}(-A^{CC}_{3/2} + A^{CC}_{1/2})
$$
$$
\mathscr{M}(\nu n \to l^- n\pi^+) = \frac{1}{3\sqrt{2}}(A^{CC}_{3/2} + 2A^{CC}_{1/2})
$$

$$(4.11)$$

$A^{CC}_{3/2}$ comes from resonance with isospin $3/2$ and $A^{CC}_{1/2}$ comes from resonances with isospin $1/2$. According to [7] we have:

$$
\frac{1}{\sqrt{2}}A^{CC}_{3/2} = \sqrt{3}\sum_{\substack{\text{all } I = 3/2 \\ \text{resonances}}} a^{CC}(R_{3/2}),
$$
$$
\frac{1}{3}A^{CC}_{1/2} = \frac{1}{\sqrt{3}}\sum_{\substack{\text{all } I = 1/2 \\ \text{resonances}}} a^{CC}(R_{1/2}).
$$

$$(4.12)$$

where $a^{CC}(R_{3/2})$ and $a^{CC}(R_{1/2})$ are amplitudes for resonance with isospin $3/2$ and $1/2$. Therefore

$$
Ampl(\nu p \to l^- p\pi^+) = \sqrt{3}\sum_{\substack{\text{all } I = 3/2 \\ \text{resonances}}} a^{CC}(R_{3/2})
$$
$$
Ampl(\nu n \to l^- p\pi^0) = -\sqrt{\frac{2}{3}}\sum_{\substack{\text{all } I = 3/2 \\ \text{resonances}}} a^{CC}(R_{3/2}) + \sqrt{\frac{1}{3}}\sum_{\substack{\text{all } I = 1/2 \\ \text{resonances}}} a^{CC}(R_{1/2})
$$
$$
Ampl(\nu n \to l^- n\pi^+) = \sqrt{\frac{1}{3}}\sum_{\substack{\text{all } I = 3/2 \\ \text{resonances}}} a^{CC}(R_{3/2}) + \sqrt{\frac{2}{3}}\sum_{\substack{\text{all } I = 1/2 \\ \text{resonances}}} a^{CC}(R_{1/2})
$$

$$(4.13)$$

The same calculation can be done for anti-neutrino interactions and NC interactions, that is also discussed in [7]. All isospin coefficients for individual resonances in CC and NC (anti-)neutrino interactions are given in Table 4.2.

4.1.2   Helicity amplitudes for resonant Interaction

Now we need to find the helicity amplitudes for resonant interaction (RS-model) from chapter 3 (Equation 3.34). The CC cross-section for pion production (given in Equation 3.82) can be calculated for one particular resonance with $j = l + \frac{1}{2}$ (like Δ) and $P = -(-1)^l$:

$$
\begin{aligned}
\frac{d\sigma(\nu N \rightarrow lR \rightarrow lN\pi)}{dk^2 dW} = &\frac{G_F^2}{2} \cos^2\theta_C \frac{1}{(2\pi)^3} |\mathbf{q}| \frac{-k^2}{(k^L)^2} \frac{2j+1}{2} \Big\{ \\
&|C_L|^2 \big[|A_{l+}^V + A_{l+}^A|^2 + \frac{l(l+2)}{4}|(B_{l+}^V + B_{l+}^A|^2\big] \\
&+|C_R|^2 \big[|A_{l+}^V - A_{l+}^A|^2 + \frac{l(l+2)}{4}|(B_{l+}^V - B_{l+}^A|^2\big] \\
&+|C_-|^2 \frac{|\mathbf{k}|^2}{(-k^2)} \big[|S_{l+}^{(-)V} + S_{l+}^{(-)A}|^2 + |S_{l+}^{(-)V} - S_{l+}^{(-)A}|^2\big] \\
&+|C_+|^2 \frac{|\mathbf{k}|^2}{(-k^2)} \big[|S_{l+}^{(+)V} + S_{l+}^{(+)A}|^2 + |S_{l+}^{(+)V} - S_{l+}^{(+)A}|^2\big] \Big\}
\end{aligned}
\tag{4.14}
$$

Comparing Equation 4.10 with Equation 4.14 we have:

$$
\begin{aligned}
|A_{l+}^{(I)V} \pm A_{l+}^{(I)A}|^2 &= |C_{N\pi}^I|^2 \kappa^2 \chi_E |f_{BW}(R)|^2 \; |f_{\pm 1}^{CC}(R(I, j = l+1/2))|^2 \\
\frac{l(l+2)}{4}|B_{l+}^{(I)V} \pm B_{l+}^{(I)A}|^2 &= |C_{N\pi}^I|^2 \kappa^2 \chi_E |f_{BW}(R)|^2 \; |f_{\pm 3}^{CC}(R(I, j = l+1/2))|^2 \\
|S_{l+}^{(-)(I)V} \pm S_{l+}^{(-)(I)A}|^2 &= |C_{N\pi}^I|^2 \kappa^2 \chi_E |f_{BW}(R)|^2 \; |f_{\mp 0}^{(-)CC}(R(I, j = l+1/2))|^2 \\
|S_{l+}^{(+)(I)V} \pm S_{l+}^{(+)(I)A}|^2 &= |C_{N\pi}^I|^2 \kappa^2 \chi_E |f_{BW}(R)|^2 \; |f_{\mp 0}^{(+)CC}(R(I, j = l+1/2))|^2.
\end{aligned}
\tag{4.15}
$$

where $|f_{BW}(R)|^2$ is Breit-Wigner factor (Γ_R has been defined in Equation 4.3):

$$
|f_{BW}(R)|^2 = \frac{\Gamma_R}{2\pi}\left(\frac{1}{(W-M_R)^2 + \Gamma_R^2/4}\right),
\tag{4.16}
$$

and κ^2 appears here because the two cross-sections are slightly different:

$$
\kappa^2 = \left(2\pi^2\frac{W^2}{M^2}\cdot\frac{2}{2j+1}\frac{1}{|\mathbf{q}|}\right)^{\frac{1}{2}}.
\tag{4.17}
$$

Equation 4.15 is absolute square of the helicity amplitudes, therefore it does not say anything about a possible phase (sign) that might have been carried by an amplitude itself. However these phases (signs) are very important for evaluation of interferences between resonance and nonresonant amplitudes as well as among resonances themselves.

Pion production in resonant interaction consists of resonance production and its subsequent

decay into the $N\pi$ final state:

$$\langle N\pi, \lambda_2 | \varepsilon_\lambda^\alpha F_\alpha | N, \lambda_1 \rangle = \langle N\pi, \lambda_2 | R\lambda_R \rangle \langle R\lambda_R | \varepsilon_\lambda^\alpha F_\alpha | N\lambda_1 \rangle$$

$$= \langle N\pi, \lambda_2 | R\lambda_R \rangle \langle N\lambda_1 | (\varepsilon_\lambda^\alpha F_\alpha)^\dagger | R\lambda_R \rangle^* \tag{4.18}$$

where λ stands for left and right hand lepton currents. We already discussed about the resonance production, but now we are going to talk about decay amplitudes.

Decay Amplitudes

The decay amplitude is found by projecting the resonance onto the relevant $N\pi$ final state, and is also given in [5], but in RS model it is replaced by a complex Breit-Wigner amplitude:

$$f_{BW}(R) = \sqrt{\frac{\Gamma_R}{2\pi}} \left(\frac{1}{W - M_R + i\Gamma_R/2} \right), \tag{4.19}$$

where Γ_R has been given in Equation 4.3. Comparing with Equation 4.15 it is obvious that the decay amplitudes should be related to κ (Equation 4.17), $\sqrt{\chi_E}$ (Table 4.1), and the isospin Clebsch-Gordan coefficients $C_{N\pi}^I$.

Decay amplitudes in RS model [7] also carry a sign that is important for the interference effect. In principle, production and subsequent decay of a resonance have to be calculated in the same model in order to obtain a coherent prediction for the pion production and it has been done in [5]. However, RS model is replacing the latter by the Breit-Wigner factor, and the sign of the decay amplitudes is missing. Comparing with [5], RS model multiplies the missing sign to the individual resonances.

One sign is the sign of numerical value of the decay amplitudes (σ^D) given in [5], and they are given in Table 4.1 [2]. The other is the sign of angular momentum Clebsch-Gordan coefficients $C_{N\pi}^j$. The actual angular momentum Clebsch-Gordan coefficients are given in Appendix G, but from now on $C_{N\pi}^j$ is only the signs of $C_{N\pi}^j$ in Table G.1. Therefore

$$\langle N\pi, \lambda_2 | R\lambda_R \rangle = \sigma^D C_{N\pi}^j \sqrt{\chi_E} \, \kappa C_{N\pi}^I f_{BW} \tag{4.20}$$

where $\sigma^D C_{N\pi}^j$ is just a sign.

Now we are ready to define helicity amplitudes for a resonance with definite angular momentum j, as it is defined in [9]. It is reasonable to consider $F_{\mu,\lambda}^j$ and $G_{\mu,\lambda}^j$ as a vector and axial helicity amplitudes in the basis $(\mu\lambda)$ where a nucleon of helicity λ_1 goes over- via an intermediate state of helicity λ- into a nucleon of helicity λ_2 and a scalar pion. Such

---

[2]This sign is provided in the RS model for individual resonances, but it is not based on theoretical approach. Next chapter we will use an alternative way to extract the resonance's signs.

intermediate state is a resonance R ($\lambda = \lambda_R$) with angular momentum j. Therefore helicity amplitudes for a resonance can be defined as:

$$F^j_{\mu\lambda} = F^j_{-\lambda_2 \lambda_R} \tag{4.21}$$

From Equation 4.8, for instance:

$$F^j_{\mu\lambda=\frac{1}{2}} = \langle \mu | e^\alpha_R F^V_\alpha | N, \lambda_1 = \frac{1}{2} \rangle \tag{4.22}$$

Therefore

$$
\begin{aligned}
F^j_{\mu\lambda_R} = F^j_{-\lambda_2 \lambda_R = \frac{1}{2}} &= \langle N\pi, -\lambda_2 | R, \lambda_R \rangle \langle R, \lambda_R | e^\alpha_R F^V_\alpha | N, \lambda_1 \rangle \\
&= -\langle N\pi, -\lambda_2 | R, \lambda_R \rangle f^V_{-1} \qquad \text{for } \lambda_1 = -s_{z1} = \frac{1}{2} \\
F^j_{-\lambda_2, \lambda_R = \frac{3}{2}} &= -\langle N\pi, -\lambda_2 | R, \lambda_R \rangle f^V_{-3} \qquad \text{for } \lambda_1 = -s_{z1} = -\frac{1}{2},
\end{aligned}
\tag{4.23}
$$

where f^V is production amplitude for vector part. On the other hand from Equation 3.67 and Equation 3.73) we have[3]:

$$
\begin{aligned}
\tilde{F}^{e_R}_{\frac{1}{2},\frac{1}{2}}(\theta) &= -F_{-\frac{1}{2}\frac{1}{2}}(\theta) = -F^j_{-\frac{1}{2}\frac{1}{2}}(2j+1)d^j_{\frac{1}{2}-\frac{1}{2}}(\theta) \\
\tilde{F}^{e_R}_{\frac{1}{2},-\frac{1}{2}}(\theta) &= F_{-\frac{1}{2}\frac{3}{2}}(\theta) = F^j_{-\frac{1}{2}\frac{3}{2}}(2j+1)d^j_{\frac{3}{2}-\frac{1}{2}}(\theta)
\end{aligned}
\tag{4.24}
$$

for a single resonance. As it was discussed in the previous chapter, $F^j_{\mu,\lambda}$ refer to πN states of definite total angular momentum but not of definite parity. Parity eigenstates, corresponding to a definite I value are defined in Equation 3.76 and for $j = l \pm 1/2$. Similarly we have:

$$
\begin{aligned}
F^j_{\pm\frac{1}{2},\frac{1}{2}} &= -\frac{1}{\sqrt{2}}(A^V_{l+} \mp A^V_{l-}), & G^j_{\pm\frac{1}{2},\frac{1}{2}} &= \mp\frac{1}{\sqrt{2}}(A^A_{l+} \pm A^A_{l-}) \\
F^j_{\pm\frac{1}{2},\frac{3}{2}} &= \frac{\sqrt{l(l+2)}}{2\sqrt{2}}(B^V_{l+} \mp B^V_{l-}), & G^j_{\pm\frac{l}{2},\frac{1}{2}} &= \frac{\sqrt{l(l+2)}}{2\sqrt{2}}(B^A_{l+} \mp B^A_{l-}) \\
F^{(-)0j}_{\pm\frac{1}{2},\frac{1}{2}} &= \frac{1}{\sqrt{2}}\frac{|\mathbf{k}|}{\sqrt{-k^2}}(S^{(-)V}_{l+} \pm S^{(-)V}_{l-}), & G^{(-)0j}_{\pm\frac{1}{2},\frac{1}{2}} &= \frac{1}{\sqrt{2}}\frac{|\mathbf{k}|}{\sqrt{-k^2}}(S^{(-)A}_{l+} \pm S^{(-)A}_{l-}) \\
F^{(+)0j}_{\pm\frac{1}{2},\frac{1}{2}} &= \frac{1}{\sqrt{2}}\frac{|\mathbf{k}|}{\sqrt{-k^2}}(S^{(+)V}_{l+} \pm S^{(+)V}_{l-}), & G^{(+)0j}_{\pm\frac{1}{2},\frac{1}{2}} &= \frac{1}{\sqrt{2}}\frac{|\mathbf{k}|}{\sqrt{-k^2}}(S^{(+)A}_{l+} \pm S^{(+)A}_{l-})
\end{aligned}
\tag{4.25}
$$

---

[3]Here we ignore the ϕ dependence of helicity amplitudes for simplicity, because it is already factorized from cross-section in Equation 3.64.

where $l\pm$ referes to resonances with $j = l \pm 1/2$.

We can sum up over all resonances to find out the helicity amplitude. Therefore using Equation 4.25 for $j = l \pm 1/2$ we have :

$$\tilde{F}^{e_R}_{\frac{1}{2}\frac{1}{2}}(\theta) = \frac{1}{\sqrt{2}}\sum_j (2j+1)(-\langle N\pi, -\frac{1}{2}|R, \lambda_R\rangle f^V_{-1})d^j_{\frac{1}{2}-\frac{1}{2}}(\theta),$$

$$\tilde{F}^{e_R}_{\frac{1}{2}-\frac{1}{2}}(\theta) = \frac{1}{\sqrt{2}}\sum_j (2j+1)(-\langle N\pi, -\frac{1}{2}|R, \lambda_R\rangle f^V_{-3})d^j_{\frac{3}{2}-\frac{1}{2}}(\theta),$$

$$\tilde{F}^{e_R}_{-\frac{1}{2}\frac{1}{2}}(\theta) = \mp\frac{1}{\sqrt{2}}\sum_j (2j+1)(-\langle N\pi, -\frac{1}{2}|R, \lambda_R\rangle f^V_{-1})d^j_{\frac{1}{2}\frac{1}{2}}(\theta),$$

$$\tilde{F}^{e_R}_{-\frac{1}{2}-\frac{1}{2}}(\theta) = \mp\frac{1}{\sqrt{2}}\sum_j (2j+1)(-\langle N\pi, -\frac{1}{2}|R, \lambda_R\rangle f^V_{-3})d^j_{\frac{3}{2}\frac{1}{2}}(\theta). \qquad (4.26)$$

Therefore using Equation 4.15, we have:

$$\tilde{F}^{e_R}_{\frac{1}{2},\frac{1}{2}}(\theta) = -\frac{1}{\sqrt{2}}\sum_j (2j+1)\sigma^D C^j_{N\pi}\sqrt{\chi_E}\kappa C^I_{N\pi} f_{BW} f^V_{-1} d^j_{\frac{1}{2}-\frac{1}{2}}(\theta)$$

$$\tilde{F}^{e_R}_{\frac{1}{2},-\frac{1}{2}}(\theta) = -\frac{1}{\sqrt{2}}\sum_j (2j+1)\sigma^D C^j_{N\pi}\sqrt{\chi_E}\kappa C^I_{N\pi} f_{BW} f^V_{-3} d^j_{\frac{3}{2}-\frac{1}{2}}(\theta)$$

$$\tilde{F}^{e_R}_{-\frac{1}{2},\frac{1}{2}}(\theta) = \pm\frac{1}{\sqrt{2}}\sum_j (2j+1)\sigma^D C^j_{N\pi}\sqrt{\chi_E}\kappa C^I_{N\pi} f_{BW} f^V_{-1} d^j_{\frac{1}{2}\frac{1}{2}}(\theta)$$

$$\tilde{F}^{e_R}_{-\frac{1}{2},-\frac{1}{2}}(\theta) = \pm\frac{1}{\sqrt{2}}\sum_j (2j+1)\sigma^D C^j_{N\pi}\sqrt{\chi_E}\kappa C^I_{N\pi} f_{BW} f^V_{-3} d^j_{\frac{3}{2}\frac{1}{2}}(\theta). \qquad (4.27)$$

The same calculation can be done for the axial helicity amplitudes, with axial production amplitude f^A. Using $f^{CC}_{-1} = F^V_{-1} - F^A_{-1}$ we have:

$$\tilde{F}^{e_R}_{\frac{1}{2}\frac{1}{2}}(\theta) - \tilde{G}^{e_R}_{\frac{1}{2}\frac{1}{2}}(\theta) = -\sum_j \frac{2j+1}{\sqrt{2}}\sigma^D \kappa C^I_{N\pi} \sqrt{\chi_E} f_{BW}(R) f^{CC}_{-1}(R(I, j = l\pm\frac{1}{2})) d^j_{\frac{1}{2}-\frac{1}{2}}(\theta)$$

$$\tilde{F}^{e_R}_{\frac{1}{2}-\frac{1}{2}}(\theta) - \tilde{G}^{e_R}_{\frac{1}{2}-\frac{1}{2}}(\theta) = -\sum_j \frac{2j+1}{\sqrt{2}}\sigma^D \kappa C^I_{N\pi} \sqrt{\chi_E} f_{BW}(R) f^{CC}_{-3}(R(I, j = l\pm\frac{1}{2})) d^j_{\frac{3}{2}-\frac{1}{2}}(\theta)$$

$$(4.28)$$

It is very easy to calculate the helicity amplitude for e_L, using the following symmetry relations among standard helicity amplitudes:

$$F_{-\mu,-\lambda}(\theta) = -e^{i(\lambda-\mu)\pi}F_{\mu,\lambda}(\theta)$$

$$G_{-\mu,-\lambda}(\theta) = e^{i(\lambda-\mu)\pi}F_{\mu,\lambda}(\theta) \qquad (4.29)$$

where the explicit expression is given in Table 4.3: Therefore:

$$
\begin{aligned}
\tilde{F}^{e_L}_{-\frac{1}{2},\frac{1}{2}}(\theta) &= F_{\frac{1}{2}-\frac{3}{2}}(\theta) = -F_{-\frac{1}{2}\frac{3}{2}} \\
&= -\sum_j F^j_{-\frac{1}{2}\frac{3}{2}}(2j+1)d^j_{\frac{3}{2}-\frac{1}{2}}(\theta) = -\tilde{F}^{e_R}_{\frac{1}{2}-\frac{1}{2}}(\theta)
\end{aligned}
$$

$$
\begin{aligned}
\tilde{F}^{e_L}_{-\frac{1}{2},-\frac{1}{2}}(\theta) &= -F_{\frac{1}{2}-\frac{1}{2}}(\theta) = -F_{-\frac{1}{2}\frac{1}{2}}(\theta) \\
&= -\sum_j F^j_{-\frac{1}{2}\frac{1}{2}}(2j+1)d^j_{\frac{1}{2}-\frac{1}{2}}(\theta) = \tilde{F}^{e_R}_{\frac{1}{2}\frac{1}{2}}(\theta).
\end{aligned} \tag{4.30}
$$

But there is an additional minus for axial part due to Equation 4.29.

$$
\begin{aligned}
\tilde{G}^{e_L}_{-\frac{1}{2},\frac{1}{2}}(\theta) &= G_{\frac{1}{2}-\frac{3}{2}}(\theta) = G_{-\frac{1}{2}\frac{3}{2}} \\
&= \sum_j G^j_{-\frac{1}{2}\frac{3}{2}}(2j+1)d^j_{\frac{3}{2}-\frac{1}{2}}(\theta) = \tilde{G}^{e_R}_{\frac{1}{2}-\frac{1}{2}}(\theta)
\end{aligned}
$$

$$
\begin{aligned}
\tilde{G}^{e_L}_{-\frac{1}{2},-\frac{1}{2}}(\theta) &= -G_{\frac{1}{2}-\frac{1}{2}}(\theta) = G_{-\frac{1}{2}\frac{1}{2}}(\theta) \\
&= \sum_j G^j_{-\frac{1}{2}\frac{1}{2}}(2j+1)d^j_{\frac{1}{2}-\frac{1}{2}}(\theta) = -\tilde{G}^{e_R}_{\frac{1}{2}\frac{1}{2}}(\theta).
\end{aligned} \tag{4.31}
$$

All symmetry relations between the helicity amplitudes can be found in Table 4.4. Therefore:

$$
\begin{aligned}
&\tilde{F}^{e_L}_{-\frac{1}{2}\frac{1}{2}}(\theta) - \tilde{G}^{e_L}_{-\frac{1}{2}\frac{1}{2}}(\theta) \\
&= \sum_j \frac{2j+1}{\sqrt{2}}\sigma^D \, \kappa \, C^I_{N\pi} \, \sqrt{\chi_E} f_{BW}(R) \, (f^V_{-3}+f^A_{-3})(R(I,j=l\pm\tfrac{1}{2})) \, d^j_{\frac{3}{2}-\frac{1}{2}}(\theta) \\
&\tilde{F}^{e_L}_{-\frac{1}{2}-\frac{1}{2}}(\theta) - \tilde{G}^{e_L}_{-\frac{1}{2}-\frac{1}{2}}(\theta) \\
&= -\sum_j \frac{2j+1}{\sqrt{2}}\sigma^D \, \kappa \, C^I_{N\pi} \, \sqrt{\chi_E} f_{BW}(R) \, (f^V_{-1}+f^A_{-1})(R(I,j=l\pm\tfrac{1}{2})) \, d^j_{\frac{1}{2}-\frac{1}{2}}(\theta)
\end{aligned} \tag{4.32}
$$

According to [9]

$$
f^V_{-1,-3,0-}+f^A_{-1,-3,0-} = f^{V+A}_{-1,-3,0-} = \mp f^{V-A}_{+1,+3,0+} = \mp f^{CC}_{+1,+3,0+} \quad (\text{ for } j\pm\tfrac{1}{2}) \tag{4.33}
$$

Therefore

$$
\tilde{F}^{e_L}_{-\frac{1}{2}\frac{1}{2}}(\theta) - \tilde{G}^{e_L}_{-\frac{1}{2}\frac{1}{2}}(\theta)
$$
$$
= \mp \sum_j \frac{2j+1}{\sqrt{2}} \sigma^D \, \kappa \, C^I_{N\pi} \, \sqrt{\chi_E} f_{BW}(R) \, (f^{CC}_{+3})(R(I, j = l \pm \frac{1}{2})) \, d^j_{\frac{3}{2}-\frac{1}{2}}(\theta)
$$
$$
\tilde{F}^{e_L}_{-\frac{1}{2}-\frac{1}{2}}(\theta) - \tilde{G}^{e_L}_{-\frac{1}{2}-\frac{1}{2}}(\theta)
$$
$$
= \pm \sum_j \frac{2j+1}{\sqrt{2}} \sigma^D \, \kappa \, C^I_{N\pi} \, \sqrt{\chi_E} f_{BW}(R) \, (f^{CC}_{+1})(R(I, j = l \pm \frac{1}{2})) \, d^j_{\frac{1}{2}-\frac{1}{2}}(\theta) \qquad (4.34)
$$

Like Equation 4.21- 4.23, for e_- we have:

$$
F^{0(-)j}_{\mu\lambda} = F^{0(-)j}_{-\lambda_2\lambda_R} = \langle N\pi, -\lambda_2 | R, \lambda_R \rangle \langle R, \lambda_R | e^\alpha_- F^V_\alpha | N, \lambda_1 \rangle \qquad (4.35)
$$

From Equation 4.8

$$
F^j_{-\lambda_2, \lambda_R = \pm\frac{1}{2}} = \langle N\pi, -\lambda_2 | R, \lambda_R \rangle f^V_{0\pm} \text{ for } \lambda_1 = -s_{z1} = \mp\frac{1}{2}
$$
$$
\qquad (4.36)
$$

where f^V is production amplitude for vector part. On the other hand from Equation 3.67 and Equation 3.73 we have:

$$
\tilde{F}^{e_-}_{-\frac{1}{2}-\frac{1}{2}}(\theta) = -F^{0(-)}_{\frac{1}{2}\frac{1}{2}}(\theta) = -\sum_j F^{0(-)j}_{\frac{1}{2}\frac{1}{2}}(2j+1)d^j_{\frac{1}{2}\frac{1}{2}}(\theta)
$$
$$
= -\sum_j \frac{2j+1}{\sqrt{2}} (\langle N\pi, -\frac{1}{2} | R, \lambda_R \rangle \frac{|\mathbf{k}|}{\sqrt{-k^2}} f^V_{0+}) d^j_{\frac{1}{2}\frac{1}{2}}(\theta)
$$
$$
\qquad (4.37)
$$

and extra factor from Equation 4.25 should be multiplied:

$$
\tilde{F}^{e_-}_{-\frac{1}{2}-\frac{1}{2}}(\theta) - \tilde{G}^{e_-}_{-\frac{1}{2}-\frac{1}{2}}(\theta)
$$
$$
= -\frac{|\mathbf{k}|}{\sqrt{-k^2}} \sum_j \frac{2j+1}{\sqrt{2}} \sigma^D \, \kappa \, C^I_{N\pi} \, \sqrt{\chi_E} f_{BW}(R) \, f^{CC}_{0+}(R(I, j = l \pm \frac{1}{2})) \, d^j_{\frac{1}{2}\frac{1}{2}}(\theta) \qquad (4.38)
$$

It is important to notice that the sign of $C^j_{N\pi}$ is always positive sign for $j = l + \frac{1}{2}$ but it can have different signs for resonances with $j = l - \frac{1}{2}$ (see Table G.1).

Below we summarize the helicity amplitudes for all helicities:

$$\tilde{F}^{e_L}_{\frac{1}{2}\frac{1}{2}} - \tilde{G}^{e_L}_{\frac{1}{2}\frac{1}{2}} = -\sum_j \frac{2j+1}{\sqrt{2}} \sigma^D C^j_{N\pi}\, \kappa\, C^I_{N\pi}\, f_{BW}(R)\, f_{+3}(R(I,j=l\pm\tfrac{1}{2}))\, d^j_{\frac{3}{2}\frac{1}{2}}(\theta)$$

$$\tilde{F}^{e_L}_{-\frac{1}{2}\frac{1}{2}} - \tilde{G}^{e_L}_{-\frac{1}{2}\frac{1}{2}} = \mp\sum_j \frac{2j+1}{\sqrt{2}} \sigma^D C^j_{N\pi}\, \kappa\, C^I_{N\pi}\, f_{BW}(R)\, f_{+3}(R(I,j=l\pm\tfrac{1}{2}))\, d^j_{\frac{3}{2}-\frac{1}{2}}(\theta)$$

$$\tilde{F}^{e_L}_{\frac{1}{2}-\frac{1}{2}} - \tilde{G}^{e_L}_{\frac{1}{2}-\frac{1}{2}} = \sum_j \frac{2j+1}{\sqrt{2}} \sigma^D C^j_{N\pi}\, \kappa\, C^I_{N\pi}\, f_{BW}(R)\, f_{+1}(R(I,j=l\pm\tfrac{1}{2}))\, d^j_{\frac{1}{2}\frac{1}{2}}(\theta)$$

$$\tilde{F}^{e_L}_{-\frac{1}{2}-\frac{1}{2}} - \tilde{G}^{e_L}_{-\frac{1}{2}-\frac{1}{2}} = \pm\sum_j \frac{2j+1}{\sqrt{2}} \sigma^D C^j_{N\pi}\, \kappa\, C^I_{N\pi}\, f_{BW}(R)\, f_{+1}(R(I,j=l\pm\tfrac{1}{2}))\, d^j_{\frac{1}{2}-\frac{1}{2}}(\theta)$$

$$\tilde{F}^{e_R}_{\frac{1}{2}\frac{1}{2}} - \tilde{G}^{e_R}_{\frac{1}{2}\frac{1}{2}} = -\sum_j \frac{2j+1}{\sqrt{2}} \sigma^D C^j_{N\pi}\, \kappa\, C^I_{N\pi}\, f_{BW}(R)\, f_{-1}(R(I,j=l\pm\tfrac{1}{2}))\, d^j_{\frac{1}{2}-\frac{1}{2}}(\theta)$$

$$\tilde{F}^{e_R}_{-\frac{1}{2}\frac{1}{2}} - \tilde{G}^{e_R}_{-\frac{1}{2}\frac{1}{2}} = \pm\sum_j \frac{2j+1}{\sqrt{2}} \sigma^D C^j_{N\pi}\, \kappa\, C^I_{N\pi}\, f_{BW}(R)\, f_{-1}(R(I,j=l\pm\tfrac{1}{2}))\, d^j_{\frac{1}{2}\frac{1}{2}}(\theta)$$

$$\tilde{F}^{e_R}_{\frac{1}{2}-\frac{1}{2}} - \tilde{G}^{e_R}_{\frac{1}{2}-\frac{1}{2}} = -\sum_j \frac{2j+1}{\sqrt{2}} \sigma^D C^j_{N\pi}\, \kappa\, C^I_{N\pi}\, f_{BW}(R)\, f_{-3}(R(I,j=l\pm\tfrac{1}{2}))\, d^j_{\frac{3}{2}-\frac{1}{2}}(\theta)$$

$$\tilde{F}^{e_R}_{-\frac{1}{2}-\frac{1}{2}} - \tilde{G}^{e_R}_{-\frac{1}{2}-\frac{1}{2}} = \pm\sum_j \frac{2j+1}{\sqrt{2}} \sigma^D C^j_{N\pi}\, \kappa\, C^I_{N\pi}\, f_{BW}(R)\, f_{-3}(R(I,j=l\pm\tfrac{1}{2}))\, d^j_{\frac{3}{2}\frac{1}{2}}(\theta)$$

$$\tilde{F}^{e_-}_{\frac{1}{2}\frac{1}{2}} - \tilde{G}^{e_-}_{\frac{1}{2}\frac{1}{2}} = \mp\frac{|\mathbf{k}|}{\sqrt{-k^2}}\sum_j \frac{2j+1}{\sqrt{2}} \sigma^D C^j_{N\pi}\, \kappa\, C^I_{N\pi}\, f_{BW}(R)\, f^{(-)}_{0-}(R(I,j=l\pm\tfrac{1}{2}))\, d^j_{-\frac{1}{2}-\frac{1}{2}}(\theta)$$

$$\tilde{F}^{e_-}_{-\frac{1}{2}\frac{1}{2}} - \tilde{G}^{e_-}_{-\frac{1}{2}\frac{1}{2}} = -\frac{|\mathbf{k}|}{\sqrt{-k^2}}\sum_j \frac{2j+1}{\sqrt{2}} \sigma^D C^j_{N\pi}\, \kappa\, C^I_{N\pi}\, f_{BW}(R)\, f^{(-)}_{0-}(R(I,j=l\pm\tfrac{1}{2}))\, d^j_{-\frac{1}{2}\frac{1}{2}}(\theta)$$

$$\tilde{F}^{e_-}_{\frac{1}{2}-\frac{1}{2}} - \tilde{G}^{e_-}_{\frac{1}{2}-\frac{1}{2}} = \pm\frac{|\mathbf{k}|}{\sqrt{-k^2}}\sum_j \frac{2j+1}{\sqrt{2}} \sigma^D C^j_{N\pi}\, \kappa\, C^I_{N\pi}\, f_{BW}(R)\, f^{(-)}_{0+}(R(I,j=l\pm\tfrac{1}{2}))\, d^j_{\frac{1}{2}-\frac{1}{2}}(\theta)$$

$$\tilde{F}^{e_-}_{-\frac{1}{2}-\frac{1}{2}} - \tilde{G}^{e_-}_{-\frac{1}{2}-\frac{1}{2}} = -\frac{|\mathbf{k}|}{\sqrt{-k^2}}\sum_j \frac{2j+1}{\sqrt{2}} \sigma^D C^j_{N\pi}\, \kappa\, C^I_{N\pi}\, f_{BW}(R)\, f^{(-)}_{0+}(R(I,j=l\pm\tfrac{1}{2}))\, d^j_{\frac{1}{2}\frac{1}{2}}(\theta)$$

$$\tilde{F}^{e_+}_{\frac{1}{2}\frac{1}{2}} - \tilde{G}^{e_+}_{\frac{1}{2}\frac{1}{2}} = \mp \frac{|\mathbf{k}|}{\sqrt{-k^2}} \sum_j \frac{2j+1}{\sqrt{2}} \sigma^D C^j_{N\pi} \, \kappa \, C^I_{N\pi} \, f_{BW}(R) \, f^{(+)}_{0-}(R(I, j = l \pm \tfrac{1}{2})) \, d^j_{-\frac{1}{2}-\frac{1}{2}}(\theta)$$

$$\tilde{F}^{e_+}_{-\frac{1}{2}\frac{1}{2}} - \tilde{G}^{e_+}_{-\frac{1}{2}\frac{1}{2}} = - \frac{|\mathbf{k}|}{\sqrt{-k^2}} \sum_j \frac{2j+1}{\sqrt{2}} \sigma^D C^j_{N\pi} \, \kappa \, C^I_{N\pi} \, f_{BW}(R) \, f^{(+)}_{0-}(R(I, j = l \pm \tfrac{1}{2})) \, d^j_{-\frac{1}{2}\frac{1}{2}}(\theta)$$

$$\tilde{F}^{e_+}_{\frac{1}{2}-\frac{1}{2}} - \tilde{G}^{e_+}_{\frac{1}{2}-\frac{1}{2}} = \pm \frac{|\mathbf{k}|}{\sqrt{-k^2}} \sum_j \frac{2j+1}{\sqrt{2}} \sigma^D C^j_{N\pi} \, \kappa \, C^I_{N\pi} \, f_{BW}(R) \, f^{(+)}_{0+}(R(I, j = l \pm \tfrac{1}{2})) \, d^j_{\frac{1}{2}-\frac{1}{2}}(\theta)$$

$$\tilde{F}^{e_+}_{-\frac{1}{2}-\frac{1}{2}} - \tilde{G}^{e_+}_{-\frac{1}{2}-\frac{1}{2}} = - \frac{|\mathbf{k}|}{\sqrt{-k^2}} \sum_j \frac{2j+1}{\sqrt{2}} \sigma^D C^j_{N\pi} \, \kappa \, C^I_{N\pi} \, f_{BW}(R) \, f^{(+)}_{0+}(R(I, j = l \pm \tfrac{1}{2})) \, d^j_{\frac{1}{2}\frac{1}{2}}(\theta)$$

$$(4.39)$$

where $f_{\pm 1}(R)$ and $f^{(\pm)}_{0\pm}(R)$ are resonance production amplitudes given in Appendix G for both CC$^{\pm 3}$ and NC neutrino interactions.

An important point here is due to symmetry property of $d^j_{\lambda\mu}(\theta)$ [15]

$$d^j_{\lambda\mu}(\theta) = (-1)^{j+\lambda} d^j_{\lambda-\mu}(\pi - \theta), \qquad (4.40)$$

the cross-section of individual resonance is symmetric, i.e. $d\sigma/d\theta(\pi - \theta) = d\sigma/d\theta(\theta)$.

4.1.3 Form-factors

The resonance production amplitudes depend on vector and axial form-factor which is dipole in [7], but in this work we use a form-factor proposed in [17] for Δ resonance:

$$F^V(W, k^2) = \frac{1}{2}\left(1 - \frac{k^2}{(M+W)^2}\right)^{\frac{1}{2}} \sqrt{3\left(G^{f_3}_V(W, k^2)\right)^2 + \left(G^{f_1}_V(W, k^2)\right)^2} \qquad (4.41)$$

for vector form-factor where

$$G^{f_3}_V(W, k^2) = \frac{1}{2\sqrt{3}}\left[C^V_4 \frac{W^2 + k^2 - M^2}{2M^2} + C^V_5 \frac{W^2 - K^2 - M^2}{2M^2} + \frac{C^V_3}{M}(W + M)\right],$$

$$G^{f_1}_V(W, k^2) = \frac{1}{2\sqrt{3}}\left[C^V_4 \frac{W^2 + k^2 - M^2}{2M^2} + C^V_5 \frac{W^2 - K^2 - M^2}{2M^2} + C^V_3 \frac{(M+W)M - k^2}{MW}\right],$$

$$(4.42)$$

and

$$
\begin{aligned}
C_3^V &= 2.13 \left(1 - \frac{k^2}{4M_V^2}\right)^{-1} \left(1 - \frac{k^2}{M_V^2}\right)^{-2}, \\
C_4^V &= -1.51 \left(1 - \frac{k^2}{4M_V^2}\right)^{-1} \left(1 - \frac{k^2}{M_V^2}\right)^{-2}, \\
C_5^V &= 0.48 \left(1 - \frac{k^2}{4M_V^2}\right)^{-1} \left(1 - \frac{k^2}{0.776M_V^2}\right)^{-2}.
\end{aligned}
\tag{4.43}
$$

For axial vector form-factor:

$$
F^A(W, k^2) = \frac{\sqrt{3}}{2} \left(1 - \frac{k^2}{(M+W)^2}\right)^{\frac{1}{2}} \left[1 - \frac{W^2 + k^2 - M^2}{8M^2}\right] C_5^A(k^2),
\tag{4.44}
$$

where

$$
C_5^A(k^2) = \frac{C_5^A(0)}{\left(1 - \frac{k^2}{M_A^2}\right)^2}.
\tag{4.45}
$$

M_V, M_A, and $C_5^A(0)$ are adjustable parameters that can be fitted to data. $M_V = 0.84$ has been fitted to electron scattering data, but M_A and $C_5^A(0)$ should be fitted to the neutrino scattering data.

For higher resonances ($N \neq 0$) we propose a slightly different form-factor (based on [9]) but with same assumption as in [17]:

$$
\begin{aligned}
F^V(W, k^2) &= \frac{1}{2} \left(1 - \frac{k^2}{(M+W)^2}\right)^{\frac{1}{2}} \left(1 - \frac{k^2}{4M^2}\right)^{-\frac{N}{2}} \sqrt{3\left(G_V^{f_3}(W, k^2)\right)^2 + \left(G_V^{f_1}(W, k^2)\right)^2} \\
F^A(W, k^2) &= \frac{\sqrt{3}}{2} \left(1 - \frac{k^2}{(M+W)^2}\right)^{\frac{1}{2}} \left(1 - \frac{k^2}{4M^2}\right)^{-\frac{N}{2}} \left[1 - \frac{W^2 + k^2 - M^2}{8M^2}\right] C_5^A(k^2),
\end{aligned}
\tag{4.46}
$$

where N is given in Table 4.1.

4.2 Nonresonance Background

In addition to resonant interaction, pion can be also produced via nonresonant interaction, and it has been known for decades [8, 9]. The nonresonant interaction can be derived from a model called σ-model [11]. The σ-model is a field theoretical model based on
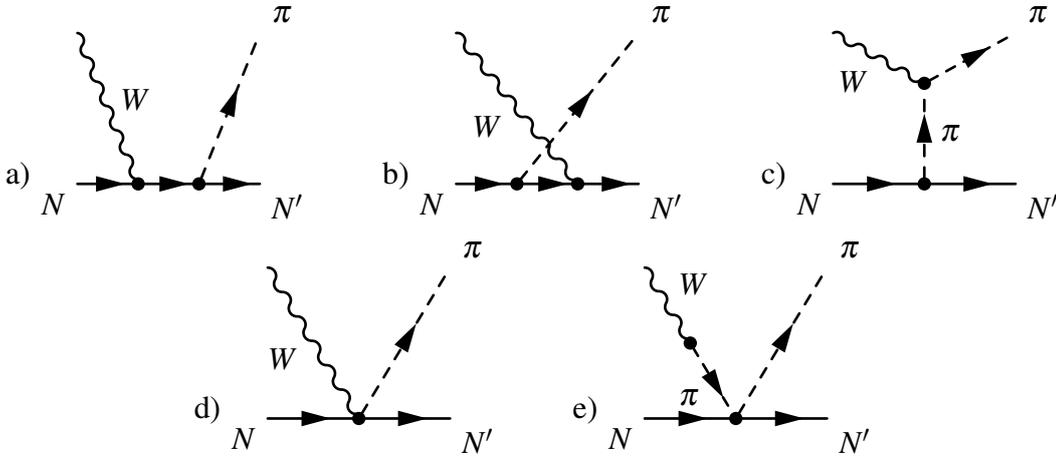
Fig. 4.1 Nonresonant pion production diagrams: a) nucleon pole (NP), b) crossed nucleon pole (CNP), c) pion-in-flight (PIF), d) contact term (CT), e) pion pole (PP)

$SU(2) \times SU(2)$ chiral symmetry and it is consistent with the symmetries of QCD in the limit of massless up and down quarks. The ingredients of the model are nucleon field ($\psi(x)$), pion field ($\phi(x)$) and a scalar σ field.

Pion is pseudoscalar and the Lagrangian should be scalar, therefore the simplest interaction lagrangian can be pseudoscalar (linear with $\phi(x)$) or pseudovector (linear with $\partial_\mu \phi(x)$), since they both give identical results for nucleons, satisfying the free Dirac equation. The lagrangian can be linear to a new (σ) field (linear σ-model) or it can be nonlinear to σ which is not a new field but a function of π field (non-linear σ-model).

The earlier work was based [8, 9] on linear σ-model with pseudoscalar interaction that provides 3 Born graphs and it has been employed by Rein [9], but the new σ particle has never been found. On the other hand there is a recent work [10], based on non-linear σ-model with pseudovector interaction, and we are going to follow this approach in this thesis.

4.2.1 Charged-Current Interactions

The diagrams (loop corrections are not included) for nonresonant charged-current interaction proposed in [10] are shown in Figure 4.1. In [10] there are two more diagrams responsible for Δ resonance, and we do not take them into account here, since RS model is responsible for resonant interaction.

The transition amplitudes for the proposed diagrams (Figure 4.1) are the following [10]:

$$\mathcal{M}_{CC}^{NP} = C^{NP} \cos\theta_C \frac{g_A}{\sqrt{2}f_\pi} \frac{1}{s-M^2} \bar{u}(p_2) \; \slashed{q} \gamma_5 (\slashed{p}_1 + \slashed{k} + M)\varepsilon^\mu [F_\mu^V - F_\mu^A] \, u(p_1),$$

$$\mathcal{M}_{CC}^{CNP} = C^{CNP} \cos\theta_C \frac{g_A}{\sqrt{2}f_\pi} \frac{1}{u-M^2} \bar{u}(p_2) \; \varepsilon^\mu [F_\mu^V - F_\mu^A] \, (\slashed{p}_2 - \slashed{k} + M) \; \slashed{q}\gamma_5 \, u(p_1),$$

$$\mathcal{M}_{CC}^{PF} = C^{PF} \cos\theta_C \frac{g_A}{\sqrt{2}f_\pi} \frac{1}{t-m_\pi^2} F_{PF}(k^2)\bar{u}(p_2) \, \gamma_5 \, [2q\varepsilon - k\varepsilon]2M \, u(p_1),$$

$$\mathcal{M}_{CC}^{CT} = C^{CT} \cos\theta_C \frac{1}{\sqrt{2}f_\pi} \; \bar{u}(p_2) \, \varepsilon^\mu\gamma_\mu \, [g_A F_{CT}^V(k^2) \; \gamma_5 - F_\rho((k-q)^2)] \, u(p_1),$$

$$\mathcal{M}_{CC}^{PP} = C^{PP} \cos\theta_C \frac{1}{\sqrt{2}f_\pi} \; \bar{u}(p_2) \frac{\varepsilon k}{k^2 - m_\pi^2} F_\rho((k-q)^2) \; \slashed{k} \, u(p_1), \tag{4.47}$$

where

$$(F^V)^\mu = 2\left[F_1^V(k^2)\gamma^\mu - \mu_V \frac{F_2^V(k^2)}{2M}[\gamma^\mu, \slashed{k}]\right],$$

$$(F^A)^\mu = -G_A(k^2)\left[\gamma^\mu\gamma_5 + \frac{\slashed{k}}{m_\pi^2 - k^2}k^\mu\gamma_5\right]. \tag{4.48}$$

The vector form factors are:

$$F_1^V(k^2) = \frac{1}{2}\left(F_2^p(k^2) - F_1^n(k^2)\right), \qquad \mu_V F_2^V(k^2) = \frac{1}{2}\left(\mu_p F_2^p(k^2) - \mu_n F_2^n(k^2)\right). \tag{4.49}$$

Like [10], we use the parametrization of Galster and collaborators [19]:

$$F_1^N = \frac{G_E^N + \tau G_M^N}{1+\tau}, \qquad \mu_N F_2^N = \frac{G_M^N - G_E^N}{1+\tau},$$

$$G_E^p = \frac{G_M^p}{\mu_p} = \frac{G_M^n}{\mu_n} = -(1+\lambda_n\tau)\frac{G_E^n}{\mu_n\tau} = \left(\frac{1}{1-k^2/M_D^2}\right)^2, \tag{4.50}$$

where $\tau = -k^2/4M^2, M_D = 0.843 GeV, \mu_p = 2.792847, \mu_n = -1.913043$ and $\lambda_n = 5.6$. The axial form factor is:

$$G_A(k^2) = \frac{g_A}{(1-k^2/M_A^2)^2}, \qquad g_A = 1.26, \tag{4.51}$$

where $M_V = 0.84$ GeV and $M_A = 1.05$ GeV, and

$$F_\rho(t) = 1/(1-t/M_\rho^2), \tag{4.52}$$

where $m_\rho = 0.7758$ GeV, as it is proposed in [10].

Conservation of Vector Current (CVC) requires (see H):

$$F_{PF}(k^2) = F_{CT}^V(k^2) = 2F_1^V(k^2). \tag{4.53}$$

$C^{NP}, C^{CNP}, C^{PF}, C^{CT}$ and C^{PP} are isospin coefficients and they are given in Table 4.5 for different neutrino and anti-neutrino channels[4]. To calculate the helicity amplitudes of the above diagrams, From Equation 3.6 and Equation 3.27, first we need to calculate invariant amplitudes (V_k and A_k) from transition amplitudes for different channels.

$$\langle N\pi | e^\rho J_\rho | N \rangle = \sum_k \bar{u}_N(p_2) \left[V_k(s,t,u)O(V_k) - A_k(s,t,u)O(A_k) \right] u_N(p_1). \tag{4.54}$$

Here we calculate the invariant amplitudes of different diagrams given in Equation 4.47 and we start with nucleon pole (NP) diagram by using Equation 4.48

$$\langle e^\rho J_\rho^{NP} \rangle^{n\pi^+} = \frac{g_A}{\sqrt{2}f_\pi} 2F_1(k^2) \frac{1}{s-M^2} \bar{u}(p_2) \not{q} \gamma_5 (\not{p}_1 + \not{k} + M) \not{\varepsilon} u(p_1) \tag{4.55}$$

$$- \frac{g_A}{\sqrt{2}f_\pi} \frac{2\mu_V F_2(k^2)}{2M} \frac{1}{s-M^2} \bar{u}(p_2) \not{q} \gamma_5 (\not{p}_1 + \not{k} + M)[\not{\varepsilon}, \not{k}] u(p_1) \tag{4.56}$$

$$- \frac{g_A}{\sqrt{2}f_\pi} G_A(k^2) \frac{1}{s-M^2} \bar{u}(p_2) \not{q} \gamma_5 (\not{p}_1 + \not{k} + M) \left(\not{\varepsilon} + \frac{\not{k}}{m_\pi - k^2}(\varepsilon k) \right) \gamma_5 u(p_1) \tag{4.57}$$

We need to expand the above equation in terms of $O(V_k)$ and $O(A_k)$ given in Table 3.1. We start with Equation 4.55 by add and subtract $\frac{q\varepsilon}{qk} \not{q}$ term

$$\frac{g_A}{\sqrt{2}f_\pi} 2F_1(k^2) \bar{u}(p_2)\gamma_5 \left\{ -\frac{1}{s-M^2} \not{q}(\not{p}_1 + \not{k} + M) \not{\varepsilon} + \frac{q\varepsilon}{qk} \not{q} - \frac{q\varepsilon}{qk} \not{q} \right\} u(p_1)$$

$$= \frac{g_A}{\sqrt{2}f_\pi} 2F_1(k^2) \bar{u}(p_2)\gamma_5 \left\{ \frac{1}{s-M^2} \left[-\not{q}(\not{p}_1 + \not{k} + M) \not{\varepsilon} + (s-M^2)\frac{q\varepsilon}{qk} \not{q} \right] - \frac{q\varepsilon}{qk} \not{q} \right\} u(p_1) \tag{4.58}$$

$$= \frac{g_A}{\sqrt{2}f_\pi} 2F_1(k^2) \bar{u}(p_2) \left\{ \frac{1}{s-M^2} \left[\frac{2M}{qk}O(V_2) + 2MO(V_1) \right] - \frac{1}{qk}O(V_3) - \gamma_5 \frac{q\varepsilon}{qk} \not{q} \right\} u(p_1). \tag{4.59}$$

---

[4]Isospin coefficients for $p\pi^+$ and $n\pi^+$ channels are given in [10], and isospin coefficients for $p\pi^0$ can be easily calculated from Table A.0.3.

From Equation 4.58 to Equation 4.59 we used

$$\bar{u}(p_2)\gamma_5\left\{-\slashed{q}(\slashed{p}_1+\slashed{k}+M)\slashed{\varepsilon}+(s-M^2)\frac{q\varepsilon}{qk}\slashed{q}\right\}u(p_1)$$

$$\bar{u}(p_2)\gamma_5\left\{-\slashed{q}(\slashed{p}_1\slashed{\varepsilon}+\slashed{k}\slashed{\varepsilon}+\slashed{\varepsilon}\slashed{p}_1)+(k^2+2p_1k)\frac{q\varepsilon}{qk}(\slashed{p}_1-\slashed{p}_2+\slashed{k})\right\}u(p_1)$$

$$\bar{u}(p_2)\gamma_5\left\{-\slashed{q}(2\varepsilon p_1+\slashed{k}\slashed{\varepsilon})+(k^2+2p_1k)\frac{q\varepsilon}{qk}(2M+\slashed{k})\right\}u(p_1)$$

$$\bar{u}(p_2)\gamma_5\left\{-\slashed{q}\slashed{k}\slashed{\varepsilon}+(2M+\slashed{k})\left[-2\varepsilon p_1+(k^2+2p_1k)\frac{q\varepsilon}{qk}\right]\right\}u(p_1) \tag{4.60}$$

and

$$\bar{u}(p_2)\gamma_5\slashed{q}\slashed{k}\slashed{\varepsilon}u(p_1)=\bar{u}(p_2)\gamma_5(\slashed{p}_1-\slashed{p}_2+\slashed{k})\slashed{k}\slashed{\varepsilon}u(p_1)$$

$$=\bar{u}(p_2)\gamma_5(\slashed{p}_1+M+\slashed{k})\slashed{k}\slashed{\varepsilon}u(p_1)$$

$$=\bar{u}(p_2)\gamma_5(\slashed{p}_1\slashed{k}\slashed{\varepsilon}+\slashed{k}\slashed{\varepsilon}\slashed{p}_1+k^2\slashed{\varepsilon})u(p_1)$$

$$=\bar{u}(p_2)\gamma_5(\slashed{p}_1\slashed{k}\slashed{\varepsilon}-\slashed{k}\slashed{p}_1\slashed{\varepsilon}+2\slashed{k}p_1\varepsilon+k^2\slashed{\varepsilon})u(p_1)$$

$$=\bar{u}(p_2)\gamma_5\left[(-2\slashed{k}p_1+2p_1k+k^2)\slashed{\varepsilon}+2(\varepsilon p_1)\slashed{k}\right]u(p_1) \tag{4.61}$$

for the first term of Equation 4.60, and

$$-2\varepsilon p_1+(k^2+2p_1k)\frac{q\varepsilon}{qk}=-\varepsilon(p_1+p_2+q-k)+(k^2+2p_1k)\frac{q\varepsilon}{qk}$$

$$=-2\varepsilon P-\varepsilon q+\varepsilon k+k(k+2p_1-q+q)\frac{q\varepsilon}{qk}$$

$$=-\varepsilon q+\varepsilon k+\frac{1}{qk}\left[-2(\varepsilon P)(qk)+k(2P)(q\varepsilon)+(qk)(q\varepsilon)\right]$$

$$=\varepsilon k-\frac{1}{qk}\left[(2P\varepsilon)(qk)-(2Pk)(q\varepsilon)\right] \tag{4.62}$$

for the second term of Equation 4.60, where $P = \frac{1}{2}(p_1 + p_2)$. Substituting Equation 4.61 and Equation 4.62) in Equation 4.60, it is straightforward to derive Equation 4.59:

$$\bar{u}(p_2)\Big\{\gamma^5\left[2\,\slashed{k}\,\slashed{p}_1\,\slashed{\varepsilon} - (2p_1k+k^2)\,\slashed{\varepsilon} - 2(\varepsilon p_1)\,\slashed{k}\right]$$

$$+2M\left[\gamma_5\varepsilon k + \frac{1}{qk}O(V_2)\right] + \gamma_5\,\slashed{k}\left[-2\varepsilon p_1 + (k^2+2p_1k)\frac{q\varepsilon}{qk}\right]\Big\}u(p_1)$$

$$=\bar{u}(p_2)\Big\{2M\left[\gamma_5\varepsilon k + \frac{1}{qk}O(V_2)\right] + \gamma_5\,\slashed{k}(2\,\slashed{p}_1\,\slashed{\varepsilon} - 4\varepsilon p_1) - \gamma_5\,\slashed{\varepsilon}(2p_1K+k^2)$$

$$+\gamma_5\,\slashed{k}(k^2+2p_1k)\frac{q\varepsilon}{qk}\Big\}u(p_1)$$

$$=\bar{u}(p_2)\Big\{2M\left[\gamma_5\varepsilon k + \frac{1}{qk}O(V_2)\right] - 2\gamma_5\,\slashed{k}\,\slashed{\varepsilon}\,\slashed{p}_1 + \gamma_5\frac{1}{qk}\left[-\slashed{\varepsilon}(qk)(2p_1K+k^2)+\slashed{k}(k^2+2p_1k)q\varepsilon\right]\Big\}u(p_1)$$

$$=\bar{u}(p_2)\Big\{\frac{2M}{qk}O(V_2) - 2M\gamma_5(\slashed{k}\,\slashed{\varepsilon} - \varepsilon k) - \frac{1}{qk}(s-M^2)O(V_3)\Big\}u(p_1) \tag{4.63}$$

where using $\varepsilon k = \frac{1}{2}\,\slashed{\varepsilon}\,\slashed{k} + \frac{1}{2}\,\slashed{k}\,\slashed{\varepsilon}$ can lead to Equation 4.59. There is yet one term in Equation 4.59 that is not expanded over $O(V_i)$. This term will be considered with PF and the vector part of CT amplitudes.

We can continue from Equation 4.56:

$$\frac{g_A}{\sqrt{2}f_\pi}\frac{2\mu_V F_2(k^2)}{2M}\frac{1}{s-M^2}\bar{u}(p_2)\{\gamma_5\,\slashed{q}(\slashed{p}_1 + \slashed{k} + M)[\slashed{\varepsilon}, \slashed{k}]\}u(p_1)$$

$$=\mathbb{B}\,\bar{u}(p_2)\gamma_5\{\slashed{q}(\slashed{p}_1 + \slashed{k} - M)[\slashed{\varepsilon}, \slashed{k}] + 2\,\slashed{q}M[\slashed{\varepsilon}, \slashed{k}]\}u(p_1)$$

$$=\mathbb{B}\,\bar{u}(p_2)\gamma_5\{\slashed{q}(\slashed{p}_1[\slashed{\varepsilon}, \slashed{k}] - [\slashed{\varepsilon}, \slashed{k}]\slashed{p}_1) + \slashed{q}\,\slashed{k}[\slashed{\varepsilon}, \slashed{k}] + 2M\,\slashed{q}[\slashed{\varepsilon}, \slashed{k}]\}u(p_1)$$

$$=\mathbb{B}\,\bar{u}(p_2)\gamma_5\{\slashed{q}[\slashed{p}_1, [\slashed{\varepsilon}, \slashed{k}]] + \slashed{k}[\slashed{\varepsilon}, \slashed{k}] + 2\,\slashed{q}M[\slashed{\varepsilon}, \slashed{k}]\}u(p_1) \tag{4.64}$$

$$=\mathbb{B}\,\bar{u}(p_2)\gamma_5\,\slashed{q}\{-4(\slashed{\varepsilon}p_1k - \slashed{k}p_1\varepsilon) - 2\left(\slashed{\varepsilon}k^2 - \slashed{k}(\varepsilon k)\right) + 2M[\slashed{\varepsilon}, \slashed{k}]\}u(p_1) \tag{4.65}$$

$$=\frac{g_A}{\sqrt{2}f_\pi}\frac{2\mu_V F_2(k^2)}{2M}\frac{1}{s-M^2}\bar{u}(p_2)\{2(k^2+2p_1k)O(V_1) - 4M[O(V_3) + O(V_4)]\}u(p_1). \tag{4.66}$$

From Equation 4.64 to Equation 4.65 we used the following relation:

$$[\gamma^\rho, [\gamma^\mu, \gamma^\nu]] = 4(\eta^{\mu\rho}\gamma^\nu - \eta^{\nu\rho}\gamma^\mu) \Rightarrow [\slashed{p}_1, [\slashed{\varepsilon}, \slashed{k}]] = 4((p_1\varepsilon)\,\slashed{k} - (p_1k)\,\slashed{\varepsilon})$$

$$\gamma^\nu, [\gamma^\mu, \gamma^\nu] = 2(\eta^{\mu\nu}\gamma^\nu - \eta^{\nu\nu}\gamma^\mu) \Rightarrow \slashed{k}[\slashed{\varepsilon}, \slashed{k}] = 2\left((\varepsilon k)\,\slashed{k} - k^2\,\slashed{\varepsilon}\right) \tag{4.67}$$

and from Equation 4.65) to Equation 4.66 we used

$$
\begin{aligned}
&\bar{u}(p_2)\gamma_5\,\slashed{q}\left\{-4(\slashed{\varepsilon}p_1k-\slashed{k}p_1\varepsilon)-2\left(\slashed{\varepsilon}k^2-\slashed{k}(\varepsilon k)\right)\right\}u(p_1)\\
&=\bar{u}(p_2)\gamma_5(\slashed{p}_1-\slashed{p}_2+\slashed{k})\left\{-2\,\slashed{\varepsilon}(2p_1k+k^2)+2\,\slashed{k}(2p_1\varepsilon+\varepsilon k)\right\}u(p_1)\\
&=\bar{u}(p_2)\gamma_5\left\{-2(2p_1k+k^2)(\slashed{p}_1+M+\slashed{k})\,\slashed{\varepsilon}+2(2p_1\varepsilon+\varepsilon k)(\slashed{p}_1+M+\slashed{k})\,\slashed{k}\right\}u(p_1)\\
&=\bar{u}(p_2)\gamma_5\left\{-2(2p_1k+k^2)(M\,\slashed{\varepsilon}-\slashed{\varepsilon}\,\slashed{p}_1+2\varepsilon p_1+\slashed{k}\,\slashed{\varepsilon})+2(2p_1\varepsilon+\varepsilon k)(M\,\slashed{k}\right.\\
&\quad\left.-\slashed{k}\,\slashed{p}_1+2kp_1+k^2)\right\}u(p_1)\\
&=\bar{u}(p_2)\gamma_5\left\{-2(2p_1k+k^2)(2\varepsilon p_1+\slashed{k}\,\slashed{\varepsilon})+2(2p_1\varepsilon+\varepsilon k)(2k\,\slashed{p}_2+k^2)\right\}u(p_1)\\
&=\bar{u}(p_2)\gamma_5\left\{2(2p_1k+k^2)(-\slashed{k}\,\slashed{\varepsilon}+k\varepsilon)\right\}u(p_1)\\
&=\bar{u}(p_2)\gamma_5\left\{2(2p_1k+k^2)(-\slashed{k}\,\slashed{\varepsilon}+\frac{1}{2}(\slashed{k}\,\slashed{\varepsilon}+\slashed{\varepsilon}\,\slashed{k}))\right\}u(p_1)\\
&=\bar{u}(p_2)\gamma_5\left\{2(2p_1k+k^2)O(v_1)\right\}u(p_1)
\end{aligned}
$$

$$(4.68)$$

and

$$
\begin{aligned}
&\bar{u}(p_2)\gamma_5 2M\,\slashed{q}[\slashed{\varepsilon},\slashed{k}]u(p_1)\\
&=2M\bar{u}(p_2)\gamma_5(\slashed{p}_1-\slashed{p}_2+\slashed{k})[\slashed{\varepsilon},\slashed{k}]u(p_1)\\
&=2M\bar{u}(p_2)\gamma_5\left\{(\slashed{p}_1+M+\slashed{k})[\slashed{\varepsilon},\slashed{k}]\right\}u(p_1)\\
&=2M\bar{u}(p_2)\gamma_5\left\{(\slashed{p}_1-M+\slashed{k})[\slashed{\varepsilon},\slashed{k}]+2M[\slashed{\varepsilon},\slashed{k}]\right\}u(p_1)\\
&=2M\bar{u}(p_2)\gamma_5\left\{[\slashed{p}_1,[\slashed{\varepsilon},\slashed{k}]]+\slashed{k}[\slashed{\varepsilon},\slashed{k}]+2M[\slashed{\varepsilon},\slashed{k}]\right\}u(p_1)\\
&=4M\bar{u}(p_2)\gamma_5\left\{2((p_1\varepsilon)\,\slashed{k}-(p_1k)\,\slashed{\varepsilon})+((\varepsilon k)\,\slashed{k}-k^2\,\slashed{\varepsilon})+M[\slashed{\varepsilon},\slashed{k}]\right\}u(p_1)\\
&=4M\bar{u}(p_2)\gamma_5\left\{\slashed{k}(k+2p_1)\varepsilon-\slashed{\varepsilon}(k+2p_1)k+M[\slashed{\varepsilon},\slashed{k}]\right\}u(p_1)\\
&=4M\bar{u}(p_2)\gamma_5\left\{\slashed{k}(q+2P)\varepsilon-\slashed{\varepsilon}(q+2P)k+M[\slashed{\varepsilon},\slashed{k}]\right\}u(p_1)\\
&=4M\bar{u}(p_2)\left\{-O(V3)-O(V_4)\right\}u(p_1)
\end{aligned}
$$

$$(4.69)$$

where we use Equation 4.67, Dirac equation and kinematics in isobaric frame given in Appendix A.

From Equation 4.57:

$$\frac{g_A}{\sqrt{2}f_\pi} G_A(k^2)\frac{1}{s-M^2} \bar{u}(p_2)\ \slashed{q}\ \gamma_5(\slashed{p}_1+\slashed{k}+M)\left(\slashed{\varepsilon}\gamma_5+\frac{\slashed{k}}{m_\pi-k^2}(\varepsilon k)\gamma_5\right)u(p_1)$$

$$=\frac{g_A}{\sqrt{2}f_\pi} G_A(k^2)\frac{1}{s-M^2} \bar{u}(p_2)\ \slashed{q}(\slashed{p}_2+\slashed{q}-M)\left(\slashed{\varepsilon}+\frac{\slashed{k}}{m_\pi-k^2}(\varepsilon k)\right)u(p_1) \qquad (4.70)$$

$$=\frac{g_A}{\sqrt{2}f_\pi} G_A(k^2)\ \bar{u}(p_2)\left\{\frac{-2M}{s-M^2}[O(A_1)+O(A_3)]+\frac{1}{M}O(A_4)-\frac{1}{m_\pi^2-k^2}\right.$$

$$\left.\left[\left(1+\frac{4M^2}{s-M^2}\right)O(A_8)+2MO(A_7)\right]\right\}u(p_1). \qquad (4.71)$$

From Equation 4.70 Equation 4.71 we use:

$$\bar{u}(p_2)\{\slashed{q}(\slashed{p}_2+\slashed{q}-M)\ \slashed{\varepsilon}\}u(p_1)$$

$$=\bar{u}(p_2)\{(-\slashed{p}_2\ \slashed{q}+2p_2.q-M\ \slashed{q}+m_\pi^2)\ \slashed{\varepsilon}\}u(p_1)$$

$$=\bar{u}(p_2)\{-2M\ \slashed{q}\ \slashed{\varepsilon}+(2p_2.q+m_\pi^2)\ \slashed{\varepsilon}\}u(p_1)$$

$$=\bar{u}(p_2)\{-M(\slashed{q}\ \slashed{\varepsilon}-\ \slashed{\varepsilon}\ \slashed{q}+2\varepsilon q)+(s-M^2)\ \slashed{\varepsilon}\}u(p_1)$$

$$=\bar{u}(p_2)\left\{-2M(O(A_1)+O(A_3))+(s-M^2)\frac{1}{M}O(A_4)\right\}u(p_1) \qquad (4.72)$$

and

$$\bar{u}(p_2)\{\slashed{q}(\slashed{p}_2+\slashed{q}-M)\ \slashed{k}\}\varepsilon k u(p_1)$$

$$=\bar{u}(p_2)\{(-\slashed{p}_2\ \slashed{q}+2p_2.q+m_\pi^2-M\ \slashed{q})\ \slashed{k}\}\varepsilon k u(p_1)$$

$$=\bar{u}(p_2)\{\slashed{k}(2p_2.q+m_\pi^2)-2M(\slashed{p}_1-\slashed{p}_2+\slashed{k})\ \slashed{k}\}\varepsilon k u(p_1)$$

$$=\bar{u}(p_2)\{\slashed{k}(s-M^2)-2M(-\ \slashed{k}\ \slashed{p}_1+2k.p_1-M\ \slashed{k}+k^2)\}\varepsilon k u(p_1)$$

$$=\bar{u}(p_2)\{(\slashed{k}-2M)(s-M^2)+4M^2\ \slashed{k}\}\varepsilon k u(p_1)$$

$$=\bar{u}(p_2)\{-(4M^2+(s-M^2))O(A_8)-2M(s-M^2)O(A_7)\}u(p_1) \qquad (4.73)$$

Now we will take into account $\langle e^\rho J_\rho^{PF}\rangle^{n\pi^+}$ and the vector part of $\langle e^\rho J_\rho^{CT}\rangle^{n\pi^+}$, and the remaining term from Equation 4.59:

$$-\frac{g_A}{\sqrt{2}f_\pi}\frac{1}{t-m_\pi^2} F_{PF}(k^2)\bar{u}(p_2)\ \gamma_5\ [2q\varepsilon-k\varepsilon]\ u(p_1)-\frac{1}{\sqrt{2}f_\pi}\ \bar{u}(p_2)\ \varepsilon^\mu\gamma_\mu\ g_A F_{CT}^V(k^2)\ \gamma_5\ u(p_1)$$

$$-\frac{g_A}{\sqrt{2}f_\pi}\ 2F_1(k^2)\ \bar{u}(p_2)\gamma_5\frac{q\varepsilon}{qk}\ \slashed{q}u(p_1)$$

$$(4.74)$$

Using $F_{PF}(k^2) = F_{CT}^V(k^2) = 2F_1(k^2) = F(k^2)$:

$$= -\frac{g_A}{\sqrt{2}f_\pi}\frac{1}{t-m_\pi^2}F(k^2)\bar{u}(p_2)\left\{2M(2\varepsilon q - k\varepsilon) + (t-m_\pi^2)\left(-\frac{q\varepsilon}{qk}\slashed{q} + \slashed{\varepsilon}\right)\right\}\gamma_5 u(p_1)$$

$$= -\frac{g_A}{\sqrt{2}f_\pi}\frac{1}{t-m_\pi^2}F(k^2)\bar{u}(p_2)\left\{2M\frac{1}{qk}(2\varepsilon q(qk) - k\varepsilon(qK)) + (k^2 - 2qk)\frac{1}{qk}(-q\varepsilon(\slashed{k} - 2M)\right.$$
$$\left. + \slashed{\varepsilon}qk)\right\}\gamma_5 u(p_1)$$

$$= -\frac{g_A}{\sqrt{2}f_\pi}\frac{1}{t-m_\pi^2}F(k^2)\frac{1}{qk}\bar{u}(p_2)\left\{4M(qk)\varepsilon q - 2M(qk)k\varepsilon + 2Mq\varepsilon(k^2 - 2qk)\right.$$
$$\left. - q\varepsilon\,\slashed{k}(k^2 - 2qk) + \slashed{\varepsilon}qk\right\}\gamma_5 u(p_1)$$

$$= -\frac{g_A}{\sqrt{2}f_\pi}\frac{1}{t-m_\pi^2}F(k^2)\frac{1}{qk}\bar{u}(p_2)\left\{2M[-(qk)k\varepsilon + (q\varepsilon)k^2] + (k^2 - 2qk)(-q\varepsilon\,\slashed{k} + \slashed{\varepsilon}qk)\right\}\gamma_5 u(p_1)$$

$$= \frac{g_A}{\sqrt{2}f_\pi}\bar{u}(p_2)\left\{\frac{F}{qk}O(V_3) - \frac{F}{t-m_\pi^2}\frac{2M}{qk}O(V_5)\right\}u(p_1) \tag{4.75}$$

The last step is $\langle e^\rho J_\rho^{PP}\rangle^{n\pi^+}$ and the axial part of the contact term $\langle e^\rho J_\rho^{CT}\rangle^{n\pi^+}$, which are related to $F_\rho((k-q)^2)$:

$$\frac{1}{\sqrt{2}f_\pi}F_\rho((k-q)^2)\bar{u}(p_2)\left[(\varepsilon k)\frac{\slashed{k}}{k^2 - m_\pi} - \slashed{\varepsilon}\right]u(p_1)$$

$$= \frac{1}{\sqrt{2}f_\pi}F_\rho((k-q)^2)\bar{u}(p_2)\left[-\frac{1}{k^2 - m_\pi}O(A_8) - \frac{1}{M}O(A_4)\right]u(p_1) \tag{4.76}$$

Therefore using Equation 4.54- 4.76, the coefficients of $O(V_k)$ and $O(A_k)$ are V_k and A_k. We summarise the invariant amplitudes of $\nu n \to \mu n \pi^+$

$$V_1^{n\pi^+} = \frac{g_A}{\sqrt{2}f_\pi}\left(\frac{4M}{s-M^2}F_1(k^2) + \frac{2\mu_V F_2(k^2)}{M}\right)$$

$$V_2^{n\pi^+} = \frac{g_A}{\sqrt{2}f_\pi}\frac{1}{qk}\frac{4M}{s-M^2}F_1(k^2)$$

$$V_3^{n\pi^+} = -\frac{g_A}{\sqrt{2}f_\pi}\frac{4}{s-M^2}\mu_V F_2(k^2)$$

$$V_4^{n\pi^+} = -\frac{g_A}{\sqrt{2}f_\pi}\frac{4}{s-M^2}\mu_V F_2(k^2)$$

$$V_5^{n\pi^+} = -\frac{g_A}{\sqrt{2}f_\pi}\frac{4M}{qk}\frac{1}{t-m_\pi^2}F_1(k^2) \tag{4.77}$$

$$A_1^{n\pi+} = -\frac{g_A}{\sqrt{2}f_\pi} \frac{2M}{s-M^2} G_A(k^2)$$

$$A_3^{n\pi+} = -\frac{g_A}{\sqrt{2}f_\pi} \frac{2M}{s-M^2} G_A(k^2)$$

$$A_4^{n\pi+} = \frac{g_A}{\sqrt{2}f_\pi} \frac{1}{M} G_A(k^2) - \frac{1}{\sqrt{2}f_\pi} \frac{1}{M} F_\rho\left((k-q)^2\right)$$

$$A_7^{n\pi+} = -\frac{g_A}{\sqrt{2}f_\pi} \frac{2M}{m_\pi^2-k^2} G_A(k^2)$$

$$A_8^{n\pi+} = -\frac{g_A}{\sqrt{2}f_\pi} \frac{1}{m_\pi^2-k^2}\left(1+\frac{4M^2}{s-M^2}\right) G_A(k^2) + \frac{1}{\sqrt{2}f_\pi} \frac{1}{m_\pi^2-k^2} F_\rho\left((k-q)^2\right)$$

$$(4.78)$$

Similarly invariant amplitude of crossed nucleon pole (CNP) diagrams can be calculated for $\nu p \to \mu p \pi+$ channel.

$$\langle e^\rho J_\rho^{CNP}\rangle^{p\pi^+} = \frac{g_A}{\sqrt{2}f_\pi} 2F_1(k^2)\frac{1}{u-M^2}\ \bar{u}(p_2)\ \not{\epsilon}(\not{p}_2-\not{k}+M)\ \not{q}\ \gamma_5 u(p_1) \qquad (4.79)$$

$$-\frac{g_A}{\sqrt{2}f_\pi} \frac{2\mu_V F_2(k^2)}{2M}\frac{1}{u-M^2}\ \bar{u}(p_2)\ [\not{\epsilon},\not{k}](\not{p}_2-\not{k}+M)\ \not{q}\ \gamma_5 u(p_1) \qquad (4.80)$$

$$-\frac{g_A}{\sqrt{2}f_\pi} G_A(k^2)\frac{1}{u-M^2}\ \bar{u}(p_2)\ \left(\not{\epsilon}+\frac{\not{k}}{m_\pi-k^2}(\epsilon k)\right)\gamma_5(\not{p}_2-\not{k}+M)\ \not{q}\ \gamma_5 u(p_1)$$

$$(4.81)$$

again we add and subtract $\frac{q\epsilon}{qk}\ \not{q}$ term to Equation 4.79, and with the Equation 4.60- 4.62 we have

$$\frac{g_A}{\sqrt{2}f_\pi} 2F_1(k^2)\ \bar{u}(p_2)\left\{\frac{1}{u-M^2}\ \not{\epsilon}(\not{p}_2-\not{k}+M)\ \not{q}+\frac{q\epsilon}{qk}\ \not{q}-\frac{q\epsilon}{qk}\ \not{q}\right\}\gamma_5 u(p_1)$$

$$=\frac{g_A}{\sqrt{2}f_\pi} 2F_1(k^2)\ \bar{u}(p_2)\left\{\frac{1}{u-M^2}\left[\not{\epsilon}\ (\not{p}_2-\not{k}+M)\ \not{q}+(u-M^2)\frac{q\epsilon}{qk}\ \not{q}\right]-\frac{q\epsilon}{qk}\ \not{q}\right\}\gamma_5 u(p_1)$$

$$(4.82)$$

$$=\frac{g_A}{\sqrt{2}f_\pi} 2F_1(k^2)\ \bar{u}(p_2)\left\{\frac{1}{u-M^2}\left[\frac{2M}{qk}O(V_2)+2MO(V_1)\right]+\frac{1}{qk}O(V_3)-\frac{q\epsilon}{qk}\ \not{q}\right\}\gamma_5 u(p_1).$$

$$(4.83)$$

From Equation 4.82) to Equation 4.83 we used

$$\bar{u}(p_2)\left\{\slashed{\varepsilon}\,(\slashed{p}_2-\slashed{k}+M)\,\slashed{q}+(u-M^2)\frac{q\varepsilon}{qk}\,\slashed{q}\right\}\gamma_5 u(p_1)$$

$$\bar{u}(p_2)\left\{(\slashed{\varepsilon}\,\slashed{p}_2+\slashed{p}_2\,\slashed{\varepsilon}-\slashed{\varepsilon}\,\slashed{k})\,\slashed{q}+(k^2-2p_2k)\frac{q\varepsilon}{qk}(\slashed{p}_1-\slashed{p}_2+\slashed{k})\right\}\gamma_5 u(p_1)$$

$$\bar{u}(p_2)\left\{(2\varepsilon p_2-\slashed{\varepsilon}\,\slashed{k})\,\slashed{q}+(k^2-2p_2k)\frac{q\varepsilon}{qk}(-2M+\slashed{k})\right\}\gamma_5 u(p_1)$$

$$\bar{u}(p_2)\left\{-\slashed{\varepsilon}\,\slashed{k}\,\slashed{q}+(2M-\slashed{k})\left[2\varepsilon p_2+(k^2-2p_2k)\frac{q\varepsilon}{qk}\right]\right\}\gamma_5 u(p_1) \tag{4.84}$$

First term of Equation 4.84 is:

$$
\begin{aligned}
\bar{u}(p_2)\,\slashed{\varepsilon}\,\slashed{k}\,\slashed{q}\gamma_5 u(p_1) &= \bar{u}(p_2)\,\slashed{\varepsilon}\,\slashed{k}(\slashed{p}_1-\slashed{p}_2+\slashed{k})\gamma_5 u(p_1) \\
&= \bar{u}(p_2)\,\slashed{\varepsilon}\,\slashed{k}(-M-\slashed{p}_2+\slashed{k})\gamma_5 u(p_1) \\
&= \bar{u}(p_2)(-\slashed{p}_2\,\slashed{\varepsilon}\,\slashed{k}-\slashed{\varepsilon}\,\slashed{k}\,\slashed{p}_2+k^2\,\slashed{\varepsilon})\gamma_5 u(p_1) \\
&= \bar{u}(p_2)(\slashed{\varepsilon}\,\slashed{p}_2\,\slashed{k}-2\varepsilon p_2\,\slashed{k}-\slashed{\varepsilon}\,\slashed{k}\,\slashed{p}_2+k^2\,\slashed{\varepsilon})\gamma_5 u(p_1) \\
&= \bar{u}(p_2)\left(\slashed{\varepsilon}[2\,\slashed{p}_2\,\slashed{k}-2kp_2+k^2]-2\varepsilon p_2\,\slashed{k}\right)\gamma_5 u(p_1)
\end{aligned}
$$

$$\tag{4.85}$$

and second term of Equation 4.84 is:

$$
\begin{aligned}
2\varepsilon p_2+(k^2-2p_2k)\frac{q\varepsilon}{qk} &= \varepsilon(p_1+p_2q+k)+(k^2-2p_2k)\frac{q\varepsilon}{qk} \\
&= 2\varepsilon P-\varepsilon q+\varepsilon k+k(k-2p_2-q+q)\frac{q\varepsilon}{qk} \\
&= -\varepsilon q+\varepsilon k+\frac{1}{qk}\left[2(\varepsilon P)(qk)-k(2P)(q\varepsilon)+(qk)(q\varepsilon)\right] \\
&= \varepsilon k+\frac{1}{qk}\left[(2P\varepsilon)(qk)-(2Pk)(q\varepsilon)\right]
\end{aligned}
$$

$$\tag{4.86}$$

Substituting Equation 4.85 and Equation 4.86 in Equation 4.84, it is straightforward to derive Equation 4.83:

$$
\bar{u}(p_2)\Big\{ - \not{\varepsilon}\, \not{k}\, \not{q} + (2M - \not{k})\Big[2\varepsilon p_2 + (k^2 - 2p_2 k)\frac{q\varepsilon}{qk}\Big]\Big\}\gamma_5 u(p_1)
$$

$$
= \bar{u}(p_2)\Big\{ - \not{\varepsilon}[2\,\not{p_2}\,\not{k} - 2kp_2 + k^2] + 2\varepsilon p_2 \not{k} + 2M[\frac{1}{qk}\gamma_5 O(V_2) - \varepsilon k]
$$

$$
+ \not{k}\Big[2\varepsilon p_2 + (k^2 - 2p_2 k)\frac{q\varepsilon}{qk}\Big]\Big\}\gamma_5 u(p_1)
$$

$$
= \bar{u}(p_2)\Big\{ 2M[\frac{1}{qk}\gamma_5 O(V_2) - \varepsilon k] + 2[\varepsilon p_2 - \not{\varepsilon}\,\not{p_2}]\,\not{k}
$$

$$
+ \not{\varepsilon}(2kp_2 - k^2) + \not{k}(k^2 - 2p_2 k)\frac{q\varepsilon}{qk}\Big\}\gamma_5 u(p_1)
$$

$$
= \bar{u}(p_2)\Big\{ \frac{2M}{qk}\gamma_5 O(V_2) - 2M\varepsilon k + 2\,\not{p_2}\,\not{\varepsilon}\,\not{k} + \frac{1}{qk}\Big[\not{\varepsilon}(qk)(2kp_2 - k^2) + \not{k}(k^2 - 2p_2 k)q\varepsilon\Big]\Big\}\gamma_5 u(p_1)
$$

$$
= \bar{u}(p_2)\Big\{ \frac{2M}{qk}\gamma_5 O(V_2) + 2M(\not{\varepsilon}\,\not{k} - \varepsilon k) + \frac{1}{qk}(u - M2)(\not{k}q\varepsilon - \not{\varepsilon}qk)\Big\}\gamma_5 u(p_1)
$$

$$
= \bar{u}(p_2)\Big\{ \frac{2M}{qk}O(V_2) + 2MO(V_1) + \frac{1}{qk}(u - M2)O(V_3)\Big\}u(p_1)
$$

$$
(4.87)
$$

where we used $\varepsilon k = \frac{1}{2}\not{\varepsilon}\,\not{k} + \frac{1}{2}\not{k}\,\not{\varepsilon}$ for the last line. There is yet one term in Equation 4.83 that is not expanded over $O(V_k)$. This term will be considered with PF and the vector part of CT amplitudes.

Equation 4.80) can be also expanded over $O(V_k)$ with the help of Equation 4.67 - 4.91:

$$
-\frac{g_A}{\sqrt{2}f_\pi}\frac{2\mu_V F_2(k^2)}{2M}\frac{1}{u - M^2}\bar{u}(p_2)\{[\not{\varepsilon}, \not{k}](\not{p_2} - \not{k} + M)\,\not{q}\}\gamma_5 u(p_1)
$$

$$
= \mathbb{B}\,\bar{u}(p_2)\{[\not{\varepsilon}, \not{k}](\not{p_2} - \not{k} - M)\,\not{q} + 2M[\not{\varepsilon}, \not{k}]\,\not{q}\}\gamma_5 u(p_1)
$$

$$
= \mathbb{B}\,\bar{u}(p_2)\{([\not{\varepsilon}, \not{k}]\,\not{p_2} - \not{p_2}[\not{\varepsilon}, \not{k}])\,\not{q} - [\not{\varepsilon}, \not{k}]\,\not{k}\,\not{q} + 2M[\not{\varepsilon}, \not{k}]\,\not{q}\}\gamma_5 u(p_1)
$$

$$
= \mathbb{B}\,\bar{u}(p_2)\{[[\not{\varepsilon}, \not{k}], \not{p_2}] - [\not{\varepsilon}, \not{k}]\,\not{k} + 2M[\not{\varepsilon}, \not{k}]\}\,\not{q}\gamma_5 u(p_1) \qquad (4.88)
$$

$$
= \mathbb{B}\,\bar{u}(p_2)\{4(\not{\varepsilon}p_2 k - \not{k}p_2\varepsilon) + 2(\not{\varepsilon}k^2 - \not{k}(\varepsilon k)) + 2M[\not{\varepsilon}, \not{k}]\}\,\not{q}\gamma_5 u(p_1) \qquad (4.89)
$$

$$
= -\frac{g_A}{\sqrt{2}f_\pi}\frac{2\mu_V F_2(k^2)}{2M}\frac{1}{u - M^2}\bar{u}(p_2)\{-2(k^2 + 2p_2 k)O(V_1) - 4M[O(V_3) - O(V_4)]\}u(p_1).
$$

$$
(4.90)
$$

From Equation 4.88 to Equation 4.89 we used Equation 4.67. From Equation 4.89 to Equation 4.90 we used Equation 4.68 and:

$$
\begin{aligned}
&\bar{u}(p_2)2M[\not{\varepsilon},\not{k}]\ \not{q}\gamma_5 u(p_1)\\
=&-2M\bar{u}(p_2)\gamma_5[\not{\varepsilon},\not{k}](\not{p}_1-\not{p}_2+\not{k})u(p_1)\\
=&-2M\bar{u}(p_2)\gamma_5\left\{[\not{\varepsilon},\not{k}](M-\not{p}_2+\not{k})\right\}u(p_1)\\
=&-2M\bar{u}(p_2)\gamma_5\left\{[\not{\varepsilon},\not{k}](-M-\not{p}_2+\not{k})+2M[\not{\varepsilon},\not{k}]\right\}u(p_1)\\
=&-2M\bar{u}(p_2)\gamma_5\left\{[\not{p}_2,[\not{\varepsilon},\not{k}]]+\not{k}[\not{\varepsilon},\not{k}]+2M[\not{\varepsilon},\not{k}]\right\}u(p_1)\\
=&-4M\bar{u}(p_2)\gamma_5\left\{2((p_2\varepsilon)\not{k}-(p_2k)\not{\varepsilon})-((\varepsilon k)\not{k}-k^2\not{\varepsilon})+M[\not{\varepsilon},\not{k}]\right\}u(p_1)\\
=&-4M\bar{u}(p_2)\gamma_5\left\{\not{k}(-k+2p_2)\varepsilon)-\not{\varepsilon}(-k+2p_2)k+M[\not{\varepsilon},\not{k}]\right\}u(p_1)\\
=&-4M\bar{u}(p_2)\gamma_5\left\{\not{k}(-q+2P)\varepsilon)-\not{\varepsilon}(-q+2P)k+M[\not{\varepsilon},\not{k}]\right\}u(p_1)\\
=&-4M\bar{u}(p_2)\gamma_5\left\{O(V3)-O(V_4)\right\}u(p_1)
\end{aligned}
\tag{4.91}
$$

and Equation 4.81 can be expanded over $O(A_k)$ by using Equation 4.72 - 4.73:

$$
\frac{g_A}{\sqrt{2}f_\pi}\,G_A(k^2)\frac{1}{u-M^2}\,\bar{u}(p_2)\left(\not{\varepsilon}\gamma_5+\frac{\not{k}}{m_\pi^2-k^2}(\varepsilon k)\gamma_5\right)(\not{p}_2-\not{k}+M)\ \not{q}\gamma_5 u(p_1)
$$

$$
\frac{g_A}{\sqrt{2}f_\pi}\,G_A(k^2)\frac{1}{u-M^2}\,\bar{u}(p_2)\left(\not{\varepsilon}+\frac{\not{k}}{m_\pi^2-k^2}(\varepsilon k)\right)(\not{p}_2-\not{k}-M)\ \not{q}u(p_1)
$$

$$
\frac{g_A}{\sqrt{2}f_\pi}\,G_A(k^2)\frac{1}{u-M^2}\,\bar{u}(p_2)\left(\not{\varepsilon}+\frac{\not{k}}{m_\pi^2-k^2}(\varepsilon k)\right)(\not{p}_1-\not{q}-M)\ \not{q}u(p_1)
\tag{4.92}
$$

$$
\begin{aligned}
=&\frac{g_A}{\sqrt{2}f_\pi}\,G_A(k^2)\,\bar{u}(p_2)\left\{\frac{-2M}{u-M^2}[O(A_1)-O(A_3)]-\frac{1}{M}O(A_4)-\frac{1}{m_\pi^2-k^2}\right.\\
&\left.\left[\left(1+\frac{4M^2}{u-M^2}\right)O(A_8)-2MO(A_7)\right]\right\}u(p_1).
\end{aligned}
\tag{4.93}
$$

From Equation 4.92 to Equation 4.93 we use:

$$
\begin{aligned}
&\bar{u}(p_2)\left\{\not{\varepsilon}(\not{p}_1-\not{q}-M)\ \not{q}\right\}u(p_1)\\
=&\bar{u}(p_2)\left\{\not{\varepsilon}(\not{p}_1\not{q}-M\not{q}-m_\pi^2)\right\}u(p_1)\\
=&\bar{u}(p_2)\left\{\not{\varepsilon}(-\not{q}\not{p}_1+2p_1q-M\not{q}-m_\pi^2)\right\}u(p_1)\\
=&\bar{u}(p_2)\left\{-2M\not{\varepsilon}\not{q}+(2p_1q-m_\pi^2)\not{\varepsilon}\right\}u(p_1)\\
=&\bar{u}(p_2)\left\{-M(\not{\varepsilon}\not{q}-\not{q}\not{\varepsilon}+2\varepsilon q)-(u-M^2)\not{\varepsilon}\right\}u(p_1)\\
=&\bar{u}(p_2)\left\{2M(-O(A_1)+O(A_3))-(u-M^2)\frac{1}{M}O(A_4)\right\}u(p_1)
\end{aligned}
\tag{4.94}
$$

and

$$\bar{u}(p_2)\left\{\slashed{k}(\slashed{p}_1-\slashed{q}-M)\,\slashed{q}\right\}(\varepsilon k)u(p_1)$$
$$=\bar{u}(p_2)\left\{\slashed{k}(\slashed{p}_1\slashed{q}-M\slashed{q}-m_\pi^2)\right\}(\varepsilon k)u(p_1)$$
$$=\bar{u}(p_2)\left\{\slashed{k}(-\slashed{q}\slashed{p}_1+2p_1q-M\slashed{q}-m_\pi^2)\right\}(\varepsilon k)u(p_1)$$
$$=\bar{u}(p_2)\left\{-2M\,\slashed{k}\,\slashed{q}+(2p_1.q-m_\pi^2)\,\slashed{k}\right\}\varepsilon k u(p_1)$$
$$=\bar{u}(p_2)\left\{-2M\,\slashed{k}(\slashed{k}+\slashed{p}_1-\slashed{p}_2-(u-M^2)\,\slashed{k}\right\}\varepsilon k u(p_1)$$
$$=\bar{u}(p_2)\left\{-2M(k^2+M\,\slashed{k}-\slashed{k}\,\slashed{p}_2)-(u-M^2)\,\slashed{k}\right\}\varepsilon k u(p_1)$$
$$=\bar{u}(p_2)\left\{-2M(k^2+M\,\slashed{k}+\slashed{p}_2\,\slashed{k}-2kp_2)-(u-M^2)\,\slashed{k}\right\}\varepsilon k u(p_1)$$
$$=\bar{u}(p_2)\left\{-2M(u-M^2)-4M^2\,\slashed{k}-(u-M^2)\,\slashed{k}\right\}\varepsilon k u(p_1)$$
$$=\bar{u}(p_2)\left\{-(4M^2+(u-M^2))O(A_8)-2M(u-M^2)O(A_7)\right\}u(p_1)\,notcompleted \quad (4.95)$$

Now we will take into account $\langle e^\rho J_\rho^{PF}\rangle^{p\pi^+}$, and the vector part of $\langle e^\rho J_\rho^{CT}\rangle^{p\pi^+}$, and the remaining term from Equation 4.79, and using Equation 4.53:

$$+\frac{g_A}{\sqrt{2}f_\pi}\frac{1}{t-m_\pi^2}F_{PF}(k^2)\bar{u}(p_2)\,2M[2q\varepsilon-k\varepsilon]\gamma_5\,u(p_1)+\frac{q_A}{\sqrt{2}f_\pi}F_{CT}^V\,\bar{u}(p_2)\,\slashed{\varepsilon}\,\gamma_5\,u(p_1)$$
$$-\frac{g_A}{\sqrt{2}f_\pi}2F_1(k^2)\,\bar{u}(p_2)\frac{q\varepsilon}{qk}\,\slashed{q}\gamma_5 u(p_1)$$
$$=\frac{g_A}{\sqrt{2}f_\pi}\frac{1}{t-m_\pi^2}F(k^2)\bar{u}(p_2)\left\{2M(2\varepsilon q-k\varepsilon)+(t-m_\pi^2)(-\frac{q\varepsilon}{qk}\,\slashed{q}+\slashed{\varepsilon})\right\}\gamma_5 u(p_1)$$
$$=\frac{g_A}{\sqrt{2}f_\pi}F(k^2)\frac{1}{t-m_\pi^2}\frac{1}{qk}\bar{u}(p_2)\left\{2M(qk)(2q-k)\varepsilon+(k^2-2qk)(-q\varepsilon(\slashed{k}-2M)+(qk)\,\slashed{\varepsilon})\right\}\gamma_5 u(p_1)$$
$$=\frac{g_A}{\sqrt{2}f_\pi}F(k^2)\frac{1}{t-m_\pi^2}\frac{1}{qk}\bar{u}(p_2)\left\{2M(qk)(2q-k)\varepsilon+2M(k-2q)k(q\varepsilon)+(k^2-2qk)[-q\varepsilon\,\slashed{k}+(qk)\,\slashed{\varepsilon}]\right\}\gamma_5 u($$
$$=\frac{g_A}{\sqrt{2}f_\pi}\bar{u}(p_2)\left\{-\frac{F}{qk}O(V_3)+\frac{F}{t-m_\pi^2}\frac{2M}{qk}O(V_5)\right\}u(p_1) \quad (4.96)$$

The last step is $\langle e^\rho J_\rho^{PP}\rangle^{p\pi^+}$ and the axial part of the contact term $\langle e^\rho J_\rho^{CT}\rangle^{p\pi^+}$, which are related to $F_\rho((k-q)^2)$:

$$\frac{1}{\sqrt{2}f_\pi}F_\rho((k-q)^2)\bar{u}(p_2)\left[\slashed{\varepsilon}-(\varepsilon k)\frac{\slashed{k}}{k^2-m_\pi}\right]u(p_1)$$
$$=\frac{1}{\sqrt{2}f_\pi}F_\rho((k-q)^2)\bar{u}(p_2)\left[\frac{1}{M}O(A_4)+\frac{1}{k^2-m_\pi}O(A_8)\right]u(p_1) \quad (4.97)$$

Therefore using Equation 4.81- 4.97 and comparing with Equation 4.54, we can extract the invariant amplitudes of $\nu p \to \mu p \pi^+$

$$
\begin{aligned}
V_1^{p\pi+} &= \frac{g_A}{\sqrt{2}f_\pi}\left(\frac{4M}{s-M^2}F_1(k^2)+\frac{2\mu_V F_2(k^2)}{M}\right) \\
V_2^{p\pi+} &= \frac{g_A}{\sqrt{2}f_\pi}\frac{1}{qk}\frac{4M}{u-M^2}F_1(k^2) \\
V_3^{p\pi+} &= \frac{g_A}{\sqrt{2}f_\pi}\left(\frac{4}{u-M^2}\mu_V F_2(k^2)\right) \\
V_4^{p\pi+} &= -\frac{g_A}{\sqrt{2}f_\pi}\frac{4}{u-M^2}\mu_V F_2(k^2) \\
V_5^{p\pi+} &= \frac{g_A}{\sqrt{2}f_\pi}\frac{1}{qk}\frac{2M}{t-m_\pi}F_\pi(k^2)
\end{aligned}
\tag{4.98}
$$

$$
\begin{aligned}
A_1^{p\pi+} &= \frac{g_A}{\sqrt{2}f_\pi}\frac{2M}{u-M^2}G_A(k^2) \\
A_3^{p\pi+} &= -\frac{g_A}{\sqrt{2}f_\pi}\left(\frac{2M}{u-M^2}G_A(k^2)\right) \\
A_4^{p\pi+} &= -\frac{g_A}{\sqrt{2}f_\pi}\frac{1}{M}G_A(k^2)+\frac{1}{\sqrt{2}Mf_\pi}F_\rho\left((k-q)^2\right) \\
A_7^{p\pi+} &= -\frac{g_A}{\sqrt{2}f_\pi}\frac{2M}{m_\pi^2-k^2}G_A(k^2) \\
A_8^{p\pi+} &= \frac{g_A}{\sqrt{2}f_\pi}\frac{1}{m_\pi^2-k^2}\left(1+\frac{4M^2}{u-M^2}\right)G_A(k^2)-\frac{1}{\sqrt{2}f_\pi}\frac{1}{m_\pi^2-k^2}F_\rho\left((k-q)^2\right)
\end{aligned}
\tag{4.99}
$$

Isospin symmetry (see A) allows us to find $V_k^{p\pi^0}$ in terms of $V_k^{p\pi^+}$ and $V_k^{n\pi^+}$, and similarly for $A_k^{p\pi^0}$:

$$
\begin{aligned}
V_k^{p\pi^0} &= -\frac{1}{\sqrt{2}}\left[V_k^{p\pi^+}-V_k^{n\pi^+}\right] \\
A_k^{p\pi^0} &= -\frac{1}{\sqrt{2}}\left[A_k^{p\pi^+}-A_k^{n\pi^+}\right]
\end{aligned}
\tag{4.100}
$$

Knowing the invariant amplitudes one can calculate the isobaric amplitudes $\mathscr{F}_k$ and $\mathscr{G}_k$, from Appendix D, and the derivation of helicity amplitudes is straightforward from Equation 3.49 - 3.56 for nonresonant contribution.

Before finishing this section it worth to mention that nonresonant interaction is different in [9] with what we introduced here, in many aspects. For instance, the nonresonant interaction

in [9] is based on 3 Born diagrams which are results of linear sigma model with PS coupling. therefore the transition amplitudes are different than what are given in Equation 4.47. As a result, the invariant amplitudes should be different.

4.2.2   Neutral Current interactions

Pion can also be produced via NC interactions, accompanied by an outgoing nucleon and a neutrino. Transition amplitude and lepton current are given in Equation 3.8. The resonance production amplitudes for NC interactions ($f^{NC}_{\pm3,\pm1}$) are given in [7] and also in Appendix G. One only needs to substitute them in Equation 4.39 for the resonant contribution with proper isospin coefficients from Table 4.1.

Detailed calculation for nonresonant interactions is given in [10], however, we will briefly talk about it in this section. Thanks to isospin symmetry, we can relate NC interaction to the CC interactions we have discussed in the previous chapter.

In terms of hadron current, the differences are isospin coefficients and the fact that the parity does not break maximally unlike CC interactions. Instead, vector and axial vector currents multiply to a factor related to the Weinberg angle ($\sin\theta_W = 0.231$).

Neutral hadron current at quark level is:

$$
\begin{aligned}
J^{\rho}_{NC} = & \bar{\psi}_u \gamma^{\rho} \left(1 - \frac{8}{3}\sin\theta_W - \gamma_5\right)\psi_u - \bar{\psi}_d \gamma^{\rho}\left(1 - \frac{4}{3}\sin\theta_W - \gamma_5\right)\psi_d \\
& - \bar{\psi}_s \gamma^{\rho}\left(1 - \frac{4}{3}\sin\theta_W - \gamma_5\right)\psi_s
\end{aligned}
\tag{4.101}
$$

Equation 4.101 can be expressed as:

$$
J^{\rho}_{NC} = \bar{\psi}_q \gamma^{\rho}\left(1 - 2\sin\theta_W - \gamma_5\right)\tau_3 \psi_q - 4\sin^2\theta_W s^{\rho}_{em,IS} - \bar{\psi}_s \gamma^{\rho}\left(1 - \gamma_5\right)\psi_s
\tag{4.102}
$$

where $\psi_q = \begin{pmatrix} \psi_u \\ \psi_d \end{pmatrix}$ and τ_3 is Pauli matrix given in Appendix A. The isoscalar part (second term) of the electromagnetic current is:

$$
s^{\rho}_{em,IS} = \frac{1}{6}\bar{\psi}_q \gamma^{\rho}\psi_q - \frac{1}{3}\bar{\psi}_s \gamma^{\rho}\psi_s.
\tag{4.103}
$$

Isospin symmetry enable us to relate the isovector (first) term of Equation 4.102 to the charged-current SPP channels (Table A.0.3):

$$
\begin{aligned}
\langle\, p\pi^0|\bar{\psi}_q\gamma^\rho\left(1-2\sin\theta_W-\gamma_5\right)\tau_3\psi_q|p\,\rangle &= \frac{1}{\sqrt{2}}\Big\{\left(1-2\sin\theta_W\right)\big[\langle\, p\pi^+|\,V_{CC}^\rho\,|p\,\rangle \\
&\quad +\langle\, n\pi^+|\,V_{CC}^\rho\,|n\,\rangle\big]-\big[\langle\, p\pi^+|\,A_{CC}^\rho\,|p\,\rangle+\langle\, n\pi^+|\,A_{CC}^\rho\,|n\,\rangle\big]\Big\} \\
\langle\, n\pi^+|\bar{\psi}_q\gamma^\rho\left(1-2\sin\theta_W-\gamma_5\right)\tau_3\psi_q|p\,\rangle &= -\Big\{\left(1-2\sin\theta_W\right)\big[\langle\, p\pi^+|\,V_{CC}^\rho\,|p\,\rangle \\
&\quad -\langle\, n\pi^+|\,V_{CC}^\rho\,|n\,\rangle\big]-\big[\langle\, p\pi^+|\,A_{CC}^\rho\,|p\,\rangle-\langle\, n\pi^+|\,A_{CC}^\rho\,|n\,\rangle\big]\Big\} \\
\langle\, n\pi^0|\bar{\psi}_q\gamma^\rho\left(1-2\sin\theta_W-\gamma_5\right)\tau_3\psi_q|n\,\rangle &= \langle\, p\pi^0|\bar{\psi}_q\gamma^\rho\left(1-2\sin\theta_W-\gamma_5\right)\tau_3\psi_q|p\,\rangle \\
\langle\, p\pi^-|\bar{\psi}_q\gamma^\rho\left(1-2\sin\theta_W-\gamma_5\right)\tau_3\psi_q|n\,\rangle &= -\langle\, n\pi^+|\bar{\psi}_q\gamma^\rho\left(1-2\sin\theta_W-\gamma_5\right)\tau_3\psi_q|p\,\rangle
\end{aligned}
\tag{4.104}
$$

As it is explained in [10], isospin symmetry can also relate the isoscalar term to the charged-current SPP channels like Equation 4.102, with an extra minus for $\nu n \to \nu n\pi^0$ and $\nu n \to \nu p\pi^-$ channels that is explained in Appendix A, therefore:

$$
\langle\, n\pi^+|s_{em,IS}^\rho\,|p\,\rangle = \langle\, p\pi^-|s_{em,IS}^\rho\,|n\,\rangle = \sqrt{2}\langle\, p\pi^0|s_{em,IS}^\rho\,|p\,\rangle = -\sqrt{2}\langle\, n\pi^0|s_{em,IS}^\rho\,|n\,\rangle \tag{4.105}
$$

For isoscalar electromagnetic current, only nucleon pole diagrams can contribute according to [10]

$$
\begin{aligned}
\langle\, p\pi^0|s_{em,IS}^\rho\,|p\,\rangle = -i\frac{g_A}{2f_\pi}\bar{u}(p_2)\Bigg\{&\not{q}\gamma_5\frac{\not{p}_1+\not{k}+M}{(p_1+k)^2-M^2+i\delta}\left[F_1^{IS}(k^2)\gamma^\rho+i\mu_{IS}\frac{F_2^{IS}}{2M}\sigma^{\rho\lambda}k_\lambda\right] \\
&+\left[F_1^{IS}(k^2)\gamma^\rho+i\mu_{IS}\frac{F_2^{IS}}{2M}\sigma^{\rho\lambda}k_\lambda\right]\frac{\not{p}_2-\not{k}+M}{(p_2-k)^2-M^2+i\delta}\not{q}\gamma_5\Bigg\}u(p_1)
\end{aligned}
\tag{4.106}
$$

where

$$
\begin{aligned}
F_1^{IS}(k^2) &= \frac{1}{2}[F_1^p(k^2)+F_1^n(k^2)], \\
\mu_{IS}F_2^{IS}(k^2) &= \frac{1}{2}[\mu_p F_2^p(k^2)+\mu_n F_2^n(k^2)],
\end{aligned}
\tag{4.107}
$$

with the Galster parametrization given in Equation 4.50. From Equation 4.105 it is straightforward to calculate the isoscalar electromagnet current for other channels.

Isoscalar operator $\bar{\psi}_s\gamma^\rho\left(1-\gamma_5\right)\psi_s$ is sensitive to the strange content of hadrons, with simple

relation between different channels:

$$\langle\, n\pi^+|\bar{\psi}_s\gamma^\rho\left(1-\gamma_5\right)\psi_s|p\,\rangle = \langle\, p\pi^-|\bar{\psi}_s\gamma^\rho\left(1-\gamma_5\right)\psi_s|n\,\rangle$$
$$= \sqrt{2}\langle\, p\pi^0|\bar{\psi}_s\gamma^\rho\left(1-\gamma_5\right)\psi_s|p\,\rangle$$
$$= -\sqrt{2}\langle\, n\pi^0|\bar{\psi}_s\gamma^\rho\left(1-\gamma_5\right)\psi_s|n\,\rangle \tag{4.108}$$

and again only nucleon pole diagrams can contribute

$$\langle\, p\pi^0|\bar{\psi}_s\gamma^\rho\left(1-\gamma_5\right)\psi_s|p\,\rangle =$$
$$-i\frac{g_A}{2f_\pi}\bar{u}(p_2)\Bigg\{ \slashed{q}\gamma_5\frac{\slashed{p}_1+\slashed{k}+M}{(p_1+k)^2-M^2+i\delta}\left[F_1^s(k^2)\gamma^\rho+i\mu_s\frac{F_2^s}{2M}\sigma^{\rho\lambda}k_\lambda-G_A^s\gamma^\rho\gamma_5\right]$$
$$+\left[F_1^s(k^2)\gamma^\rho+i\mu_s\frac{F_2^s}{2M}\sigma^{\rho\lambda}k_\lambda-G_A^s\gamma^\rho\gamma_5\right]\frac{\slashed{p}_2-\slashed{k}+M}{(p_2-k)^2-M^2+i\delta}\,\slashed{q}\gamma_5\Bigg\}u(p_1) \tag{4.109}$$

where F_1^s, F_2^s and G_A^s are the strange vector and axial nucleon form factors, and from [10]

$$G_A^s(k^2) = \frac{g_s}{(1-k^2/(M_A^s)^2)^2}, \qquad F_1^s(k^2) = \mu_s F_2^s(k^2) = 0, \tag{4.110}$$

with $g_s = -0.15$ and $M_A^s = M_A = 1.05$ GeV.

4.3 Resonance Contribution and Nonresonant Background

In chapter 3, we defined the general form of the differential cross-section in terms of helicity amplitudes, and in this chapter, the helicity amplitudes of resonant and nonresonant interactions are given. They provide us with everything about neutrino-nucleon single pion production via resonance excitation and nonresonant interaction, however we need to know how to add the different helicity amplitudes.

A primary constraint on the pion production amplitudes is Watson theorem, which is derived by assuming unitarity. The RS model [7] violates Watson theorem because it is not a unitarized model. As we discussed before in section 4.1, we take into account 17 resonances from RS model. Helicity amplitudes of a resonance is a complex amplitudes due to a complex Breit-Wigner amplitudes, but it is unitarized, i.e.

$$A = |A|e^{i\delta} \tag{4.111}$$

where A is a multipole part of the amplitudes for definite quantum number that is explained in subsection 3.2.1.

All resonant and nonresonant multipoles are unitarized individually, but they are not unitarized as a model unless you define proper phases to make it unitarized [37]. Therefore RS model is not unitarized above Δ region ($W > 1.4 GeV$).

Now assume you have only one resonance and nonresonant multipoles (A_R and A_B), with phase δ_R and δ_B:

$$A = |A_B| \exp[i\delta_B] + |A_R| \exp[i(\delta_R + \phi)]. \tag{4.112}$$

The phase ϕ should be constrained such that Equation 4.111 is satisfied.

$$A = |A_R| \{ \chi \exp[i\delta_B] + \exp[i(\delta_R + \phi)] \} \tag{4.113}$$

where $\chi = |A_B|/|A_R|$. Now we assume $\delta_B = \delta_R - \delta$:

$$
\begin{aligned}
A &= |A_R| \{ \chi \exp[i\delta_B] + \exp[i(\delta_B + \delta + \phi)] \} \\
&= |A_R| \{ \chi \exp[i(\delta_B - \delta)] + \exp[i(\delta_B + \phi)] \} e^{i\delta}
\end{aligned}
\tag{4.114}
$$

To satisfy Equation 4.111, the curly bracket in Equation 4.114 should be real:

$$
\begin{aligned}
\sin(\delta_B + \phi) &= \chi \sin(\delta - \delta_B) \\
\delta_B + \phi &= \sin^{-1}[\chi \sin(\delta - \delta_B)] \\
\phi &= -\delta_B + \sin^{-1}[\chi \sin(\delta - \delta_B)]
\end{aligned}
\tag{4.115}
$$

In our case the nonresonant background multipoles are real and $\delta_B = 0$ and $\delta = \delta_R$, therefore:

$$\phi = \sin^{-1}[\chi \sin(\delta_R)] \tag{4.116}$$

In the described model with 17 resonances and nonresonant background, it is not practical to calculate all phases between multipoles.

4.4 Summary

The theoretical calculation of the proposed model was given in chapter 3 and in this chapter. The general definition for helicity amplitudes and cross-section derivations was given in chapter 3. In section 4.1, the helicity amplitudes of the resonances were given by using

Equation 3.82 and the RS model. In section 4.2 we derived the helicity amplitudes of the
five diagrams introduced in [10] for the nonresonant interaction. We also discussed about the
isospin coefficients for charged and neutral-currents, resonant and nonresonant interactions.
Knowing the cross-section in Equation 3.60, and the helicity amplitudes with proper isospin
coefficients for different channels, one can calculate a full kinematics differential cross-
section for all channels in Equation 3.1 - 3.4, as a function of W, Q^2 and θ, ϕ in the isobaric
frame and neutrino energy (E_ν) in the lab frame. The model proposed in these chapters
has a very suitable format for implementation. One can easily write a program to get the
numerical value of the differential cross-sections in order to compare the model predictions
with available data. This is going to be discussed in the next chapter.

Table 4.1 Properties of resonances below $2GeV/c^2$ from [78].

Resonance	M_R	Γ_0	χ_E	σ^D	N
$P_{33}(1232)$	1232	117	1	+	0
$P_{11}(1440)$	1430	350	0.65	+	2
$D_{13}(1520)$	1515	115	0.60	-	1
$S_{11}(1535)$	1535	150	0.45	-	1
$P_{33}(1600)$	1600	320	0.18	+	2
$S_{31}(1620)$	1630	140	0.25	+	1
$S_{11}(1650)$	1655	140	0.70	+	1
$D_{15}(1675)$	1675	150	0.40	+	1
$F_{15}(1680)$	1685	130	0.67	+	2
$D_{13}(1700)$	1700	150	0.12	-	1
$D_{33}(1700)$	1700	300	0.15	+	1
$P_{11}(1710)$	1710	100	0.12	-	2
$P_{13}(1720)$	1720	250	0.11	+	2
$F_{35}(1905)$	1880	330	0.12	-	2
$P_{31}(1910)$	1890	280	0.22	-	2
$P_{33}(1920)$	1920	260	0.12	+	2
$F_{37}(1950)$	1930	285	0.40	+	2

resonances are identified with isospin (I) and angular momentum (j); $L_{2I,2j}(M_R)$, where M_R are old measurements for averaged Breit-Wigner mass and we kept them for identification but the updated mass is also given.

Table 4.2 Isospin coefficients for RS model CC and NC (anti-)neutrino channels.

ν Channels	$\bar\nu$ Channels	$C_{N\pi}^{3/2}$	$C_{N\pi}^{1/2}$
$\nu p \to l^- p\pi^+$	$\bar\nu n \to l^+ n\pi^-$	$\sqrt{3}$	0
$\nu n \to l^- p\pi^0$	$\bar\nu p \to l^+ n\pi^0$	$-\sqrt{\frac{2}{3}}$	$\sqrt{\frac{1}{3}}$
$\nu n \to l^- n\pi^+$	$\bar\nu p \to l^+ p\pi^-$	$\sqrt{\frac{1}{3}}$	$\sqrt{\frac{2}{3}}$
$\nu p \to \nu p\pi^0$	$\bar\nu p \to \bar\nu p\pi^0$	$\sqrt{\frac{2}{3}}$	$-\sqrt{\frac{1}{3}}$
$\nu p \to \nu n\pi^+$	$\bar\nu p \to \bar\nu n\pi^+$	$-\sqrt{\frac{1}{3}}$	$-\sqrt{\frac{2}{3}}$
$\nu n \to \nu n\pi^0$	$\bar\nu n \to \bar\nu n\pi^0$	$\sqrt{\frac{2}{3}}$	$\sqrt{\frac{1}{3}}$
$\nu n \to \nu p\pi^-$	$\bar\nu n \to \bar\nu p\pi^-$	$\sqrt{\frac{1}{3}}$	$-\sqrt{\frac{2}{3}}$

Table 4.3 Symmetry relation among standard helicity amplitudes

Vector	Axial vector
$F_{-\frac{1}{2}-\frac{1}{2}} = -F_{\frac{1}{2}\frac{1}{2}}$	$G_{-\frac{1}{2}-\frac{1}{2}} = G_{\frac{1}{2}\frac{1}{2}}$
$F_{-\frac{1}{2}-\frac{3}{2}} = e^{-2i\phi}F_{\frac{1}{2}\frac{3}{2}}$	$G_{-\frac{1}{2}-\frac{3}{2}} = -e^{-2i\phi}G_{\frac{1}{2}\frac{3}{2}}$
$F_{\frac{1}{2}-\frac{1}{2}} = e^{-2i\phi}F_{-\frac{1}{2}\frac{1}{2}}$	$G_{\frac{1}{2}-\frac{1}{2}} = -e^{-2i\phi}G_{-\frac{1}{2}\frac{1}{2}}$
$F_{\frac{1}{2}-\frac{3}{2}} = -e^{-4i\phi}F_{-\frac{1}{2}\frac{3}{2}}$	$G_{-\frac{1}{2}\frac{3}{2}} = e^{-4i\phi}G_{-\frac{1}{2}\frac{3}{2}}$
$F^{(\pm)0}_{-\frac{1}{2}-\frac{1}{2}} = -F^{(\pm)0}_{\frac{1}{2}\frac{1}{2}}$	$G^{(\pm)0}_{-\frac{1}{2}-\frac{1}{2}} = G^{(\pm)0}_{\frac{1}{2}\frac{1}{2}}$
$F^{(\pm)0}_{-\frac{1}{2}\frac{1}{2}} = e^{2i\phi}F^{(\pm)0}_{\frac{1}{2}-\frac{1}{2}}$	$G^{(\pm)0}_{-\frac{1}{2}\frac{1}{2}} = -e^{2i\phi}G^{(\pm)0}_{\frac{1}{2}-\frac{1}{2}}$

Table 4.4 Symmetry relations between Helicity Amplitudes $\tilde{F}_{\lambda_2\lambda_1}(\theta,\phi)$, $\tilde{G}_{\lambda_2\lambda_1}(\theta,\phi)$

Vector	Axial vector
$\tilde{F}^{e_L}_{\frac{1}{2}\frac{1}{2}} = e^{-4i\phi}\tilde{F}^{e_R}_{-\frac{1}{2}-\frac{1}{2}}$	$\tilde{G}^{e_L}_{\frac{1}{2}\frac{1}{2}} = -e^{-4i\phi}\tilde{G}^{e_R}_{-\frac{1}{2}-\frac{1}{2}}$
$\tilde{F}^{e_L}_{-\frac{1}{2}\frac{1}{2}} = -e^{-2i\phi}\tilde{F}^{e_R}_{\frac{1}{2}-\frac{1}{2}}$	$\tilde{G}^{e_L}_{-\frac{1}{2}\frac{1}{2}} = e^{-2i\phi}\tilde{G}^{e_R}_{\frac{1}{2}-\frac{1}{2}}$
$\tilde{F}^{e_L}_{\frac{1}{2}-\frac{1}{2}} = -e^{-2i\phi}\tilde{F}^{e_R}_{-\frac{1}{2}\frac{1}{2}}$	$\tilde{G}^{e_L}_{\frac{1}{2}-\frac{1}{2}} = e^{-2i\phi}\tilde{G}^{e_R}_{-\frac{1}{2}\frac{1}{2}}$
$\tilde{F}^{e_L}_{-\frac{1}{2}-\frac{1}{2}} = \tilde{F}^{e_R}_{\frac{1}{2}\frac{1}{2}}$	$\tilde{G}^{e_L}_{-\frac{1}{2}-\frac{1}{2}} = -\tilde{G}^{e_R}_{\frac{1}{2}\frac{1}{2}}$
$\tilde{F}^{e-}_{\frac{1}{2}\frac{1}{2}} = -e^{-2i\phi}\tilde{F}^{e-}_{-\frac{1}{2}frac12}$	$\tilde{G}^{e-}_{\frac{1}{2}\frac{1}{2}} = e^{-2i\phi}\tilde{\tilde{G}}^{e-}_{-\frac{1}{2}-\frac{1}{2}}$
$\tilde{F}^{e-}_{-\frac{1}{2}\frac{1}{2}} = \tilde{F}^{e-}_{\frac{1}{2}-\frac{1}{2}}$	$\tilde{G}^{e-}_{-\frac{1}{2}\frac{1}{2}} = -\tilde{G}^{e-}_{\frac{1}{2}-\frac{1}{2}}$

Table 4.5 Isospin coefficients for neutrino and anti-neutrino channels.

CC Channels	C_{NP}	C_{CNP}	C_{PF}	C_{CT}	C_{PP}
$\nu p \to l^- p \pi^+$	0	1	1	1	1
$\nu n \to l^- p \pi^0$	$\frac{1}{\sqrt{2}}$	$-\frac{1}{\sqrt{2}}$	$-\sqrt{2}$	$-\sqrt{2}$	$-\sqrt{2}$
$\nu n \to l^- n \pi^+$	1	0	-1	-1	-1
$\bar{\nu} n \to l^+ n \pi^-$	0	1	1	1	1
$\bar{\nu} p \to l^+ n \pi^0$	$-\frac{1}{\sqrt{2}}$	$\frac{1}{\sqrt{2}}$	$\sqrt{2}$	$\sqrt{2}$	$\sqrt{2}$
$\bar{\nu} p \to l^+ p \pi^-$	1	0	-1	-1	-1

Chapter 5

Model predictions for free nucleon and Data comparisons

The model described in the previous chapters has full kinematics description (including pion angles) of the final state particles for charged and neutral-current (anti-)neutrino-nucleon interactions. It has been calculated in the helicity basis which is very suitable for implementation, and very fast.

The model has been implemented as Cross-Section Calculation (CSC) code using $C++$ by the author of this thesis. The CSC code is capable of returning the differential cross-section (given in Equation 3.60), by knowing W, Q^2 and θ, ϕ in the isobaric frame and energy (E_ν) in the lab frame. Differential (total) cross-section can be calculated as a function of any of the variable(s) [1]. It includes all (anti-)neutrino charged and neutral-current channels illustrated in Equation 3.1 - 3.4, for free nucleon.

The resonance part of the model (which is the RS model) includes resonances up to $M_R = 2 GeV$ (see Table 4.1), therefore it is valid up to $W = 2$ GeV. For nonresonant interactions and as we mentioned before the model is based on the chiral symmetry and it is not reliable at high energy and high W. A practical solution to have a complete model with resonant and nonresonant interactions, is to multiply a form-factor to the virtual pion propagator of PIF diagram in Figure 4.1, in order to reduce the nonresonant contributions, smoothly, in the 1.4 GeV $\leq W \leq$ 1.6 GeV region.

$$F_{vir}(W) = \begin{cases} 1 & \text{if } W < 1.4 \text{ GeV} \\ -23.31W^2 + 64.92W - 44.2 & \text{if } 1.4 \text{ GeV} \leq W \leq 1.6 \text{ GeV} \\ 0 & \text{if } W > 1.6 \text{ GeV} \end{cases} \qquad (5.1)$$

---

[1]The code for integrating by part was written by Dr. Zmuda from Wroclaw University.

The conservation of vector current (CVC) requires to include this form factor in several other amplitudes (see Appendix H), therefore nonresonant interaction will have no effect at $W \geq 1.6$ GeV.

The model for resonant interaction contains form-factors. the vector form factors can be related to the electromagnetic form factors measured in electron-nucleon elastic scattering experiments. The axial form-factor should be extracted from neutrino-nucleon data. Therefore we firs need to fit the resonance's axial form-factor (Equation 4.45) with two adjustable parameters M_A and $C_5^A(0)$ to the neutrino data. This is the first job we should do before any data comparison.

Then we will discuss about the resonance's signs (σ_D introduced in subsection 4.1.2) in subsection 5.2.2.

For the rest of this chapter, we show the comparison between model prediction and all available measurements for neutrino Energy (E_ν), invariant mass W and pion angular distribution (θ, ϕ) on free nucleon.

5.1   Bubble chamber experiments

Several experiments have studied single pion production interactions with neutrino and anti-neutrino beam at various incident energies. Almost all of them measure the total cross-section, and some of them also measure the differential cross-section in terms of Q^2, W, θ and ϕ or they only report the number of events distributions. Here we give a brief summary of the bubble chamber experiments which we will use their measurements for the model comparison.

- **ANL** The experiment was performed at the Zero Gradient Synchrotron using the wide-band neutrino beam incident on the Argonne 12 ft (3.6 m) bubble chamber filled with hydrogen and deuterium. The neutrino energy spectrum peaks at 0.5 GeV and has a tail extending to 6 GeV. The chamber has been in operation for physics runs from September 1970 to October 1979.

  Data we are using in this work is from 1115 selected evens published in [38] for three CC neutrino channels (Equation 3.1). ANL also has selected a few events for NC exclusive channels and the data in this work is from [43, 44]. The measurements have been done with 47 and 25 signal events for $\nu p \pi^-$ and $\nu n \pi^+$ final states respectively.

- **BNL** The experiment was carried out at Brookhaven National Laboratory using the 7 ft (~ 2.1 m) bubble chamber filled with deuterium and the Alternating Gradient Synchrotron (AGS) wide-band neutrino beam peaked at 1.2 GeV and extended up to
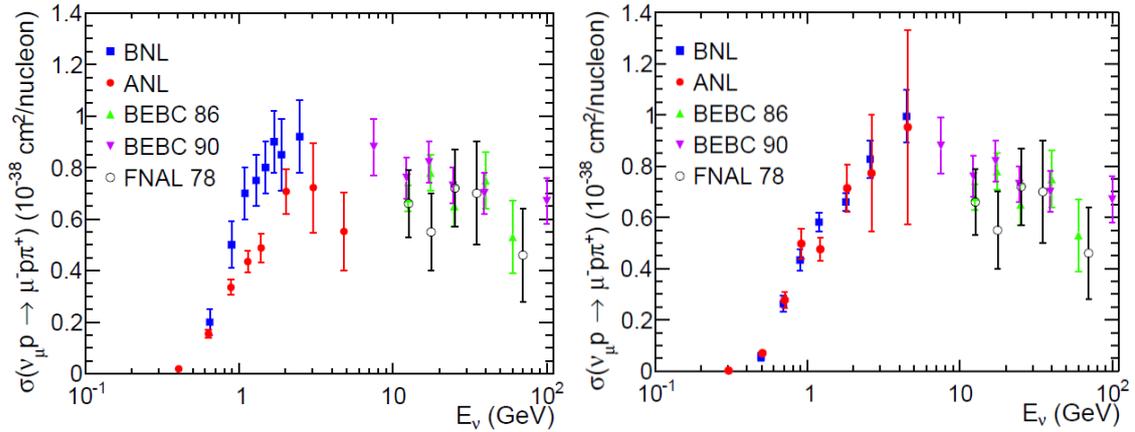
Fig. 5.1 The published (left) and extracted (right) ANL [38] and BNL [39] data are compared with other measurements of $\nu p \rightarrow \mu p \pi^+$ on hydrogen or deuterium targets. Pictures are taken from [53]

15 GeV.

Data in this work is from [39] for three CC neutrino channels. The measurement has been done on 1803 $\mu^- p p i^+$, 896 $\mu^- p \pi^0$ and 732 $\mu^- n \pi^+$ events where they have taken from 1974 to 1984.

There is a discrepancy between ANL [38] and BNL[39] bubble chamber cross-section measurements at the same range of energy. This was first studied in Reference [52]. In Reference [54] it is shown that there is a good agreement for the ratio of number of events in $CC1pi^+$ and $CCQE$, between ANL and BNL. This suggests that the cause of the discrepancy is the flux prediction. A simple reanalysis of the ANL and BNL data which removed the flux uncertainty by taking ratios with the well understood CCQE channel found good agreement between ANL and BNL data. The published and reanalyzed data are shown in Figure 5.1.

- **BEBC** Big European Bubble Chamber (BEBC) was a cylinder with 32 m^3 volume filled with deuterium during operation. Data has been obtained duing $1977 - 1984$ in the wide band neutrino and anti-neutrino beam at Cern Super Proton Synchrotron (SPS). Almost two-thirds of obtained data were exposed to the wide band anti-neutrino beam and the rest of running with the neutrino beam. In total, 27575 ν and 16896 $\bar{\nu}$ events were obtained with the two beam settings. Data we are using in this work are the measurements for five CC (anti-)neutrino channels from [40] and [49]:

$$\nu_\mu + p \rightarrow \ \mu p \pi^+ \ , \qquad\qquad \bar{\nu}_\mu + n \rightarrow \ \mu^+ n \pi^-$$
$$\nu_\mu + n \rightarrow \ \mu p \pi^0 \ , \qquad\qquad \bar{\nu}_\mu + p \rightarrow \ \mu^+ p \pi^-$$
$$\nu_\mu + n \rightarrow \ \mu n \pi^+ \ ,$$

with an invariant mass $W < 2$ GeV cut in the hadron's final states, which is perfect for the model comparison, because the model is valid in this region.

- **FNAL** Fermilab 15 ft (~ 4.5 m)bBubble Chamber filled with hydrogen, exposed to a wide-band horn-focused neutrino beam. The neutrino event energy spectrum peaks at about 15 GeV with 90% of the spectrum below 100 GeV.
  The FNAL data [41] on a hydrogen target is selected for $\nu p \rightarrow \mu p \pi^+$ channel with an invariant mass cut of $W < 1.4$ GeV, in order to isolate the Δ contribution to the cross-section. The first run started in 1972 and the data from reference [41] is published in 1978.

- **Gargamelle** big heavy liquid bubble chamber Gargamelle ($8 \ m^3$ of visible and $\sim 3 m^3$ of fiducial volume) was filled with propane and a small admixture of heavy freon CF3Br and exposed to the CERN PS neutrino and antineutrino beam (peaked at $E_\nu \sim 1.5$ GeV). It started taking data from 1971, and the analysed data we are using here was published in 1978.
  Propane is a heavy target but it is possible to do hydrogen event study with it, and the separation of neutron-proton can be achieved for single pion production. The method is to fit events to the hydrogen hypothesis (the energy-momentum conservation). This method had been tested on a sample of reactions on bound nucleons selected by a nuclear fit, and only a few events pass through the hydrogen fit.
  Data we are using is this work is the total cross-section as a function of energy for two CC anti-neutrino channels from reference [48], and NC channels from reference [46]. The total cross-sections are deduced from the corrected number of events (246 ± 17 for $\mu^+ \pi^- p$ and 227 ± 17 for $\mu^+ \pi^- n$) taking into account the percentage of neutrons and protons in the liquid (45% and 55%, respectively). The data are with ($W < 1.4$) and without an invariant mass cut, however, due to the low energy, we are allowed to draw the data without the invariant mass cut against the model prediction with $W < 2$GeV cut.

5.2 Results for Free Nucleon

In this section, the model predictions will be compared with all available bubble chamber data, but first, we should fit the two free parameters M_A and $C_5^A(0)$ in the resonance's axial form-factor to the available data in order to have definitive predictions from the model. Then we will discuss the resonance decay's signs that have been introduced in subsection 4.1.2.

5.2.1 Fitting M_A and C_A^5

The axial form-factor of resonance interaction with two adjustable parameters (M_A and C_A^5) should be fitted to neutrino data. The dipole form-factor (Equation 4.45) is a function of Q^2, and the parameters affect both the absolute value of the cross-section and the shape of the Q^2 distribution. Therefore we need to fit the adjustable parameters to $d\sigma/dQ^2$ measurements. ANL experiment [38] provided this measurement for $\nu_\mu p \to \mu^- p \pi^+$ with the selections $0.5\,\text{GeV} < E < 6\,\text{GeV}$ and $W < 1.4\,\text{GeV}$. Furthermore ANL data shows small correction for the flux as it is shown in [54]. This is why the Q^2-differential cross-section measured by ANL experiment is chosen for the fit.[2]

To fit the axial form-factor's parameters flux[3]-averaged prediction of $d\sigma/dQ^2$ is calculated with the same cut for ANL measurement. The best value of the free parameters can be found by minimizing the χ^2 function similar to Reference [52]:

$$\chi^2(M_A, C_5^A) = \sum_{i=1}^{n} \left[\frac{\left(\frac{d\sigma}{dQ^2}\right)_i^{exp} - \left(\frac{d\sigma}{dQ^2}(M_A, C_5^A)\right)_i^{th}}{\Delta\left(\frac{d\sigma}{dQ^2}\right)_i} \right] \tag{5.2}$$

where $\left(\frac{d\sigma}{dQ^2}\right)_i^{exp}$ is the measured differential cross-section for single pion production (resonant and nonresonant) in the i-th bin with the uncertainty $\Delta\left(\frac{d\sigma}{dQ^2}\right)_i$, and $\left(\frac{d\sigma}{dQ^2}(M_A, C_5^A)\right)_i^{th}$ is the flux-averaged differential cross-section of the full model including the resonant and nonresonant interaction, in the i-th bin.

The best fit parameters are:

$$M_A = 0.733 \pm 0.068\,\text{GeV}, \qquad C_5^A = 0.993 \pm 0.101\,\text{GeV} \tag{5.3}$$

and the correlation matrix (Table 5.1) shows that parameters are strongly anticorrelated. Figure 5.2 shows the result of the fit with ANL data within 1σ error.

---

[2]For example BNL experiment [39] only provides the event distribution of Q^2.
[3]From Reference [50].

Table 5.1 Correlation Matrix

	M_A	C_5^A
M_A	1	-0.858
C_A^0	-0.858	1

Fig. 5.2 Differential cross-section as a function of Q^2. The curve is the model's prediction for $\frac{d\sigma}{dQ^2}$ averaged over ANL flux and for the best fit values of the free parameters, and the shaded area accounts for the variation of the results when M_A changes within its error interval. The model prediction include a $W < 1.4$GeV cut in the final pion-nucleon invariant mass.
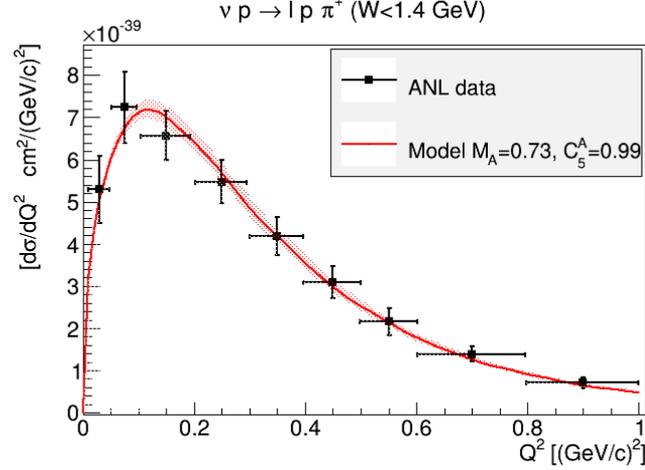
Changing M_A has its main effects on the shape of $d\sigma/dQ^2$. To show this, the model predictions for different M_A has been shown in Figure 5.3.

The best values for M_A and $C_A^5(0)$ parameters obtained from the fit in the Δ region (and for one channel) will be fixed as constant values from now on to do all predictions for CC and NC (anti-)neutrino SPP channels in this work.

We can turn off the nonresonant background in the MK-model. The best fit parameters are:

$$M_A = 0.776 \pm 0.056 \text{ GeV} , \qquad C_5^A = 1.125 \pm 0.085 \text{ GeV} \qquad (5.4)$$

Fig. 5.3 Differential cross-section as a function of Q^2. Curves are the model's prediction for $\frac{d\sigma}{dQ^2}$ averaged over ANL flux and for the different values of M_A. Solid-red is for the best value, and the dotted-blue and dashed-black are for different M_A while they are normalized to the solid-red curve to show the changes in shape. The model prediction include a $W < 1.4$GeV cut in the final pion-nucleon invariant mass.
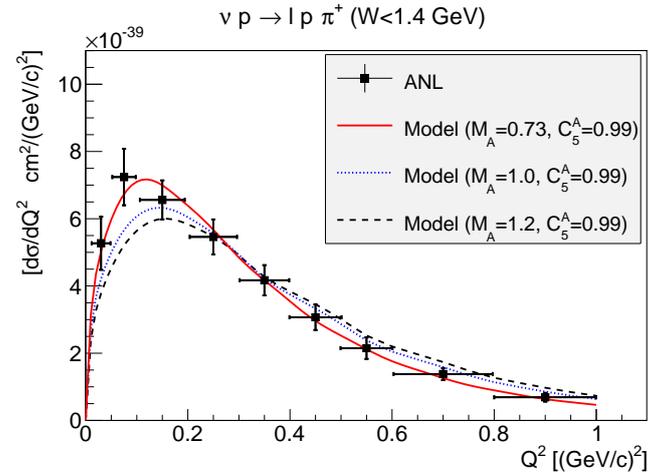
and the correlation matrix (Table 5.2) also shows that parameters are strongly anticorrelated. The minimum of reduced χ^2 is 0.199 which is very similar to what we got with nonresonant

Table 5.2 Correlation Matrix

	M_A	C_5^A
M_A	1	-0.829
C_5^A	-0.849	1

contribution.

In reference [17], the RS model with GS form-factor and with no background is taking into account and the fitting result is consistent with the best fit value in this work. If we use the RS form-factors with one parameter, M_A (which is used in the RS model [7] and the Rein model [9]), we get a similar result as Reference [9] with full MK-model, i.e. $M_A = 1$ GeV. Fitting results with more data sets and discussions can be found in I.

5.2.2 Resonance's Signs from Bubble Chambers Data

As discussed in subsection 4.1.2 about the decay amplitude of resonant interactions, it is replaced by Breit-Wigner factor (multiplied by branching ratio) taken from experimental data, and isospin coefficients and the resonance's sign (σ_D in Table 4.1), as it is displayed in Equation 4.20. In the RS model, σ_D is taken from the numerical value of decay amplitude from FKR model [5].

In the same way, as the RS model defines resonance's shape by Breit-Wigner factor to best describe the data, we can also choose the sign to get the best description of data. The procedure is to use the experimental data sensitive to the interference terms to extract signs related to the individual resonances and nonresonant helicity amplitudes. Such data exists from BEBC experiment [40] where decay angular distributions of the nucleon-pion system are investigated by means of a spherical harmonics expansion. The expansion in terms of spherical harmonics with coefficients as a function of $N\pi$ invariant mass W are:

$$
\begin{aligned}
\frac{d\sigma}{dW d\Omega} &= a_{00}^{\nu,\bar{\nu}}(W)Y_0^0(\Omega) + a_{10}^{\nu,\bar{\nu}}(W)Y_1^0(\Omega) + a_{20}^{\nu,\bar{\nu}}(W)Y_2^0(\Omega) + ... \\
&+ a_{11}^{\nu,\bar{\nu}}(W)\operatorname{Re}Y_1^1(\Omega) + a_{21}^{\nu,\bar{\nu}}(W)\operatorname{Re}Y_2^1(\Omega) + a_{22}^{\nu,\bar{\nu}}(W)\operatorname{Re}Y_2^2(\Omega) + ... \\
&+ b_{11}^{\nu,\bar{\nu}}(W)\operatorname{Im}Y_1^1(\Omega) + b_{21}^{\nu,\bar{\nu}}(W)\operatorname{Im}Y_2^1(\Omega) + b_{22}^{\nu,\bar{\nu}}(W)\operatorname{Im}Y_2^2(\Omega) + ... \quad (5.5)
\end{aligned}
$$

where $Y_l^m(\theta,\phi)$ are spherical harmonics functions. Therefore the coefficients are:

$$
a_{ij}^{\nu,\bar{\nu}}(W) = \int d\Omega \frac{d\sigma}{dW d\Omega}\operatorname{Re}Y_i^j(\Omega), \qquad b_{ij}^{\nu,\bar{\nu}}(W) = \int d\Omega \frac{d\sigma}{dW d\Omega}\operatorname{Im}Y_i^j(\Omega) \qquad (5.6)
$$

where $a_{00}^{\nu,\bar{\nu}}(W)$ is used for the normalization, and the measured quantities are:

$$\hat{a}_{ij} = a_{ij}/a_{00} \quad , \qquad \hat{b}_{ij} = b_{ij}/a_{00} \tag{5.7}$$

On the other hand from Equation 3.64:

$$\frac{d\sigma^{\nu,\bar{\nu}}}{dWd\Omega} = T_1^{\nu,\bar{\nu}}(W,\theta) + \quad \cos\phi\, T_2^{\nu,\bar{\nu}}(W,\theta) + \sin\phi\, T_3^{\nu,\bar{\nu}}(W,\theta)$$
$$+ \quad \cos 2\phi\, T_4^{\nu,\bar{\nu}}(W,\theta) + \sin 2\phi\, T_5^{\nu,\bar{\nu}}(W,\theta). \tag{5.8}$$

It is easy to do the integration over ϕ in Equation 5.6, using Equation 5.8:

$$a_{l0}^{\nu,\bar{\nu}} = 2\pi\sqrt{\frac{2l+1}{4\pi}} \int d\cos\theta\, T_1^{\nu,\bar{\nu}}(W,\theta) P_l(\cos\theta)$$

$$a_{l1}^{\nu,\bar{\nu}} = \pi\sqrt{(2l+1)\frac{(l-1)!}{(l+1)!}} \int d\cos\theta\, T_2^{\nu,\bar{\nu}}(W,\theta) P_l^1(\cos\theta) \qquad (\text{For } l > 0)$$

$$b_{l1}^{\nu,\bar{\nu}} = \pi\sqrt{(2l+1)\frac{(l-1)!}{(l+1)!}} \int d\cos\theta\, T_3^{\nu,\bar{\nu}}(W,\theta) P_l^1(\cos\theta) \qquad \text{For } l > 0 \tag{5.9}$$

where $P_l(\cos\theta)$ are Legendre functions, and $P_l^m(\cos\theta)$ are associated Legendre functions. These coefficients (which is called the averaged value of spherical harmonics due to Equation 5.6) are measured in terms of W which allows to distinguish individual resonance's regions approximately. But unfortunately measurement is for the ratio of the coefficients in Equation 5.7, that make it more difficult to guess about resonance's regions.

For a_{00} (which is actually $d\sigma/dW$ multiplied to a constant), one can look at specific W region and conclude about the signs, although regions of resonances are not separated due to the interfering resonances with same (l, j) numbers, and interference effects between resonant and nonresonant interactions. For other coefficients it is more difficult because the cross-section is additionally multiplied to a Legendre function which will change the interference terms.

Figure 5.4 shows the averaged value of spherical harmonics (Equation 5.7) for $\bar{\nu}p \rightarrow \mu^+ p\pi^-$ channel measured by BEBC experiment. The model prediction with resonance's signs proposed in RS model is compared with data, and it shows disagreement for the leading coefficients especially at high W. We change the signs to obtain the best description of the data. We can repeat the same procedure for all resonances and extract the sign for different resonances, as they are given in Table 5.3. The result shows significantly better agreement with data for the extracted signs as it is displayed in Figure 5.4.

Since the main difference appears in the leading coefficients we will present precise cal-

Table 5.3 Resonance signs from Rein-Sehgal (RS) model [7] and new signs proposed in this work.

Resonance	M_R	Γ_0	χ_E	$RS-signs$	$MK-signs$
$P_{33}(1232)$	1232	117	1	+	+
$P_{11}(1440)$	1430	350	0.65	+	-
$D_{13}(1520)$	1515	115	0.60	-	-
$S_{11}(1535)$	1535	150	0.45	-	-
$P_{33}(1600)$	1600	320	0.18	+	+
$S_{31}(1620)$	1630	140	0.25	+	-
$S_{11}(1650)$	1655	140	0.70	+	+
$D_{15}(1675)$	1675	150	0.40	+	-
$F_{15}(1680)$	1685	130	0.67	+	+
$D_{13}(1700)$	1700	150	0.12	-	-
$D_{33}(1700)$	1700	300	0.15	+	+
$P_{11}(1710)$	1710	100	0.12	-	-
$P_{13}(1720)$	1720	250	0.11	+	-
$F_{35}(1905)$	1880	330	0.12	-	+
$P_{31}(1910)$	1890	280	0.22	-	-
$P_{33}(1920)$	1920	260	0.12	+	-
$F_{37}(1950)$	1930	285	0.40	+	+
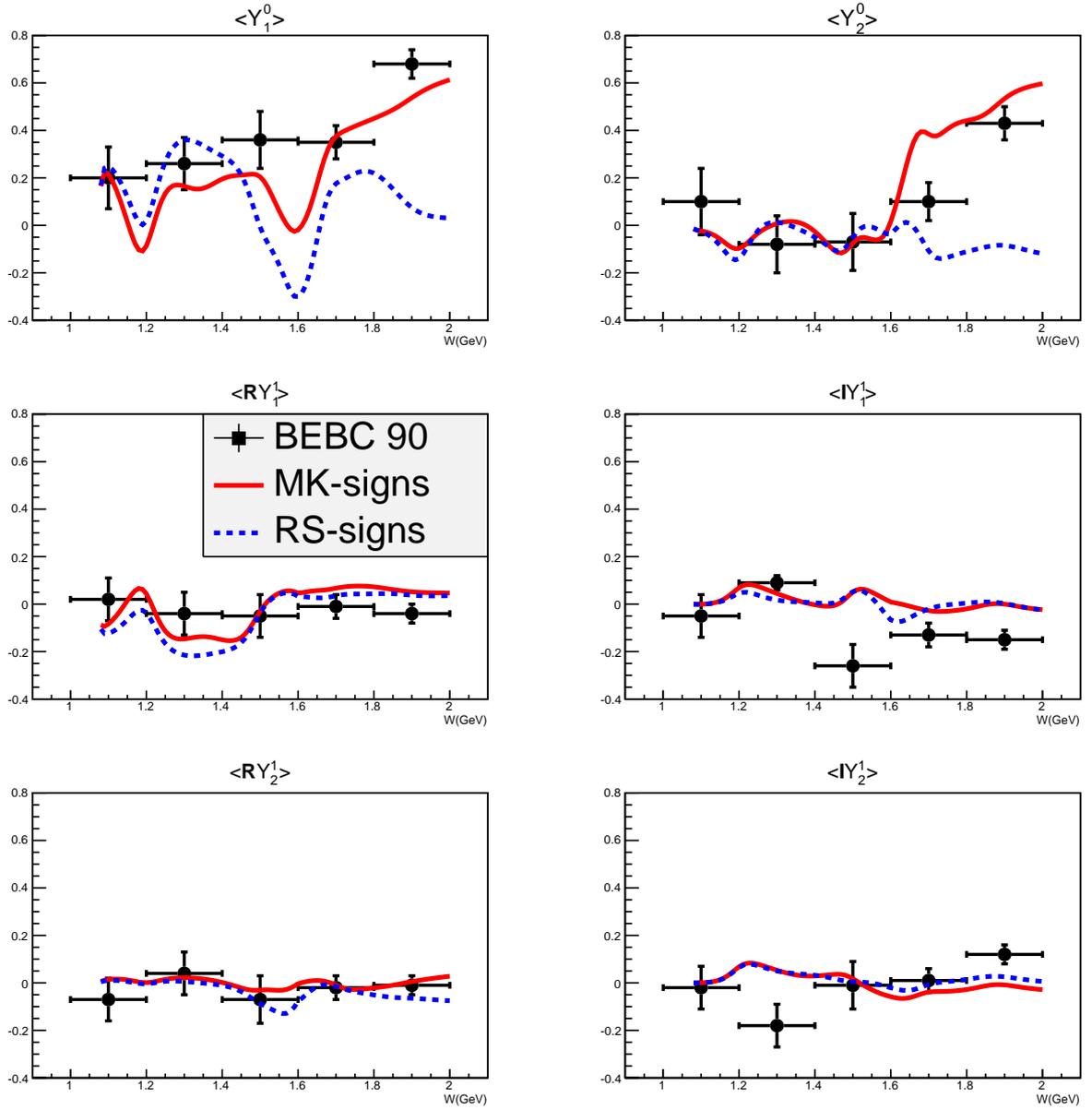
Fig. 5.4 Averaged values of the spherical harmonics for $\bar{\nu}p \to \mu^+ p\pi^-$ reaction from [40]. Curves show the model's prediction for RS-signs (dashed-blue) and the new extracted signs (solid-red). $\langle Y_i^j \rangle = \hat{a}_{ij}$.

culation for $\langle Y_1^0 \rangle \hat{a}_{10}$, assuming the MK-model has only Δ resonance, i.e. we ignore other resonances and nonresonant interaction. Therefore the angular part of the helicity amplitudes of

$$
\begin{aligned}
T_1(W,\theta) \;=\; & \int dk^2 \, \frac{G_F^2}{2} \frac{1}{(2\pi)^4} \frac{|\mathbf{q}|}{4} \frac{-k^2}{(k^L)^2} \sum_{\lambda_2,\lambda_1} \Bigg\{ \\
& |C_L|^2 |\tilde{F}^{e_L}_{\lambda_2\lambda_1}(\theta) - \tilde{G}^{e_L}_{\lambda_2\lambda_1}(\theta)|^2 + |C_R|^2 |\tilde{F}^{e_R}_{\lambda_2\lambda_1}(\theta) - \tilde{G}^{e_R}_{\lambda_2\lambda_1}(\theta)|^2 \\
+ \; & |C_-|^2 \, |\tilde{F}^{e_-}_{\lambda_2\lambda_1}(\theta) - \tilde{G}^{e_-}_{\lambda_2\lambda_1}(\theta)|^2 + |C_+|^2 \, |\tilde{F}^{e_+}_{\lambda_2\lambda_1}(\theta) - \tilde{G}^{e_+}_{\lambda_2\lambda_1}(\theta)|^2 \Bigg\} \quad (5.10)
\end{aligned}
$$

are $d^{3/2}_{\lambda\mu}$, and for a specific helicity $\lambda = 1/2$ and $\mu = 1/2$

$$
d^{3/2}_{1/2,1/2} = \frac{1}{2}cos\theta/2(3cos\theta - 1), \tag{5.11}
$$

we have:

$$
\begin{aligned}
\frac{a_{10}}{a_{00}} &= \frac{\int_{-1}^{1} d\cos\theta \, \cos^2(\theta/2)[3\cos\theta - 1]^2 P_1(\cos\theta)}{\int_{-1}^{1} d\cos\theta \, \cos^2(\theta/2)[3\cos\theta - 1]^2} \\
&= \frac{\int_{-1}^{1} d\cos\theta \, [1+\cos\theta][3\cos\theta - 1]^2 \cos\theta}{\int_{-1}^{1} d\cos\theta \, [1+\cos\theta][3\cos\theta - 1]^2}
\end{aligned} \tag{5.12}
$$

which is a negligible number (~ 0.03). This is the same for all single resonances and with different helicities, therefore, the interference effect is significantly visible in $\hat{a}_{10}$ in absence of resonances. Same calculation and conclusion can be made for $\hat{a}_{20}$ as well.

To do more investigation we also show the model predictions for individual coefficients a_{00}, a_{10} and a_{20} in Figure 5.5, rather than the ratio that was presented in top plots of Figure 5.4.

Plots in the right side of Figure 5.5 show the full model predictions (i.e resonant, nonresonant contribution with interference effects) with RS and MK signs. The top plot shows a_{00} where the significant change appears in the Δ region due to the interference between resonant and nonresonant interactions. This is shown on the top-right plot where the different ingredients are shown separately. This plot has few messages:

- changing resonance's signs will change the resonance contribution, only a little bit, due to the interference between resonances at higher W where the MK-signs are different for $P_{33}(1920)$, $F_{35}(1905)$ and $P_{13}(1720)$.

- At low W, changing the sign of $P_{11}(1440)$[4] reflects the contribution of interference with the nonresonant background. Figure 5.6 shows the separate contributions for individual resonance (with different sings and Δ ($P_{33}(1232)$) resonance) and nonresonant background, where the top plots shows the interference contributions is the main reason for a_{00} modification at low W due to the superposition of Δ and $P_{11}(1440)$ resonances.

- The nonresonant background is obviously unaffected by changing the resonance's signs, however, the contribution is significant (especially for this channel) up to $W < 1.6$ GeV region.

- The interference between resonant and nonresonant for both RS and MK signs show significant changes in $W < 1.6$ GeV region, and this is the main reason for the modification in the Δ region of a_{00} in the top right plot.

The middle plots of Figure 5.5 show the model predictions for a_{10} with RS and MK signs. The resonance contribution is changing in $W > 1.2$ GeV because all resonance can interfere with each other after multiplying the Legendre function $P_1(\cos\theta)$. On the other hand, the interference (between resonance and nonresonant interaction) effect has a large contribution in $W < 1.6$ GeV region. They are significantly different (between RS and MK signs) everywhere, but its effect in $W < 1.2$ GeV region is the main reason to see different result for a_{10} (right plot) in this region.

The ratio of a_{10}/a_{00} between top-right and middle-right plots of Figure 5.5 is consistent with the top-right plot of Figure 5.4 where the different resonance's signs cause significant change in the model predictions.

Similar arguments can be made for a_{20} (bottom-right plot of Figure 5.5) where the main change for higher W comes from the interference between resonances and for low W ($W < 1.6$ GeV) is due to the interference between all multipoles. The ratio of a_{20}/a_{00}, between top-right and bottom-right plots of Figure 5.5, is consistent with the top-left plot of Figure 5.4 where the different resonance's signs cause the model predictions with RS and MK signs modify significantly.

From now on, "RS-signs" refers to resonance's signs proposed in RS model and presented in the 5th column of the Table 5.3, and "MK-signs" refers to the new extracted signs proposed in this work (6th column of Table 5.3).

---

[4]This is called Roper resonance. As it is discussed in [7, 9], the RS-sign sign for Roper resonance is different with the sign as required by photoproduction. Therefore the extracted MK-sign is consistent with the sign of the photoproduction amplitude.
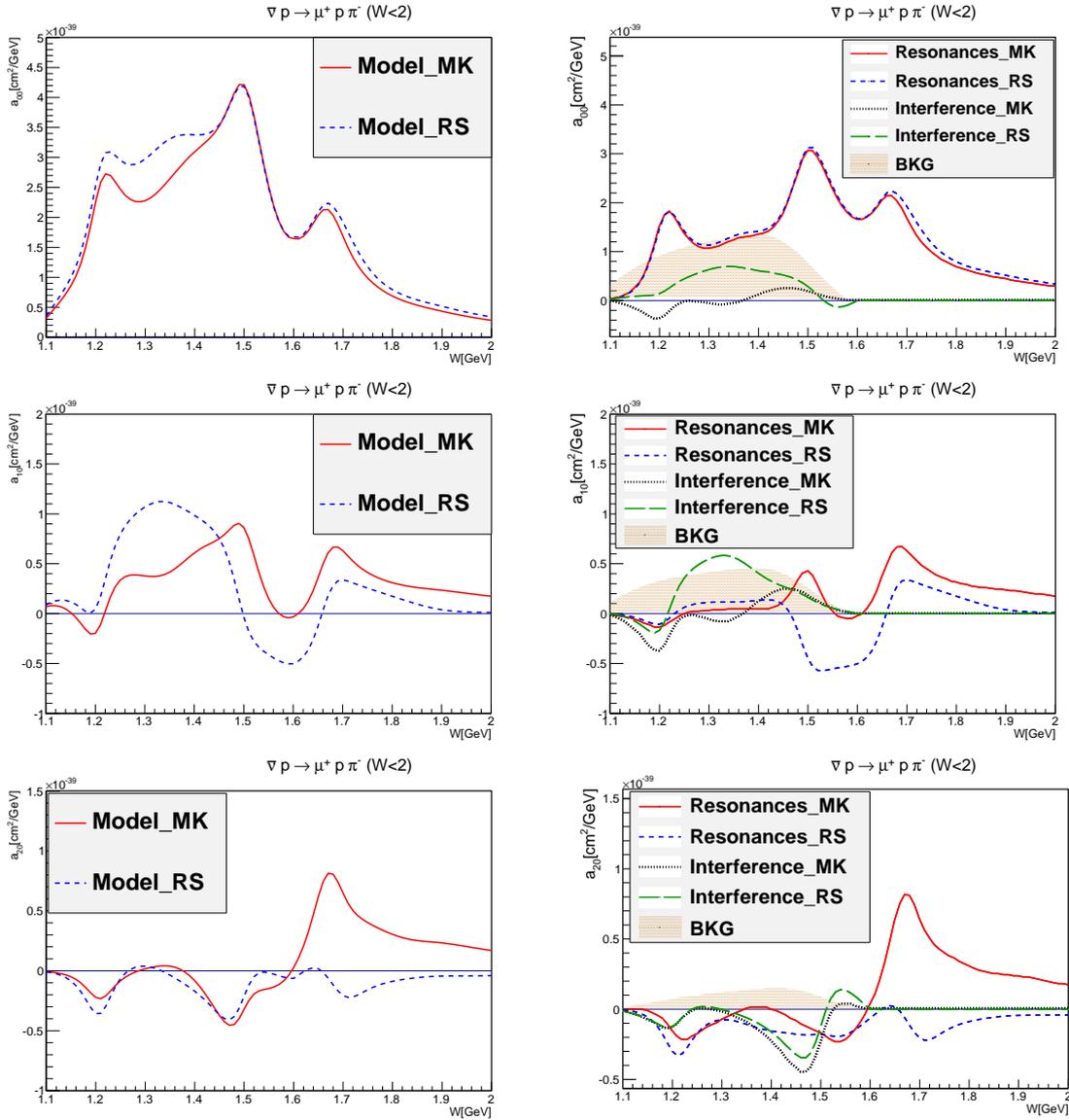
Fig. 5.5 The model predictions for leading coefficients in Equation 5.6, i.e. a_{00}, a_{10} and a_{20}. Right plots are the full model with MK (solid-red) and RS (dashed-blue) signs. In left plots, different ingredients of the model (i.e. resonances, nonresonant background and the interference between them) are shown separately.
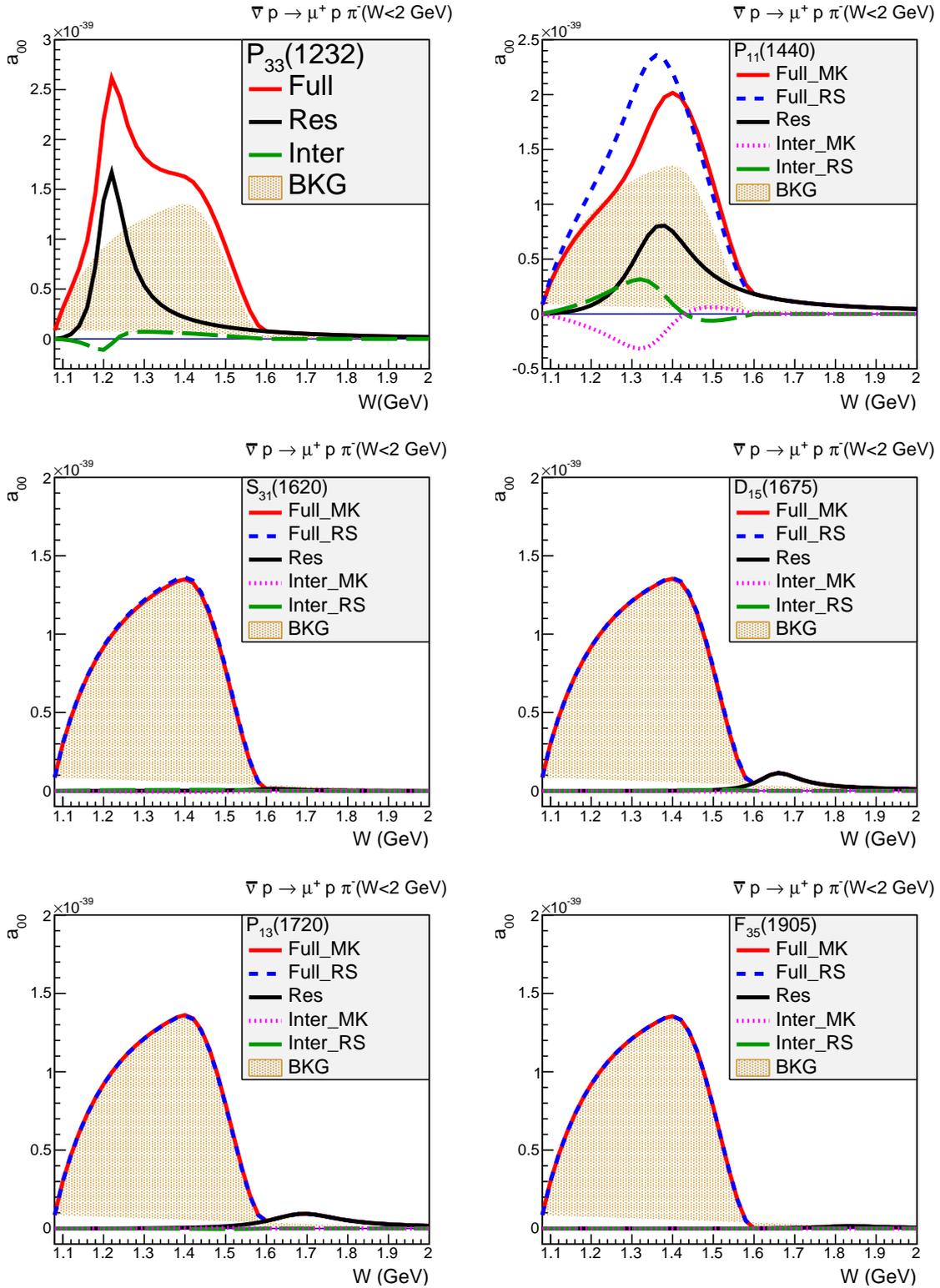
Fig. 5.6 Averaged values of the spherical harmonics for $\bar{\nu} p \rightarrow \mu^+ p \pi^-$ reaction from [40]. Curves show the model's prediction for RS-signs (dashed-blue) and the new extracted signs (solid-red)
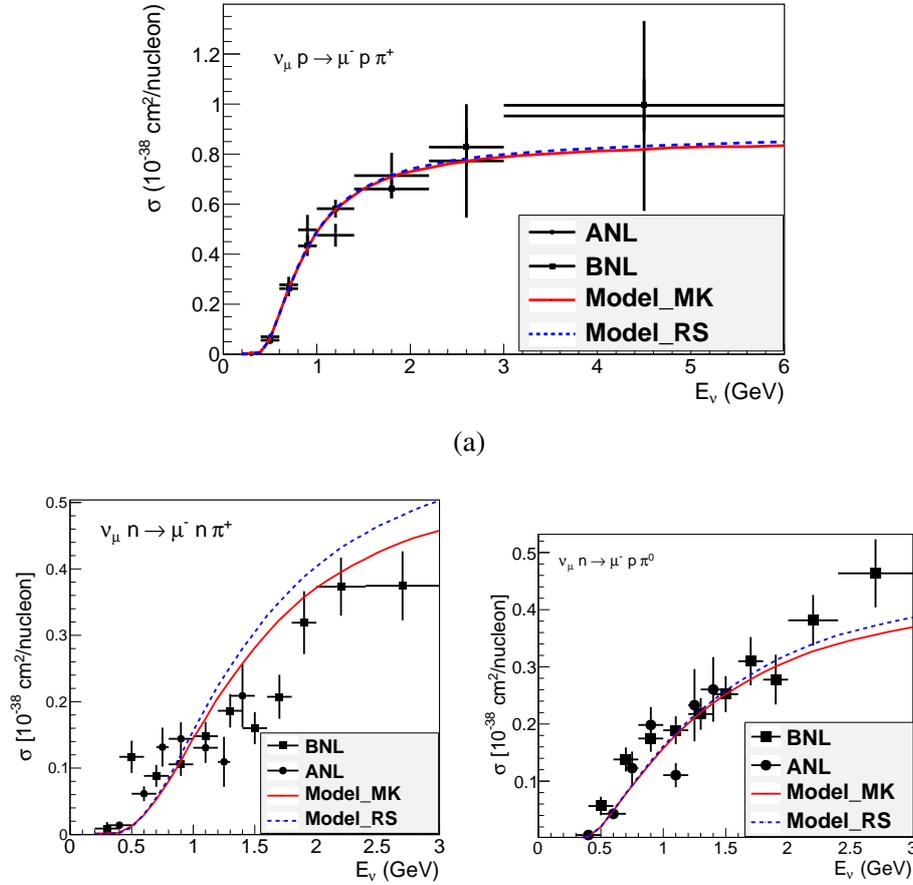
Fig. 5.7 Total cross-section for CC neutrino channels with RS-signs (dashed blue), and with MK-signs (solid red). Reanalysed ANL and BNL data are from [54, 55].

5.2.3   Total cross-section

Several bubble-chamber experiments have published their measurements for total cross-section as a function of neutrino energy. ANL [38] and BNL [39] experiments have made the measurement with the low energy neutrino beam, and they have been reanalyzed later (see section 5.1). Model predictions for CC neutrino channels (Equation 3.2) for both RS-signs and MK-signs are compared with reanalysed data from [54, 55] in Figure 5.7. Changing resonance's signs has a visible effect in $\nu n \rightarrow \mu n \pi^+$ channel due to the significant contribution from $P_{11}(1440)$ resonance.

 Now we look at CC antineutrino data for two channels $\bar{\nu} p \rightarrow \mu^+ p \pi^-$ and $\bar{\nu} n \rightarrow \mu^+ n \pi^-$. For the BEBC data [40] on deuterium target and Gargamelle data [48] on propane target the total cross-section as a function of neutrino energy is published. The comparison between data and the model with an invariant mass cut $W < 2$ GeV is shown on Figure 5.8. Gargamelle
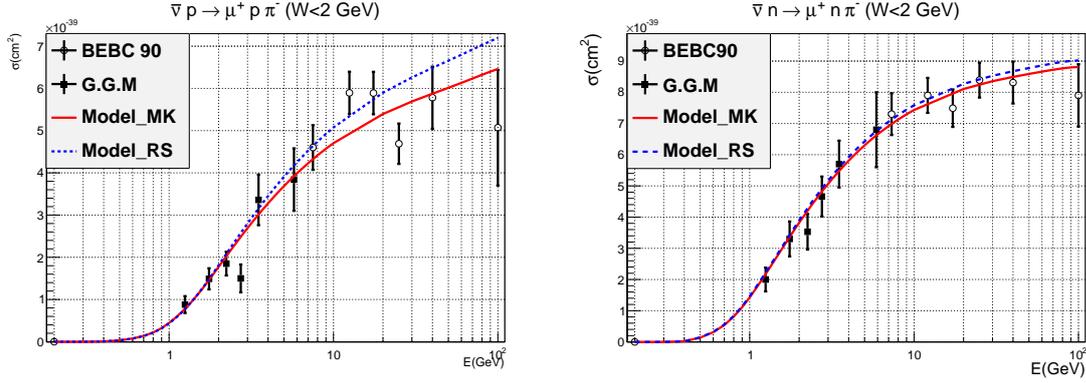
Fig. 5.8 Total cross-section for two channels $\bar{\nu}p \to \mu^+ p\pi^-$ (left) and $\bar{\nu}n \to \mu^+ n\pi^-$ (right), as a function of neutrino energy. Data are from BEBC [40] and Gargamelle [49], and curves are integrated cross-section for the model with an invariant mass cut $W < 2$ GeV for MK-signs (solid red) and RS-signs (dashed blue).

Fig. 5.9 Integrated cross-section as a function of neutrino energy for $\nu n \to \nu p\pi^-$ channel. The model has an invariant mass cut $W \leq$ GeV2 for RS-signs (dashed blue) and MK-signs (solid red).
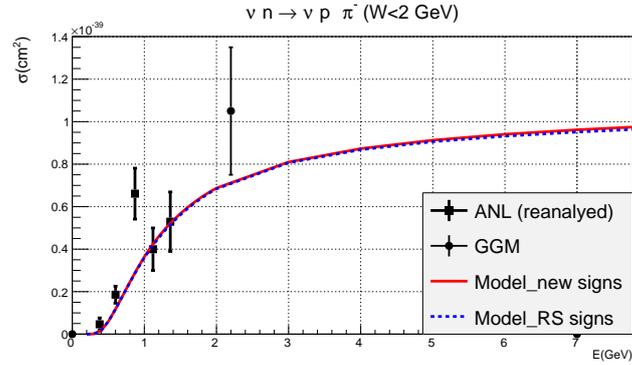
data is normalized to the cross-section on free nucleon [49] using the relation:

$$\sigma_{propane}(n\pi^-) = f_n \sigma_n(n\pi^-),$$
$$\sigma_{propane}(N\pi^-) = f_n \sigma_n(n\pi^-) + f_p \sigma_p(p\pi^-), \tag{5.13}$$

where $f_p = 0.55$ and $f_n = 0.45$ are derived from number of protons and neutrons in the target material [49].

There are few available bubble-chamber data for NC single pion production from ANL on deuterium target and Gargamelle on propane. For $\nu n \to \nu p\pi^-$ channel, reanalyzed ANL data (based on [55]), Gargamelle data and the model prediction with both RS-signs and MK-signs are shown in Figure 5.9.

There are also few measurements for other NC neutrino and antineutrino channels (Equation 3.3, 3.4), by Gargamelle [46] and Auchen-Padova spark chamber [47]. All available data and the model prediction with RS-signs and MK-signs are shown in Figure 5.10.
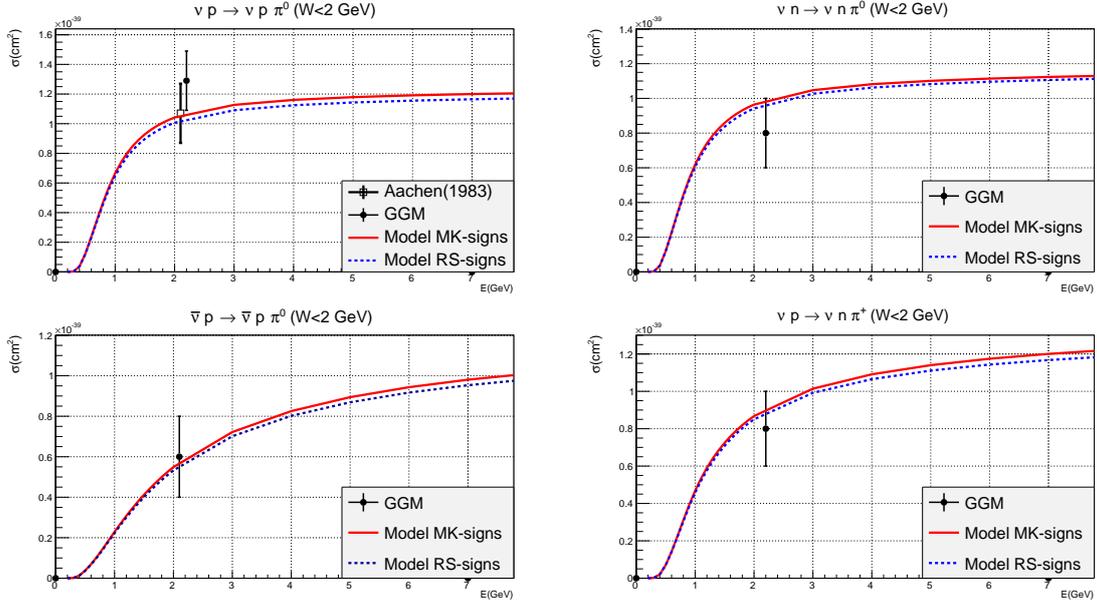
Fig. 5.10 NC (anti)neutrino channels for single pion production. data are from [45] and [47], and curves are model prediction with invariant mass cut $W < 2$ GeV for RS resonance's signs (dashed blue) and the MK-sign (solid red).

The comparisons between data and model for total differential cross-section as a function of energy show very good agreements for different CC and NC (anti-)neutrino channels in this section.

5.2.4 W distribution

The *W* distribution provides us information about individual resonance contributions. For example Δ ($P_{33}(1232)$) with mass $M_R = 1232$ MeV and width $\Gamma_0 = 117$ MeV has a clear bump in 1115 MeV $\leq W \leq$ 1349 MeV region.

In Figure 5.11, we present the distribution of W events for five CC channels (Equation 3.1,3.2) from exposures of BEBC to (anti-)neutrino beam. High neutrino energy in this experiment allowed us to see a clear pattern of resonances. To do the shape comparison we need to calculate the BEBC's flux[5] averaged $d\sigma/dW$, and normalize it to the area. Both predictions with RS-signs and MK-signs are shown in Figure 5.11. To show the effects of background contribution we also show the model prediction without the background and with RS-signs (i.e. the RS-model with GS form-factors) for parameters defined in Equation 5.4.

It is apparent that $\nu p \to \mu p \pi^+$ and $\bar{\nu} n \to \mu^+ n \pi^-$ channels (with isospin 3/2 resonances) are dominated by $\Delta(1232)$ resonance production. Other channels are a combination of

---

[5]From Reference [49]

both isospin 1/2 and 3/2 resonances and the isospin coefficients are given in Table 4.2. In $\nu n \to \mu n \pi^+$, $\nu n \to \mu p \pi^0$ and $\bar{\nu} p \to \mu^+ p \pi^-$ channels, the resonances with isospin 1/2 can also contribute. These resonances contribute significantly around $W = 1500$ MeV and $W = 1700$ MeV as it is clear in the Figure 5.11.

Different resonance's signs change the shape only a little bit. but the effect of nonresonant background is significant especially for channels with isospin 1/2 resonances.

Figure 5.12 shows the event distribution for W that measured by ANL experiment [38]. The flux averaged $d\sigma/dW$ predicted by the full model with MK-signs and RS-signs are shown in this figure. To show the effect of the nonresonant background, the model prediction (with RS-signs) without background is also shown in Figure 5.12. This is actually the RS-model with GS form-factor and fitted parameters from Equation 5.4.

5.3 Model and NEUT comparison with bubble chamber data

In this section we compare the MK-model and NEUT [56](the primary neutrino interaction generator used by T2K experiment), with the bubble chamber data for single pion production. The model introduced in this work with all fitted parameters and MK-signs is called MK-model (refers to the author) from now on. The single pion production model in NEUT 5.3.6 is the Rein-Sehgal model with the isospin 1/2 background terms with an adjustable coefficient defined in the original paper [7] and it is called ISO BKG parameter in NEUT. The Form-factors are the same in both models (from reference [17]), with two adjustable parameters (M_A^{RES} and $C5A$). All three parameters in NEUT 5.3.6 are fitted to ANL and BNL data for CC neutrino channels. They are $M_A^{RES} = 1.07$ GeV, $C5A = 0.96$ GeV and ISO BKG=0.96 GeV.

First we start with the total cross-section of CC neutrino channels which is shown Figure 5.13. For this channels, NEUT has good agreements with all ANL and BNL data because the three parameters are fitted to this particular data.

Reanalyzed ANL and BNL data for $\nu p \to \mu p \pi^+$ channel (shown in Figure 5.13a) is for low energy, however data from BEBC [40] and FNAL [41] are also included for comparisons at higher energies in Figure 5.14. The model prediction with MK-signs[6] and an invariant mass cut $W < 2$ GeV is also shown for comparison.

The discrepancy between NEUT and model appears for anti-neutrino data as it is shown in Figure 5.15. This discrepancy will also appears in the next chapter when we compare

---

[6]the model predicts same result for both RS and MK signs as it is shown in Figure 5.7a.
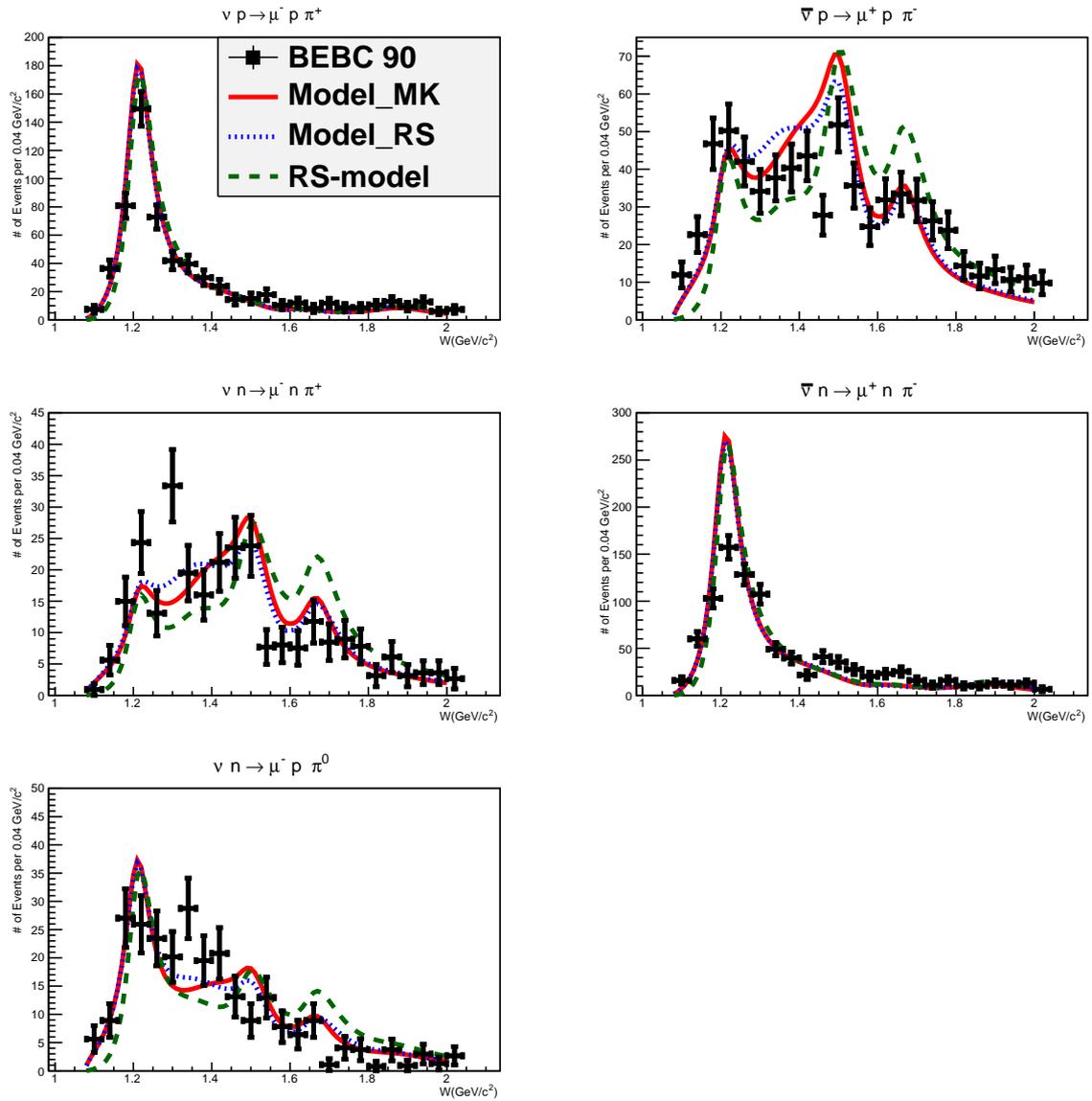
Fig. 5.11 W-distribution for different neutrino and antineutrino CC channels from [40]. Curves are the model prediction (normalized to data) for RS-signs (dashed blue), and MK-signs (solid red)
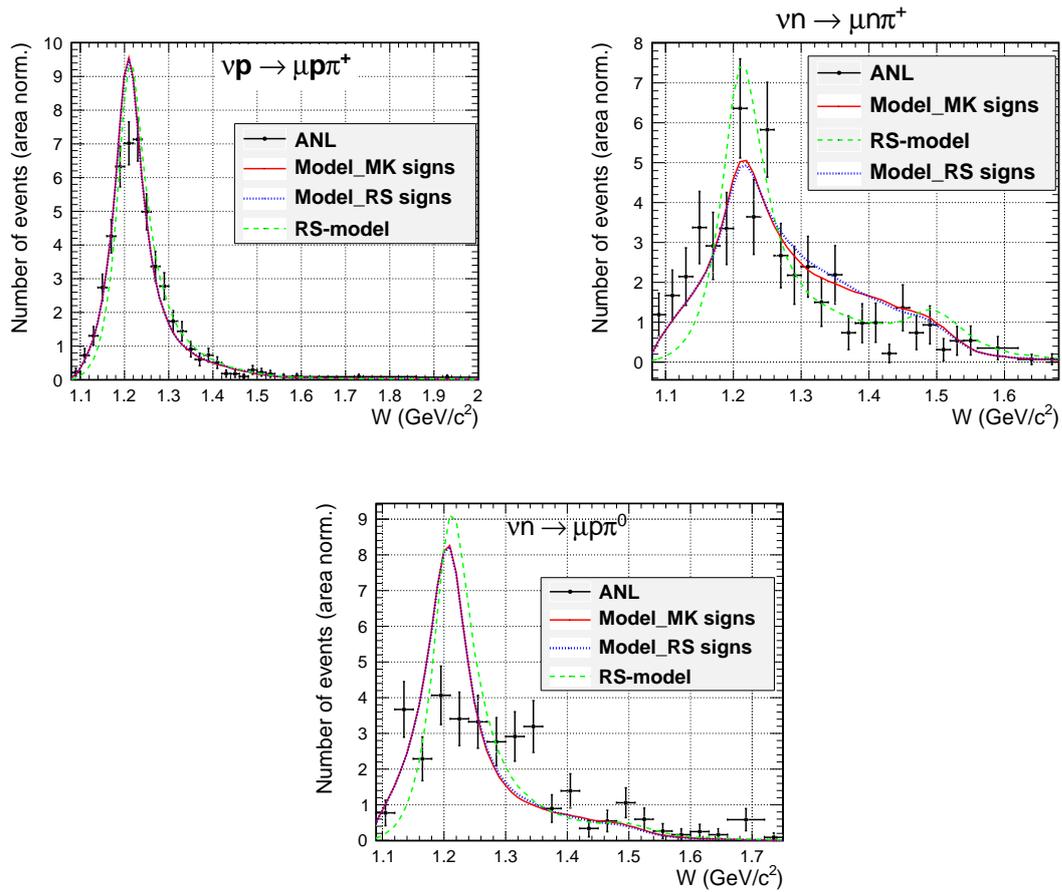
Fig. 5.12 W-distribution for different neutrino CC channels from [38]. Curves are the model prediction (normalized to data) for RS-signs (dotted blue), and MK-signs (solid red). The dashed green curve is the model without background with RS-signs (RS model with GS form-factors).

(a)
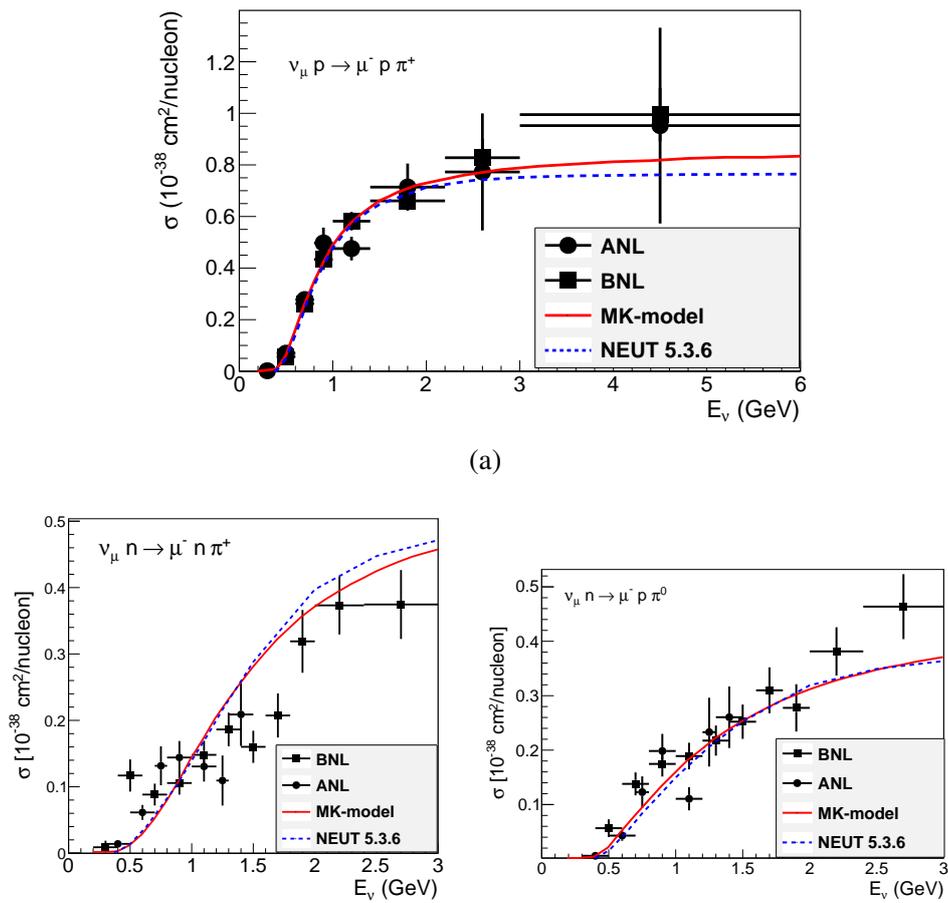
Fig. 5.13 Total cross-section for CC neutrino channels model with MK-signs (solid red) and the NEUT prediction (dashed blue). Reanalysed ANL and BNL data are from [54, 55]

.
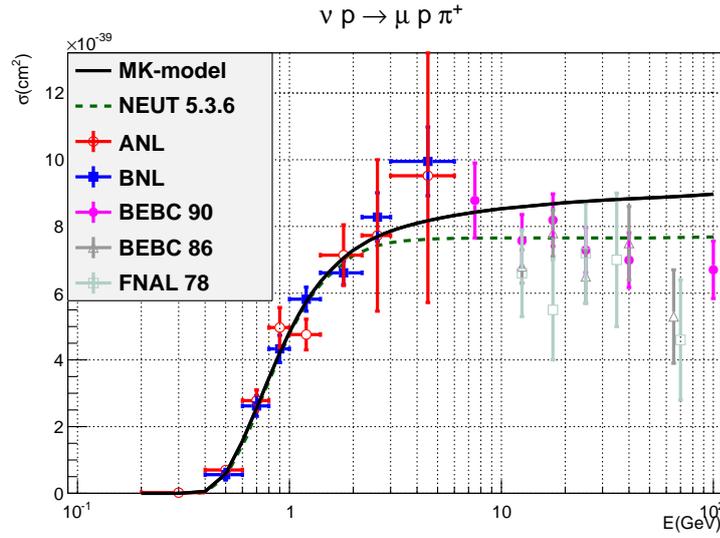
Fig. 5.14 Cross-section for $\nu p \to \mu p \pi^+$ channel from reanalysed ANL and BNL data for low energy and BEBC [40, 49] and FNAL [41] for high neutrino energy. Both Model and data have an invariant mass cut $W < 2$ GeV, except ANL and BNL data that has no cut on the event selection.

NEUT 5.3.6 (with the RS model) and NEUT with the MK-model. The main reason for the discrepancy is due to the background and its interference with resonance contribution in the MK-model while the RS-model treat differently with nonresonant background and has no interference effects.

The comparison between NEUT5.3.6, the MK-model and bubble chambers data for neutral current channels are shown in Figure 5.16 and 5.17. The discrepancy between NEUT5.3.6 and MK-model is not negligible and same discrepancy will be visible also in the next chapter. The reason is due to the background effects and because the parameters are already fitted to the CC neutrino channels.

Pion momentum is a direct observable, unlike W and Q^2 that have to be constructed from final state particles. Therefore it is very important to check consistency of model prediction with data.

ANL has published pion momentum distribution in the lab frame for two CC channels $\nu_\mu + p \to \mu p \pi^+$ and $\nu_\mu n \to \mu n \pi^+$ in [44]. To compare the model prediction in the lab frame one needs to generate events in the isobaric frame and boost it to the lab frame. Figure 5.18 shows the comparison between ANL data and the model prediction for two CC channels. The NEUT5.3.6 prediction is also shown in Figure 5.18 for comparison. The MK-model has an obviously better agreement with data.
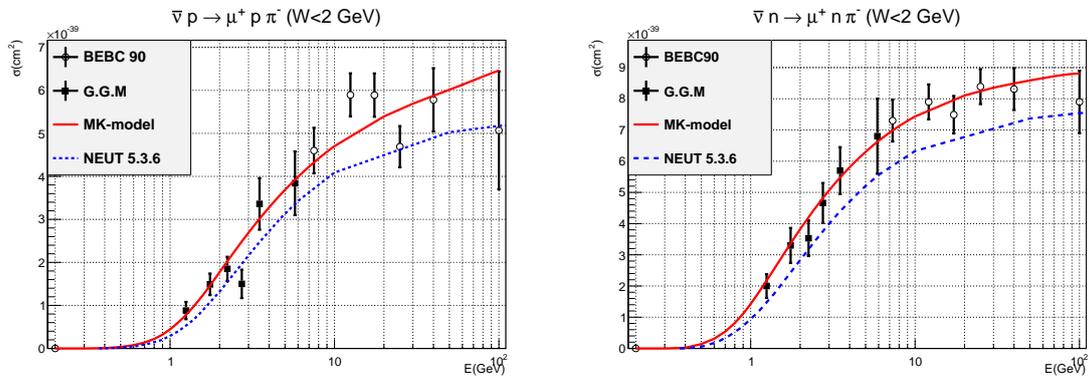
Fig. 5.15 Total cross-section for two channels $\bar{\nu}p \rightarrow \mu^+ p\pi^-$ (left) and $\bar{\nu}n \rightarrow \mu^+ n\pi^-$ (right), as a function of neutrino energy. Data are from BEBC [40] and Gargamelle [49]. Curves are total cross-section predicted by MK-model (solid-red) and RS-model (dashed-blue) with an invariant mass cut $W < 2$ GeV.
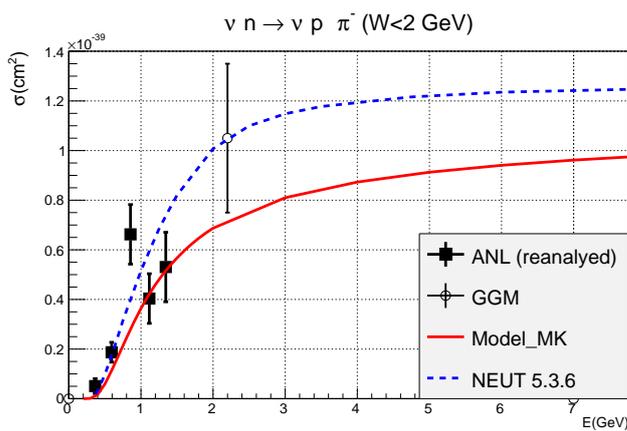
Fig. 5.16 Integrated cross-section as a function of neutrino energy for $\nu n \rightarrow \nu p\pi^-$ channel. The model with MK-signs (solid red) and NEUT prediction(dashed blue) have an invariant mass cut $W < 2$ GeV.
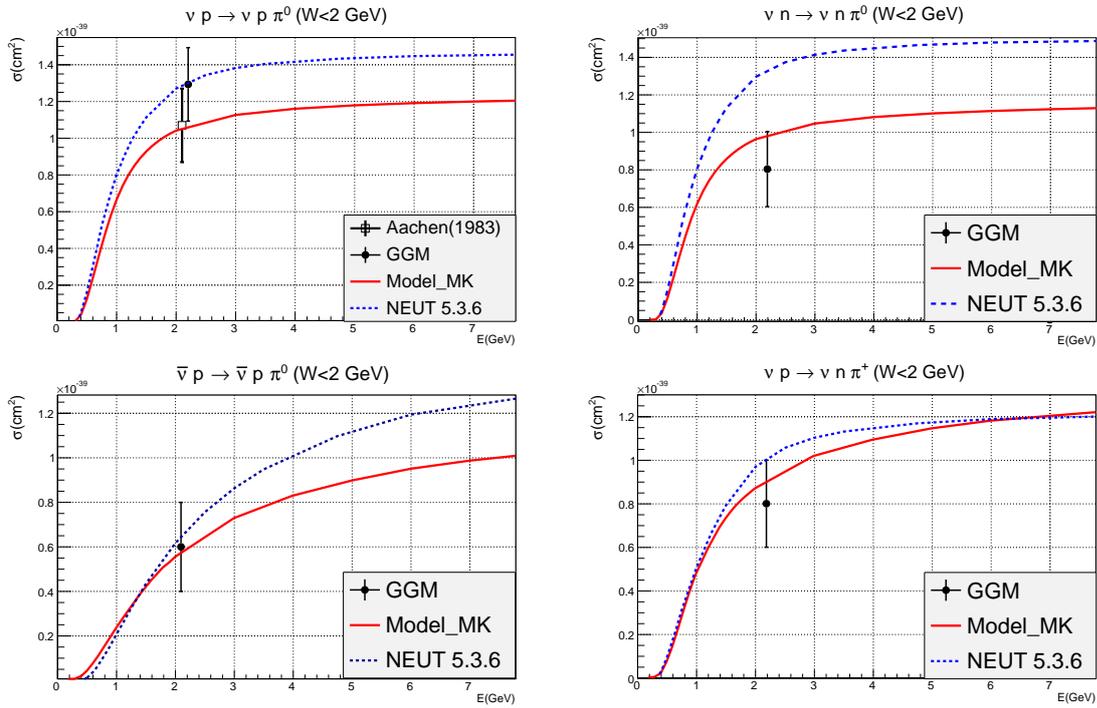
Fig. 5.17 NC (anti-)neutrino channels for single pion production. data are from [45] and [47], and curves are model with MK-sign (solid red) and NEUT (dashed blue) prediction with invariant mass cut $W < 2$ GeV.
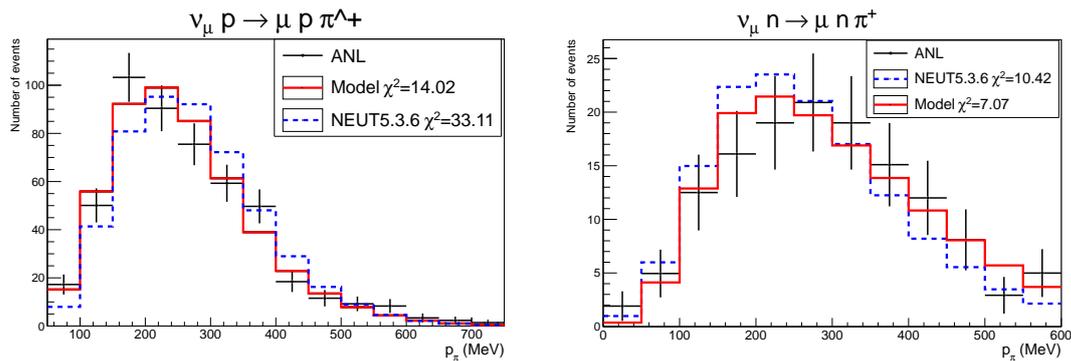
Fig. 5.18 Pion momentum distribution for $\nu p \to \mu p \pi^+$ (left) and $\nu n \to \mu n \pi^+$ (right) channels from ANL [44]. The MK-model(solid-red) and NEUT5.3.6 (dashed-blue) predictions of flux averaged p_π-differential cross-section (with $W < 2$ GeV cut), normalized to data for two CC neutrino channels. The plots is made by NUISANCE [84]. The degrees of freedom is 14(12) for left(right) plot.
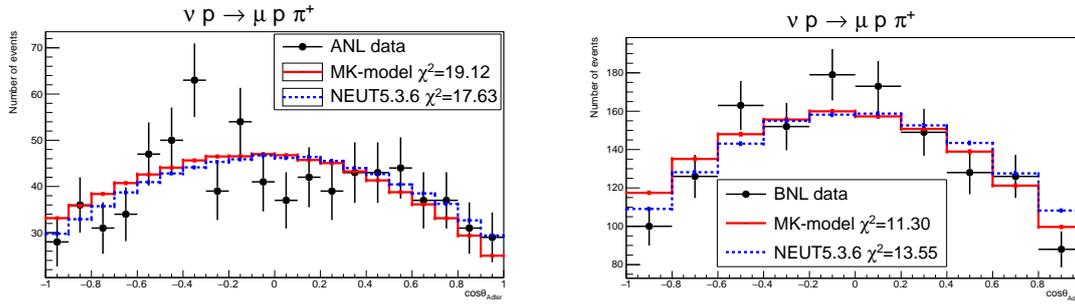
Fig. 5.19 Event distribution in the pion polar angle for ANL (left) and BNL (right) from References [38, 39]. Curves are flux-averaged, area-normalized prediction of the MK-model (solid-red) and NEUT5.3.6 (dashed-blue). Plots are made with NUISANCE [84]. The degrees of freedom is 20(10) for left(right) plot.

5.4 Angular distribution

Polar (θ) and azimuthal (ϕ) angles are shown in the isobaric or $N\pi$ rest frame in Figure 3.3. The θ-distribution of individual resonance is symmetric in the $N\pi$ rest frame[7], therefore any modification from the symmetric pattern is cased by the interference effects between resonant and nonresonant interactions. θ-distribution for $\nu p \to \mu p \pi^+$ channel has been measured by ANL [38] and BNL [39] experiments, The data is compared with the flux averaged differential cross-section normalized to data in Figure 5.19.

To show the effects of nonresonant interactions as well as its interference with resonances we compare the full model in this work (resonant and nonresonant) and RS-model (only resonance) in Figure 5.20 for three CC channels. We also include the symmetric Δ contribution for comparison. Curves are differential cross-section averaged over T2K near detector's flux for different models as described before. To show the effect of resonance signs we also show same comparisons with the RS-signs in Figure 5.21.

It is apparent from Figure 5.20, that the nonresonance interference has a significant effect on θ distribution (compare solid-red curve with blue-dotted curves), and the interference between resonances has also non-negligible effects especially on channels with isospin 1/2. For $\nu p \to \nu p \pi^+$ channel, only resonances with isospin 3/2 can contribute and Δ is dominant, therefore interference effects are not significant.

In terms of pion angles, neutrino generators like NEUT [56] only have contribution for Δ resonance, and missing all the other resonances and their interferences, as well as the nonresonance effects. Therefore we also include the RS-model only for Δ resonance in Figure 5.20 to show the comparison between the full model and what is currently available in the generator.

---

[7]See the symmetry property of resonance helicity amplitudes at the end of subsection 4.1.2.
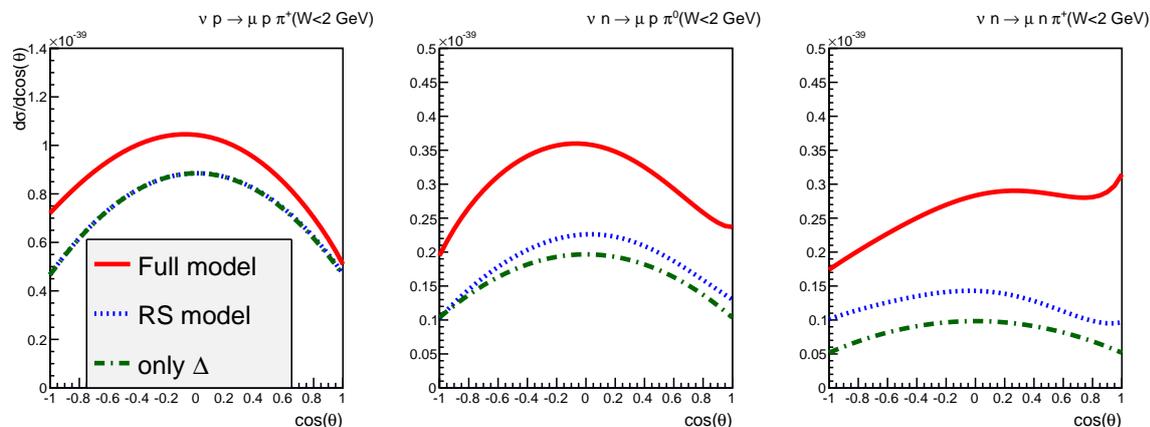
Fig. 5.20 The differential cross-section averaged over T2K flux in terms of the polar angle for MK-signs. The blue dotted curve shows the RS model, i.e. all resonances (up to $W = 2GeV$) and their interference, while green (dashed) curve is only for the dominant Δ resonance. Red (solid) curve shows the full model.
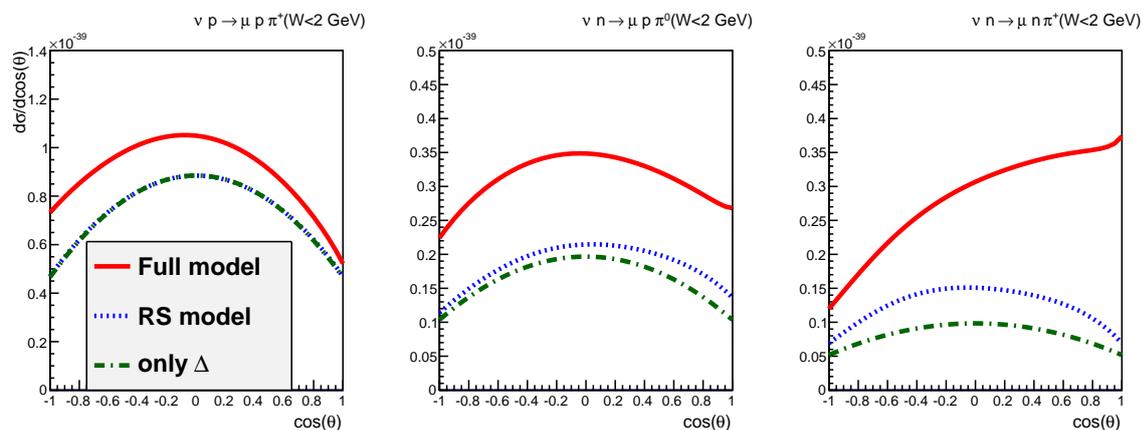
Fig. 5.21 The differential cross-section averaged over T2K flux in terms of the polar angle for RS-signs. The blue dotted curve shows the RS model, i.e. all resonances (up to $W = 2GeV$) and their interference, while the Green (dashed) curve is only for the dominant Δ resonance. The Red (solid) curve shows the full model.
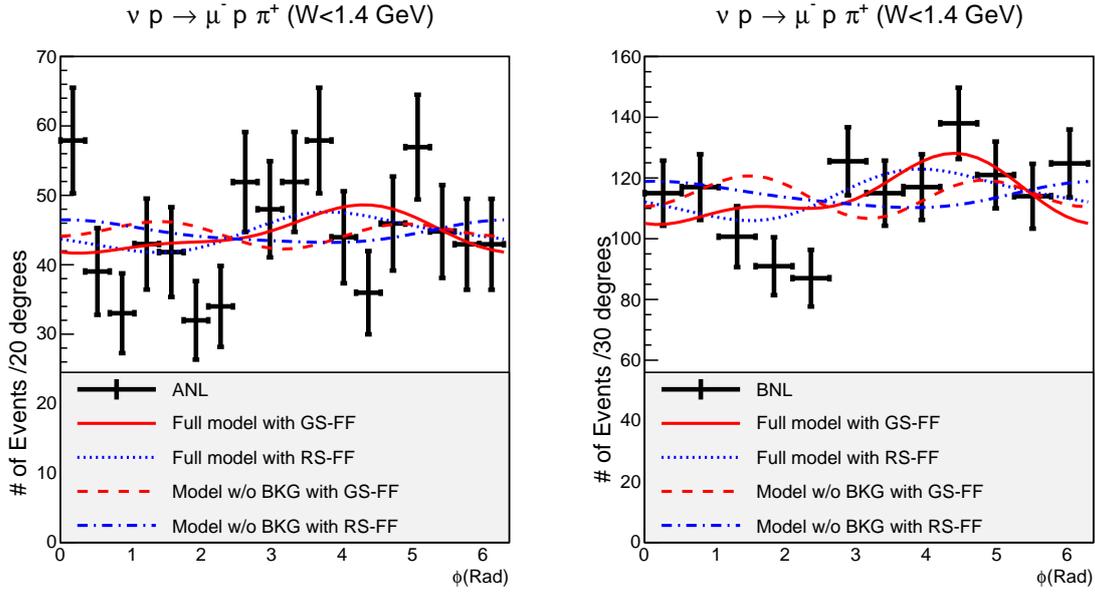
Fig. 5.22 ANL and BNL distribution of events in the pion azimuthal angle in πN rest frame with $W < 1.4 GeV$ for $\mu^- p \pi^+$ final state. Curves are flux-averaged, area-normalized prediction of the model for $d\sigma/d\phi$.

The azimuthal angle (ϕ) in the plane perpendicular to the momentum transfer (see Figure 3.3) is also sensitive to the interference effects like polar angle, but it is also a good observable to extract form-factors. For the RS-model and resonant interactions there are two different available form-factors on the market i.e. the dipole (RS) form-factors from the original RS model [7], and the form-factors introduced by Graczyk and Sobczyk (GS) [17], and the latter are used in this work.

Figure 5.22 shows different distributions between RS-model and the model proposed in this work, with different form-factors. The model predictions as a function of ϕ differential cross-section are normalized to ANL [38] and BNL [39] data in Figure 5.22.

From Figure 5.22 we can conclude:

- the nonresonant interference term has a significant effect on the ϕ distribution. This is visible when comparing two (solid and dashed) red curves for the full model in this work and RS model only for resonances.

- The different form-factor will change the ϕ distribution significantly which is visible by comparing pairs of red and blue curves.

- The best agreement with data is the full model with the Graczyk-Sobczyk form-factor [17] which is the default form-factor in this work.

According to [59], the ϕ distribution (only shape) is almost unaffected by nuclear effects, therefore experiments with a nuclear target can also be a good probe to extract the axial form-factors in the neutrino-nucleon models, while bubble chamber data is not precise enough to distinguish different models. Many experiments are currently measuring differential cross-sections precisely, on nuclear targets. If they will measure precise ϕ distribution, it can shed light on the axial form-factor.

5.5   The Rein model

The first idea of how to add the non-resonant amplitudes to the RS model helicity amplitudes, in this work, came from Rein model [9]. The Rein model use three Born graphs as for the nonresonant background contribution which is based on linear sigma model [11]. It also neglect the charged lepton mass. In Rein's model the multipoles for different angular momentum is calculated[8] for the Born graphs, and only multipoles with $l \geq 2$ is taking into account. The MK-model and Rein model are similar for the resonant interaction and they both use the RS model. The differences are the nonresonant background contribution and the charged lepton mass that is restored in the MK-model.

In this section we show some result from the Rein model and compare it with data and the MK-model. This will show us how much a different nonresonant model can change the predictions. Figure 5.24 show the W-distribution of BEBC experiment with the Rein model and MK-model predictions. Since both models have the same RS-model for resonance contribution, We also show the MK-model without the background contribution (RS-model with GS form-factos) for fitted parameters in Equation 5.4.

 The other comparison is for Q2-differential cross-section for BEBC flux with two different invariant mass cuts, i.e. in two $W < 1.4$ GeV and 1.4 GeV $< W < 2$ GeV regions. The Rein model uses the RS form-factor [9], while MK-model is using the GS form-factor [17] in the Delta region, but we use same treatment for the higher resonances. Although both models use the same data sets for extracting the axial form-factor, but their predictions are significantly different in normalization and shape which can be also due to the background.

5.6   Conclusion

Existing bubble-chamber data on light nucleon are old with large error and this situation is very unlikely to be improved. This data is used to validate cross-section models defined in

---

[8]This is very CPU consuming and not good for neutrino generators
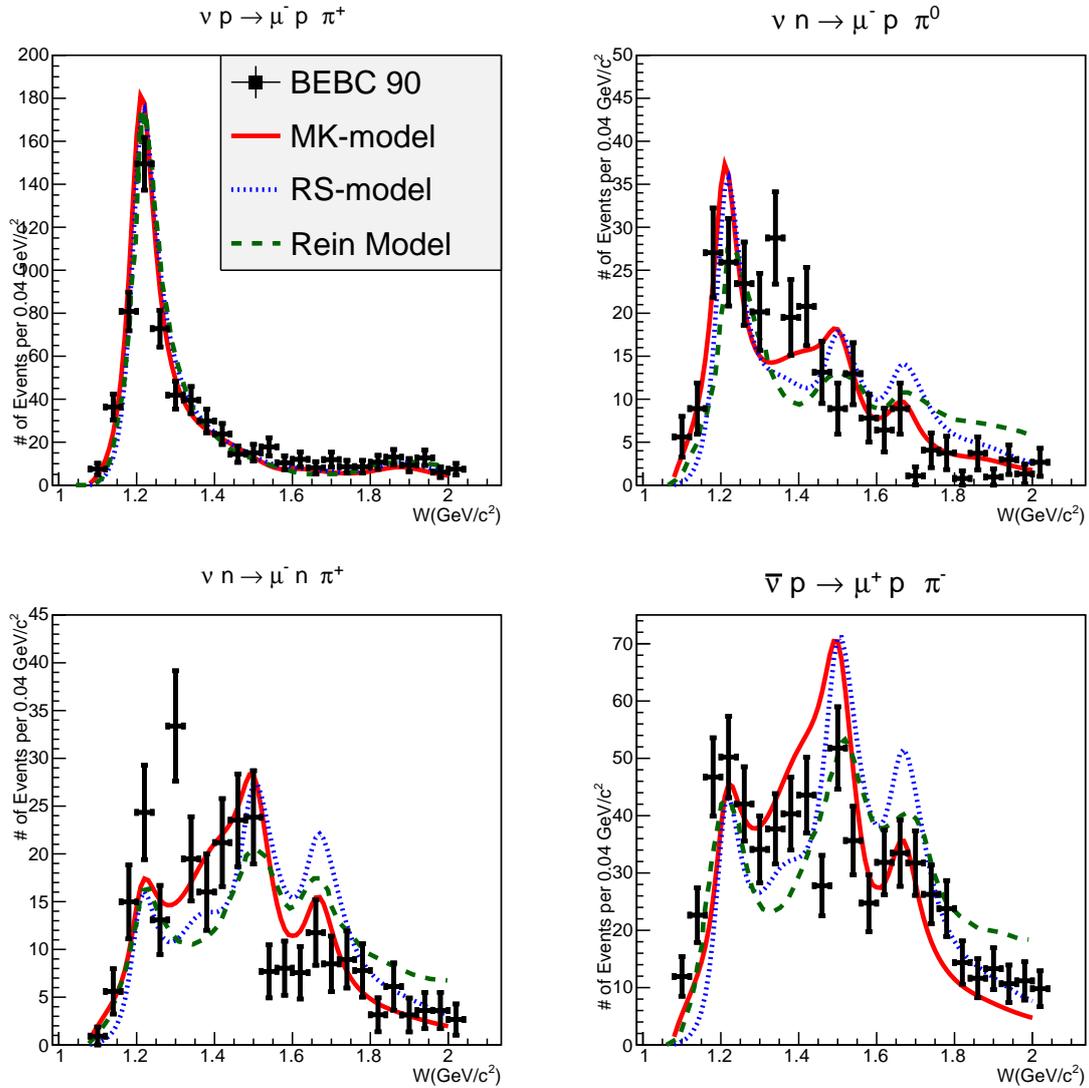
Fig. 5.23 W-distribution for different neutrino and antineutrino CC channels from [40]. Curves are the Rein's model (dashed green) and MK-model (solid red) and RS-model with GS form-factors (dotted-blue). All curves are normalized to the data. The Rein model prediction is digitized from reference [40].
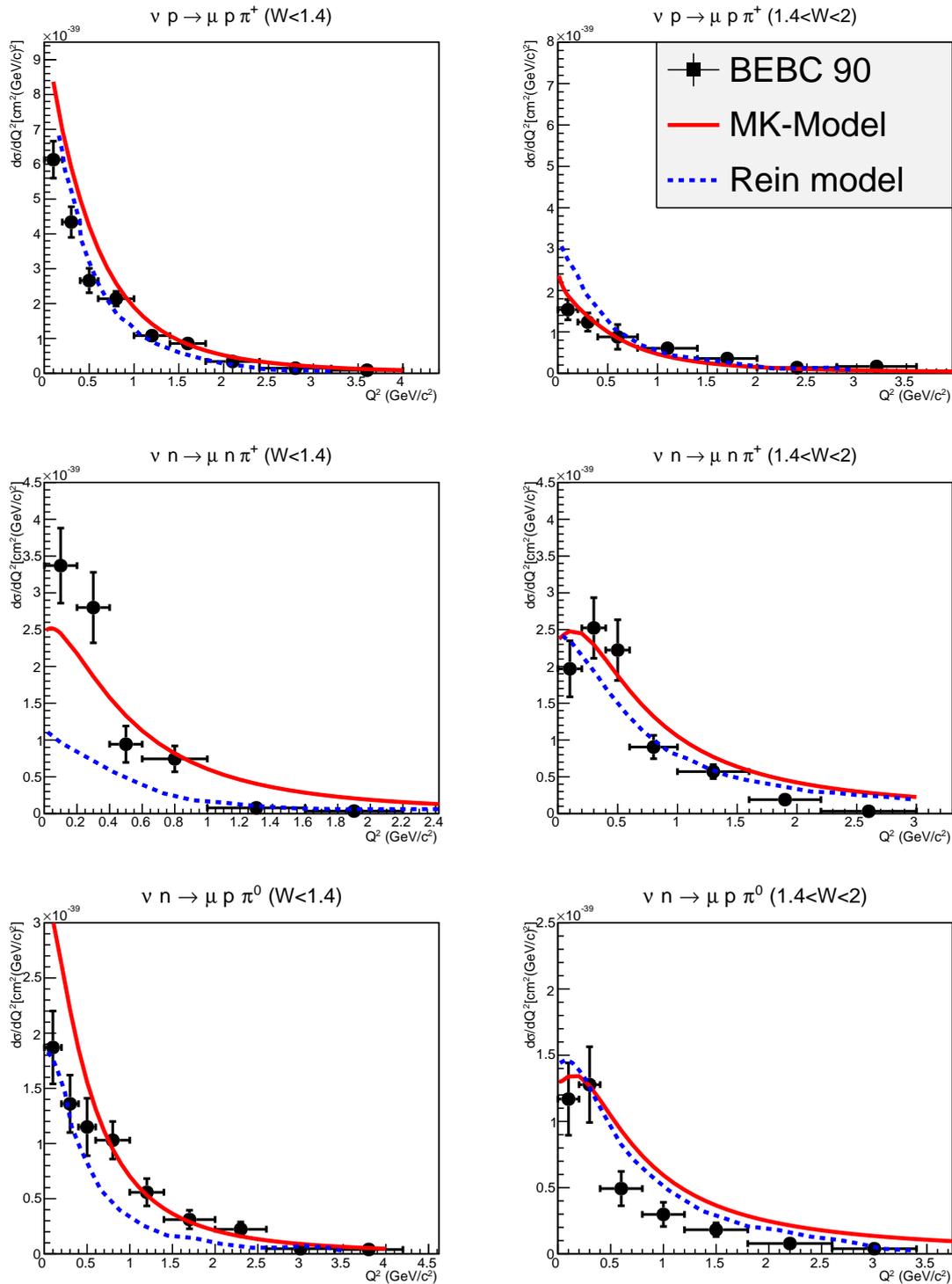
Fig. 5.24 Q2-differential cross-section for different neutrino CC channels from [40]. Curves are the Rein's model (dashed blue) and MK-model prediction (solid red) for $W < 1.4$ GeV and 1.4 GeV $< W < 2$ GeV invariant mass regions. The Rein model prediction is digitized from reference [40].

section 2.1 and to extract the axial form-factors. The single pion production (SPP) model proposed in the previous chapters is also a cross-section model, and it should be validated with the bubble-chamber data. This was the main goal in this chapter to extract the axial form-factor in resonant interactions and show the consistency between model and data.

The single pion production model described in this work with all fitted parameters and signs(described in this chapter) is called MK-model. The model describes the neutrino-nucleon interactions and it does not include the deuterium effects. The MK-model has several advantages compared with several other SPP models in the market:

- It consists of resonant and nonresonant interactions including the interference effects.

- It is valid up to $W = 2$ GeV, which is a suitable range of W for neutrino generators like NEUT.
  Models described in [8] and [10] for instance, are only valid in the Δ region.

- It is a full kinematics model i.e. the full differential cross-section is $d\sigma/dWdQ^2d\Omega$. The output of RS model is $d\sigma/dWdQ^2$, and in terms of pion angles the model defines density matrix which has very difficult form and not suitable for generators, therefore NEUT [56] and GENIE[57] have only Δ implementation, and the result shows a significant difference in pion angle distributions compared to what NEUT predicts.

- It has a suitable form for implementation.

- It has good agreement with almost all available bubble chamber's data (within a large error) for CC and NC (anti-)neutrino channels in the different range of neutrino energy with neutrino and antineutrino beams.

The available models for single pion production satisfy some of the items described above. For instance, the Rein-Sehgal model [7] does not include a reliable model for nonresonant interaction while the described model in References [10, 8] are only valid in the Δ region. The Rein model [9] on the other hand, is very CPU consuming to calculate all multipoles (for different angular momentum) and not suitable for the neutrino generators.

Chapter 6

Implementation of the Single Pion Production Model in NEUT

In the previous chapters, a new model has been introduced that describes single pion production in the neutrino-nucleon interactions. However, its results can be only compared with old bubble chamber measurements on light nucleus such as hydrogen and deuterium as they are presented in chapter 5. The satisfactory results for free nucleon motivated us to include the nuclear effects in order to check the model predictions for nuclear targets like carbon and oxygen which are typical target materials in the current neutrino experiments with high statistics. The impact of nuclear effects on single pion production was described in subsection 2.1.2 within two processes of initial state interaction and the final state interaction (FSI). To this end, we will use neutrino generators because they include the nuclear effects.

NEUT and GENIE are designed such that the total cross-section as a function of energy for each mode is computed before the event generation and stored in tables. This allows the probability of each interaction modes for a selected neutrino energy. An event can then be generated for the interaction mode selected, where the momentum and direction of every outgoing particle are specified. After the simulation of an interaction, the outgoing particles are propagated through the nuclear medium where they are allowed to interact.

A model in a Monte Carlo-based generator must be efficient and fast enough. This has been already checked for the MK-model using the cross-section calculation code, introduced in chapter 5. It was also the main focus while developing the MK-model, and the calculation (in chapter 3 and 4) had been revised several times in order to address the requirement.

In this chapter, we will talk about the single pion production model implemented in the two Monte Carlo (MC) neutrino interaction generators which are used by the current neutrino experiments. Then we describe the implementation of the proposed MK-model into NEUT.

Then details of the implementation in NEUT and validation plots will be given. Finally, we will show NEUT predictions with presently used models and with the new MK-model implementation (the result of work presented in this thesis) on nucleon and nuclear targets. Results in this chapter and next chapter are given for the parameters given in item 2 which is fitted to all CC neutrino data (ANL, BNL).

6.1   Monte Carlo generators of the neutrino interactions

In the following, we briefly describe the single pion production model in two Monte Carlo (MC) neutrino interaction generators: NEUT [56], the official generator of the Super-Kamiokande and T2K collaborations; and GENIE [57], which is widely used by the neutrino scattering and oscillation communities.
Both NEUT and GENIE use the Rein-Sehgal model [7] although there are some differences between the implementations. Here we summarize the differences:

- NEUT has 18 resonances implemented from the original paper [7] up to $W \leq 2$ GeV with the interferences among resonances, while GENIE implemented 16 resonances up to $W \leq 1.7$ GeV, without the interference effects.

- NEUT implemented the lepton mass based on Berger-Sehgal paper [13], while GENIE has only the lepton mass correction on the phase space.

- NEUT implemented Graczyk-Sobczyk resonance's form-factor from [17], while GENIE has RS form-factor from [7].

- For nonresonant background, NEUT implemented the nonresonant contribution for isospin 1/2 resonances from the original RS paper [7], while GENIE did not implement it.

Pion angular distributions in the RS-model are described by density matrix for all resonances, however both NEUT and GENIE only implemented the $\Delta(1232)$ resonance, i.e. both generators predict a symmetric distribution for θ angle as it is described in section 5.4.

6.2   Details of the implementation in NEUT

The implementation of the MK-model in the NEUT generator follows the existing implementation of the RS-model [7]. There are three channels for CC (anti-)neutrino channels and four channels for NC (anti-)neutrino given in Equation 3.1 - 3.4. Altogether there are 7

neutrino channels and similarly 7 antineutrino channels.

The basic event generation algorithm for single pion production in the current NEUT is as follows:

1. Randomly select a neutrino energy (E_v).

2. Randomly select the initial state nucleon momentum from a nuclear model (chapter 2). The probability of finding a nucleon with three-momentum and energy within Fermi gas model is related to the Fermi momentum and binding energy of the nucleus.

3. Randomly select a neutrino interaction for the selected E_v. Probability of each channel is based on precalculated $\sigma(E_v)$ table. If it picks single pion production channels, then goto step 4.

4. randomly generate W in allowed region:

$$M + m_\pi \leq W \leq W_{max},$$

   where W_{max} is the maximum value of W. In full phase space $W_{max} = \sqrt{2ME_v + M^2} - m_l$[1], but if $W_{cut} < \sqrt{2ME_v + M^2} - m_l$ then $W_{max} = W_{cut}$.

5. Get a maximum cross-section for the selected E_v. We step around the region in W and Q^2 that we expect to get the maximum cross-section. For W we expect to get the maximum cross-section around the Δ peak ($1.15 \leq W \leq 1.25$) and we expect to get the maximum cross-section at low Q^2 ($0.08 \leq Q^2 \leq 0.18$). At different energy and channels the maximum cross-section can be at secondary resonance peak but comparable to the Δ peak, therefore the maximum cross-section is multiplied to a safety factor (which is 1.5 in NEUT) to make sure that this is largest value in the whole phase space.

6. Generate a random cross-section up to the maximum cross-section from step 5.

7. Randomly generate $0 \leq Q^2 \leq 4E_v^2$. If it is not in kinematically allowed region:

$$-m_l^2 + \frac{ME_v}{2ME_v + M^2}(2ME_v + M^2 + m_l^2 - W^2 - \sqrt{\lambda}) \leq Q^2 \leq$$
$$-m_l^2 + \frac{ME_v}{2ME_v + M^2}(2ME_v + M^2 + m_l^2 - W^2 + \sqrt{\lambda})$$
$$\text{where } \lambda = (2ME_v + M^2 - m_l^2 - W^2)^2 - 4.*m_l^2 W^2 \tag{6.1}$$

   then go back to step 5.

---

[1] M, m_π and m_l are mass of nucleon, pion and lepton respectively.

8. Calculate the differential cross-section ($d\sigma/dWdQ^2$) from the RS-model for the selected event.

9. If the value in 6 is larger than the value in step 8, we reject the event and go back to the step 7. Otherwise we accept it and continue.

10. Randomly generate θ and ϕ such that $0 \le \theta \le \pi$ and $0 \le \phi \le 2\pi$.

11. The angular distribution of Δ resonance with the aid of the density matrix, in terms of spherical harmonics is given in the RS-model [7]. One can easily find a maximum value of the angular distribution.

12. Generate a random cross-section up to the maximum value from step 11.

13. Calculate the exact value of angular distribution for Δ resonance by knowing the pion angles from step 10.

14. If the value in step 12 is larger than the value in step 13, we reject the event and go back to the step 10. Otherwise we accept it and continue.

15. The cross-section in steps 5 and 9 and the angular distribution in steps 11 and 13 are calculated in the isobaric frame, therefore we need to boost it to the lab frame.

16. Apply Pauli blocking to the outgoing nucleon, if an event is Pauli blocked, NEUT leaves it as Pauli-blocked event, i.e. set all outgoing particles inactive and the cross-section does not take into account this event[2].

Steps 5- 10 are related to the RS-model while steps 2 and 16 are related to the nuclear model. Therefore replacing MK-model with RS-model, one need to modify all steps 5- 14. Besides the cross-section table in step 3 should be filled with the MK-model predictions for all channels.

RS-model provides $d\sigma/dWdQ^2$, therefore we only need to generate a random number for W and Q^2 to calculate the cross-section. If the event in the step 10 is accepted, the angular distributions (based on density matrix given in [7]) will be provided later. However the density matrix which is implemented in NEUT is not complete and it only includes Δ resonance for simplicity, as it mentioned in section 6.1. On the other hand, the MK-model provides a full kinematic cross-section ($d\sigma/dWdQ^2d\Omega$), and the event is generated in one step and there is no assumption in the angular calculation. Therefore the angular distribution of the existing RS-model is only from Δ resonance while the angular distribution of the MK-model

---

[2]NEUT keeps these event to check the consistency with cross-sections in table.

implementation takes into account all resonant and nonresonant ingredients including all interference terms. Here is the new algorithm for the MK-model implementation:

1. Randomly select a neutrino energy (E_ν).

2. Randomly select the initial state nucleon momentum from a nuclear model (chapter 2).

3. Randomly select a neutrino interaction for the selected E_ν. Probability of each channel is based on precalculated $\sigma(E_\nu)$ of the MK-model. If any channels of single pion production, then goto step 4.

4. Randomly generate W in allowed ($M + m_\pi \leq W \leq W_{max}$) region.

5. Get a maximum cross-section for the selected E_ν. We step around the region in W and Q^2 that we expect to get the maximum cross-section. θ and ϕ have almost a flat distributions therefore we step around whole phase space to find the maximum cross-section. The same safety factor (which is 1.5, like before) is also multiplies to make sure that this is the largest value in whole phase space.

6. Generate a random cross-section up to maximum cross-section.

7. Randomly generate $0 \leq Q^2 \leq 4E_\nu^2$, and check if it is in the kinematically allowed region. If not, then go to step 5.

8. Randomly generate θ and ϕ, such that $0 \leq \theta \leq \pi$ and $0 \leq \phi \leq 2\pi$.

9. Calculate the differential cross-section from MK-model ($d\sigma/dWdQ^2d\Omega$ in Equation 3.60) for the selected event.

10. If the value in 6 is larger than the value in step 9, we reject the event and go back to the step 7. Otherwise we accept it and continue.

11. The cross-section in steps 5 and 9 is calculated in the isobaric frame, therefore we need to boost it to the lab frame.

12. Apply Pauli blocking to the outgoing nucleon.

6.3   Validation of the implementation

As discussed in chapter 5, MK-model is implemented in the cross-section calculation (CSC) code that can provide differential cross-section in variables like Q^2, invariant mass W and

$\cos\theta$ in the isobaric frame[3]. In this chapter the MK-model is implemented in NEUT. Now we will compare the output of NEUT for free nucleon (the MK-model) with the output of CSC code for Q^2, W, and $\cos\theta$ differential cross-sections with fixed neutrino energy. Note that the model is the same but integration methods are different in the cross-section calculation code and Monte Carlo generator, therefore we expect to get exactly the same result if we generate enough events in NEUT.

Figure 6.1 shows both results for $\nu p \rightarrow \mu p \pi^+$ channel, as a function of Q^2 W and $\cos\theta$ in the isobaric frame for a fixed energy $E_\nu = 1$ GeV.

We should do the same for all other CC and NC (anti-)neutrino channels. In Figure 6.2 we
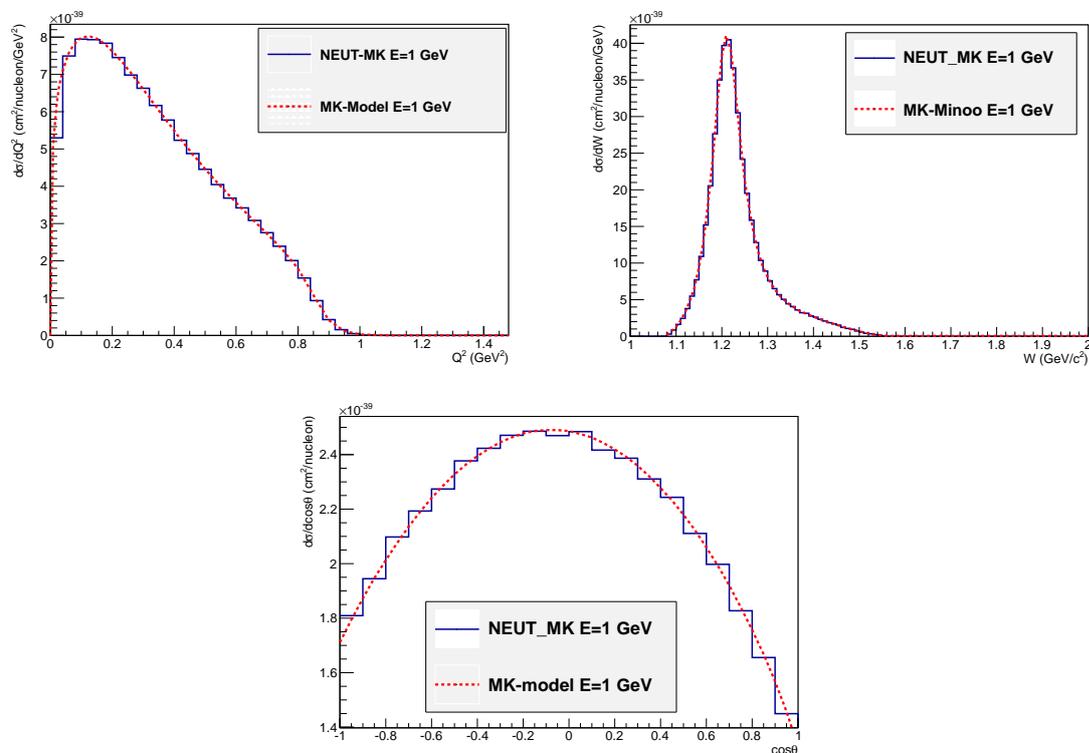
Fig. 6.1 Differential cross-section in Q^2 (top-left), W (top-right) and $\cos\theta$ in the isobaric frame (bottom) for a fixed energy $E_\nu = 1$ GeV. The blue histograms are the output of NEUT (with 500000 events), and the dashed-red curves are the output of CRC. As we see the results are identical.

show some of the validation plots i.e. the differential cross-section as a functions of Q^2 and W for different channels.

The exact agreement between cross-section calculation code and NEUT in the validation plots is a confirmation that MK-model is implemented in NEUT correctly. Now we are

---

[3]That is why we could compare the model prediction with bubble chamber data.
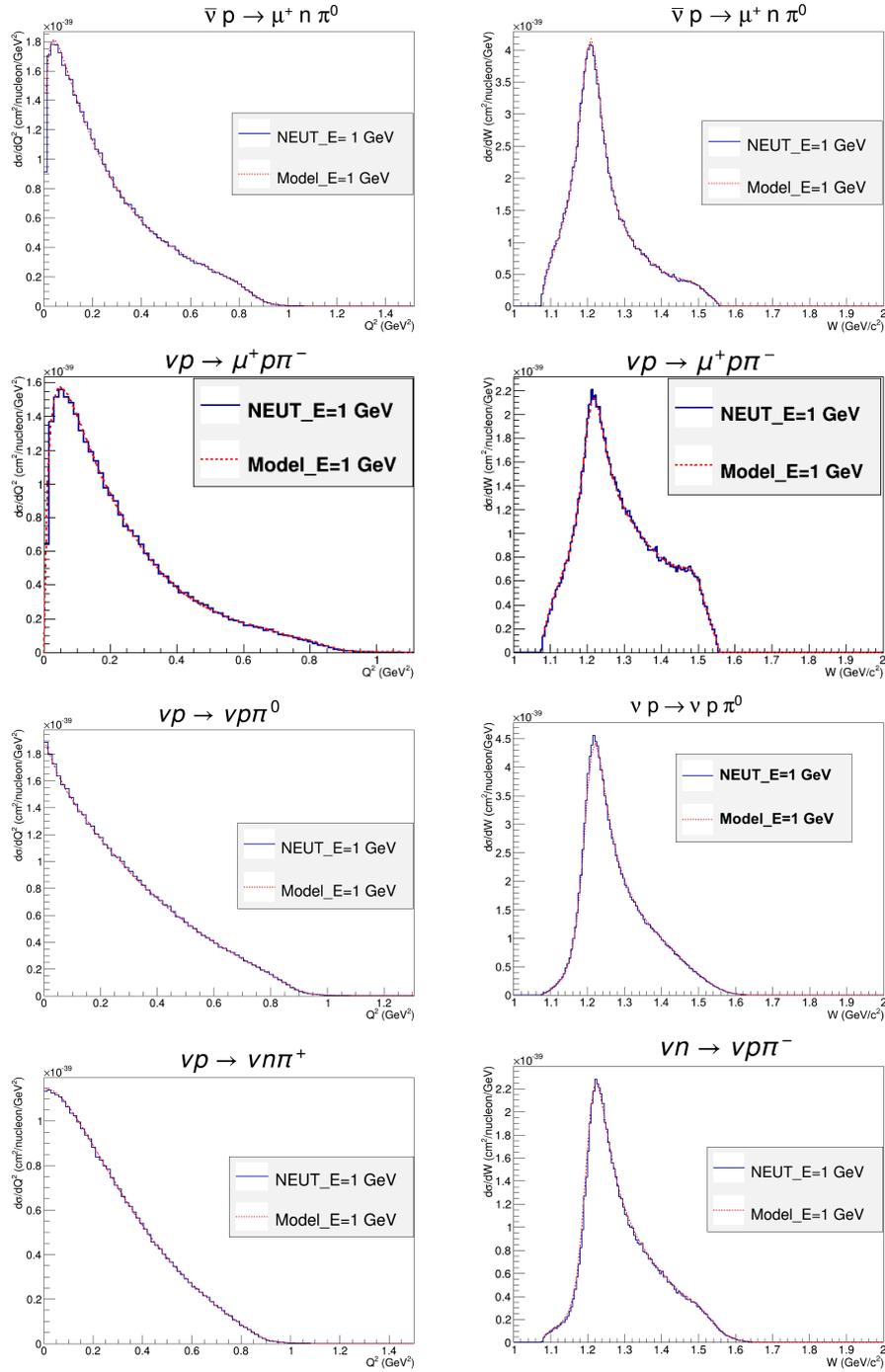
Fig. 6.2 Differential cross-section as a functions of Q^2 (left), W (right) for different channels and fixed energy $E_\nu = 1$ GeV. The blue histograms are the output of NEUT, and the dashed-red curves are the output of CSC code. As we see the results are identical.

allowed to move forward and do the Monte Carlo comparisons to analyse differences of the new MK-model with respect to the existing RS-model.

6.4   NEUT RS-model vs NEUT MK-model

The MK-model is implemented successfully as it is discussed in the previous section. Now we are able to show the NEUT predictions with the MK-model for different targets and all interesting variables.

In this section, we compare the outputs of NEUT 5.3.6 (RS models) and same version of NEUT with the MK-model (instead of RS-model). The RS-model in NEUT 5.3.6 has three adjustable parameters; M_A and C_5^A for Graczyk-Sobczyk form-factors [17], similar to MK-moodel. The RS-model proposed a helicity amplitudes of nonresonant contribution for resonant background with isospin 1/2 multiplied by an adjustable parameter. The comparisons consist of differential cross-section as a function pion and muon momenta and angles in the lab frame, for free nucleon and nuclear target.

The main goal in this section is to show how much the MK-model modifies NEUT predictions for T2K simulation. For this reason we generate events with T2K (near detector) flux [60] and CH target[4].

6.4.1   Nucleon target

All CC and NC (anti-)neutrino-nucleon channels are shown in Equations 3.1 - 3.4. Here we show NEUT comparisons for few selected channels on free nucleon with invariant mass $W < 2$ GeV cut. The differential cross-section are a functions of W and Q^2, pion and muon momenta in the lab frame (p_μ, p_π), the angle between pion and neutrino in lab frame (θ_π), the angle between muon and neutrino in lab frame (θ_μ).

For CC neutrino interaction we choose $\nu p \to \mu p \pi^+$ and $\nu n \to \mu n \pi^+$ channels. Figure 6.3 shows the NEUT predictions with RS-model and the MK-model for $\nu p \to \mu p \pi^+$ channel with isospin 3/2, which is dominated by Δ resonance. It shows similar normalization (area below histogram which is cross-section) but different shapes for pion kinematics.

As discussed in subsection 5.2.1 the axial form-factor is extracted from bubble chamber data for $\nu p \to \mu p \pi^+$ channel. The adjustable parameters in NEUT 5.3.6 are also fitted to the same data set, therefore we expect to have similar cross-section (normalization) comparing RS-model with MK-model. In this channel, Δ resonance is dominant and it is clearly visible in $d\sigma/dW$ (top-right plot) where the histogram has a significant peak around $W = 1.22$ GeV.

---

[4]Next chapter we will talk about T2K near detector (ND280).

The different shapes on tail are due to the nonresonant interactions and the interference effects. For $d\sigma/d\cos\theta_\pi$ (right-bottom plot), the MK-model predicts less pion at forwards direction which is consistent with same cross-section in the Adler frame[5] (compare shapes of solid and dashed curves in Figure 5.20).

Figure 6.4 shows the same comparisons for $\nu n \to \mu n \pi^+$ channel where all resonances (with isospin 1/2 and 3/2) can contribute. This is visible in $d\sigma/dW$ (top-right plot), where Δ resonance is not the only peak. This plot also shows the effect of different form-factors at higher W (see Figure 6.4). Figure 6.4 shows that NEUT predictions are different (between RS and MK model) in both shape and normalization which is due to the nonresonant background that has significant effects in this channel.

For CC anti-neutrino interaction we choose $\bar{\nu} n \to \mu^+ n \pi^-$ and $\bar{\nu} p \to \mu^+ p \pi^-$ channels. Figure 6.5 shows the NEUT predictions with RS-model and the MK-model for $\bar{\nu} n \to \mu^+ n \pi^-$ channel with isospin 3/2, which is clearly dominated by Δ resonance in $d\sigma/dW$ (top-right plot). All plots in Figure 6.5 show different normalization and different shapes. We expected to see different normalization from Figure 5.15, where the MK-model predicts larger cross-section and apparently better agreement with data.

Figure 6.6 shows the NEUT comparisons for $\bar{\nu} p \to \mu^+ p \pi^-$ channel where all resonances contribute. This channel has the same isospin (1/2 and 3/2) combinations as $\nu n \to \mu n \pi^+$ channel as it is clear from $d\sigma/dW$ (top-right) plot. It shows that NEUT predictions are different (between RS and MK model) in both shape and normalization. We expected to see different normalization from Figure 5.15, where the MK-model predicts larger cross-section and apparently better agreement with data. The shape discrepancy is due to the nonresonant contribution and interferences effects.

For NC neutrino interaction we choose $\nu p \to \nu p \pi^0$ and $\nu p \to \nu n \pi^+$ channels. All NC channels are a mixture of both isospins 1/2 and 3/2 with different isospin coefficients. Figure 6.7 shows the NEUT predictions with RS-model and the MK-model for $\nu p \to \nu p \pi^0$ channel where all plots show different normalization and shape. We expected to see different normalization from Figure 5.17, where the MK-model predicts larger cross-section.

Figure 6.8 shows the same comparisons for $\nu p \to \nu n \pi^+$ channel. Similar to other channels it shows that NEUT predictions are different (between RS and MK model) in both shape and normalization. We expected to see different normalization from Figure 5.17, where the MK-model predicts less cross-section. The shape discrepancy is due to the nonresonant contribution and interferences effects.

Unfortunately, there is no reliable data for neutral-current interactions except very few events from bubble chambers with large errors. However NC1π^0 sample is particularly

---

[5]We can do this only for the forward bins and for this channel since we have similar normalization.
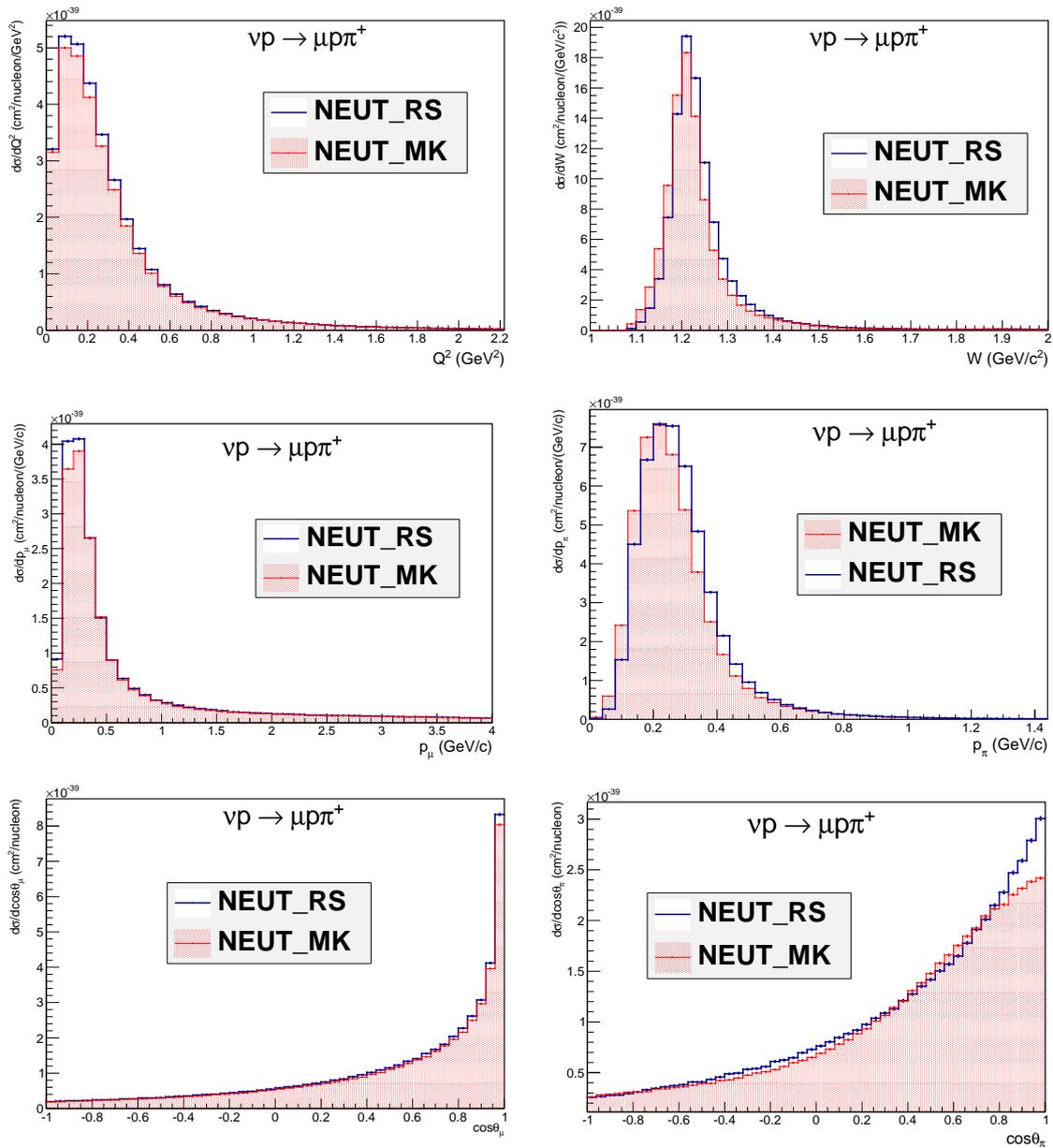
Fig. 6.3 Differential cross-section of $\nu p \to \mu^- p \pi^+$ channel for T2K energy, as a functions of lepton kinematics (left plots) and hadron kinematic (right plots) as it is predicted by NEUT 5.3.6 for RS model (blue) and the MK-model (red).
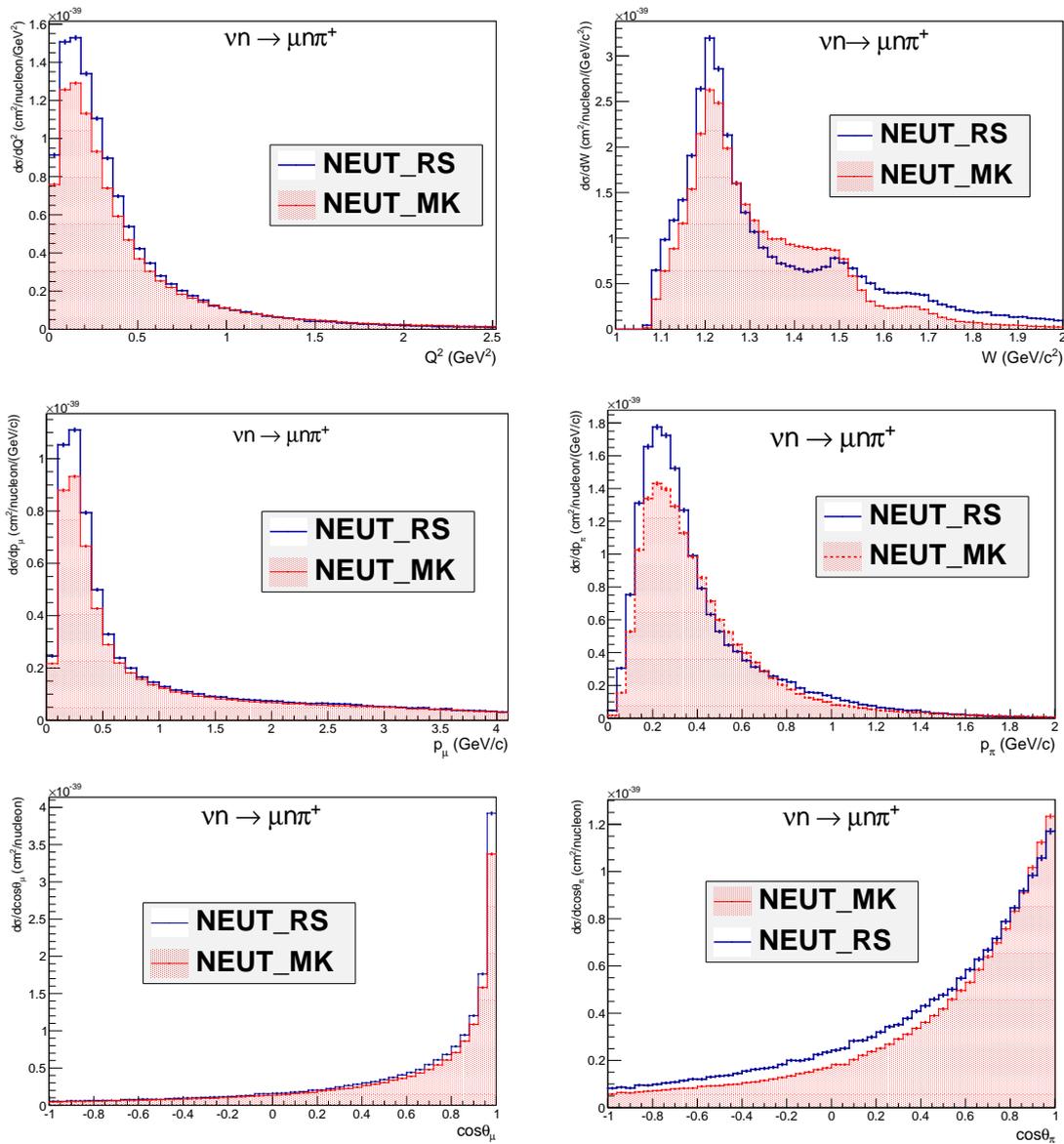
Fig. 6.4 Differential cross-section of $\nu n \rightarrow \mu^- n \pi^+$ channel for T2K energy, as a functions of lepton kinematics (left plots) and hadron kinematic (right plots) as it is predicted by NEUT 5.3.6 for RS model (blue) and the MK-model (red).
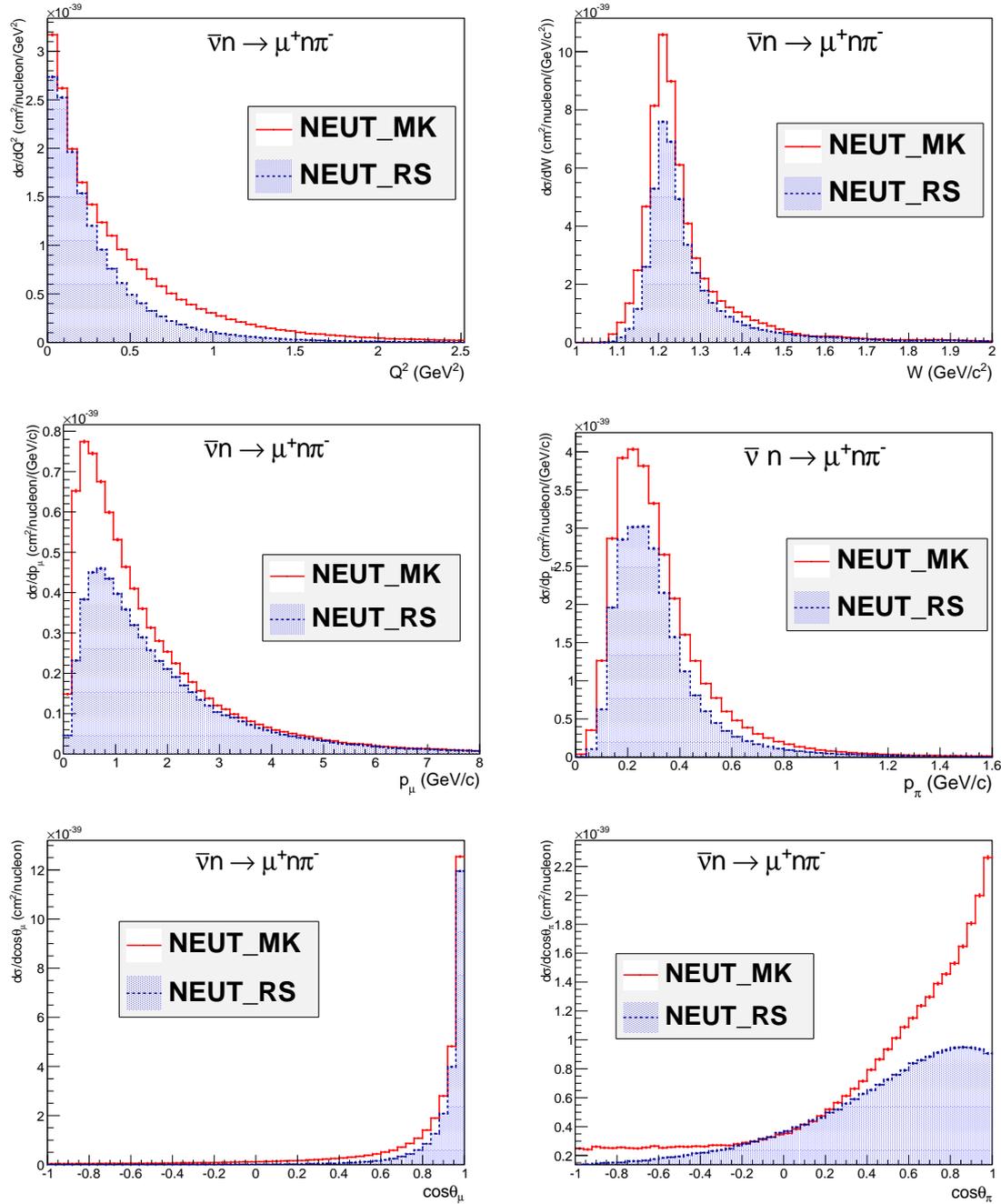
Fig. 6.5 Differential cross-section of $\bar{\nu}n \to \mu^+ n\pi^-$ channel for T2K energy, as a functions of lepton kinematics (left plots) and hadron kinematic (right plots) as it is predicted by NEUT 5.3.6 for RS model (blue) and the MK-model (red).
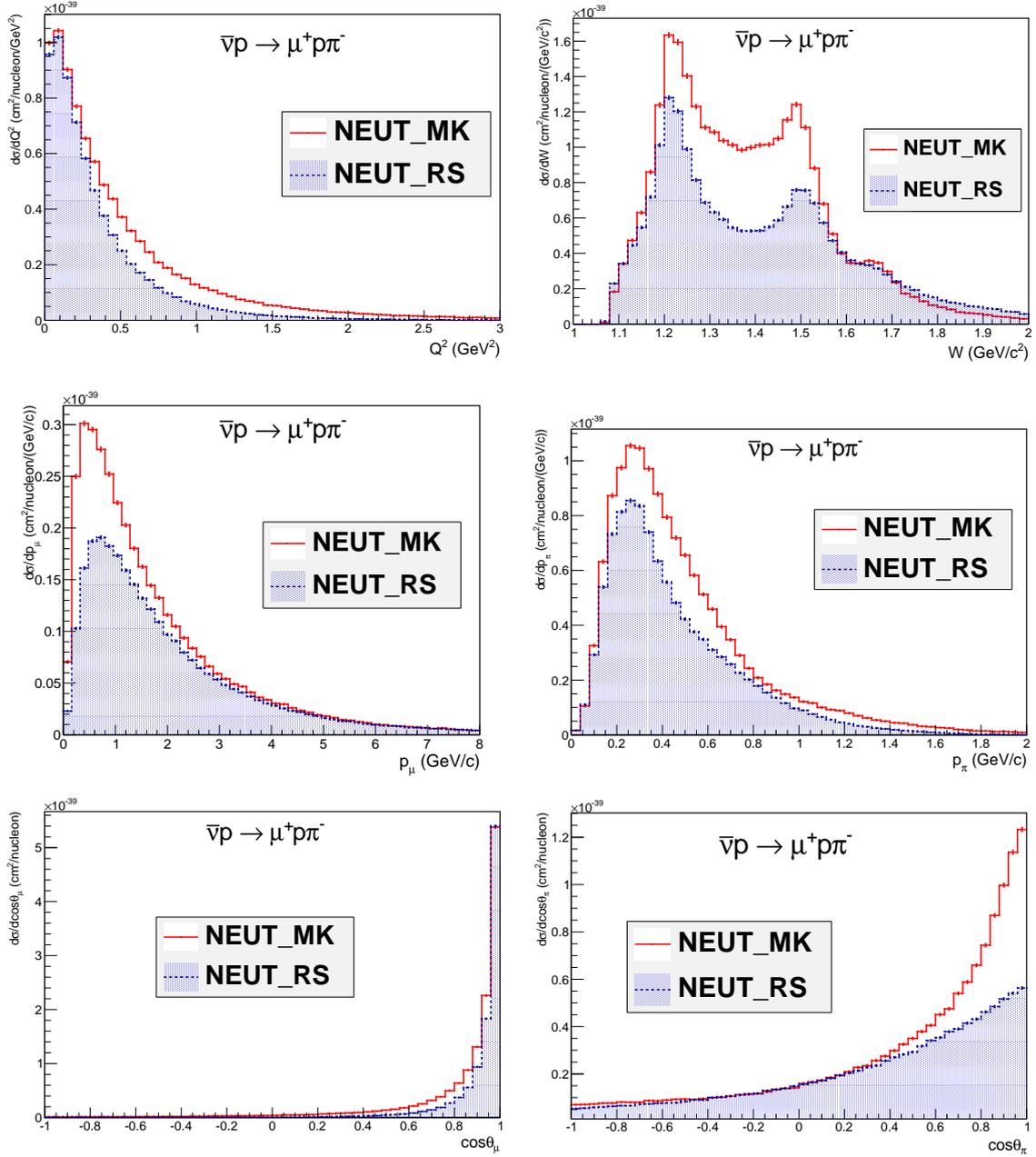
Fig. 6.6 Differential cross-section of $\bar{\nu}p \to \mu^+ p\pi^-$ channel for T2K energy, as a functions of lepton kinematics (left plots) and hadron kinematic (right plots) as it is predicted by NEUT 5.3.6 for RS model (blue) and the MK-model (red).
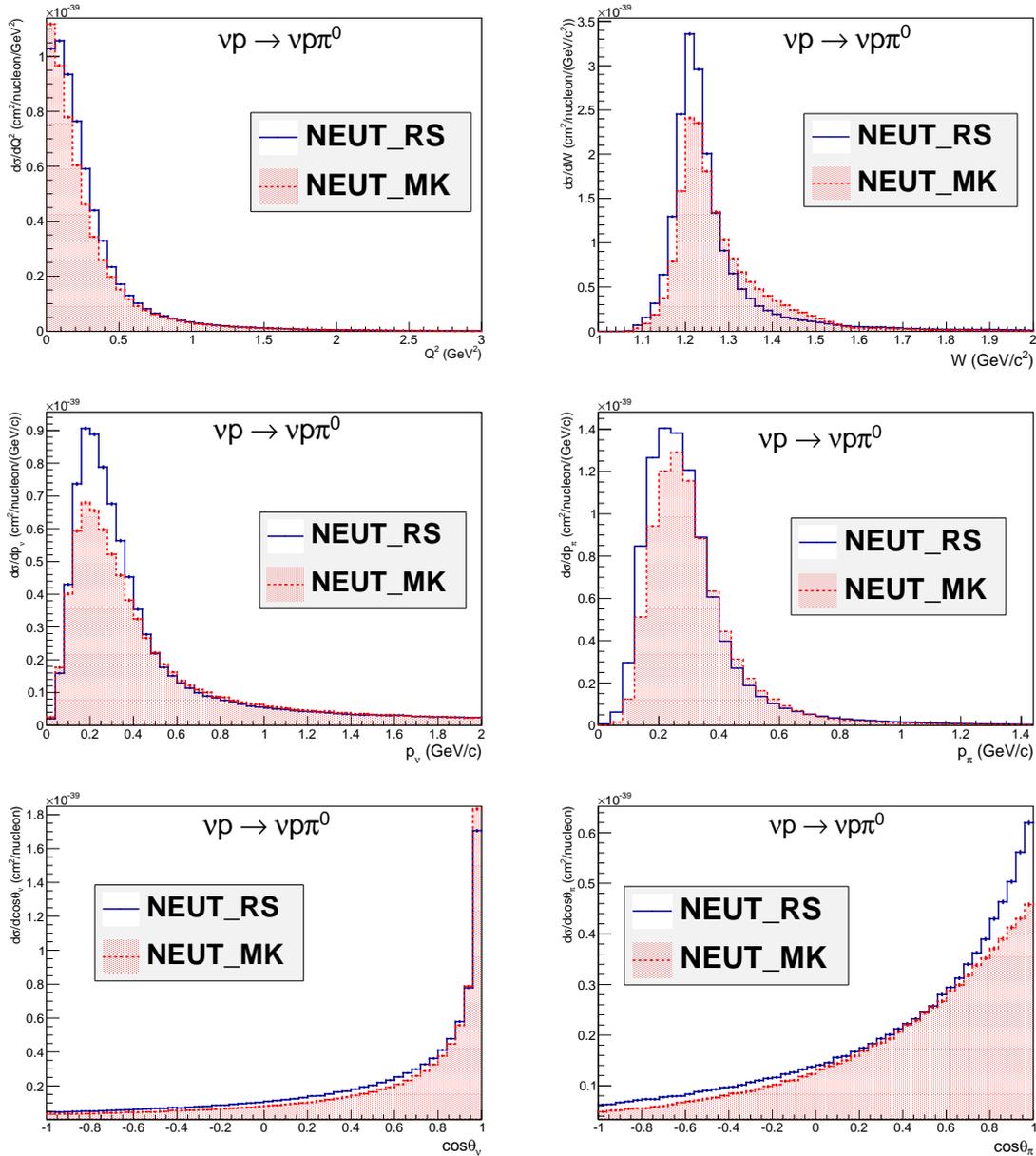
Fig. 6.7 Differential cross-section of $\nu p \to \nu p \pi^0$ channel for T2K energy, as a functions of lepton kinematics (left plots) and hadron kinematic (right plots) as it is predicted by NEUT 5.3.6 for RS model (blue) and the MK-model (red).
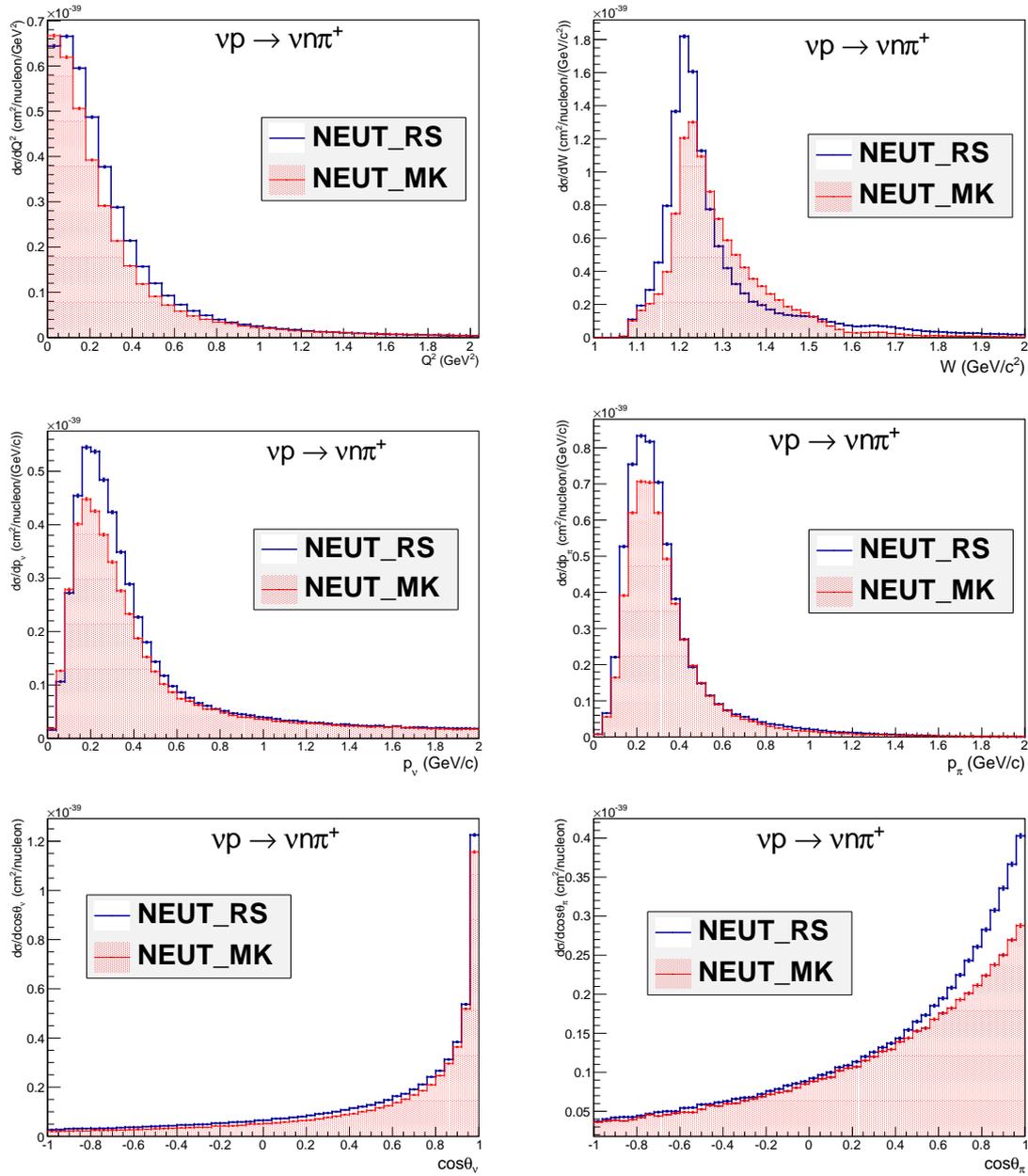
Fig. 6.8 Differential cross-section of $\nu p \to \nu n \pi^+$ channel for T2K energy, as a functions of lepton kinematics (left plots) and hadron kinematic (right plots) as it is predicted by NEUT 5.3.6 for RS model (blue) and the MK-model (red).

important for water Cherenkov detector like Super-Kamiokande [64]. NC1π^0 is the main background in ν_e appearance searches because NC1π^0 might be misidentified as charge current $\nu_e N \rightarrow eN$ interaction since they produce similar rings[6]. Therefore a reliable model is crucial for neutrino oscillation experiment like T2K.

6.4.2 Neutrino-Nucleus interactions

To study the nuclear effects (as it was explained in subsection 2.1.2) we run NEUT with CH target, which is a target used in many current experiments. Similar to the previous section we do the comparison between NEUT 5.3.6 with RS-model and NEUT with MK-model, however, the comparison can not be based on channels because the initially produced hadrons in neutrino-nucleon interactions can be different than the outgoing particles being detected at the end due to the FSI effects. Therefore the comparison is based on different samples. Note that nuclear models are the same for both cases.

For CC1π^+ we select events with one muon and one π^+, and at least one nucleon in the final states. Figure 6.9 shows NEUT predictions with MK-model and RS-model in various kinematic variables for CC1π^+ sample on CH target. All plots show discrepancy in normalization and shape where this is due to the different cross-section (RS vs MK) models. It is similar to the discrepancy presented in Figure 6.3 and Figure 6.4 for $\nu p \rightarrow \mu p \pi^+$ and $\nu n \rightarrow \mu n \pi^+$ channels. For easier comparison we also show the CC1π^+ sample on nucleon (i.e. summation of the two channels) in Appendix J.

For anti-neutrino interactions, we also compare the NEUT predictions with both models for CC1π^- sample on the CH target in Figure 6.10. The discrepancy in normalization and shape is very similar to the discrepancy presented in Figure 6.3 and Figure 6.4 for $\bar{\nu} n \rightarrow \mu^+ n \pi^-$ and $\bar{\nu} p \rightarrow \mu^+ p \pi^-$ channels. For easier comparison we also show the CC1π^+ sample on nucleon (i.e. summation of the two channels) in Appendix J.

Figure 6.9 and Figure 6.10 clearly show that the discrepancy at initial interaction remains after final state interaction in nucleus. The nuclear effects reduce the total cross-section in both CC1π^+ (compare Figure 6.9 with Figure J.1) and CC1π^- (compare Figure 6.10 with Figure J.2) samples, mainly due to pion absorption in the final state interaction.

---

[6]This will be discussed in next chapter with Super-Kamiokande detector, in subsection 7.1.3.
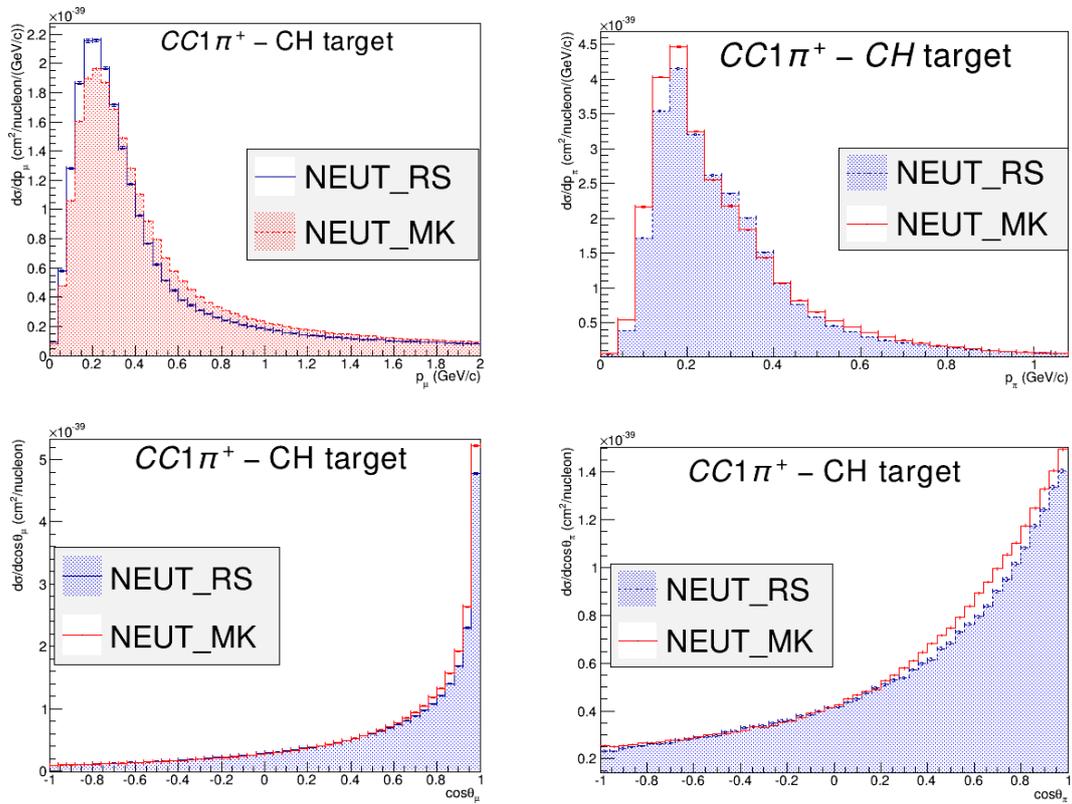
Fig. 6.9 Differential cross-section of CC1π^+ sample on CH target for T2K energy, as a functions of lepton kinematics (left plots) and hadron kinematic (right plots) as it is predicted by NEUT for RS model (blue) and the new model (red).
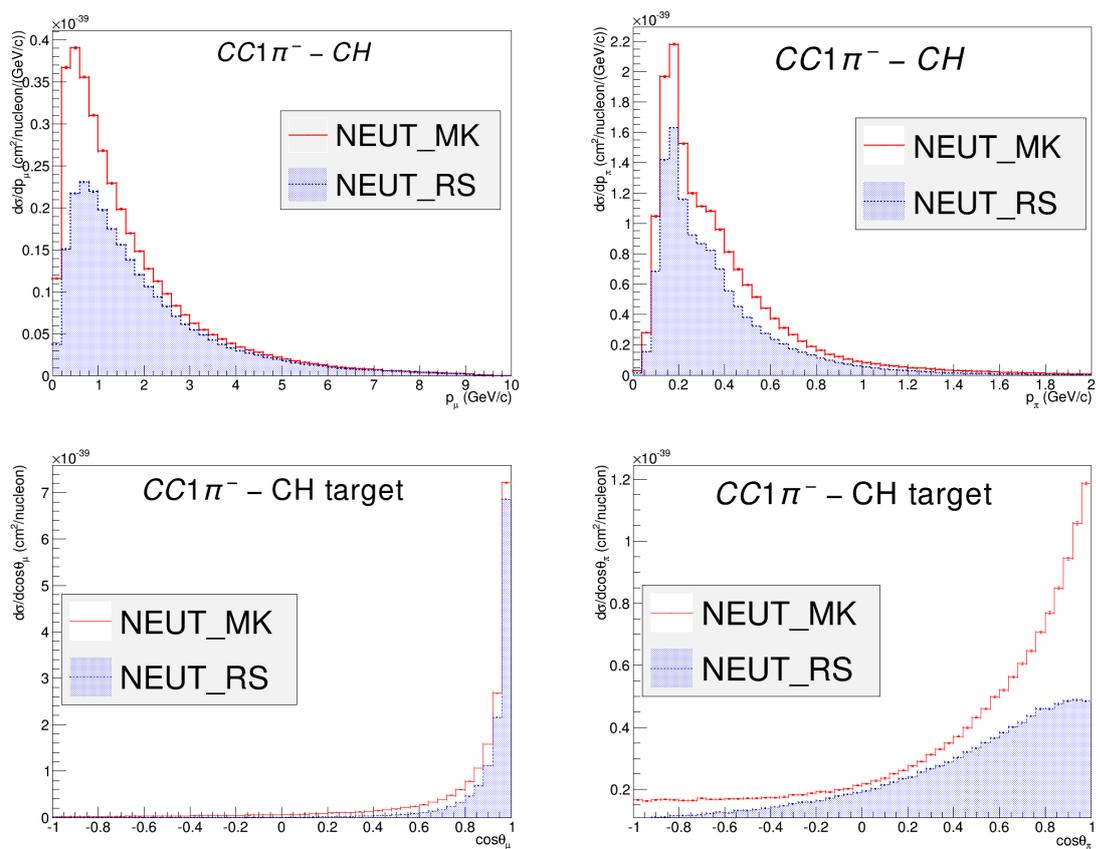
Fig. 6.10 Differential cross-section of CC1π^- samples on CH target for T2K energy, as a functions of lepton kinematics (left plots) and hadron kinematic (right plots) as it is predicted by NEUT for RS model (blue) and the new model (red).

6.5 Conclusion

The MK-model has been implemented in NEUT, and its prediction was compared with the current NEUT to show how different they are. The MK-model is a complete model with no assumption neither in calculation nor in the implementation. There are different approaches for nonresonant background in the two models. The RS-model rely on ad hoc terms proposed in the RS-model [9] with an adjustable parameter which is fitted to the charged-current neutrino channels, while the MK-model includes a sophisticated model for nonresonant interaction.

Distinction between RS-model which is currently used for the T2K analysis and MK-model appeared in both shape and normalization of differential cross-section as a function of different variables. Unlike $CC1\pi^+$ channels, CC anti-neutrino show a large discrepancy between the two models for all comparisons. The large discrepancy in the normalization turned out to be a strong point of the MK-model when we look at the comparison with bubble chamber data in the previous chapter.

Apart from the normalization, there is a large discrepancy in the shape comparison for all samples due to the nonresonant interaction and the interference effects. This is significant for the pion polar angle especially in the very forward bins, which also affects on pion momentum distributions.

To summarize, the implementation of MK-model in NEUT provides a complete description of single pion production in the initial state interaction, which is significantly different than the RS-model's predictions that is currently used for T2K analysis. For more investigation, next chapter is devoted to data (on nuclear target) comparison with NEUT prediction for both models.

Chapter 7

Monte Carlo Predictions and Comparison with Neutrino-Nucleus Data

Several modern neutrino experiments have measured the charged-current single pion production on nuclear targets, with a wide/narrow band of a few-GeV energy (muon neutrino) beam. In the previous chapter, we assumed that single pion production model is the only cross-section model responsible for single pions. However, they can also be produced via nucleon rescatterings of CCQE interactions and the coherent scattering, as they were discussed in section 2.1. Deep inelastic scattering is responsible for single pion with $W > 2$ GeV in NEUT.

In this chapter we describe three neutrino experiments; T2K, MINERνA and MiniBooNE. They all provided measurements of the CC single pion production cross-section on various target materials and with different (anti-)neutrino beams. To do the Monte Carlo comparison with published data we should:

1. Choose the target and flux for individual experiments, in order to generate events[1].

2. Analyze the events as it is done for data analysis, by selecting similar samples and applying same selection.

For the second step, we are using NUISANCE [84] software in this chapter. The NUISANCE is a software package to simplify the task of comparing neutrino event generators with published cross-section data. More information about NUISANCE is in Reference [84].

At the end of each section, the first comparisons between NEUT with the MK-model and data will be presented. To show the effects of the MK-model, we will also include the current NEUT predictions with RS-model. Note that all models used in NEUT, except the model for single pion production, are the same for the comparisons.

---

[1]we generate 15000 events with NEUT for all experiments.

7.1   The T2K experiment

The T2K [63](Tokai to Kamioka) experiment is a long-baseline neutrino oscillation experiment designed to study various neutrino oscillation parameters through ν_μ disappearance and ν_e appearance, using a high intensity off-axis ν_μ beam.

A high purity ν_μ beam is produced at the Japan Proton Accelerator Research Complex (J-PARC) on the east coast of Japan. There is a near detector complex located 280 m downstream of the target, which is designed to measure the unoscillated beam intensity, purity and direction to high precision. The flavour composition of the beam is then measured 295 km downstream of the production point at the far detector, Super-Kamiokande [64], which measures the oscillation parameters.

Both far detector and the off-axis near detector are placed $2.5°$ off-axis with respect to the neutrino beam. This technique produces a narrow-band beam, which allows precision measurements to be made. The baseline between the neutrino production point and the far detector, 295 km, is carefully chosen to correspond to the first minimum in the ν_μ survival probability at the peak neutrino beam energy of 0.6 GeV in order to maximise the effect of neutrino oscillation at the far detector. The near detector can make the cross-section measurements, therefore we also show (in Figure 7.1) the contribution of interaction types in the narrow-band beam.

7.1.1   T2K beamline

Accelerator gives protons at 30 GeV, they are led to the primary target. The primary beamline is used to bend the 30 GeV proton beam towards the detectors. The secondary beamline consists of the target station, decay volume and beam dump, as shown in Figure 7.2.

Protons enter the target station where they will be focused toward target by magnetic horns. The target itself is a 91.4 cm long, 2.6 cm diameter graphite rod located within the first magnetic horn. The results of collisions are secondary mesons (mostly pions and kaons). The charged mesons which are focused by the magnetic horns enter a 96 m long decay volume. In this volume, the mesons decay to produce muon neutrinos and antineutrinos. The current driving the magnetic horns can be inverted to focus either positively or negatively- charged mesons, resulting in a predominantly neutrino or anti-neutrino beam.

At the downstream end of the decay volume, a 75 t graphite beam dump stops all hadrons and most muons below 5.0 GeV and leaves the neutrinos to pass.
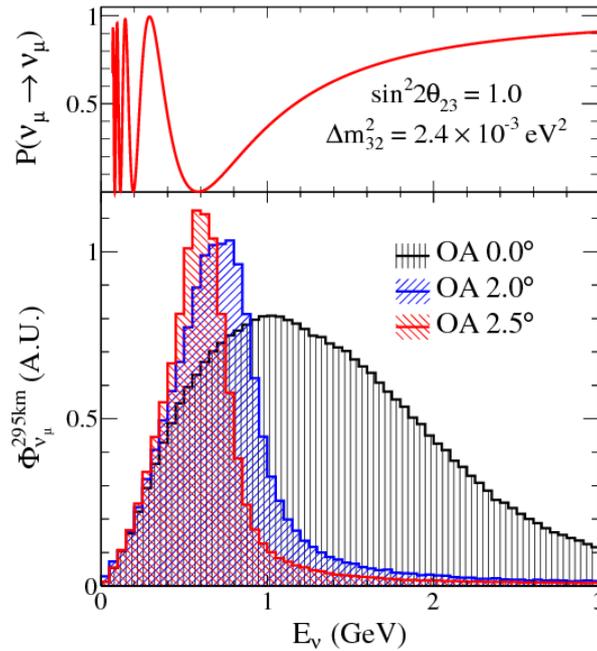
Fig. 7.1 The top plot shows the muon neutrino survival probability for the T2K baseline and the bottom plot shows the T2K neutrino flux as a function of energy for different off-axis angles. The neutrino flux peaks at 0.6 GeV for an off-axis angle of $2.5°$, which corresponds to the first oscillation maximum for T2K. Figure from Reference [63].

7.1.2   ND280 - the T2K Near detector

The off-axis ND280 detector is designed to reduce uncertainties in the flux and cross-section predictions. It consists of a few subdetectors as it is shown in Figure 7.3. The central part contains of a π^0 detector (the PØD), the tracker region, as well as the downstream electromagnetic calorimeter (DsECal). The tracker consists of two fine-grained detectors (FGDs), which provide a target (carbon and oxygen) for neutrino interactions with high resolution around the interaction vertex, and three time projection chambers (TPCs) are then used to measure the interaction products, and give very good momentum resolution and particle identification. A sample single pion production event is also shown in Figure 7.3. FGD1 is more upstream and is composed of 30 layers scintillator bars with layers in the x
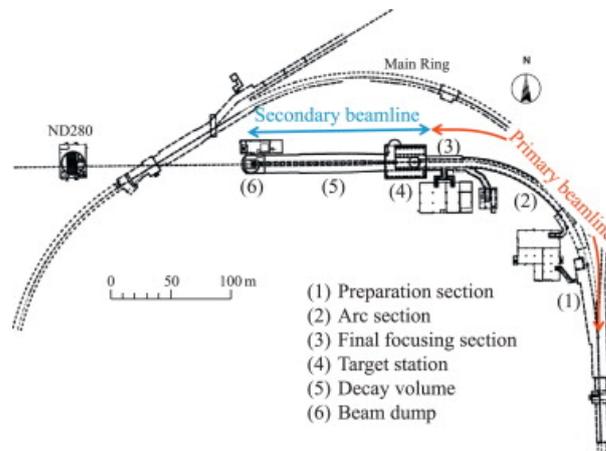
Fig. 7.2 Overview of the T2K beamline. Figure from [63]

and y directions allowing 3D tracking of charged particles. The downstream FGD2 has a total of 14 layers of scintillator bars, arranged in pairs of XY layers between which there are six 2.5 cm thick layers of water.

Although the other ND280 subdetectors are also important for the cross-section program, we will not discuss them here. For more details, see References [65–69].

7.1.3 Far detector (Super-Kamiokande)

Super-Kamiokande (SK) [64] is a large water Cherenkov detector. It serves as the far detector of the T2K experiment and is located in the Kamioka mine, 295 km in straight line from J-PARC facility. SK has been operating since 1996, long before the T2K experiment, with a broad physics program. It is composed of two huge cylindrical constructions, one within the other. The entire container is filled with 50 kt of ultra-pure water and is a target for neutrino interactions.

Charged particles produced by neutrino interactions emit Cherenkov radiation in a cone as they travel through water, and will be detected by the PMTs on the walls of the detector, where they form a ring-shaped hit pattern. Note that Cherenkov light is only produced by charged particles with sufficient energy to travel faster than the speed of light in the medium through which they are passing; typically, nucleons are below threshold so are unseen by SK. Muons and electrons can be distinguished at the SK by ring-shaped patterns (see Figure 7.4) produced by the Cherenkov light cones. Muons have a relatively large mass and do not rescatter as they pass through the water in the detector, producing a "sharp" ring, while electrons rescatter and generally induce electromagnetic showers at SK energies which produce a "fuzzy" ring, a sum of multiple Cherenkov light cones.
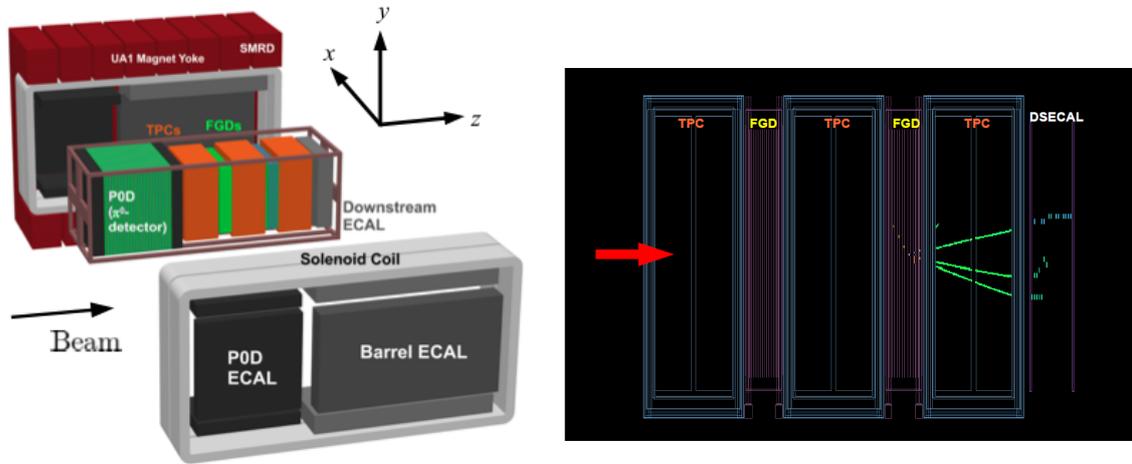
Fig. 7.3 Left: components of ND280 (T2K near detector) from Reference [63]. Right: a single pion production event in ND280 tracker (FGD 2).

An important point related to the single pion production is that $NC1\pi^0$ sample is a serious
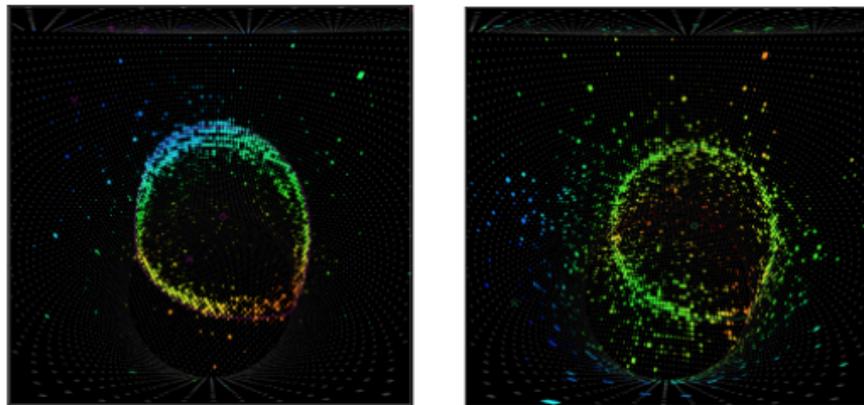
Fig. 7.4 Example events in Super-Kamiokande for a muon (left), and an electron (right) event. The colour scale represents arrival time of light at a PMT, ranging from early (violet) to late (red) times.

background for the single-ring electron-like sample in Super-Kamiokande. The single π^0 produced from the interaction of a neutrino with water target will decay immediately to two photons, which Compton scatter and produce $e^- - e^+$ pairs. These result in Cherenkov rings that are indistinguishable from those produced by electrons from CCQE scattering. If one of the two rings is not reconstructed or the rings overlap, it will look identical to a ν_e CCQE event.

7.1.4   T2K data and Monte Carlo predictions

T2K collaboration provided measurements of the CC single π^+ production (CC1π^+) cross-sections on water target (FGD2) with the T2K near detector [70]. CC1π^+ events are selected by requiring one muon, one positive pion, no other additional pions and any number of nucleons, i.e.

$$\nu_\mu + H_2O \rightarrow \mu^- \pi^+ + X \tag{7.1}$$

where X is any number of nucleons in the final state.

The analysis also restricts the kinematic phase-space to the region defined by

$$\begin{aligned} p_\pi > 200 \text{ GeV} , &\qquad \cos\theta_\pi > 0.3 \\ p_\mu > 200 \text{ GeV} , &\qquad \cos\theta_\mu > 0.3 \end{aligned} \tag{7.2}$$

to increase the efficiency of reconstruction for the CC1π^+ sample. The predicted neutrino beam flux (peaks at 0.6 GeV) is given in [60]. To do the comparison we use the same target and flux. We also apply same cuts described before.

Figure 7.5 shows the comparison between the T2K data [70] and the NEUT predictions with MK-model and RS-model as single pion cross-section model. The comparisons have been made for CC1π^+ differential cross-sections as a function of pion kinematics, muon kinematics, the angle between pion-muon and reconstructed neutrino energy in the reduced phase-space (Eq. 7.2).

 All plots show better agreements with the MK-model and as we expected, there is more discrepancy between the two models in pion kinematics than muon kinematics, but the largest discrepancy appears in differential cross-section as a function of $\cos\theta_{\mu,\pi}$, shown in the bottom right plot of Figure 7.5.

Note that current NEUT with RS-model has three adjustable parameters (see chapter 5), and they have been already fitted to bubble chamber data, for various kinematics in order to reduce the T2K systematic uncertainty. On the other hand, the MK-model has two parameters, and they are only fitted to ANL Q^2-differential cross-section to extract the axial form-factors for resonant interaction, as it was explained in subsection 5.2.1.

According to Figure 7.5, the T2K data on water prefers MK-model, even without additional free parameter and extra fitting with bubble chamber data.
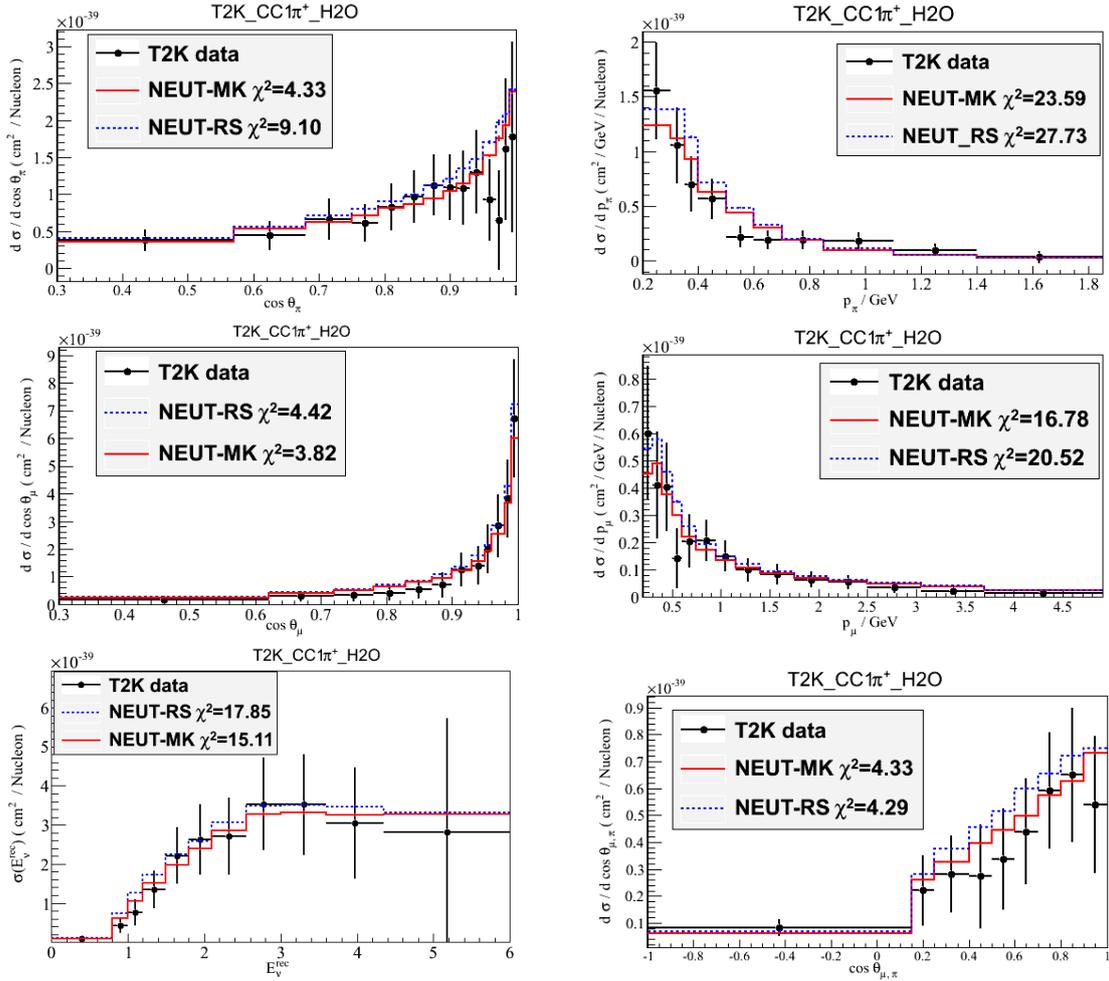
Fig. 7.5 T2K measurements on water for CC1π^+ differential cross-sections as a function of pion kinematics (top), muon kinematics (center), $\cos\theta_{\mu,\pi}$(bottom right) and reconstructed neutrino energy (bottom left) in the reduced phase-space of $p_{\pi^+} > 200$ MeV/c, $p_\mu > 200$ MeV/c, $\cos\theta_\pi > 0.3$ and $\cos\theta_\mu > 0.3$. Histograms show NEUT predictions with MK-model (solid-red) and RS-model (dashed-blue). Degrees of freedom are different (between 9-14).

7.2   The MINERνA experiment

The MINERνA experiment (Main INjector ExpeRiment ν-A) [71] is designed to make high precision measurements of neutrino-nucleus scattering cross-sections. It uses a fine-grained, plastic-scintillator tracking detector [71] in conjunction with the magnetized MINOS near detector [73], to record interactions of neutrinos and antineutrinos from the high-intensity Neutrinos at the Main Injection (NuMI) beam at Fermilab [72]. The MINOS near detector is located downstream of the main MINERνA detector, and is used as a muon spectrometer. As the MINOS detector is magnetised, it is enabling the unmagnetised MINERνA detector to measure the momentum and charge of the muons.

The NuMI beam is described in Reference [72]. The primary 120 GeV proton beam is delivered by the Fermilab Main Injector and strikes a graphite target. The results discussed in this thesis used the low-energy NuMI beam, which produces a wide-band beam with neutrino energies extending from 1 GeV to greater than 20 GeV and a peak energy of 3 GeV.

The main part of the MINERνA detector is separated into inner and outer detector regions. The inner detector is composed of four distinct regions: the nuclear targets region, the tracker region, an electromagnetic calorimeter, and a hadronic calorimeter as it is shown in Figure 7.6. Each region is divided into modules which consist mostly of hexagonal scintillator planes.

The fully active tracker region is the target for the cross-section measurements used in
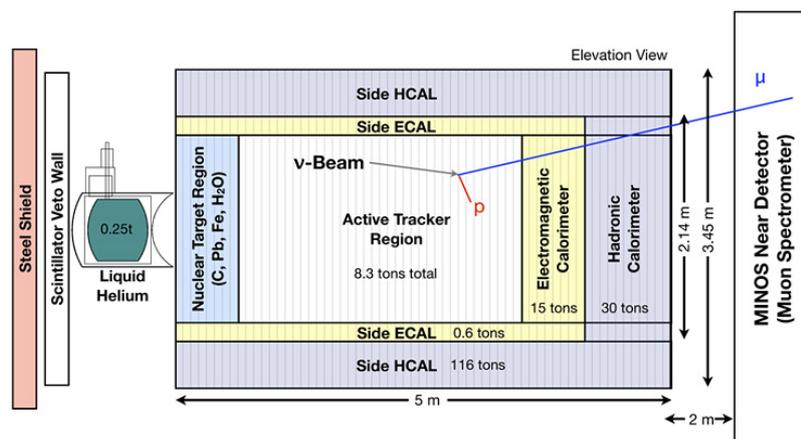
Fig. 7.6 Front view of a single MINERνA detector module. Figure is from Reference [71].

this thesis. The target material is therefore the scintillator itself, composed of long-chain hydrocarbons, which can be treated as a CH target. For more details, see Reference [71].
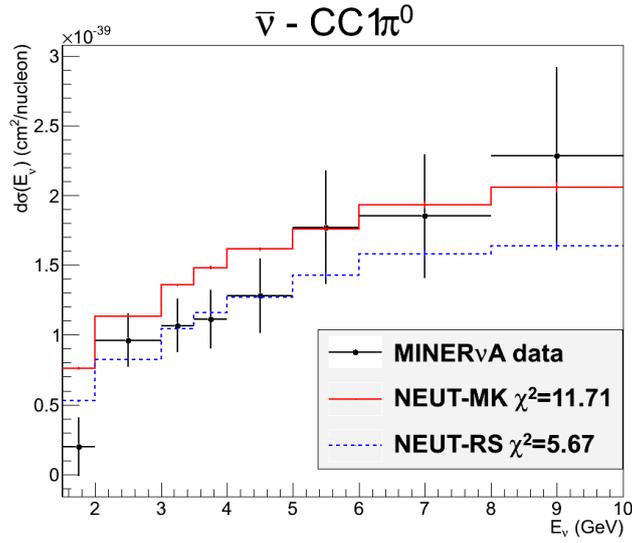
Fig. 7.7 MINERvA measurements on CH for $\bar{\nu}$-CC1π^0 total cross-sections as a function of energy. Histograms show NEUT predictions with MK-model (solid-red) and RS-model (dashed-blue). Degree of freedom is 8.

7.2.1 MINERvA anti-neutrino data and Monte Carlo predictions

The data we are using here is from Reference [75] - the latest single pion production measurements with anti-neutrino beam (published in 2016), with improved flux results. The measurement is on hydrocarbon (CH) target, in the following channel:

$$\bar{\nu}_\mu + CH \rightarrow \mu^+ + \pi^0 + X \tag{7.3}$$

The sample is restricted to events having only one π^0 and one μ^+. In the analysis, the anti-neutrino flux [74] with the energy restricted to 1.5 GeV $< E_\nu <$ 10 GeV is used. Further restriction is that hadronic mass is $W \leq 1.8$ GeV. In the MC simulations we apply similar cuts as those above.

To show the comparison between the MINERvA data and NEUT predictions with the MK-model and the RS-model, we start with the total cross-section as a function of E_ν. Figure 7.7 shows that the MK-model has a better agreements at higher energy while the RS-model has better agreement at lower energy. It also shows that MK-model predicts larger cross-section in all the energy range.

The Q^2 differential cross-section is shown in the left plot of Figure 7.8. Comparing MK-model and the RS-model in this plot does not reveal which model is better, but we should keep in mind that the RS-model has been the default model for single pion cross-section model in NEUT for years, with three adjustable parameters fitted to the single pion production data,
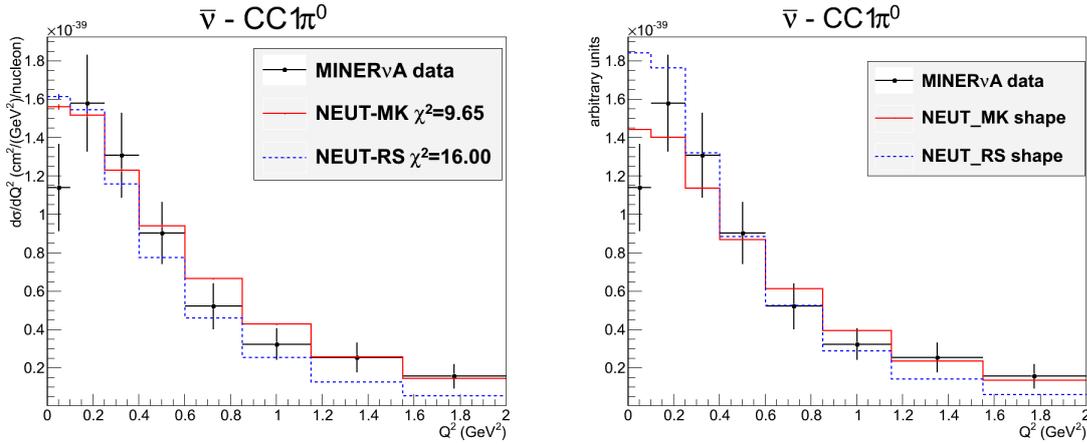
Fig. 7.8 The Data-NEUT comparison for Q^2-differential cross-section. Data is from Reference [75], the MINERνA measurements on CH for $\bar{\nu}$-CC1π^0 sample. Histograms show the cross-section (left), and normalized cross-section to the data (right) of the NEUT predictions with MK-model (solid-red) and RS-model (dashed-blue). Degree of freedom is 8.

before producing the systematic uncertainties.

We also show the shape comparison of the Q^2 differential cross-section in the right plot of Figure 7.8, where the NEUT predictions are normalized to the MINERνA data. Here it is clear that the two models predict different Q^2 distribution.

The next comparison we present in Figure 7.9 is for the muon kinematics. The differential cross-section as a function of muon momentum and muon polar angle in the lab frame is measured by the MINERνA experiment. The NEUT predictions are with the RS-model and the MK-model. We also show the shape comparison where the NEUT prediction is normalized to the data. The plots show that the two modes are not just different in the normalization, but they also predicts different distributions for the muon kinematics.

The pion kinematics and especially the pion angle is where we expect to see the main differences between two models. Figure 7.10 shows the differential cross-section as a function of pion kinetic energy and pion angle in the lab frame. The data is from Reference [75]; the MINERνA measurements on CH for $\bar{\nu}$-CC1π^0 sample. To do the comparison we also show the NEUT predictions with the MK-model and the RS-model for the T_π-differential cross-section and θ_π-differential cross-section in top plots, where the NEUT prediction is significantly different for the MK-model and the RS-model, especially for the pion angle. The same data are presented in bottom plots of Figure 7.10, but the histograms are normalized to the data to show the shape comparisons, where the two models also predicts different shapes especially for the pion angle.
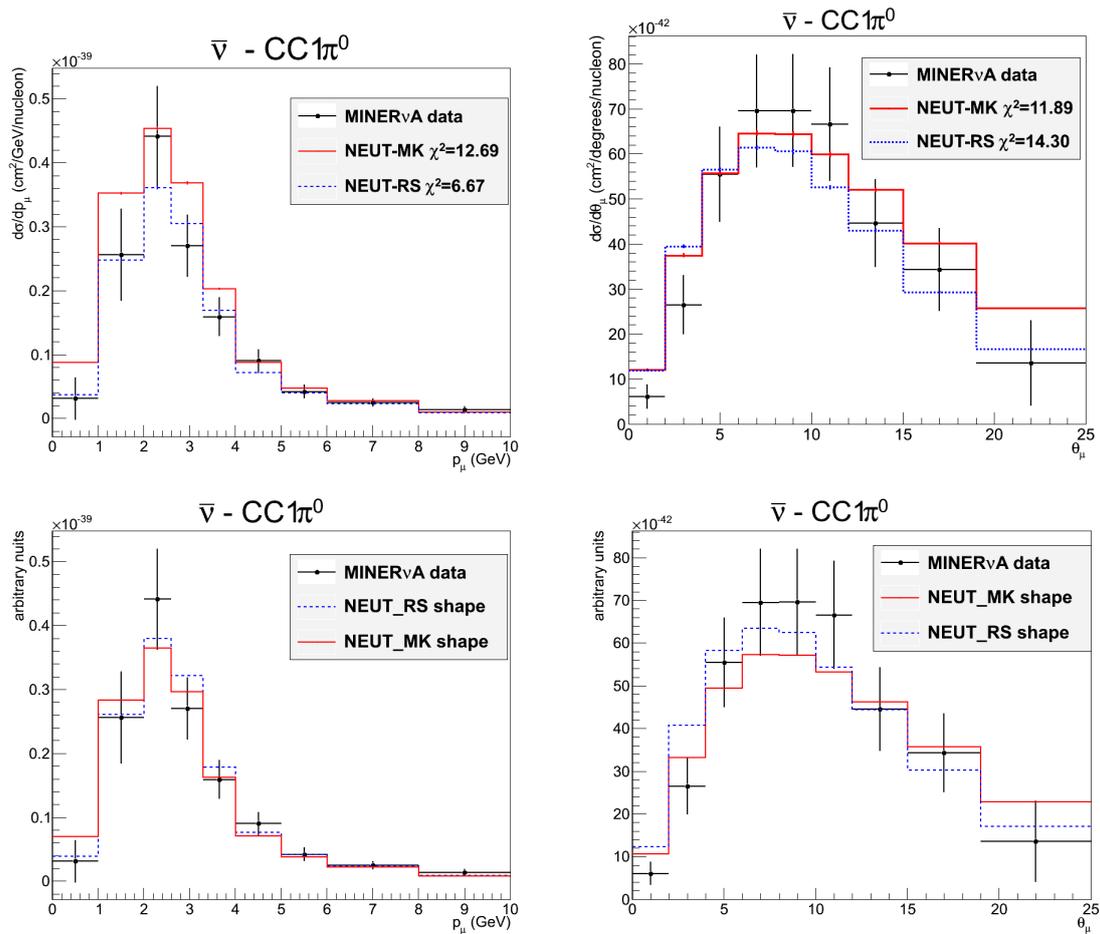
Fig. 7.9 MINER*v*A measurements on CH for $\bar{v}$-CC1π^0 differential cross-sections as a function of muon momentum(top-left) and muon angle (top-right) in the lab frame. Histograms show the NEUT predictions with MK-model (solid-red) and RS-model (dashed-blue) for the cross-section (top), and normalized cross-section to the data (bottom). Degree of freedom is 9.
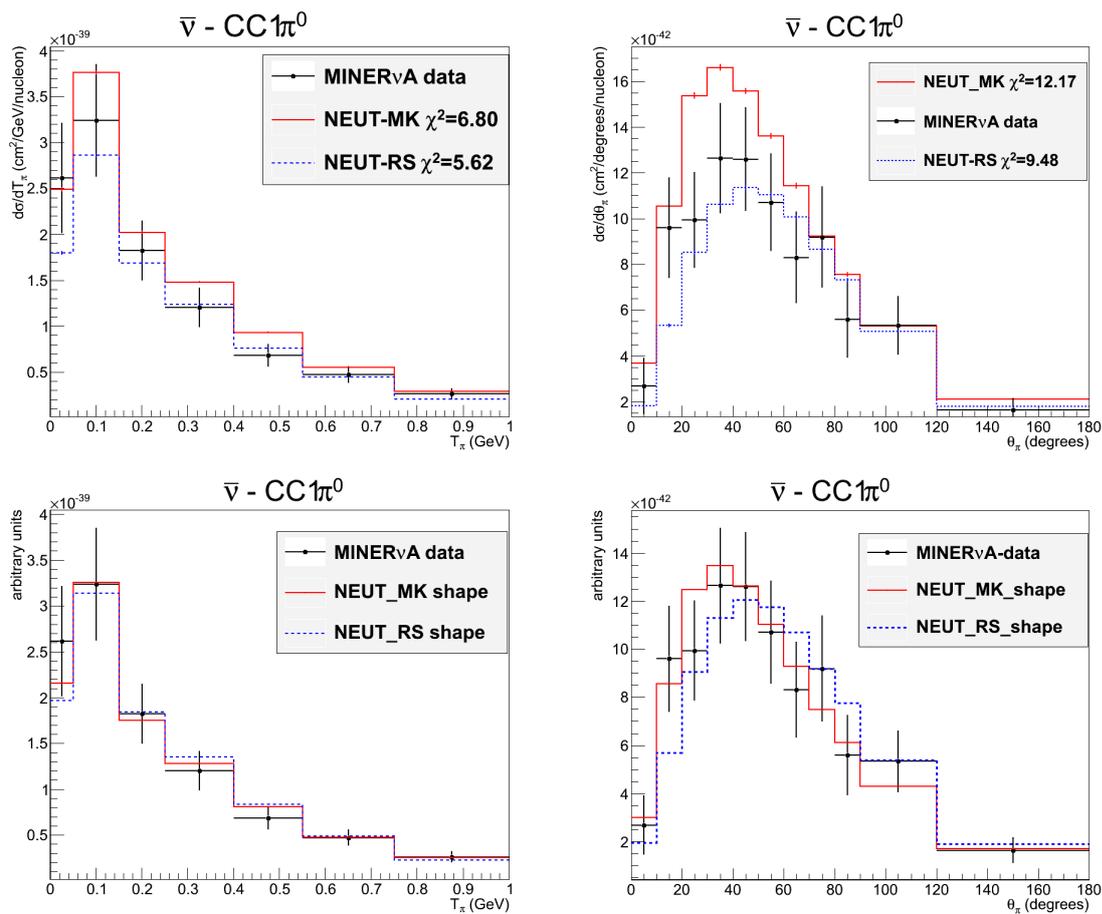
Fig. 7.10 MINERνA measurements on CH for $\bar{\nu}$-CC1π^0 differential cross-sections as a function of pion kinetic energy (left) and pion angle (right). Histograms show NEUT predictions with MK-model (solid-red) and RS-model (dashed-blue) and it bottom they are normalized to the data. Degree of freedom is 7 for the kinetic energy and 11 for pion angle.
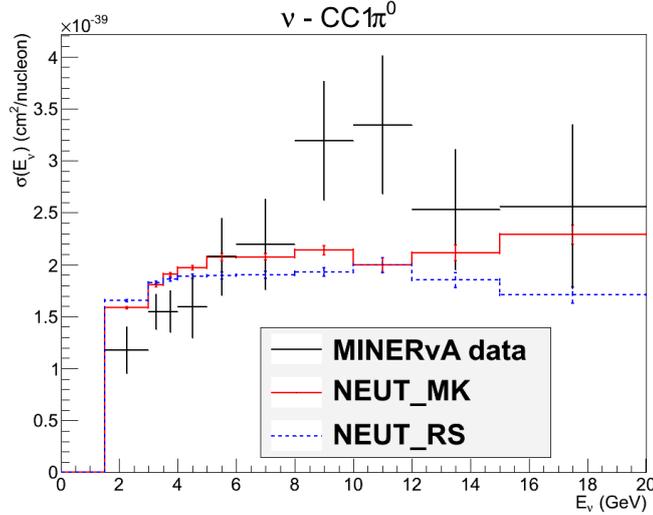
Fig. 7.11 MINERvA measurements on CH for ν-CC1π^0 total cross-sections as a function of energy. Histograms show NEUT predictions with MK-model (solid-red) and RS-model (dashed-blue).

7.2.2   MINERvA neutrino data and Monte Carlo predictions

The data we are using here is from Reference [86]- very recent (August 2017) single pion production measurements with neutrino beam. The measurement is on hydrocarbon (CH) target, in the following channel:

$$\nu_\mu + CH \rightarrow \mu^- + \pi^0 + X \tag{7.4}$$

The sample is restricted to events having only one π^0 and one μ^-. In the analysis, the neutrino flux [74] with the energy restricted to 1.5 GeV $< E_\nu <$ 20 GeV is used. Further restriction is that hadronic mass is $W \leq 1.8$ GeV. In the MC simulations we apply similar cuts as those above.

To show the comparison between the MINERvA data and NEUT predictions with the MK-model and the RS-model, we start with the total cross-section as a function of E_ν. Figure 7.11 shows that both models predict similar cross-sections at low energy ($E_\nu <$ 4 GeV), and this is what we expected from Figure 5.13. However, they have different predictions at higher energy where MK-model predicts larger cross-section.

The Q^2 differential cross-section is shown in the left plot of Figure 7.12. Comparing MK-model and the RS-model in this plot does not reveal which model is better, but it seems the MK-model has better prediction at very low Q^2 (less than 2.5 GeV^2 while RS-model is better at 2.5 GeV$^2 < Q^2 < 6$ $textGeV^2$.
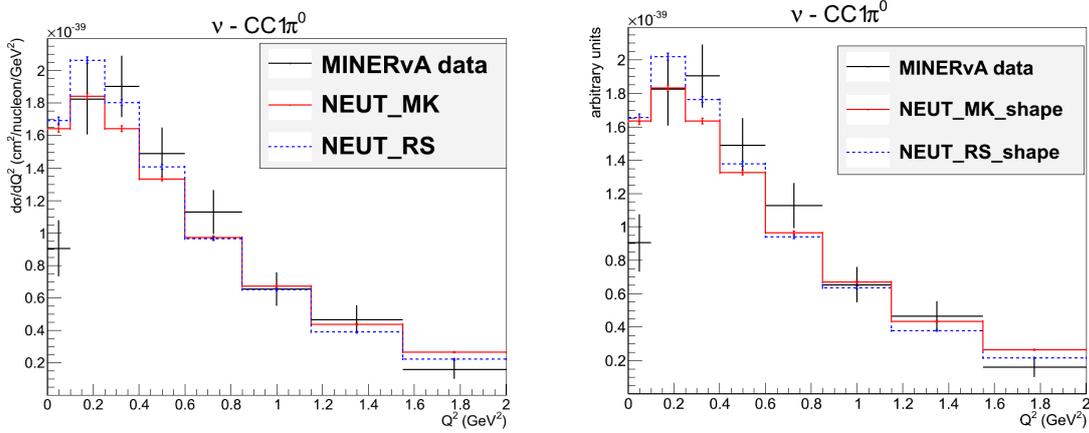
Fig. 7.12 The Data-NEUT comparison for Q^2-differential cross-section. Data is from Reference [86], the MINERνA measurements on CH for ν-CC1π^0 sample. Histograms show the cross-section (left), and normalized cross-section to the data (right) of the NEUT predictions with MK-model (solid-red) and RS-model (dashed-blue).

We also show the shape comparison of the Q^2 differential cross-section in the right plot of Figure 7.12, where the NEUT predictions are normalized to the MINERνA data, and it is very similar to the left plot which means NEUT predictions and data have almost same normalizations.

Figure 7.13 shows the differential cross-section as a function of pion kinetic energy and pion angle in the lab frame. To do the comparison, the NEUT predictions with the MK-model and the RS-model for the T_π-differential cross-section and θ_π-differential cross-section in top plots, where the NEUT prediction with MK-model predicts more pions at lower T_π and forward direction ($\theta_\pi < 50°$) than RS-model. The same data are presented in bottom plots of Figure 7.13, but the histograms are normalized to the data to show the shape comparisons, where the MK-model shows better agreement with data at forward direction i.e. $\theta_\pi < 60°$.

Recent MINERνA result also reports the differential cross-section as a function of $p\pi^0$ invariant mass in Δ region ($W < 1.4$ GeV) and higher $W < 1.8$ GeV region. The invariant mass, $M_{p\pi^0}$, is calculated from the reconstructed π^0 and the leading proton. In this analysis, events are required to have a leading proton in the final state with kinetic energy $T_p > 100$ MeV. The MINERνA data and NEUT prediction for $M_{p\pi^0}$-differential cross-section is shown in Figure 7.14 where MK-model predicts more pion at $M_{p\pi^0} < 1.2$ GeV region due to the nonresonant background. This is consistent to the top-left plot in Figure 7.13 where the T_{π^0}- differential cross-section by MK-model is higher at low kinetic energy.

 The next comparison is for the muon kinematics. The differential cross-section as a function of muon momentum and muon polar angle in the lab frame is measured by the MINERνA
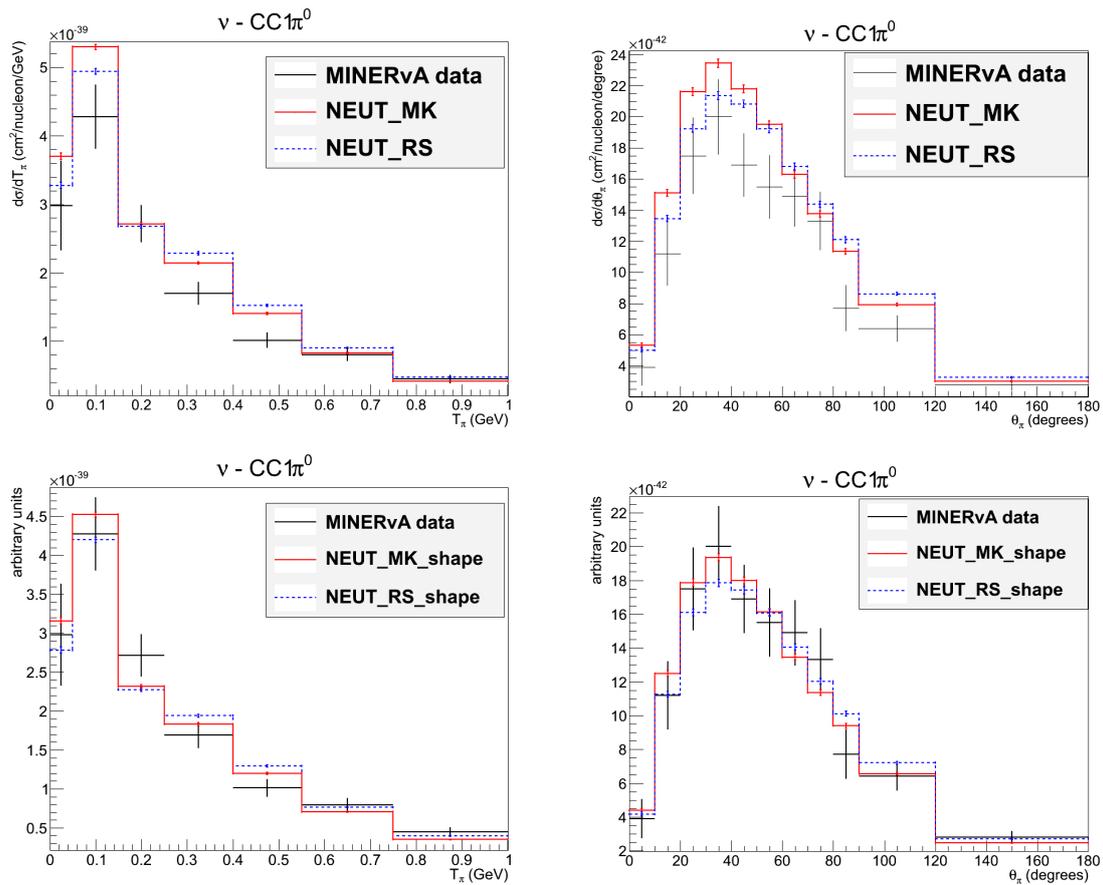
Fig. 7.13 Pion kinetic energy (left) and pion angle (right) differential cross-section in the lab frame for ν-CC1π⁰ sample. Histograms show NEUT predictions with MK-model (solid-red) and RS-model (dashed-blue). They are normalized to the data in the bottom plots.
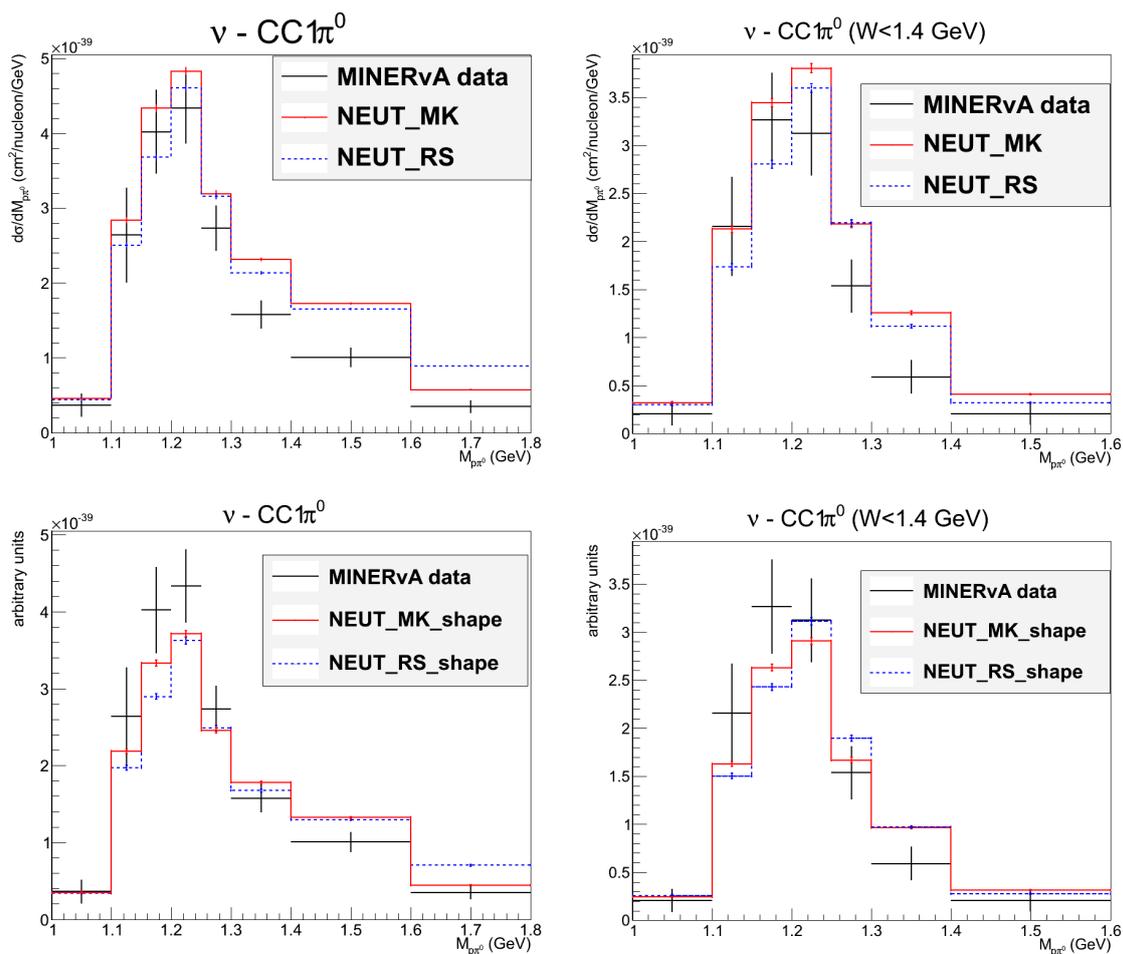
Fig. 7.14 Differential cross-section as a function of $p\pi^0$ invariant mass with $W < 1.8$ GeV (left) and $W < 1.4$ GeV (right) for ν-CC1π^0 sample. Histograms show NEUT predictions with MK-model (solid-red) and RS-model (dashed-blue). They are normalized to data in the bottom plots.
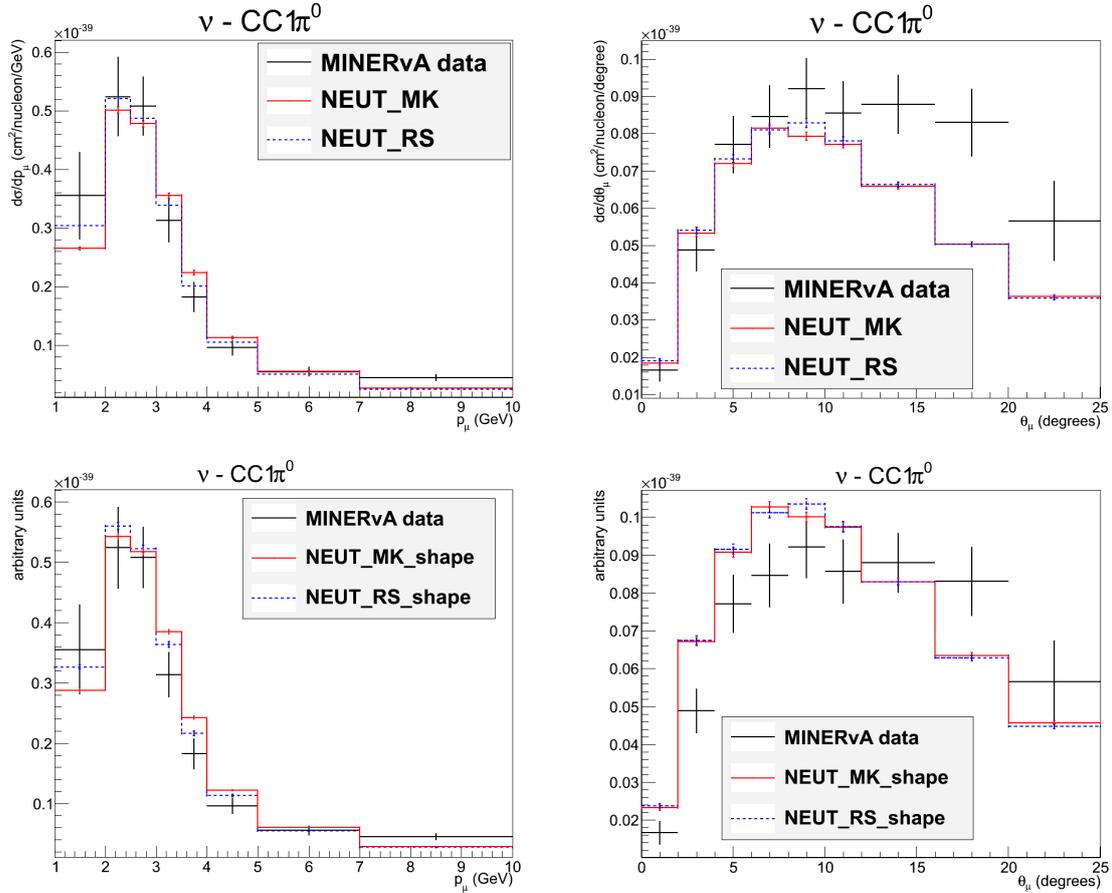
Fig. 7.15 Differential cross-sections as a function of muon momentum(top-left) and muon angle (top-right) in the lab frame. Histograms show the NEUT predictions with MK-model (solid-red) and RS-model (dashed-blue) for the cross-section (top), and normalized cross-section to the data (bottom).

experiment. Figure 7.15 show data and the NEUT predictions with the RS-model and the MK-model where the NEUT predictions are very similar. We also show the shape comparison where the NEUT prediction is normalized to the data.

7.3 The MiniBooNE experiment

The MiniBooNE experiment [76] was designed to test $\bar{\nu}_\mu \to \bar{\nu}_e$ oscillation signal. Mini-BooNE uses the Booster Neutrino Beam(BNB) at Fermilab, which has a peak energy of approximately 700 MeV. The BNB at Fermilab [83] uses 8 GeV protons from the Fermilab booster. The same booster feeds the Main Injector used by the MINERνA experiment. The protons strike a beryllium target inside a single magnetic horn, which focuses the beam of

secondary mesons of a given charge (selected by changing the polarity of the horn). The secondary beam is directed down a 50m long decay pipe, where most mesons decay in flight. The MiniBooNE detector [76] can detect neutrino interactions in a 12 m diameter sphere of pure(undoped) mineral oil. The MiniBooNE detector is divided into signal (inner) and veto (outer) regions as it is shown in Figure 7.16. MiniBooNE is a Cherenkov detector.
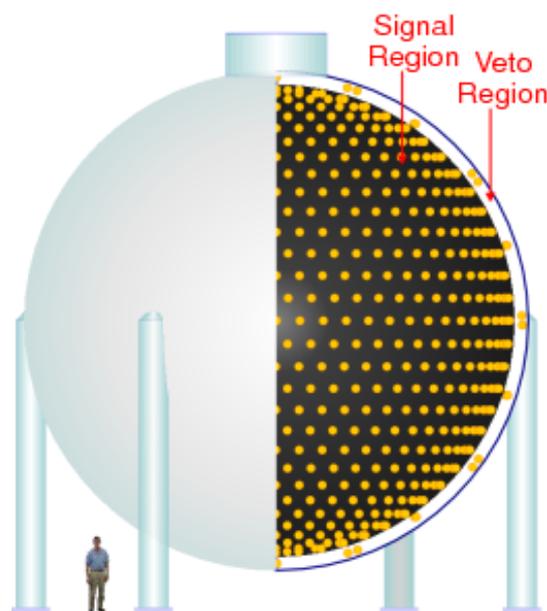
Fig. 7.16 The MiniBooNE detector tank from Reference [76]

The neutrino interactions with the carbon nucleus or protons in the mineral oil produce charged particles (muons, electrons, pions...) which will produce Cherenkov light if they have sufficient velocity (energy). The cone of light produced by a charged particle projects to a well-defined pattern on the photomultiplier array.

7.3.1 MiniBooNE data and Monte Carlo predictions

The MiniBooNE collaboration reported cross-sections for ν_μ-induced charged-current single π^0 production on mineral oil (CH2) over an energy range of $0.5 - 2$ GeV in Reference [77]. To do the comparison we chose CH target in NEUT, which is very similar to CH2 (MiniBooNE target). The MiniBooNE flux for this measurements is given in Reference [77]. The MiniBooNE data is controversial since there is a discrepancy [61] with other published data. We also see some discrepancy for the NEUT predictions with both models in Figure 7.17. The discrepancy is significant for muon kinematics, and generally the NEUT prediction with RS-model has better agreement with the MiniBooNE data.

 To show the discrepancy is not the pure normalization, especially for the angular distributions,
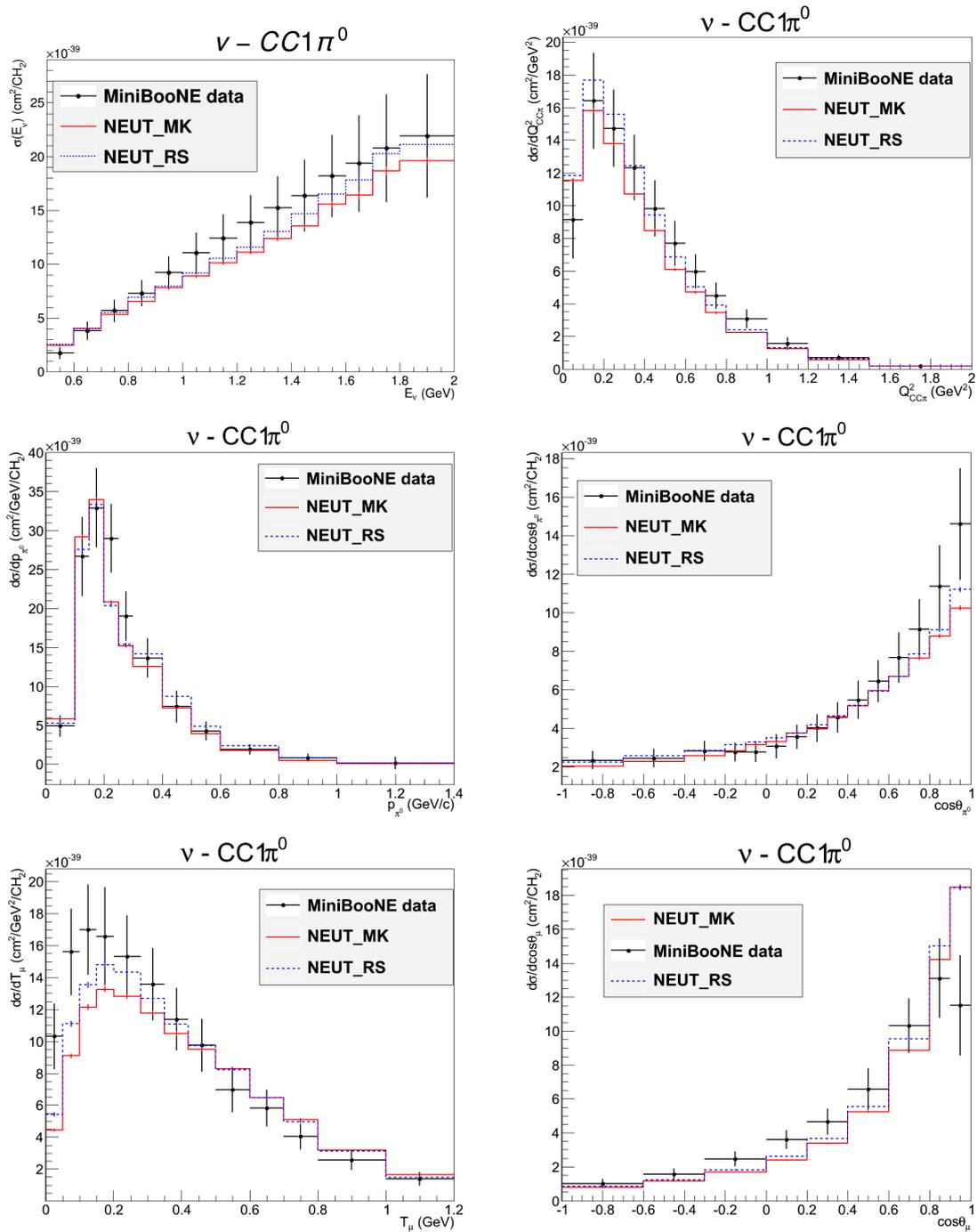
Fig. 7.17 MiniBooNE data for CC1π^0 sample from Reference [77]. The total cross-section in terms of energy (top left), the Q^2-differential cross-section (top right), the differential cross-sections as a function of pion kinematics (center), muon kinematics (bottom). Histograms show NEUT predictions with MK-model (solid-red) and RS-model (dashed-blue).

we also show the shape comparison in Figure 7.18 for the same MiniBooNE data presented in Figure 7.17, but the NEUT predictions are normalized to the data.

7.4 Conclusion

The primary purpose of T2K's Neutrino Interactions Working Group (NIWG group in the T2K collaboration) is to include new models in NEUT, and to produce uncertainties for the parameters of the model to be used as inputs to T2K oscillation analyses, and for T2K cross-section analyses. The fitting tool is used by the NIWG group to constrain model's parameters for various interactions [85], and a new model implemented in the NEUT should be used in a fit to the available data.

The MK-model implemented in the NEUT, is now ready to be used as a single pion production model for T2K, and will be included in the next generation NIWG fitting procedure using the existing framework. For the next step, the model's parameters (M_A and C_5^{A2}) will be fitted to the single pion production bubble chamber data, and then cross-section errors will be estimated using all available single pion production data.

In this chapter, the NEUT prediction with MK-model was compared with the single pion production data on nuclear targets, and it shows good agreement with both T2K and MINERvA data.To show the effects of MK/RS-model replacement, we also presented the current NEUT prediction which is only different in the single pion production model.

The large discrepancy between the NEUT predictions indicates that the nonresonant background effect is not negligible and it has significant impact on predictions for single pion production especially on pion polar angle as it was discussed in the previous chapters. Comparing NEUT predictions for CC1π^0 sample and neutrino flux between MINERvA ($E_\nu > 1.5$ GeV) and MiniBooNE ($E_\nu < 2$ GeV) shows MK-model predicts higher cross-section for higher energy (MINERvA flux) and less cross-section for lower energy (MiniBooNE flux). The discrepancy between MK-model and RS-model is less for MiniBooNE flux than MINERvA flux with larger phase space. This is because both model are fitted to data at low energy ($E_\nu \approx 1$ GeV). Comparing NEUT predictions for CC1π^0 sample between neutrino and anti-neutrino MINERvA fluxes show although the discrepancy in normalization is larger for anti-neutrino (this was discussed in section 5.3), but the shape discrepancy is very similar especially for pion kinematics.

---

[2]these are the MK-model's parameters by now. New parameter(s) might be added to the model by NIWG group.
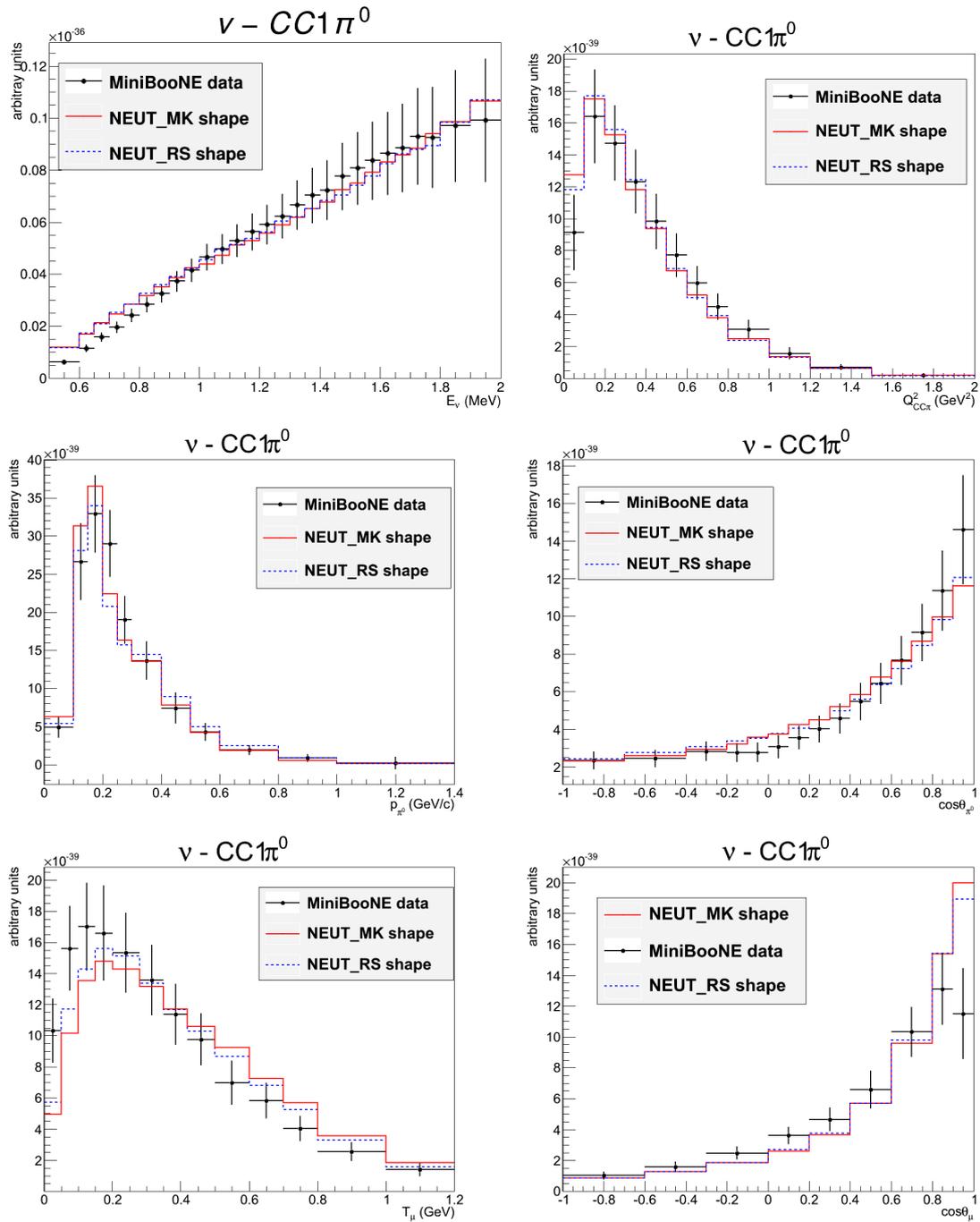
Fig. 7.18 MiniBooNE data for CC1π^0 sample from Reference [77]. The total cross-section in terms of energy (top left), the Q^2-differential cross-section (top right), the differential cross-sections as a function of pion kinematics (center), muon kinematics (bottom). Histograms show NEUT predictions with MK-model (solid-red) and RS-model (dashed-blue), normalized to the data.

Chapter 8

Summary and Concluding remarks

The main goal of this thesis was to develop a new single pion production cross-section model. A motivation is to use it in Monte Carlo simulation in the T2K experiment for precision measurements of neutrino oscillation. The present (Rein-Sehgal) model in NEUT is not satisfactory. It is particularly missing a reliable model for nonresonant interaction and its interference with the resonant interaction. Besides, the model is not implemented completely for the angular distribution, and for simplicity only Δ resonance contribute. Therefore the single pion production model in NEUT is not efficient for simulation. In this work, we introduced a complete model, including all the effects, in order to get better descriptions.

The model proposed in this work (we call it MK-model) consists of resonant and non-resonant interactions including the interference effects between all resonances as well as nonresonant contributions. In chapter 3 the general framework for the helicity amplitude calculation is provided. This was introduced in References [8, 9] for neglected lepton mass, but in this chapter the lepton mass is restored. The full kinematic differential cross-section in terms of helicity amplitudes is also given in this chapter which includes the discussion of angular distributions. In chapter 4 the helicity amplitudes of the RS-model [7] for resonant interaction and HNV-model [10] for nonresonant interaction is calculated. For resonant calculation, we follow up the idea from Reference [9]. THe MK-model has a suitable format for the neutrino generators.

The resonant interaction has axial form-factor with two unknown parameters, and their best values were obtained from fitting to the bubble chamber data. we also defined the resonance's signs to get the best description of data, where we got different signs for few resonances compare to the RS-model. Fixing the parameters and the signs of resonances in the cross-section calculation (CSC) code, we were able to get the numerical values of the

differential cross-section to compare with the bubble chamber data on light targets. The better agreements of the MK-model with data compare to NEUT5.3.6 (especially for anti-neutrino channels) presented in the chapter 5, confirmed that the model is doing a good job, and we will probably see less systematic error in the next T2K analysis.

The full kinematic cross-section, $d\sigma/dWdQ^2d\Omega$, which is the output of MK-model is implemented in NEUT for all CC and NC (anti-)neutrino channels. In chapter 6, we compared various differential cross-sections predicted by NEUT 5.3.6 (RS-model), and NEUT with the MK-model. The comparisons have been done for several channels on free nucleon and few samples on CH target, and they clearly show discrepancy in shape and normalization. The disagreements is significant for the pion kinematics due to the interference effects and the simplified implementation (for pion angles[1]) of the RS-model in the current NEUT.

The MK-model is successfully implemented in the NEUT and all necessary checks were done as described in the chapter 6, and it is ready to be used for the future T2K analyses, However there are still more tests that should be done within the T2K collaboration, particularly the free parameters of the MK-model needs to be fitted to other data available for the single pion production. This is going to be done with the T2K software as it was done before for the presently used models in NEUT.

In chapter 7 we presented the first comparisons between NEUT predictions with the RS-model (NEUT5.3.6) and the MK-model and recent data on the nuclear targets. The results show that the discrepancy between two models is clearly visible even after the nuclear effects and the kinematic cuts. The value for χ^2 in each comparison shows better agreements for Mk-model with the T2K and MINERνA data.

The Neutrino Interactions Working Group (NIWG group in the T2K collaboration) is responsible for providing central values and uncertainties for the cross-section parameters which are used in the oscillation analyses. There are currently 22 cross-section parameters for all models in the NEUT where three of them are related to the single pion production model. The better agreements between NEUT and the data constrain the cross-section systematics which is used for systematic error estimation in oscillation fits.

---

[1]In the current NEUT, pion angles are implemented separately (they are not included in the cross-section formula) and only includes the Δ resonance.

Chapter 9

Summary

The main goal of this thesis is to develop a new single pion production cross-section model. A motivation is to use it in Monte Carlo simulation in the T2K experiment for precision measurements of neutrino oscillation. The present (Rein-Sehgal) model in NEUT is not satisfactory. It is particularly missing a reliable model for nonresonant interaction and its interference with the resonant interaction. Besides, the model is not implemented completely for the angular distribution, and for simplicity only Δ resonance contribute. Therefore the single pion production model in NEUT is not efficient for simulation. In this work, we introduced a complete model, including all the effects, in order to get better descriptions.

The model proposed in this work (we call it MK-model) consists of resonant and nonresonant interactions including the interference effects between all resonances as well as nonresonant contributions. In chapter 3 the general framework for the helicity amplitude calculation is provided. This was introduced in References [8, 9] for neglected lepton mass, but in this chapter the lepton mass is restored. The full kinematic differential cross-section in terms of helicity amplitudes is also given in this chapter which includes the discussion of angular distributions. In chapter 4 the helicity amplitudes of the RS-model [7] for resonant interaction and HNV-model [10] for nonresonant interaction is calculated. For resonant calculation, we follow up the idea from Reference [9]. THe MK-model has a suitable format for the neutrino generators.

The resonant interaction has axial form-factor with two unknown parameters, and their best values were obtained from fitting to the bubble chamber data. we also defined the resonance's signs to get the best description of data, where we got different signs for few resonances compare to the RS-model. Fixing the parameters and the signs of resonances in the cross-section calculation (CSC) code, we were able to get the numerical values of the

differential cross-section to compare with the bubble chamber data on light targets. The better agreements of the MK-model with data compare to NEUT5.3.6 (especially for anti-neutrino channels) presented in the chapter 5, confirmed that the model is doing a good job, and we will probably see less systematic error in the next T2K analysis.

The full kinematic cross-section, $d\sigma/dWdQ^2d\Omega$, which is the output of MK-model is implemented in NEUT for all CC and NC (anti-)neutrino channels. In chapter 6, we compared various differential cross-sections predicted by NEUT 5.3.6 (RS-model), and NEUT with the MK-model. The comparisons have been done for several channels on free nucleon and few samples on CH target, and they clearly show discrepancy in shape and normalization. The disagreements is significant for the pion kinematics due to the interference effects and the simplified implementation (for pion angles[1]) of the RS-model in the current NEUT.

The MK-model is successfully implemented in the NEUT and all necessary checks were done as described in the chapter 6, and it is ready to be used for the future T2K analyses, However there are still more tests that should be done within the T2K collaboration, particularly the free parameters of the MK-model needs to be fitted to other data available for the single pion production. This is going to be done with the T2K software as it was done before for the presently used models in NEUT.

In chapter 7 we presented the first comparisons between NEUT predictions with the RS-model (NEUT5.3.6) and the MK-model and recent data on the nuclear targets. The results show that the discrepancy between two models is clearly visible even after the nuclear effects and the kinematic cuts. The value for χ^2 in each comparison shows better agreements for Mk-model with the T2K and MINERνA data.

---

[1]In the current NEUT, pion angles are implemented separately (they are not included in the cross-section formula) and only includes the Δ resonance.

Appendix A

Convention

The four vectors are:

$$
\begin{aligned}
x^\mu &= \left(x^0, \ \mathbf{x} \right) \ \text{contravariant} \\
x_\mu &= \left(x^0, \ -\mathbf{x} \right) \ \text{covariant}
\end{aligned}
\tag{A.0}
$$

where $x^\mu = \eta^{\mu\nu} x_\nu$, and η is our metric:

$$
\eta^{\mu,\nu} = \begin{pmatrix} 1 & 0 & 0 & 0 \\ 0 & -1 & 0 & 0 \\ 0 & 0 & -1 & 0 \\ 0 & 0 & 0 & -1 \end{pmatrix}
\tag{A.0}
$$

Therefore, the four-vector contraction is:

$$
x^\mu x_\mu = x_0^2 - \mathbf{x}^2.
\tag{A.0}
$$

For all on-shell particles with mass m and momentum p we have following relation for four-momentum:

$$
p^\mu = \left(E(\mathbf{p}), \ \mathbf{p} \right) = \left(\sqrt{\mathbf{p}^2 + m^2}, \ \mathbf{p} \right)
\tag{A.0}
$$

Therefore $p^\mu p_\mu = m^2$.

A.0.1 Dirac Equation and Dirac matrices

Free Dirac equation of motion is:

$$
(i \ \slashed{\partial} - M) \psi(x) = 0
\tag{A.0}
$$

where $\not{\partial} = \gamma^\mu \partial_\mu$, and in this thesis we generally have $\not{A} = \gamma^\mu A_\mu$. Dirac matrices are:

$$\gamma^0 = \begin{pmatrix} \mathbb{1}_2 & 0 \\ 0 & -\mathbb{1}_2 \end{pmatrix}, \quad \gamma^k = \begin{pmatrix} 0 & \sigma^k \\ -\sigma^k & 0 \end{pmatrix}, \quad \gamma^5 = \begin{pmatrix} 0 & \mathbb{1}_2 \\ \mathbb{1}_2 & 0 \end{pmatrix} \tag{A.1}$$

where σ^k are 2×2 Pauli matrices:

$$\sigma_1 = \begin{pmatrix} 0 & 1 \\ 1 & 0 \end{pmatrix}, \quad \sigma_2 = \begin{pmatrix} 0 & -i \\ i & 0 \end{pmatrix}, \quad \sigma_3 = \begin{pmatrix} 1 & 0 \\ 0 & -1 \end{pmatrix}, \quad \mathbb{1}_2 = \begin{pmatrix} 1 & 0 \\ 0 & 1 \end{pmatrix}. \tag{A.2}$$

$$\{\gamma^\mu, \gamma^\nu\} = 2\eta^{\mu\nu} \tag{A.3}$$

Dirac equation in momentum space is:

$$\begin{aligned} (i \not{p} - M)u_s(p) &= 0 \\ (i \not{p} + M)v_s(p) &= 0, \end{aligned} \tag{A.3}$$

and Dirac spinors are the solution of this equation:

$$\begin{aligned} u_s(p) &= \sqrt{E(p)+M} \begin{pmatrix} \chi_s \\ \frac{\boldsymbol{\sigma}\cdot\mathbf{p}}{E(p)+M}\chi_s \end{pmatrix} \\ v_s(p) &= \sqrt{E(p)+M} \begin{pmatrix} \frac{\boldsymbol{\sigma}\cdot\mathbf{p}}{E(p)+M}\chi_s \\ \chi_s \end{pmatrix} \end{aligned} \tag{A.3}$$

where χ_s are Pauli spinors with two components, and

$$\boldsymbol{\sigma} = \vec{\sigma} = \sigma_1\hat{i} + \sigma_2\hat{j} + \sigma_3\hat{k}. \tag{A.3}$$

Dirac spinors are normalized as follows:

$$\bar{u}_s(p)u'_s(p) = -\bar{v}_s(p)v'_s(p) = 2M\delta_{ss'} \tag{A.4}$$

A.0.2 Isospin Operators

- **Nucleon and isospin $1/2$ resonances**

  The proton and neutron (like all isospin $1/2$ resonances) form an isospin $SU(2)$ doublet:

$$|p\rangle = \begin{pmatrix} 1 \\ 0 \end{pmatrix}, \quad |n\rangle = \begin{pmatrix} 0 \\ 1 \end{pmatrix} \tag{A.4}$$

The isospin matrices form a vector in isospin space:

$$\boldsymbol{\tau} = \left(\tau_1, \tau_2, \tau_3 \right) \tag{A.4}$$

where τ_k are Pauli matrices given in Eq. A.2. Proton and neutron have isospin $\frac{1}{2}$ and $-\frac{1}{2}$ respectively. We can define

$$\tau_{\pm} = \frac{1}{2}(\tau_1 \pm i\tau_2) \tag{A.4}$$

to change the isospin

$$\tau_-|p\rangle = |n\rangle, \;\; \tau_+|n\rangle = |p\rangle, \quad \tau_+|p\rangle = \tau_-|n\rangle = 0 \tag{A.4}$$

- **Pions**

   Pion fields can be defined in Cartesian isospin coordinate:

$$\boldsymbol{\phi} = \left(\phi_1, \phi_2, \phi_3 \right) \tag{A.4}$$

   We can also define
$$\phi_{\pm} = \frac{1}{\sqrt{2}}(\phi_1 \pm i\phi_2), \quad \phi_0 = \phi_3, \tag{A.4}$$

   where ϕ_- creates a π^- or annihilate a π^+, and ϕ_+ creates a π^+ or annihilate a π^-. Its scalar product with the isospin $1/2$ matrix is:

$$\boldsymbol{\tau}.\boldsymbol{\phi} = \tau_1\phi_1 + \tau_2\phi_2 + \tau_3\phi_3 = \sqrt{2}(\tau_+\phi_- + \tau_-\phi_+) + \tau_3\phi_0. \tag{A.4}$$

A.0.3   Isospin structure of hadron current

We can decompose the hadron currents to different isospins[1]:

$$\langle\, N\pi|\, J_\rho^V\, |N\,\rangle = a^{(+)}V_\rho^{(+)} + a^{(-)}V_\rho^{(-)}$$
$$\langle\, N\pi|\, J_\rho^A\, |N\,\rangle = a^{(+)}A_\rho^{(+)} + a^{(-)}A_\rho^{(-)}$$

---

[1]Isospin convention is from Reference [8]

where

$$a^{(\pm)} = \chi_2^\dagger \psi_{\pi c}^\dagger \frac{1}{2}(\tau_c \tau_d \pm \tau_d \tau_c) \psi_{Wd} \chi_1.$$

Here χ_1 and χ_2 are nucleon isospinors and ψ_ϕ isospin matrix of final pion :

$$\psi_\phi = \frac{1}{\sqrt{2}} \begin{pmatrix} 1 \\ \pm i \\ 0 \end{pmatrix} \text{ For } \pi^\pm, \quad \psi_\phi = \begin{pmatrix} 0 \\ 0 \\ 1 \end{pmatrix} \text{ For } \pi^0$$

ψ_W describes the isospin character of the weak currents:

$$\psi_W = \frac{1}{2} \begin{pmatrix} 1 \\ i \\ 0 \end{pmatrix} \text{ For } W^+, \quad \psi_W = \frac{1}{2} \begin{pmatrix} 0 \\ 0 \\ 1 \end{pmatrix} \text{ For } Z^0$$

It is useful to introduce linear combination of $V_\rho^{(\pm)}$ and $A_\rho^{(\pm)}$ to $V_\rho^{(1/2,3/2)}$ and $A_\rho^{(1/2,3/2)}$ which describe transitions to pure isospin states of pion and nucleon.

$$a^{(+)}V_\rho^{(+)} + a^{(-)}V_\rho^{(-)} = a^{(1/2)}V_\rho^{(1/2)} + a^{(3/2)}V_\rho^{(3/2)}$$
$$V_\rho^{(1/2)} = V_\rho^{(+)} + 2V_\rho^{(-)}, \quad V_\rho^{(3/2)} = V_\rho^{(+)} - V_\rho^{(-)}$$
$$a^{(1/2)} = \frac{1}{3}(a^{(+)} + a^{(-)}) \;, \quad a^{(3/2)} = \frac{1}{3}(2a^{(+)} - a^{(-)}).$$

The numerical values of the isospin matrix elements for different SPP channels are given in Table A.1. Using isospin symmetry you can find all charged current interaction in terms of two of them. For example:

$$\langle p\pi^0 | J^{CC} | n \rangle = -\frac{1}{\sqrt{2}} \left[\langle p\pi^+ | J^{CC} | p \rangle - \langle n\pi^+ | J^{CC} | n \rangle \right].$$

We can also have:

$$\bar{\psi}_u \psi_d = \bar{\psi}_q \frac{\tau^+}{\sqrt{2}} \psi_q \qquad \text{where } \psi_q = \begin{pmatrix} \psi_u \\ \psi_d \end{pmatrix},$$

Table A.1 Isospin Clebsch-Gordan coefficients for CC and NC (anti-)neutrino channels.

ν Channels	$\bar{\nu}$ Channels	$a^{(+)}$	$a^{(-)}$	$a^{1/2}$	$a^{3/2}$
$\nu p \to l^- p\pi^+$	$\bar{\nu}n \to l^+ n\pi^-$	$\frac{1}{\sqrt{2}}$	$-\frac{1}{\sqrt{2}}$	0	$\frac{1}{\sqrt{2}}$
$\nu n \to l^- p\pi^0$	$-(\bar{\nu}p \to l^+ n\pi^0)$	0	1	$\frac{1}{3}$	$-\frac{1}{3}$
$\nu n \to l^- n\pi^+$	$\bar{\nu}p \to l^+ p\pi^-$	$\frac{1}{\sqrt{2}}$	$\frac{1}{\sqrt{2}}$	$\frac{\sqrt{2}}{3}$	$\frac{1}{3\sqrt{2}}$
$\nu p \to \nu p\pi^0$	$\bar{\nu}p \to \bar{\nu}p\pi^0$	$\frac{1}{2}$	0	$\frac{1}{6}$	$\frac{1}{3}$
$\nu p \to \nu n\pi^+$	$\bar{\nu}p \to \bar{\nu}n\pi^+$	0	$\frac{1}{\sqrt{2}}$	$\frac{1}{3\sqrt{2}}$	$-\frac{\sqrt{2}}{3}$
$\nu n \to \nu n\pi^0$	$\bar{\nu}n \to \bar{\nu}n\pi^0$	$\frac{1}{2}$	0	$\frac{1}{6}$	$\frac{1}{3}$
$\nu n \to \nu p\pi^-$	$\bar{\nu}n \to \bar{\nu}p\pi^-$	0	$-\frac{1}{\sqrt{2}}$	$-\frac{1}{3\sqrt{2}}$	$\frac{1}{3\sqrt{2}}$

therefore the matrix elements of the isovector part of electromagnetic current ($s^\mu_{IV} = \bar{\psi}_q \gamma^\mu \frac{\tau_3}{2} \psi_q$) are related to the charged current interaction from Table A.1:

$$\langle p\pi^+ | J^V_{CC} | p\rangle = \sqrt{2}\langle n\pi^0 | s^{IV} | n\rangle + \langle p\pi^- | s^{IV} | n\rangle$$
$$\langle n\pi^+ | J^V_{CC} | n\rangle = \sqrt{2}\langle p\pi^0 | s^{IV} | p\rangle - \langle p\pi^- | s^{IV} | n\rangle.$$

For isoscalar operators ($s^\mu_{IS} = \frac{1}{2}\bar{\psi}_q \gamma^\mu \psi_q$) you only need to replace τ_3 with $\mathbb{1}_2$ for τ_d in Eq. A.0.3. and as a result a minus will be multiplied to $\nu n \to \nu n\pi^0$ and $\nu n \to \nu p\pi^-$ isospin coefficients given in Table A.1.

Appendix B

Pauli Spinors in the Isobaric frame

We need to define the Spinors of fermions like leptons and nucleon. they can be define when the the momentum of fermions (**p**) are fixed in the framework (isobaric frame in this case)

$$\hat{\mathbf{p}}.\mathbf{s}\,|\lambda\rangle = \hbar\lambda\,|\lambda\rangle \Rightarrow \hat{\mathbf{p}}.\sigma\,|\lambda\rangle = \lambda\,|\lambda\rangle \tag{B.1}$$

Fig. (B.1) and Fig. (B.2) show the momentum of fermions in the isobaric frame. Knowing their unit vector we can calculate spinors.
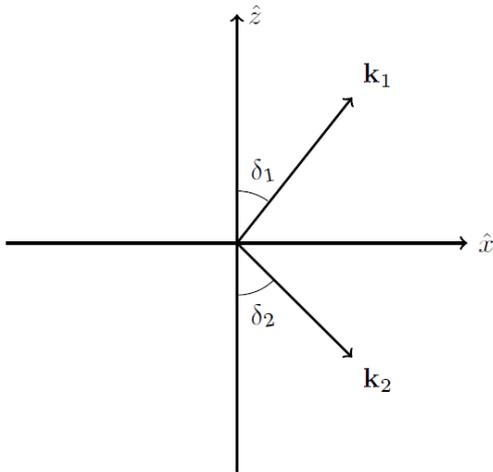
Fig. B.1 Lepton's momentums in the isobaric frame.
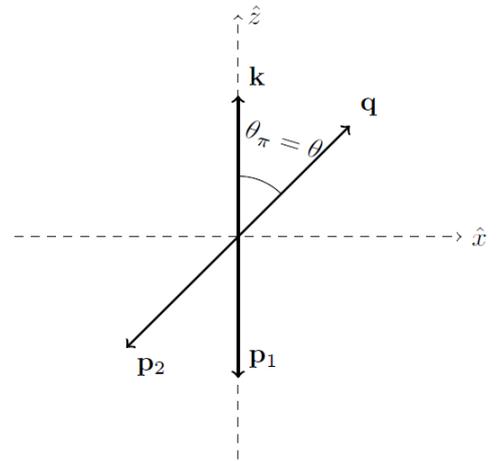
Fig. B.2 hadron's momentums in the isobaric frame.

• **Incident neutrino**

$$\hat{k_1} = \sin\delta_1\hat{x} + \cos\delta_1\hat{z} \tag{B.2}$$

$$\hat{\mathbf{k}}_1.\sigma |\lambda\rangle = \begin{pmatrix} \cos \delta_1 & \sin \delta_1 \\ \sin \delta_1 & -\cos \delta_1 \end{pmatrix} |\lambda\rangle = \lambda |\lambda\rangle \qquad (B.3)$$

The eigenvalues are $\lambda = \pm$ related to the right and left helicities. Neutrino is left handed, therefore

$$\begin{pmatrix} \cos \delta_1 & \sin \delta_1 \\ \sin \delta_1 & -\cos \delta_1 \end{pmatrix} \begin{pmatrix} a \\ b \end{pmatrix} = -\begin{pmatrix} a \\ b \end{pmatrix}. \qquad (B.4)$$

we can calculate a and b and the neutrino's spinor is

$$|\Downarrow\rangle_v = \begin{pmatrix} -\sin \delta_1/2 \\ \cos \delta_1/2 \end{pmatrix}. \qquad (B.5)$$

- **Outgoing lepton**

$$\hat{k}_2 = \sin \delta_2 \hat{x} - \cos \delta_2 \hat{z} \qquad (B.6)$$

$$\hat{\mathbf{k}}_2.\sigma |\lambda\rangle = \begin{pmatrix} -\cos \delta_2 & \sin \delta_2 \\ \sin \delta_2 & \cos \delta_2 \end{pmatrix} \begin{pmatrix} a \\ b \end{pmatrix} = \pm \begin{pmatrix} a \\ b \end{pmatrix} \qquad (B.7)$$

$$|\Downarrow\rangle_l = \begin{pmatrix} \cos \delta_2/2 \\ -\sin \delta_2/2 \end{pmatrix}, \qquad |\Uparrow\rangle_l = \begin{pmatrix} \sin \delta_2/2 \\ \cos \delta_2/2 \end{pmatrix}. \qquad (B.8)$$

- **incoming nucleon**

$$\hat{\mathbf{p}}_1 = -\hat{\mathbf{z}} \Rightarrow \hat{\mathbf{p}}_1.\sigma = \begin{pmatrix} -1 & 0 \\ 0 & 1 \end{pmatrix}, \qquad (B.9)$$

and the eigenvectors are:

$$|\Downarrow\rangle_{N_1} = \begin{pmatrix} -1 \\ 0 \end{pmatrix}, \qquad |\Uparrow\rangle_{N_1} = \begin{pmatrix} 0 \\ 1 \end{pmatrix}. \qquad (B.10)$$

- **Outgoing nucleon**

$$\hat{\mathbf{p}}_2 = -\sin\theta\cos\phi\hat{\mathbf{x}} - \sin\theta\sin\phi\hat{\mathbf{y}} - \cos\theta\hat{\mathbf{z}}, \tag{B.11}$$

$$\hat{\mathbf{p}}_2.\sigma = \begin{pmatrix} -\cos\theta & -\sin\theta e^{-i\phi} \\ -\sin\theta e^{i\phi} & \cos\theta \end{pmatrix}, \tag{B.12}$$

and the eigenvectors are:

$$|\downarrow\rangle_{N_2} = \begin{pmatrix} \cos\theta/2e^{-i\phi} \\ \sin\theta/2 \end{pmatrix}, \qquad |\uparrow\rangle_{N_2} = \begin{pmatrix} \sin\theta/2 \\ -e^{i\phi}\cos\theta/2 \end{pmatrix}. \tag{B.13}$$

Appendix C

Lepton Current

The general form of lepton currents are defined in section 3.1:

$$\varepsilon_\lambda^\alpha = \bar{u}_{l_\lambda}(k_2, s_2)\gamma^\alpha(1 - \gamma_5)u_{\nu_L}(k_1, s_1), \tag{C.1}$$

where λ is the helicity[1], $k_{1(2)}$ and $s_{1(2)}$ are the momentum and spin on incoming (outgoing) leptons respectively. Dirac matrices are:

$$\gamma^0 = \begin{pmatrix} I_2 & 0 \\ 0 & -I_2 \end{pmatrix}, \quad \gamma^k = \begin{pmatrix} 0 & \sigma^k \\ -\sigma^k & 0 \end{pmatrix}, \quad \gamma^5 = \begin{pmatrix} 0 & I_2 \\ I_2 & 0 \end{pmatrix} \tag{C.2}$$

where σ^k are 2×2 Pauli matrices:

$$\sigma_1 = \begin{pmatrix} 0 & 1 \\ 1 & 0 \end{pmatrix}, \quad \sigma_2 = \begin{pmatrix} 0 & -i \\ i & 0 \end{pmatrix}, \quad \sigma_3 = \begin{pmatrix} 1 & 0 \\ 0 & -1 \end{pmatrix}, \quad I_2 = \begin{pmatrix} 1 & 0 \\ 0 & 1 \end{pmatrix}. \tag{C.3}$$

Dirac spinors are $u_\lambda(k_i, s_i) = N_i \begin{pmatrix} \chi_{s_i,\lambda} \\ \frac{\boldsymbol{\sigma}.\mathbf{k}_i}{k_{0i}+m_i}\chi_{s_i,\lambda} \end{pmatrix}$, with normalization $N_i = \sqrt{E_i + m_i}$ for $i = 1, 2$, where χ_{s_i} are Pauli spinors.

$$\bar{u}_{l_\lambda}(k_2, s_2)\gamma^\alpha = N_2^* \left(\chi_{(s_2,\lambda)}^\dagger, \; \chi_{(s_2,\lambda)}^\dagger \frac{\boldsymbol{\sigma}.\mathbf{k}_2}{k_{02} + m_l} \right) \gamma^0 \gamma^\alpha \tag{C.4}$$

$$(\text{if } \alpha = 0) \quad = N_2^* \left(\chi_{(s_2,\lambda)}^\dagger, \; \chi_{(s_2,\lambda)}^\dagger \frac{\boldsymbol{\sigma}.\mathbf{k}_2}{k_{02} + m_l} \right) \tag{C.5}$$

$$(\text{if } \alpha = j) \quad = N_2^* \left(\chi_{(s_2,\lambda)}^\dagger \frac{\boldsymbol{\sigma}.\mathbf{k}_2}{k_{02} + m_l} \sigma^j, \; \chi_{(s_2,\lambda)}^\dagger \sigma^j \right) \tag{C.6}$$

---

[1] u_{ν_L} is neutrino spinor and left handed.
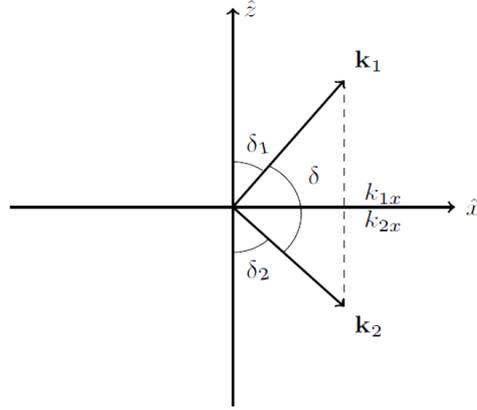
Fig. C.1 Lepton momentum in Isobaric frame

and

$$(1 - \gamma_5)u_{\nu_L}(k_1, s_1) = N_1 \begin{pmatrix} (1 - \frac{\boldsymbol{\sigma}.\mathbf{k}_1}{k_{01}})\chi_{s_1} \\ -(1 - \frac{\boldsymbol{\sigma}.\mathbf{k}_1}{k_{01}})\chi_{s_1} \end{pmatrix}.$$

Therefore

$$\varepsilon_\lambda^0 = N_1 N_2^* \, \chi_{(s_2,\lambda)}^\dagger \left(1 - \frac{\boldsymbol{\sigma}.\mathbf{k}_2}{k_{02} + m_l}\right)\left(1 - \frac{\boldsymbol{\sigma}.\mathbf{k}_1}{k_{01}}\right) \chi_{s_1}, \tag{C.7}$$

$$\varepsilon_\lambda^j = N_1 N_2^* \, \chi_{(s_2,\lambda)}^\dagger \left(1 - \frac{\boldsymbol{\sigma}.\mathbf{k}_2}{k_{02} + m_l}\right)(-\sigma^j)\left(1 - \frac{\boldsymbol{\sigma}.\mathbf{k}_1}{k_{01}}\right) \chi_{s_1}. \tag{C.8}$$

We can calculate ε_λ^0 and ε_λ^j in isobaric frame (Fig. C.1) where

$$\mathbf{k} = \mathbf{k_1} - \mathbf{k_2} = |\mathbf{k}|\hat{z}.$$

It is convenient to neglect y comonents, i.e. $k_{1y} = k_{2y} = 0$, therefore:

$$k_{1x} = k_{2x},$$
$$|\mathbf{k}| = |k_{1z} - k_{2z}|. \tag{C.7}$$

For incoming neutrino ($m_\nu = 0$):

$$k_{1x}^2 + k_{1z}^2 = k_{01}^2$$
$$(\frac{k_{1x}}{k_{01}})^2 + (\frac{k_{1z}}{k_{01}})^2 = 1, \tag{C.7}$$

and for outgoing lepton with $m_l \neq 0$:

$$
\begin{aligned}
k_{2x}^2 + k_{2z}^2 = k_{02}^2 - m_l^2 &= p_l^2 \\
\left(\frac{k_{2x}}{p_l}\right)^2 + \left(\frac{k_{2z}}{p_l}\right)^2 &= 1.
\end{aligned}
\tag{C.7}
$$

where
$$
\begin{aligned}
\frac{k_{1x}}{k_{01}} &= sin\delta_1, & \frac{k_{2x}}{p_l} &= sin\delta_1, \\
\frac{k_{1z}}{k_{01}} &= cos\delta_1, & \frac{k_{2z}}{p_l} &= -cos\delta_1.
\end{aligned}
\tag{C.8}
$$

Now we can calculate ε^0 by knowing the Pauli spinors (Appendix B) and pauli matrices:

$$
\varepsilon_\lambda^0 = N_1 N_2^* \, \chi_{(s_2,\lambda)}^\dagger \left(1 - \frac{\boldsymbol{\sigma}.\mathbf{k}_2}{k_{02}+m_l}\right)\left(1 - \frac{\boldsymbol{\sigma}.\mathbf{k}_1}{k_{01}}\right) \chi_{s_1}
\tag{C.9}
$$

$$
\begin{aligned}
\left(1 - \frac{\boldsymbol{\sigma}.\mathbf{k}_1}{k_{01}}\right)\chi_{s_1} &= \begin{pmatrix} 1 - \frac{k_{1z}}{k_{01}} & -\frac{k_{1x}}{k_{01}} \\ -\frac{k_{1x}}{k_{01}} & 1 + \frac{k_{1z}}{k_{01}} \end{pmatrix} \chi_{s_1} \\
&= \begin{pmatrix} 1 - \cos\delta_1 & -\sin\delta_1 \\ -\sin\delta_1 & 1 + \cos\delta_1 \end{pmatrix} \begin{pmatrix} -\sin\delta_1/2 \\ \cos\delta_1/2 \end{pmatrix} \\
&= \begin{pmatrix} -2\sin\delta_1/2 \\ 2\cos\delta_1/2 \end{pmatrix}
\end{aligned}
\tag{C.9}
$$

$$
\tag{C.10}
$$

and

$$
\chi_{(s_2,\lambda)}^\dagger \left(1 - \frac{\boldsymbol{\sigma}.\mathbf{k}_2}{k_{02}+m_l}\right) = \chi_{(s_2,\lambda)}^\dagger \begin{pmatrix} 1 - \frac{k_{2z}}{k_{02}+m_l} & -\frac{k_{2x}}{k_{02}-m_l} \\ -\frac{k_{2x}}{k_{02}+m_l} & 1 + \frac{k_{2z}}{k_{02}+m_l} \end{pmatrix}.
\tag{C.10}
$$

For left handed lepton:

$$
\begin{aligned}
&= \begin{pmatrix} \cos\delta_2/2 & -\sin\delta_2/2 \end{pmatrix} \begin{pmatrix} 1 + \left(\frac{k_{02}-m_l}{k_{02}+m_l}\right)^{1/2}\cos\delta_2 & -\left(\frac{k_{02}-m_l}{k_{02}+m_l}\right)^{1/2}\sin\delta_2 \\ -\left(\frac{k_{02}-m_l}{k_{02}+m_l}\right)^{1/2}\sin\delta_2 & 1 - \left(\frac{k_{02}-m_l}{k_{02}+m_l}\right)^{1/2}\cos\delta_2 \end{pmatrix} \\
&= \left(1 + \sqrt{\frac{k_{02}-m_l}{k_{02}+m_l}}\right)\begin{pmatrix} \cos\delta_2/2 & -\sin\delta_2/2 \end{pmatrix}
\end{aligned}
\tag{C.10}
$$

and for right handed lepton, Equation C will be:

$$
= \left(\sin \delta_2/2 \quad \cos \delta_2/2 \right) \begin{pmatrix} 1 + \left(\frac{k_{02}-m_l}{k_{02}+m_l} \right)^{1/2} \cos \delta_2 & - \left(\frac{k_{02}-m_l}{k_{02}+m_l} \right)^{1/2} \sin \delta_2 \\ - \left(\frac{k_{02}-m_l}{k_{02}+m_l} \right)^{1/2} \sin \delta_2 & 1 - \left(\frac{k_{02}-m_l}{k_{02}+m_l} \right)^{1/2} \cos \delta_2 \end{pmatrix}
$$

$$
= \left(1 - \sqrt{\frac{k_{02}-m_l}{k_{02}+m_l}} \right) \left(\sin \delta_2/2 \quad \cos \delta_2/2 \right) \tag{C.10}
$$

Therefore:

$$
\begin{aligned}
\varepsilon_L^0 &= N_1 N_2^* \left(1 + \sqrt{\frac{k_{02}-m_l}{k_{02}+m_l}} \right) \left(\cos \delta_2/2 \quad -\sin \delta_2/2 \right) \begin{pmatrix} -2\sin \delta_1/2 \\ 2\cos \delta_1/2 \end{pmatrix} \\
&= -2\sqrt{2k_{01}(k_02 + p_l)} \, \sin \left(\frac{\delta_1}{2} + \frac{\delta_2}{2} \right) \\
&= -2\sqrt{2k_{01}(k_02 + p_l)} \, \sqrt{\frac{1 - \cos(\delta_1 + \delta_2)}{2}} \\
&= -2\sqrt{k_{01}(k_02 + p_l)} \, \sqrt{1 + \cos \delta},
\end{aligned} \tag{C.8}
$$

$$
\begin{aligned}
\varepsilon_R^0 &= N_1 N_2^* \left(1 - \sqrt{\frac{k_{02}-m_l}{k_{02}+m_l}} \right) \left(\sin \delta_2/2 \quad \cos \delta_2/2 \right) \begin{pmatrix} -2\sin \delta_1/2 \\ 2\cos \delta_1/2 \end{pmatrix} \\
&= 2\sqrt{2k_{01}(k_02 - p_l)} \, \cos \left(\frac{\delta_1}{2} + \frac{\delta_2}{2} \right) \\
&= 2\sqrt{2k_{01}(k_02 - p_l)} \, \sqrt{\frac{1 + \cos(\delta_1 + \delta_2)}{2}} \\
&= 2\sqrt{k_{01}(k_02 - p_l)} \, \sqrt{1 - \cos \delta},
\end{aligned} \tag{C.6}
$$

where $\delta = \pi - (\delta_1 + \delta_2)$, the angle between leptons in the isobaric frame. We can do the same calculation for ε_λ^j

$$
\varepsilon_\lambda^j = N_1 N_2^* \, \chi_{(s_2,\lambda)}^\dagger \left(1 - \frac{\boldsymbol{\sigma}.\boldsymbol{k}_2}{k_{02}+m_l} \right) \left(-\sigma^j \right) \left(1 - \frac{\boldsymbol{\sigma}.\mathbf{k}_1}{k_{01}} \right) \chi_{s_1} \tag{C.7}
$$

$$
\begin{aligned}
\varepsilon_L^1 &= -N_1 N_2^* \left(1 + \sqrt{\frac{k_{02} - m_l}{k_{02} + m_l}}\right) \left(\cos \delta_2/2 \quad -\sin \delta_2/2\right) \begin{pmatrix} 0 & 1 \\ 1 & 0 \end{pmatrix} \begin{pmatrix} -2\sin \delta_1/2 \\ 2\cos \delta_1/2 \end{pmatrix} \\
&= -2\sqrt{2k_{01}(k_02 + p_l)} \cos\left(\frac{\delta_2}{2} - \frac{\delta_1}{2}\right) \\
&= -2\sqrt{k_{01}(k_02 + p_l)} \sqrt{1 + \cos(\delta_2 - \delta_1)} \\
&= -2\sqrt{k_{01}(k_02 + p_l)} \sqrt{1 - \frac{k_{1z}}{k_{01}}\frac{k_{2z}}{p_l} + \frac{k_{1x}}{k_{01}}\frac{k_{2x}}{p_l}} \\
&= \frac{-2}{\sqrt{2k_{01}p_l}} \sqrt{k_{01}(k_02 + p_l)} \sqrt{2k_{01}p_l - 2k_{1z}k_{2z} + 2k_{1x}k_{2x}}
\end{aligned}
\tag{C.4}
$$

After some simplification via Equation C.8

$$
\begin{aligned}
\varepsilon_L^1 &= \frac{-2}{\sqrt{2k_{01}p_l}} \sqrt{k_{01}(k_02 + p_l)} \frac{(k_{01} + p_l)}{|k|} \sqrt{(k_{1z} - k_{2z})^2 - (k_{01} - p_l)^2} \\
&= -2\sqrt{k_{01}(k_{02} + p_l)} \frac{(k_{01} + p_l)}{|k|} \sqrt{1 - \frac{k_{1z}}{k_{01}}\frac{k_{2z}}{p_l} - \frac{k_{1x}}{k_{01}}\frac{k_{2x}}{p_l}} \\
&= -2\sqrt{k_{01}(k_{02} + p_l)} \frac{(k_{01} + p_l)}{|k|} \sqrt{1 + \cos(\delta_1 + \delta_2)} \\
&= -2\sqrt{k_{01}(k_{02} + p_l)} \frac{(k_{01} + p_l)}{|k|} \sqrt{1 - \cos \delta}.
\end{aligned}
\tag{C.2}
$$

Similarly

$$
\begin{aligned}
\varepsilon_L^2 &= 2i\sqrt{2k_{01}(k_{02} + p_l)} \cos\left(\frac{\delta_1}{2} + \frac{\delta_2}{2}\right) \\
&= 2i\sqrt{k_{01}(k_{02} + p_l)} \sqrt{1 - \cos \delta}, \\
\varepsilon_L^3 &= 2\sqrt{2k_{01}(k_02 + p_l)} \sin\left(\frac{\delta_1}{2} - \frac{\delta_2}{2}\right) \\
&= -2\sqrt{k_{01}(k_{02} + p_l)} \frac{|k_{01} - p_l|}{|k|} \sqrt{1 + \cos \delta}
\end{aligned}
\tag{C.2}
$$

and for right handed ε_R^j:

$$
\begin{aligned}
\varepsilon_R^1 &= 2\sqrt{2k_{01}(k_{02}-p_l)}\,\sin\left(\frac{\delta_1}{2}-\frac{\delta_2}{2}\right) \\
&= 2\sqrt{k_{01}(k_{02}-p_l)}\,\frac{(k_{01}-p_l)}{|k|}\,\sqrt{1+\cos\delta} \quad\quad\quad\quad (C.2) \\
\varepsilon_R^2 &= 2i\sqrt{2k_{01}(k_{02}-p_l)}\,\sin\left(\frac{\delta_1}{2}+\frac{\delta_2}{2}\right) \\
&= 2i\sqrt{k_{01}(k_{02}-p_l)}\,\sqrt{1+\cos\delta} \quad\quad\quad\quad\quad\quad\quad (C.2) \\
\varepsilon_R^3 &= 2\sqrt{2k_{01}(k_{02}-p_l)}\,\cos\left(\frac{\delta_1}{2}+\frac{\delta_2}{2}\right) \\
&= 2\sqrt{k_{01}(k_{02}-p_l)}\,\frac{(k_{01}+p_l)}{|k|}\,\sqrt{1-\cos\delta}. \quad\quad\quad (C.2)
\end{aligned}
$$

Appendix D

Linear Transformation Between Invariant and Isobar Frame Amplitudes

Helicity amplitudes in Equation 3.49 - 3.56 are related to $\mathscr{F}_i$ and $\mathscr{G}_i$. We give here the linear transformations relating the isobaric frame amplitudes and invariant amplitudes (V_k and A_k). Equation 3.30 shows $O(V_k)$ and $O(A_k)$ in terms of Pauli matrices by using the following relations:

$$
\begin{aligned}
\gamma^0 \gamma^k &= \sigma^k \begin{pmatrix} 0, \mathbb{1}_2 \\ \mathbb{1}_2, 0 \end{pmatrix} \\
\gamma^i \gamma^j &= -\sigma^i \sigma^j \mathbb{1}_4
\end{aligned}
\tag{D.0}
$$

where γ^μ are Dirac matrices and given in Appendix C. First we show detailed derivation for $O(A_1)$ that has been given in Eq. (3.30).

$$
\begin{aligned}
O(A_1) &= \frac{1}{2} \left[(\gamma q)(\gamma \varepsilon) - (\gamma \varepsilon)(\gamma q) \right] \\
&= \frac{1}{2} \left[(\gamma^0 q_0 - \gamma^k q_k)(\gamma^0 \varepsilon_0 - \gamma^j \varepsilon_j) - (\gamma^0 \varepsilon_0 - \gamma^j \varepsilon_j)(\gamma^0 q_0 - \gamma^k q_k) \right] \\
&= \frac{1}{2} \left[q_0 \varepsilon_0 - \gamma^k \gamma^0 q_k \varepsilon_0 - \gamma^0 \gamma^j q_0 \varepsilon_j + \gamma^k \gamma^j q_k \varepsilon_j \right] \\
&= -\frac{1}{2} \left[\varepsilon_0 q_0 - \gamma^0 \gamma^k \varepsilon_0 q_k - \gamma^j \gamma^0 \varepsilon_j q_0 + \gamma^j \gamma^k \varepsilon_j q_k \right].
\end{aligned}
$$

Using Equation D.1

$$O(A_1) = \frac{1}{2}\left[2\gamma^0\gamma^k\varepsilon_0 q_k + 2\gamma^j\gamma^0\varepsilon_j q_0 + \gamma^k\gamma^j q_k\varepsilon_j + \gamma^k\gamma^j\varepsilon_j q_k + 2\vec{\varepsilon}.\vec{q}\right]$$

$$= \left[(\vec{q}.\vec{\sigma})\varepsilon^0 - (\vec{\varepsilon}.\vec{\sigma})q^0\right]\begin{pmatrix}0, \mathbb{1}_2 \\ \mathbb{1}_2, 0\end{pmatrix} + \left[(\vec{\varepsilon}.\vec{q}) - (\vec{\sigma}.\vec{q})(\vec{\sigma}.\vec{\varepsilon})\right]\mathbb{1}_4$$

where $\vec{\sigma} = \sigma_1\hat{i} + \sigma_2\hat{j} + \sigma_3\hat{k}$, and σ_k are Pauli matrices.

$\mathscr{F}_k$ and $\mathscr{G}_k$ can be found by equating the right hand sides of Equation 3.27 and Equation 3.29 for both vector and axial parts, therefore first we need to rewrite Equation 3.27 in terms of Pauli spinors and matrices (Appendix A). Here we will calculate $\mathscr{G}_k$ related to $O(A_1)$ contribution, but first we introduce new conventions and useful relations for the derivation:

$$O_{1\pm} = \left[(W_\pm^2 - k^2)(W_\pm^2 - m_\pi^2)\right]^{\frac{1}{2}}/2W = \left[(p_{10} \pm M)(P_{20} \pm M)\right]^{1/2}$$

$$O_{2\pm} = \left[(W_\pm^2 - k^2)/(W_\pm^2 - m_\pi^2)\right]^{\frac{1}{2}} = \left(\frac{p_{10} \pm M}{p_{20} \pm M}\right)^{1/2}$$

$$O_{1\pm} = |q|\left(\frac{p_{10} \pm M}{p_{10} \mp M}\right)^{1/2}O_{2\pm}$$

$$\frac{1}{O_{2\pm}} = \left(\frac{p_{20} \pm M}{p_{10} \pm M}\right)^{1/2} = \frac{|\mathbf{p}_2|}{|\mathbf{p}_1|}O_{2\mp} = \frac{|\mathbf{q}|}{|\mathbf{k}|}O_{2\mp} = \frac{1}{|\mathbf{k}|}\left(\frac{p_{10} \mp M}{p_{10} \pm M}\right)^{1/2}O_{1\pm}$$

where $W_\pm = W \pm M$, and $(p_1 + p_2)k + qk = W_+W_-$.

Dirac spinors for nucleons are $u(p_i, s_i) = N_i\begin{pmatrix}\chi_{s_i} \\ \frac{\vec{\sigma}.\vec{p}_i}{p_{0i}+M}\chi_{s_i}\end{pmatrix}$, with normalization $N_i = \sqrt{E_i + M}$ for $i = 1, 2$, where χ_{s_i} are Pauli spinors. Using this we start with axial part of Equation 3.27 for $k = 1$ with the help of Eq. D.

$$A_1\bar{u}(p_2, s_2)O(A_1)u(p_1, s_1) =$$

$$A_1 N_1 N_2 \left\{ \chi_{s2}^\dagger\left[(\vec{q}.\vec{\sigma})\varepsilon^0 - (\vec{\varepsilon}.\vec{\sigma})q^0\right]\frac{\vec{\sigma}.\vec{p}_1}{p_{01}+M} - \frac{\vec{\sigma}.\vec{p}_2}{p_{02}+M}\left[(\vec{q}.\vec{\sigma})\varepsilon^0 - (\vec{\varepsilon}.\vec{\sigma})q^0\right]\chi_{s1}\right.$$

$$\left. + \chi_{s2}^\dagger\left[(\vec{\varepsilon}.\vec{q}) - (\vec{\sigma}.\vec{q})(\vec{\sigma}.\vec{\varepsilon})\right] - \frac{\vec{\sigma}.\vec{p}_2}{p_{02}+M}\left[(\vec{\varepsilon}.\vec{q}) - (\vec{\sigma}.\vec{q})(\vec{\sigma}.\vec{\varepsilon})\right]\frac{\vec{\sigma}.\vec{p}_1}{p_{01}+M}\chi_{s1}\right\}$$

$$= A_1\chi_{s2}^\dagger\left\{\left[(\vec{q}.\vec{\sigma})\varepsilon^0 - (\vec{\varepsilon}.\vec{\sigma})q^0\right]\left(-|q|O_{2-}\hat{k}.\vec{\sigma}\right) + \left[(\vec{q}.\vec{\sigma})\varepsilon^0 - (\vec{\varepsilon}.\vec{\sigma})q^0\right]\left(|q|O_{2+}\hat{q}.\vec{\sigma}\right)\right.$$

$$\left. + \left[(\vec{\varepsilon}.\vec{q}) - (\vec{\sigma}.\vec{q})(\vec{\sigma}.\vec{\varepsilon})\right]O_{1+} - O_{1-}(\vec{\varepsilon}.\vec{q})(\hat{q}.\vec{\sigma})(\hat{k}.\vec{\sigma}) + O_{1-}|q|(\vec{\varepsilon}.\vec{\sigma})(\hat{k}.\vec{\sigma})\right\}$$

using $O_{1\pm} = O_{2\pm}(p_{02} \pm M)$

$$= A_1\chi_{s2}^\dagger\Bigg\{ \left[(\vec{\varepsilon}.\vec{q})O_{1+} + |q|^2\varepsilon_0 O_{2+}\right] - \left[(\vec{\varepsilon}.\vec{q})O_{1-} + |q|^2\varepsilon_0 O_{2-}\right](\vec{\sigma}.\hat{q})(\vec{\sigma}.\hat{k})$$

$$-(\vec{\sigma}.\hat{q})(\vec{\sigma}.\vec{\varepsilon})|q|\left[q_0 O_{2+} + (p_{02}+M)O_{2+}\right] + (\vec{\sigma}.\hat{k})(\vec{\sigma}.\vec{\varepsilon})|q|\left[q_0 O_{2-} + (p_{02}-M)O_{2-}\right]\Bigg\}\chi_{s1}$$

$$= A_1\chi_{s2}^\dagger\Bigg\{ -|q|O_{2+}W_+(\vec{\sigma}.\hat{q})(\vec{\sigma}.\vec{\varepsilon}) + |q|O_{2-}W_-(\vec{\sigma}.\hat{k})(\vec{\sigma}.\vec{\varepsilon})$$

$$+ O_{1+}\left[(\vec{\varepsilon}.\vec{q}) + \varepsilon_0(p_{02}-M)\right] - O_{1-}\left[(\vec{\varepsilon}.\vec{q}) + \varepsilon_0(p_{02}+M)\right](\vec{\sigma}.\hat{q})(\vec{\sigma}.\vec{k})\Bigg\}\chi_{s1}$$

Now we define $\Delta = k_0(q_0 k_0 - (qk))\mathbf{k^2}$ and we use an auxiliary term which is zero:

$$\mathbb{C} = O_{1+}\Bigg\{ \left[-\frac{|\mathbf{k}|}{k_0}(p_{02}-M) - \sqrt{\frac{p_{01}-M}{p_{01}+M}}W_- - (\vec{q}.\hat{k})\right] + \frac{|\mathbf{k}|}{k_0}\left[\Delta + p_{02} - M + \frac{k_0 W_-}{p_{01}+M}\right]\Bigg\}$$

$$-O_{1-}\Bigg\{ -\left[\frac{|\mathbf{k}|}{k_0}(p_0+M) + \sqrt{\frac{p_{01}+M}{p_{01}-M}}W_+ + (\vec{q}.\hat{k})\right] + \frac{|\mathbf{k}|}{k_0}\left[\Delta + p_{02} + M + \frac{k_0 W_+}{p_{01}-M}\right]\Bigg\}(\vec{\sigma}.\hat{q})(\vec{\sigma}.\hat{k})$$

$\mathbb{C} = 0$, therefore we can add $\mathbb{C}(\hat{k}.\vec{\varepsilon})$ to Eq. D.

$$= A_1\chi_{s2}^\dagger\Bigg\{ -|q|O_{2+}W_+(\vec{\sigma}.\hat{q})(\vec{\sigma}.\vec{\varepsilon}) + |q|O_{2-}W_-(\vec{\sigma}.\hat{k})(\vec{\sigma}.\vec{\varepsilon})$$

$$+ O_{1+}\Bigg[|q|\left((\vec{\varepsilon}.\hat{q}) - (\hat{q}.\hat{k})(\hat{k}.\vec{\varepsilon})\right) + \frac{k\varepsilon}{k_0}(p_{02}-M) - \sqrt{\frac{p_{01}-M}{p_{01}+M}}W_-(\hat{k}.\vec{\varepsilon})$$

$$+ \frac{|\mathbf{k}|}{k_0}\left(\Delta + p_{02} - M + \frac{k_0 W_-}{p01+M}\right)(\hat{k}.\vec{\varepsilon})\Bigg]$$

$$- O_{1-}\Bigg[|q|\left((\vec{\varepsilon}.\hat{q}) - (\hat{q}.\hat{k})(\hat{k}.\vec{\varepsilon})\right) + \frac{k\varepsilon}{k_0}(p_{02}+M) - \sqrt{\frac{p_{01}+M}{p_{01}-M}}W_+(\hat{k}.\vec{\varepsilon})$$

$$+ \frac{|\mathbf{k}|}{k_0}\left(\Delta + p_{02} + M + \frac{k_0 W_+}{p01+M}\right)(\hat{k}.\vec{\varepsilon})\Bigg](\vec{\sigma}.\hat{q})(\vec{\sigma}.\hat{k})\Bigg\}\chi_{s1}$$

$$= A_1\chi_{s2}^\dagger\Bigg\{ |q|O_{2+}W_+\Lambda_1 + |q|O_{2-}\Lambda_2 + |q|O_{1-}\Lambda_3 - |q|O_{1+}\Lambda_4$$

$$+ O_{1-}(\Delta + P_{20} + M + k_0 W_+/(p_{01}-M))\Lambda_5 - O_{1+}(\Delta + P_{20} - M + k_0 W_-/(p_{01}+M))\Lambda_6$$

$$+ O_{1-}(P_{02}+M)\Lambda_7 - O_{1+}(P_{02}-M)\Lambda_8\Bigg\}\chi_{s1}$$

From Eq. D we can extract $\mathcal{G}_k$, but only terms related to A_1. One needs to calculate all terms related to A_k and V_k.

Here we summarize $\mathcal{F}_i$ and $\mathcal{G}_i$ in terms of V_k and A_k

$$
\begin{aligned}
\mathcal{F}_i &= K_i^V.F_i \\
\mathcal{G}_i &= K_i^A.G_i,
\end{aligned}
\tag{D.-23}
$$

where

$$
\begin{aligned}
K_1^V &= W_- O_{1+} & K_4^V &= q^2 W_+ O_{2-} \\
K_2^V &= W_+ O_{1-} & K_5^V &= 1/O_{2+} \\
K_3^V &= q^2 W_+ O_{2-} & K_6^V &= 1/O_{2-}
\end{aligned}
\tag{D.-23}
$$

and

$$
\begin{aligned}
K_1^A &= |\mathbf{q}| O_{2+} & K_5^A &= O_{1-} \\
K_2^A &= |\mathbf{q}| O_{2-} & K_6^A &= O_{1+} \\
K_3^A &= |\mathbf{q}| O_{1-} & K_7^A &= O_{1-} \\
K_4^A &= |\mathbf{q}| O_{1+} & K_8^A &= O_{1+}
\end{aligned}
\tag{D.-23}
$$

For vector part

$$
\begin{aligned}
F_1 &= V_1 + (V_3 - V_4)(qk)/W_- + V_4 W_- - V_6 k^2/W_- \ , \\
F_2 &= -V_1 + (V_3 - V_4)(qk)/W_+ + V_4 W_+ - V_6 k^2/W_+ \ , \\
F_3 &= V_3 - V_4 + V_{25}/W_+ \ , \\
F_4 &= V_3 - V_4 - V_{25}/W_- \ , \\
F_5 &= V_1(W_+^2 - k^2)/2W - V_2(qk)(W_+^2 - k^2 + 2WW_-)/2W + (V_3 - V_4)(W_+ q_0 - (qk)) \\
&\quad + V_4(W_+^2 - k^2)W_-/2W - V_5(qk)k_0 - V_6(W_+^2 - k^2)W_-/2W + q_0 V_{25} \ , \\
F_6 &= -V_1(W_-^2 - k^2)/2W + V_2(qk)(W_+^2 - k^2 + 2WW_-)/2W + (V_3 - V_4)(W_- q_0 - (qk)) \\
&\quad + V_4(W_-^2 - k^2)W_+/2W + V_5(qk)k_0 - V_6(W_-^2 - k^2)W_+/2W - q_0 V_{25} \ ,
\end{aligned}
\tag{D.-22}
$$

and for axial part of Eq: (D.-23) are

$$G_1 = W_+ A_1 - M A_4 \ ,$$

$$G_2 = -W_- A_1 - M A_4 \ ,$$

$$G_3 = A_1 + A_2 - A_3 + (A_5 - A_6) W_+ \ ,$$

$$G_4 = -A_1 - A_2 + A_3 + (A_5 - A_6) W_- \ ,$$

$$G_5 = \left[\Delta + (W_+^2 - m_\pi^2)/2W + 2W k_0 W_+/(W_-^2 - k^2) \right] A_1 + (\Delta + p_{02} + W) A_2 + (q_0 - \Delta) A_3$$

$$\quad - M \left[W_-/(p_{01} - M) \right] A_4 + W_+ \left[(\Delta + p_{02} + W) A_5 + (q_0 - \Delta) A_6 \right] \ ,$$

$$G_6 = - \left[\Delta + (W_-^2 - m_\pi^2)/2W + 2W k_0 W_-/(W_+^2 - k^2) \right] A_1 + (\Delta + p_{02} + W) A_2 - (q_0 - \Delta) A_3$$

$$\quad - M \left[W_+/(p_{01} + M) \right] A_4 + W_- \left[(\Delta + p_{02} + W) A_5 + (q_0 - \Delta) A_6 \right] \ ,$$

$$G_7 = (W_+^2 - m_\pi^2) A_1/2W + (p_{01} + p_{02}) A_2 + q_0 A_3 - M A_4 + k_0 A_7$$

$$\quad + W_+ \left[(p_{01} + p_{02}) A_5 + q_0 A_6 + k_0 A_8 \right] \ ,$$

$$G_8 = -(W_-^2 - m_\pi^2) A_1/2W - (p_{01} + p_{02}) A_2 - q_0 A_3 - M A_4 - k_0 A_7$$

$$\quad + W_- \left[(p_{01} + p_{02}) A_5 + q_0 A_6 + k_0 A_8 \right] \ ,$$

(D.-21)

where

$$V_{25} = W_+ W_- V_2 + k^2 V_5$$

$$\Delta = k_0(q_0 k_0 - (qk)) \mathbf{k^2}.$$

(D.-21)

Appendix E

General Cross-section expression

The general expression of the differential cross section for the collision of two particles ($i = 1, 2$) and N outgoing particles ($f = 1, ..., N$) is given as:

$$d\sigma = \frac{(2\pi)^4}{4[(p_1 . p_2)^2 - m_1^2 m_2^2]^{1/2}} \delta^4\left(\sum_f p_f - \sum_i p_i\right) \left(\prod_f \frac{d^3 p_f}{(2\pi)^3 2p^0}\right) |\mathcal{M}|^2, \tag{E.1}$$

where for particles on their mass shell

$$\frac{d^3 p}{(2\pi)^3 2p^0} = \frac{\mathbf{p}^2 d\mathbf{p} d\Omega}{(2\pi)^3 2p^0} = \frac{1}{(2\pi)^3} \frac{\sqrt{p^{02} - m^2}}{2} dp^0 d\Omega. \tag{E.2}$$

For single pion production

$$\nu(k_1) + N(p_1) \to l(k_2) + N(p_2) + \pi(q), \tag{E.3}$$

$N = 3$, and the differential cross-section is :

$$d\sigma = \frac{(2\pi)^4}{4(k_1 . p_1)} \delta^4(k_2 + p_2 + q - k_1 - p_1) \frac{d^3 p_2}{(2\pi)^3 2p_2^0} \frac{d^3 k_2}{(2\pi)^3 2k_2^0} \frac{d^3 q}{(2\pi)^3 2q^0} |\mathcal{M}|^2, \tag{E.4}$$

$$\tag{E.5}$$

where $[(p_1 . p_2)^2 - m_1^2 m_2^2]$ is invariant and it is easier to calculate it in the lab frame where nucleon is at rest and neutrino is massless.
$\frac{d^3 k_2}{(2\pi)^3 2k_2^0}$ is also invariant and can be calculated in the lab frame:

$$\left[\frac{d^3 k_2}{(2\pi)^3 2k_{02}}\right]_{Lab} = \frac{|\mathbf{k}_{2L}|^2}{2k_{02}^L} d|\mathbf{k}_{2L}| d\Omega_{k_{2L}} = \frac{|\mathbf{k}_{2L}|}{2} dk_{02}^L d\phi_{k_{2L}} d\cos\delta_{k_{2L}}. \tag{E.6}$$

$dk_{02}^L = \frac{W}{M} dk_2^0$, where k_{02} is the lepton energy in the isobaric frame, and

$$Q^2 = -(k_{1L} - k_{2L})^2 = m_l^2 - 2k_{1L}^0 k_{2L}^0 + 2|\mathbf{k}_{1L}||\mathbf{k}_{2L}|\cos\delta_{k_{2L}}$$
$$\Rightarrow dQ^2 = 2|\mathbf{k}_{1L}||\mathbf{k}_{2L}| \, d\cos\delta_{k_{2L}}. \tag{E.6}$$

Therefore:

$$\frac{d^3 k_2}{(2\pi)^3 2k_{02}} = \frac{|\mathbf{k}_{2L}|}{2} \frac{W}{M} dk_{02}d\phi_{k_{2L}} \frac{1}{2|\mathbf{k}_{1L}||\mathbf{k}_{2L}|}dQ^2 \tag{E.7}$$

Substituting Equation E.7 in Equation E.4, and using $\mathbf{k}_1 - \mathbf{k}_2 + \mathbf{p}_1 = 0$ in the isobaric frame we will have:

$$d\sigma = \frac{2\pi}{4ME_\nu}\delta(k_{02} + p_{02} + q_0 - k_{01} - p_{01})\delta^3(\mathbf{p}_2 + \mathbf{q})\frac{d^3 p_2}{(2\pi)^3 2p_{02}}\frac{d^3 q}{(2\pi)^3 2q_0}$$
$$\times \left(\frac{1}{4E_\nu}\frac{W}{M} dk_{02}d\phi_{k_{2L}}dQ^2\right)|\mathscr{M}|^2. \tag{E.7}$$

In the isobaric frame $\mathbf{p}_2 + \mathbf{q} = 0 \Rightarrow p_{02} = \sqrt{|\mathbf{q}|^2 + M^2}$, and we can integrate over $d_{\mathbf{p}_2}^3$:

$$d\sigma = \frac{2\pi}{4ME_\nu}\frac{1}{(2\pi)^3}\frac{1}{4}\frac{\delta\left[(k_{02} - k_{01} - p_{01}) + \sqrt{|\mathbf{q}|^2 + M^2} + \sqrt{|\mathbf{q}|^2 + m_\pi^2}\right]}{\sqrt{|\mathbf{q}|^2 + M^2} \cdot \sqrt{|\mathbf{q}|^2 + m_\pi^2}}$$
$$\times |\mathbf{q}|^2 d|\mathbf{q}|\frac{d|\Omega_\pi|}{(2\pi)^3}\left(\frac{1}{4E_\nu}\frac{W}{M} dk_{02}d\phi_{k_{2L}}dQ^2\right)|\mathscr{M}|^2. \tag{E.7}$$

$$W = \sqrt{|\mathbf{q}|^2 + M^2} + \sqrt{|\mathbf{q}|^2 + m_\pi^2} \Rightarrow dW = \frac{W|\mathbf{q}|d|\mathbf{q}|}{\sqrt{|\mathbf{q}|^2 + M^2}\sqrt{|\mathbf{q}|^2 + m_\pi^2}} \tag{E.8}$$

Therefore:

$$d\sigma = \frac{2\pi}{4ME_\nu}\frac{1}{(2\pi)^6}\frac{|\mathbf{q}|}{4}\delta(k_{02} - k_{01} - p_{01} + W)\frac{1}{4E_\nu}\frac{W}{M}\frac{dW}{W}$$
$$\times dk_2^0 d\phi_{k_{2L}}dQ^2 d|\Omega_\pi||\mathscr{M}|^2. \tag{E.8}$$

Now we can integrate over dk_{02} and $d\phi_{k_2}$

$$d\sigma = \frac{1}{(2\pi)^4}\frac{1}{(4ME_\nu)^2}\frac{|\mathbf{q}|}{4} dW \, dQ \, d\Omega_\pi|\mathscr{M}|^2. \tag{E.9}$$

Appendix F

Angular Momentum States

To classify the possible polarized states of a particle, we can use the component of spin along a fixed direction. We can also use the component of spin along the direction of momentum of the particle, which is called helicity quantum number (λ). Imagine you have a plane-wave solution for a free particle with momentum p and energy E. If $m \neq 0$, there are $2s + 1$ linearly independent states with definite helicity:

$$\lambda = s, s-1, ..., -s+1, -s.$$

if $m = 0$ then $\lambda = \pm s$. These states characterized by p and λ, form a complete orthogonal set of states for a free particle. They have the following properties:

- λ is invariant under ordinary rotation; i.e. if we apply a rotation to our solutions, we will obtain states with different $\vec{p}$, but same λ. Therefore we can construct states with definite J for all particles with definite λ.

- λ will flip the signs under a space reflection:

$$Y\psi_{p,\lambda} = \eta(-1)^{s-\lambda}\psi_{p,-\lambda}$$

  where η is parity, and Eq. F will be derived later.

- Suppose we have states $\psi_{p\lambda}$ with $\vec{p} = |p|\hat{z}$. Then we can find states with $\vec{p}'$ in an arbitrary direction (θ, ϕ), $|\mathbf{p}|, \theta, \phi; \lambda\rangle$ with a suitable rotation

$$|\theta, \phi; \lambda\rangle = \mathscr{R}_{\phi, \theta, -\phi}\psi_{p,\lambda} = e^{i\phi\lambda}\mathscr{R}_{\phi, \theta, 0}\psi_{p,\lambda}$$

where

$$\mathscr{R}_{\alpha,\beta,\gamma} = \exp(-i\alpha J_z)\exp(-i\beta J_y)\exp(-i\gamma J_z)$$

is Euler rotation.

F.1   Two free particles along $\hat{z}$ direction

For two free particles with (s_1, m_1) and (s_2, m_2) in the center of mass frame $\vec{p}_1 = -\vec{p}_2 = p\hat{z}$.
We can have $\psi_{p_1,\lambda_1}(1)$ states for particle (1) and $\psi'_{p_2,\lambda_2}(2)$ for particle (2).
We can define the product of two states as one state with momentum $\vec{p} = p\hat{z}$, and from Eq. (F) we have:

$$\psi_{p,\lambda_1,\lambda_2} = \psi_{p\lambda_1}(1)\psi'_{p\lambda_2}(2) = \psi_{p\lambda_1}(1)(-1)^{s_2-\lambda_2}\psi_{p-\lambda_1}(1)$$

F.2   Two free particles in (θ, ϕ) direction

Eq. (F.1) gives us states of two free particle along $\hat{z}$. By applying a rotation (Eq. F) on $\psi_{p,\lambda_1,\lambda_2}$ we can find this system along an arbitrary direction (θ, ϕ):

$$|p,\theta,\phi;\lambda_1,\lambda_2\rangle = \mathscr{R}_{\phi\theta-\phi}\psi_{p\lambda_1\lambda_2} = e^{i\lambda\phi}\mathscr{R}_{\phi\theta 0}\psi_{p\lambda_1\lambda_2},$$

where $\lambda = \lambda_1 - \lambda_2$.

F.3   States with definite angular momentum and helicity

Now we can construct states with definite J and its component $J_z = M$; $|p;JM,\lambda_1\lambda_2\rangle$[1].

$$\begin{aligned}
|p,\theta,\phi;\lambda_1,\lambda_2\rangle &= \mathscr{R}_{\phi\theta-\phi}\psi_{p\lambda_1\lambda_2} \\
&= \sum_{J,M}|p;JM,\lambda_1\lambda_2\rangle\langle p;JM,\lambda_1\lambda_2|p,\theta,\phi;\lambda_1,\lambda_2\rangle \\
&= \sum_{J,M}\mathscr{D}^J_{M,\lambda}(\phi\theta-\phi)|p;JM,\lambda_1\lambda_2\rangle
\end{aligned}$$

---

[1]Since the magnitude p and helicities λ_1 and λ_2 are invariant under rotation, we can assign difinite values to them, together with J and M

where $\lambda = \lambda_1 - \lambda_2$, and

$$D^J_{M,M'}(\alpha,\beta,\gamma) = e^{-iM\alpha} \, d^J_{M,M'}(\beta) \, e^{-iM'\gamma} \qquad \text{(F.-1)}$$

is the matrix corresponding to $\mathscr{R}_{\alpha\beta\gamma}$ in the irreducible representation $\mathscr{D}^J$, and $\sqrt{\frac{2j+1}{4\pi}} d^j_{\lambda,\mu}(\theta) e^{i(\lambda-\mu)\phi}$
are mutually orthonormal functions where $d^j_{\lambda,\mu}$ are define in Equation 3.74. Therefore:

$$\int d\Omega \mathscr{D}^{J'}_{M'\lambda'}{}^*(\phi\theta-\phi)|p,\theta,\phi;\lambda_1,\lambda_2\rangle = \sum_{JM} \int d\Omega \mathscr{D}^{J'}_{M'\lambda'}{}^*(\phi\theta-\phi)\mathscr{D}^J_{M\lambda}(\phi\theta-\phi)|p;JM,\lambda_1\lambda_2\rangle$$

$$= \frac{1}{\mathfrak{R}}|p;JM,\lambda_1\lambda_2\rangle.$$

To calculate the normalization factor R, we use Eq. F.-1, and $d^j_{\lambda,\mu}$ properties:

$$\sum_{JM} \int d\Omega \mathscr{D}^{J'}_{M'\lambda'}{}^*(\phi\theta-\phi)\mathscr{D}^J_{M\lambda}(\phi\theta-\phi)$$

$$= \sum_{JM} \int d\Omega e^{iM'\phi} d^{j'}_{M'\lambda'}{}^*(\theta)e^{-i\lambda'\phi}e^{-iM\phi} d^J_{M\lambda}(\theta)e^{i\lambda\phi} = \frac{4\pi}{2j+1}$$

$$\Rightarrow \mathfrak{R} = \sqrt{\frac{2j+1}{4\pi}}$$

Therefore:

$$|p;JM,\lambda_1\lambda_2\rangle = \mathfrak{R} \int d\Omega \mathscr{D}^J_{M\lambda}{}^*(\phi\theta-\phi)|p,\theta\phi;\lambda_1\lambda_2\rangle$$

From this we can derive reflection (F). Parity (P) is reflection from the origin ($xyz \to -x,-y,-z$), then a reflection in the xz plane is

$$Y\psi_{0,\lambda} = e^{-i\pi J_y} P\psi_{0,\lambda} = \eta \sum_{\lambda'} d^s_{\lambda'\lambda}(\pi)\psi_{0,\lambda'}, \qquad \text{(F.-4)}$$

where

$$d^s_{\lambda'\lambda}(\pi) = (-1)^{(s-\lambda)}\delta_{\lambda',-\lambda}. \qquad \text{(F.-4)}$$

Therefore Equation F.3 will be F.

In order to construct states with definite angular momentum and helicity, we have to have standard particle's states if we have more than one particle. In isobaric (Adler) or πN rest frame (Figure 3.3), incident nucleon spinor (χ_1) is at $-\hat{z}$ direction and should be reflected to $\hat{z}$ (the direction of gauge boson), and outgoing nucleon is at $(-\theta,-\phi)$ direction and it should to be changed to (θ,ϕ) direction which is outgoing pion direction. This is equivalent to a

reflection and rotation along $\hat{z}$ with $-2\phi = 2\pi - 2\phi$ angle

$$
\begin{aligned}
\chi_{\lambda_1} \to \chi'_{\lambda_1} &= (-1)^{s-\lambda_1}\chi_{-\lambda_1} \text{ reflection along } \hat{z} \\
\chi^*_{\lambda_2} \to \chi'^*_{\lambda_2} &= e^{i\pi J_y}e^{i(2\pi-2\phi)J_z}\chi^*_{\lambda_2} \\
&= (-1)e^{-2i\phi(\lambda_2)}(-1)^{s-\lambda_2}\chi^*_{-\lambda_2} \text{ reflection along } (\theta,\phi)
\end{aligned}
\tag{F.-5}
$$

Then we will have a system of two particles along $\hat{z}$ for incoming nucleon and gauge boson (with helicity λ_k), $\psi_{\lambda_k - \lambda_1}$, and a state for two particles along (θ,ϕ) i.e. outgoing nucleon and pion (with helicity λ_q); $\psi\lambda_q - \lambda_2$. Therefore for $s = 1/2$ we have;

$$
\begin{aligned}
F_{\mu\lambda}(\theta,\phi) &= (-1)^{-(\lambda_1+\lambda_2)}e^{2i\phi\lambda_2}\tilde{F}^{\lambda_k}_{\lambda_2\lambda_1}(\theta,\phi) = e^{i[\lambda_1\pi+\lambda_2(\pi+2\phi)]}\tilde{F}^{\lambda_k}_{\lambda_2\lambda_1}(\theta,\phi) \\
G_{\mu\lambda}(\theta,\phi) &= (-1)^{-(\lambda_1+\lambda_2)}e^{2i\phi\lambda_2}\tilde{G}^{\lambda_k}_{\lambda_2\lambda_1}(\theta,\phi) = e^{i[\lambda_1\pi+\lambda_2(\pi+2\phi)]}\tilde{G}^{\lambda_k}_{\lambda_2\lambda_1}(\theta,\phi)
\end{aligned}
\tag{F.-5}
$$

where $\mu = \lambda_\pi - \lambda_2 = -\lambda_2$ and $\lambda = \lambda_k - \lambda_1$.

Appendix G

Resonance Production Amplitudes

In this appendix we list all helicity amplitudes for 17 resonances in Table 4.1, given in [7] and [13]. First we need to define required notation:

$$T^V = T = \frac{\sqrt{\Omega}}{3\sqrt{2}W} F^V(k^2)$$

$$R^V = R = \frac{\sqrt{2}M}{W} \frac{(W+M)|\mathbf{k}^L|}{(W+M)^2 - k^2} F^V(k^2)$$

$$S^- = \frac{\sqrt{-k^2}}{|\mathbf{k}^L|^2} \frac{\varepsilon_-^3 k_0 - |\mathbf{k}|\varepsilon_-^0}{C_-} \left(\frac{1}{6} - \frac{k^2}{6M^2} - \frac{W}{2M}\right) F^V(k^2)$$

$$S^+ = \frac{\sqrt{-k^2}}{|\mathbf{k}^L|^2} \frac{\varepsilon_+^3 k_0 - |\mathbf{k}|\varepsilon_+^0}{C_+} \left(\frac{1}{6} - \frac{k^2}{6M^2} - \frac{W}{2M}\right) F^V(k^2)$$

$$T^A = \frac{\sqrt{2\Omega}}{3} \frac{M\mathbf{k}_L}{W((W+M)^2 - k^2)} G(k^2)$$

$$R^A = \frac{\sqrt{2}}{6W} \left[W + M + \frac{2n\Omega W}{(W+M)2 - k^2}\right] G(k^2)$$

$$C^- = \frac{\sqrt{-k^2}}{C_-} \left[(\varepsilon_L^0 |\mathbf{k}| - k_0 \varepsilon_L^3)(\frac{1}{3} + \frac{k_0}{aM}) \right.$$
$$\left. + \left(\frac{2}{3}W + \frac{k^2}{aM} + \frac{n\Omega}{3aM}\right) \left[\varepsilon_L^3 + (\varepsilon_L^0 - \varepsilon_L^3 |\mathbf{k}|)\frac{|\mathbf{k}|}{m_\pi^2 - k^2}\right] \right] \frac{G^A(k^2)}{2W|\mathbf{k}|}$$

$$C^+ = \frac{\sqrt{-k^2}}{C_-} \left[(\varepsilon_R^0 |\mathbf{k}| - k_0 \varepsilon_R^3)(\frac{1}{3} + \frac{k_0}{aM}) \right.$$
$$\left. + \left(\frac{2}{3}W + \frac{k^2}{aM} + \frac{n\Omega}{3aM}\right) \left[\varepsilon_R^3 + (\varepsilon_R^0 - \varepsilon_R^3 |\mathbf{k}|)\frac{|\mathbf{k}|}{m_\pi^2 - k^2}\right] \right] \frac{G^A(k^2)}{2W|\mathbf{k}|}$$

Table G.1 Angular momentum Clebsch-Gordan coefficients

j	l	$\begin{pmatrix} \frac{1}{2} & l & j \\ \frac{1}{2} & 0 & \frac{1}{2} \end{pmatrix}$	$\begin{pmatrix} \frac{1}{2} & l & j \\ \frac{1}{2} & 1 & \frac{1}{2} \end{pmatrix}$	$\begin{pmatrix} \frac{1}{2} & l & j \\ -\frac{1}{2} & 1 & \frac{1}{2} \end{pmatrix}$	$\begin{pmatrix} \frac{1}{2} & l & j \\ -\frac{1}{2} & 2 & \frac{1}{2} \end{pmatrix}$	
$\frac{1}{2}$	0	$+1$	0	0	0	$j = l + \frac{1}{2}$
$\frac{3}{2}$	1	$+\sqrt{\frac{2}{3}}$	$+1$	$+\sqrt{\frac{1}{3}}$	0	
$\frac{5}{2}$	2	$+\sqrt{\frac{3}{5}}$	$+\sqrt{\frac{4}{5}}$	$+\sqrt{\frac{2}{5}}$	$+\sqrt{\frac{1}{5}}$	
$\frac{7}{2}$	3	...	...	...	...	
$\frac{1}{2}$	1	$-\sqrt{\frac{1}{3}}$	0	$+\sqrt{\frac{2}{3}}$	0	$j = l - \frac{1}{2}$
$\frac{3}{2}$	2	$-\sqrt{\frac{2}{5}}$	$-\sqrt{\frac{1}{5}}$	$+\sqrt{\frac{3}{5}}$	$+\sqrt{\frac{4}{5}}$	
$\frac{5}{2}$	3	...	...	...	...	

where n is a number of oscillators for resonances where $n = 0$ for Δ resonance.

$$\Omega = 1.05 \, GeV$$

$$\lambda = \sqrt{\frac{2}{\Omega} \frac{M}{W}} |\mathbf{k}^L|$$

$$a = 1 + \frac{W^2 - k^2 + M^2}{2MW}$$

and

$$T^{\pm} = -(T^V \pm T^A)$$

$$R^{\pm} = -(R^V \pm R^A)$$

Table G.2 Production amplitudes for charged and neutral current weak interaction from Reference [7]   .

Resonance	Helicity	Weak CC	Weak NC (p)	Weak NC (n)
$P_{33}(1232)$	f_{-3}	$\sqrt{6}R^-$	$-\sqrt{6}(R^- + 2xR)$	
	f_{-1}	$\sqrt{2}R^-$	$-\sqrt{6}(R^- + 2xR)$	
	f_{+1}	$-\sqrt{2}R^+$	$-\sqrt{6}(R^- + 2xR)$	
	f_{+3}	$-\sqrt{6}R^+$	$-\sqrt{6}(R^- + 2xR)$	$n = p$
	$f_{0+}^{(-)}$	$-2\sqrt{2}C^-$	$2\sqrt{2}C^-$	
	$f_{0-}^{(-)}$	$-2\sqrt{2}C^-$	$2\sqrt{2}C^-$	
	$f_{0+}^{(+)}$	$-2\sqrt{2}C^+$	$2\sqrt{2}C^+$	
	$f_{0-}^{(+)}$	$-2\sqrt{2}C^+$	$2\sqrt{2}C^+$	
$P_{11}(1440)$	f_{-1}	$-\frac{5}{6}\sqrt{3}\lambda^2 R^-$	$\frac{5}{12}\sqrt{3}(R^- + 2x(\frac{6}{5})R)$	$\frac{5}{12}\sqrt{3}(R^- + 2x(\frac{4}{5})R)$
	f_{+1}	$-\frac{5}{6}\sqrt{3}\lambda^2 R^+$	$\frac{5}{12}\sqrt{3}(R^+ + 2x(\frac{6}{5})R)$	$\frac{5}{12}\sqrt{3}(R^+ + 2x(\frac{4}{5})R)$
	$f_{0+}^{(-)}$	$-\sqrt{\frac{3}{4}}\lambda^2 S^- - \frac{5}{6}\sqrt{3}\lambda(\lambda C^- - 2B^-)$	$-\frac{1}{2}\sqrt{\frac{3}{4}}\lambda^2 S^-(1-4x) - \frac{5}{12}\sqrt{3}\lambda(\lambda C^- - 2B^-)$	$\frac{1}{2}\sqrt{\frac{3}{4}}\lambda^2 S^- + \frac{5}{12}\sqrt{3}\lambda(\lambda C - 2B^-)$
	$f_{0-}^{(-)}$	$-\sqrt{\frac{3}{4}}\lambda^2 S^- + \frac{5}{6}\sqrt{3}\lambda(\lambda C^- - 2B^-)$	$-\frac{1}{2}\sqrt{\frac{3}{4}}\lambda^2 S^-(1-4x) + \frac{5}{12}\sqrt{3}\lambda(\lambda C^- - 2B^-)$	$\frac{1}{2}\sqrt{\frac{3}{4}}\lambda^2 S^- - \frac{5}{12}\sqrt{3}\lambda(\lambda C^- - 2B^-)$
	$f_{0+}^{(+)}$	$-\sqrt{\frac{3}{4}}\lambda^2 S^+ - \frac{5}{6}\sqrt{3}\lambda(\lambda C^+ - 2B^+)$	$-\frac{1}{2}\sqrt{\frac{3}{4}}\lambda^2 S^+(1-4x) - \frac{5}{12}\sqrt{3}\lambda(\lambda C^+ - 2B^+)$	$\frac{1}{2}\sqrt{\frac{3}{4}}\lambda^2 S^+ + \frac{5}{12}\sqrt{3}\lambda(\lambda C^+ - 2B^+)$
	$f_{0-}^{(+)}$	$-\sqrt{\frac{3}{4}}\lambda^2 S^+ + \frac{5}{6}\sqrt{3}\lambda(\lambda C^+ - 2B^+)$	$-\frac{1}{2}\sqrt{\frac{3}{4}}\lambda^2 S^+(1-4x) + \frac{5}{12}\sqrt{3}\lambda(\lambda C^+ - 2B^+)$	$\frac{1}{2}\sqrt{\frac{3}{4}}\lambda^2 S^+ - \frac{5}{12}\sqrt{3}\lambda(\lambda C^+ - 2B^+)$
$D_{13}(1520)$	f_{-3}	$2\sqrt{\frac{9}{2}}T^-$	$\sqrt{\frac{9}{2}}(T^- + 2xT)$	$-\sqrt{\frac{9}{2}}(T^- + 2xT)$
	f_{-1}	$\sqrt{6}T^- - \frac{4}{\sqrt{3}}\lambda R^-$	$\sqrt{\frac{3}{2}}(T^- + 2xT) - \sqrt{\frac{4}{3}}\lambda(R^- + 2x(\frac{3}{2})R$	$-\sqrt{\frac{3}{2}}(T^- + 2xT) + \sqrt{\frac{4}{3}}\lambda(R^- + 2x(\frac{3}{2})R$
	f_{+1}	$\sqrt{6}T^+ - \frac{4}{\sqrt{3}}\lambda R^+$	$\sqrt{\frac{3}{2}}(T^+ + 2xT) - \sqrt{\frac{4}{3}}\lambda(R^+ + 2x(\frac{3}{2})R$	$-\sqrt{\frac{3}{2}}(T^+ + 2xT) + \sqrt{\frac{4}{3}}\lambda(R^+ + 2x(\frac{3}{2})R$
	f_{+3}	$2\sqrt{\frac{9}{2}}T^+$	$\sqrt{\frac{9}{2}}(T^+ + 2xT)$	$-\sqrt{\frac{9}{2}}(T^+ + 2xT)$
	$f_{0+}^{(-)}$	$-2\sqrt{3}\lambda S^- - \sqrt{\frac{4}{3}}\lambda C^-$	$-\sqrt{3}\lambda S^-(1-2x) - \frac{2}{\sqrt{3}}\lambda C^-$	$+\sqrt{3}\lambda S^-(1-2x) + \frac{2}{\sqrt{3}}\lambda C^-$
	$f_{0-}^{(-)}$	$-2\sqrt{3}\lambda S^- + \sqrt{\frac{4}{3}}\lambda C^-$	$-\sqrt{3}\lambda S^-(1-2x) + \frac{2}{\sqrt{3}}\lambda C^-$	$+\sqrt{3}\lambda S^-(1-2x) - \frac{2}{\sqrt{3}}\lambda C^-$
	$f_{0+}^{(+)}$	$-2\sqrt{3}\lambda S^+ - \sqrt{\frac{4}{3}}\lambda C^+$	$-\sqrt{3}\lambda S^+(1-2x) - \frac{2}{\sqrt{3}}\lambda C^+$	$+\sqrt{3}\lambda S^-(1-2x) + \frac{2}{\sqrt{3}}\lambda C^+$

Table G.2 Production amplitudes for charged and neutral current weak interaction from Reference [7]   .

Resonance	Helicity	Weak CC	Weak NC (p)	Weak NC (n)
	$f_{0-}^{(+)}$	$-2\sqrt{3}\lambda S^+ + \sqrt{\frac{4}{3}}\lambda C^+$	$-\sqrt{3}\lambda S^+(1-2x) + \frac{2}{\sqrt{3}}\lambda C^+$	$+\sqrt{3}\lambda S^-(1-2x) - \frac{2}{\sqrt{3}}\lambda C^+$
$S_{11}(1535)$	f_{-1}	$2\sqrt{3}T^- + \frac{4}{\sqrt{6}}\lambda R^-$	$\sqrt{3}(T^- + 2xT) + \sqrt{\frac{2}{3}}\lambda(R^- + 2x(\frac{3}{2})R)$	$-\sqrt{3}(T^- + 2xT) - \sqrt{\frac{2}{3}}\lambda(R^- + 2x(\frac{1}{2})R)$
	f_{+1}	$-2\sqrt{3}T^- - \frac{4}{\sqrt{6}}\lambda R^-$	$-\sqrt{3}(T^+ + 2xT) - \sqrt{\frac{2}{3}}\lambda(R^+ + 2x(\frac{3}{2})R)$	$\sqrt{3}(T^+ + 2xT) + \sqrt{\frac{2}{3}}\lambda(R^+ + 2x(\frac{1}{2})R)$
	$f_{0+}^{(-)}$	$\sqrt{6}\lambda S^- + 2\sqrt{\frac{2}{3}}(\lambda C^- - 3B^-)$	$\sqrt{\frac{3}{2}}\lambda S^-(1-2x) + \sqrt{\frac{2}{3}}(\lambda C^- - 3B^-)$	$-\sqrt{\frac{3}{2}}\lambda S^-(1-2x) - \sqrt{\frac{2}{3}}(\lambda C^- - 3B^-)$
	$f_{0-}^{(-)}$	$-\sqrt{6}\lambda S^- + 2\sqrt{\frac{2}{3}}(\lambda C^- - 3B^-)$	$-\sqrt{\frac{3}{2}}\lambda S^-(1-2x) + \sqrt{\frac{2}{3}}(\lambda C^- - 3B^+)$	$\sqrt{\frac{3}{2}}\lambda S^-(1-2x) - \sqrt{\frac{2}{3}}(\lambda C^- - 3B^-)$
	$f_{0+}^{(+)}$	$\sqrt{6}\lambda S^+ + 2\sqrt{\frac{2}{3}}(\lambda C^+ - 3B^+)$	$\sqrt{\frac{3}{2}}\lambda S^+(1-2x) + \sqrt{\frac{2}{3}}(\lambda C^+ - 3B^+)$	$-\sqrt{\frac{3}{2}}\lambda S^+(1-2x) - \sqrt{\frac{2}{3}}(\lambda C^+ - 3B^-)$
	$f_{0-}^{(+)}$	$-\sqrt{6}\lambda S^+ + 2\sqrt{\frac{2}{3}}(\lambda C^+ - 3B^+)$	$-\sqrt{\frac{3}{2}}\lambda S^-(1-2x) + \sqrt{\frac{2}{3}}(\lambda C^+ - 3B^+)$	$\sqrt{\frac{3}{2}}\lambda S^+(1-2x) - \sqrt{\frac{2}{3}}(\lambda C^+ - 3B^+)$
$P_{33}(1600)$	f_{-3}	$-\frac{1}{\sqrt{2}}\lambda^2 R^-$	$\frac{1}{\sqrt{2}}(R^- + 2xR)$	
	f_{-1}	$-\frac{1}{\sqrt{6}}\lambda^2 R^-$	$\frac{1}{\sqrt{6}}(R^- + 2xR)$	
	f_{+1}	$\frac{1}{\sqrt{6}}\lambda^2 R^+$	$-\frac{1}{\sqrt{6}}(R^+ + 2xR)$	
	f_{+3}	$\frac{1}{\sqrt{2}}\lambda^2 R^+$	$-\frac{1}{\sqrt{2}}(R^+ + 2xR)$	
	$f_{0+}^{(-)}$	$\sqrt{\frac{2}{3}}\lambda(\lambda C^- - 2B^-)$	$-\sqrt{\frac{2}{3}}\lambda(\lambda C^- - 2B^-)$	$n = p$
	$f_{0-}^{(-)}$	$\sqrt{\frac{2}{3}}\lambda(\lambda C^- - 2B^-)$	$-\sqrt{\frac{2}{3}}\lambda(\lambda C^- - 2B^-)$	
	$f_{0+}^{(+)}$	$\sqrt{\frac{2}{3}}\lambda(\lambda C^+ - 2B^+)$	$-\sqrt{\frac{2}{3}}\lambda(\lambda C^+ - 2B^+)$	
	$f_{0-}^{(+)}$	$\sqrt{\frac{2}{3}}\lambda(\lambda C^+ - 2B^+)$	$-\sqrt{\frac{2}{3}}\lambda(\lambda C^+ - 2B^+)$	
$S_{31}(1620)$	f_{-1}	$-\sqrt{3}T^- + \frac{1}{\sqrt{6}}\lambda R^-$	$\sqrt{3}(T^- + 2xT) - \sqrt{\frac{1}{6}}\lambda(R^- + 2xR)$	
	f_{+1}	$\sqrt{3}T^+ - \frac{1}{\sqrt{6}}\lambda R^+$	$-\sqrt{3}(T^+ + 2xT) + \sqrt{\frac{1}{6}}\lambda(R^+ + 2xR)$	
	$f_{0+}^{(-)}$	$-\sqrt{\frac{3}{2}}\lambda S^- + \sqrt{\frac{1}{6}}(\lambda C^- - 3B^-)$	$\sqrt{\frac{3}{2}}\lambda S^-(1-2x) - \sqrt{\frac{1}{6}}(\lambda C^- - 3B^-)$	$n = p$
	$f_{0-}^{(-)}$	$\sqrt{\frac{3}{2}}\lambda S^- + \sqrt{\frac{1}{6}}(\lambda C^- - 3B^-)$	$-\sqrt{\frac{3}{2}}\lambda S^-(1-2x) - \sqrt{\frac{1}{6}}(\lambda C^- - 3B^-)$	
	$f_{0+}^{(+)}$	$-\sqrt{\frac{3}{2}}\lambda S^+ + \sqrt{\frac{1}{6}}(\lambda C^+ - 3B^+)$	$\sqrt{\frac{3}{2}}\lambda S^+(1-2x) - \sqrt{\frac{1}{6}}(\lambda C^+ - 3B^+)$	

Table G.2 Production amplitudes for charged and neutral current weak interaction from Reference [7]   .

Resonance	Helicity	Weak CC	Weak NC (p)	Weak NC (n)
	$f_{0-}^{(+)}$	$+\sqrt{\frac{3}{2}}\lambda S^{+}+\sqrt{\frac{1}{6}}(\lambda C^{+}-3B^{+})$	$-\sqrt{\frac{3}{2}}\lambda S^{+}(1-2x)-\sqrt{\frac{1}{6}}(\lambda C^{+}-3B^{+})$	
$S_{11}(1650)$	f_{-1}	$\frac{1}{\sqrt{6}}\lambda R^{-}$	$\frac{1}{2}\frac{1}{\sqrt{6}}\lambda R^{-}$	$-\frac{1}{2}\sqrt{\frac{1}{6}}\lambda(R^{-}+4xR)$
	f_{+1}	$-\frac{1}{\sqrt{6}}\lambda R^{+}$	$-\frac{1}{2}\frac{1}{\sqrt{6}}\lambda R^{+}$	$\frac{1}{2}\sqrt{\frac{1}{6}}\lambda(R^{+}+4xR)$
	$f_{0+}^{(-)}$	$-\sqrt{\frac{2}{3}}(\lambda C^{-}-3B^{-})$	$-\sqrt{\frac{1}{6}}(\lambda C^{-}-3B^{-})$	$\sqrt{\frac{1}{6}}(\lambda C^{-}-3B^{-})$
	$f_{0-}^{(-)}$	$-\sqrt{\frac{2}{3}}(\lambda C^{-}-3B^{-})$	$-\sqrt{\frac{1}{6}}(\lambda C^{-}-3B^{-})$	$\sqrt{\frac{1}{6}}(\lambda C^{-}-3B^{-})$
	$f_{0+}^{(+)}$	$-\sqrt{\frac{2}{3}}(\lambda C^{+}-3B^{+})$	$-\sqrt{\frac{1}{6}}(\lambda C^{+}-3B^{+})$	$\sqrt{\frac{1}{6}}(\lambda C^{+}-3B^{+})$
	$f_{0-}^{(+)}$	$-\sqrt{\frac{2}{3}}(\lambda C^{+}-3B^{+})$	$-\sqrt{\frac{1}{6}}(\lambda C^{+}-3B^{+})$	$\sqrt{\frac{1}{6}}(\lambda C^{+}-3B^{+})$
$D_{15}(1675)$	f_{-3}	$-\sqrt{\frac{3}{5}}R^{-}$	$-\frac{1}{2}\sqrt{\frac{3}{5}}R^{-}$	$\frac{1}{2}\sqrt{\frac{3}{5}}\lambda(R^{-}+4xR)$
	f_{-1}	$-\sqrt{\frac{3}{10}}R^{-}$	$-\frac{1}{2}\sqrt{\frac{3}{10}}R^{-}$	$\frac{1}{2}\sqrt{\frac{3}{10}}\lambda(R^{-}+4xR)$
	f_{+1}	$-\sqrt{\frac{3}{10}}R^{+}$	$\frac{1}{2}\sqrt{\frac{3}{10}}R^{+}$	$-\frac{1}{2}\sqrt{\frac{3}{10}}\lambda(R^{+}+4xR)$
	f_{+3}	$-\sqrt{\frac{3}{5}}R^{+}$	$\frac{1}{2}\sqrt{\frac{3}{5}}R^{+}$	$-\frac{1}{2}\sqrt{\frac{3}{5}}\lambda(R^{+}+4xR)$
	$f_{0+}^{(-)}$	$\sqrt{\frac{6}{5}}\lambda C^{-}$	$\sqrt{\frac{3}{10}}C^{-}$	$-\sqrt{\frac{3}{10}}C^{-}$
	$f_{0-}^{(-)}$	$\sqrt{\frac{6}{5}}\lambda C^{-}$	$\sqrt{\frac{3}{10}}C^{-}$	$-\sqrt{\frac{3}{10}}C^{-}$
	$f_{0+}^{(+)}$	$\sqrt{\frac{6}{5}}\lambda C^{+}$	$\sqrt{\frac{3}{10}}C^{+}$	$-\sqrt{\frac{3}{10}}C^{+}$
	$f_{0-}^{(+)}$	$\sqrt{\frac{6}{5}}\lambda C^{+}$	$\sqrt{\frac{3}{10}}C^{+}$	$-\sqrt{\frac{3}{10}}C^{+}$
$F_{15}(1680)$	f_{-3}	$-\sqrt{\frac{18}{5}}\lambda T^{-}$	$-\frac{1}{2}\sqrt{\frac{18}{5}}(T^{-}+4xT)$	$\frac{1}{2}\sqrt{\frac{18}{5}}\lambda T^{-}$
	f_{-1}	$-\sqrt{\frac{9}{5}}\lambda T^{-}+\sqrt{\frac{5}{2}}\lambda^{2}R^{-}$	$-\frac{1}{2}\sqrt{\frac{9}{5}}(T^{-}+4xT)+\frac{1}{2}\sqrt{\frac{5}{2}}\lambda^{2}(R^{-}+2x(\frac{6}{5})R)$	$\frac{1}{2}\sqrt{\frac{9}{5}}\lambda T^{-}-\frac{1}{2}\sqrt{\frac{5}{2}}\lambda^{2}(R^{-}+2x(\frac{4}{5})R)$
	f_{+1}	$-\sqrt{\frac{9}{5}}\lambda T^{+}+\sqrt{\frac{5}{2}}\lambda^{2}R^{+}$	$-\frac{1}{2}\sqrt{\frac{9}{5}}(T^{+}+4xT)+\frac{1}{2}\sqrt{\frac{5}{2}}\lambda^{2}(R^{+}+2x(\frac{6}{5})R)$	$\frac{1}{2}\sqrt{\frac{9}{5}}\lambda T^{+}-\frac{1}{2}\sqrt{\frac{5}{2}}\lambda^{2}(R^{+}+2x(\frac{4}{5})R)$
	f_{+3}	$-\sqrt{\frac{18}{5}}\lambda T^{+}$	$-\frac{1}{2}\sqrt{\frac{18}{5}}(T^{+}+4xT)$	$\frac{1}{2}\sqrt{\frac{18}{5}}\lambda T^{+}$

Table G.2 Production amplitudes for charged and neutral current weak interaction from Reference [7]   .

Resonance	Helicity	Weak CC	Weak NC (p)	Weak NC (n)
	$f_{0+}^{(-)}$	$\sqrt{\frac{9}{10}}\lambda^2 S^- + \sqrt{\frac{5}{2}}\lambda^2 C^-$	$\frac{1}{2}\sqrt{\frac{9}{10}}\lambda^2 S^-(1-4x) + \frac{1}{2}\sqrt{\frac{5}{2}}\lambda^2 C^-$	$-\frac{1}{2}\sqrt{\frac{9}{10}}\lambda^2 S^-(1-4x) - \frac{1}{2}\sqrt{\frac{5}{2}}\lambda^2 C^-$
	$f_{0-}^{(-)}$	$\sqrt{\frac{9}{10}}\lambda^2 S^- - \sqrt{\frac{5}{2}}\lambda^2 C^-$	$\frac{1}{2}\sqrt{\frac{9}{10}}\lambda^2 S^-(1-4x) - \frac{1}{2}\sqrt{\frac{5}{2}}\lambda^2 C^-$	$-\frac{1}{2}\sqrt{\frac{9}{10}}\lambda^2 S^-(1-4x) + \frac{1}{2}\sqrt{\frac{5}{2}}\lambda^2 C^-$
	$f_{0+}^{(+)}$	$\sqrt{\frac{9}{10}}\lambda^2 S^+ + \sqrt{\frac{5}{2}}\lambda^2 C^+$	$\frac{1}{2}\sqrt{\frac{9}{10}}\lambda^2 S^+(1-4x) + \frac{1}{2}\sqrt{\frac{5}{2}}\lambda^2 C^+$	$-\frac{1}{2}\sqrt{\frac{9}{10}}\lambda^2 S^+(1-4x) - \frac{1}{2}\sqrt{\frac{5}{2}}\lambda^2 C^+$
	$f_{0-}^{(+)}$	$\sqrt{\frac{9}{10}}\lambda^2 S^+ - \sqrt{\frac{5}{2}}\lambda^2 C^+$	$\frac{1}{2}\sqrt{\frac{9}{10}}\lambda^2 S^+(1-4x) - \frac{1}{2}\sqrt{\frac{5}{2}}\lambda^2 C^+$	$-\frac{1}{2}\sqrt{\frac{9}{10}}\lambda^2 S^+(1-4x) + \frac{1}{2}\sqrt{\frac{5}{2}}\lambda^2 C^+$
$D_{13}(1700)$	f_{-3}	$\sqrt{\frac{9}{10}}\lambda R^-$	$\frac{1}{2}\sqrt{\frac{9}{10}}\lambda R^-$	$-\frac{1}{2}\sqrt{\frac{9}{10}}\lambda(R^- + 4xR)$
	f_{-1}	$\sqrt{\frac{1}{30}}\lambda R^-$	$\frac{1}{2}\sqrt{\frac{1}{30}}\lambda R^-$	$-\frac{1}{2}\sqrt{\frac{1}{30}}\lambda(R^- + 4xR)$
	f_{+1}	$\sqrt{\frac{1}{30}}\lambda R^+$	$\frac{1}{2}\sqrt{\frac{1}{30}}\lambda R^+$	$-\frac{1}{2}\sqrt{\frac{1}{30}}\lambda(R^+ + 4xR)$
	f_{+3}	$\sqrt{\frac{9}{10}}\lambda R^+$	$\frac{1}{2}\sqrt{\frac{9}{10}}\lambda R^+$	$-\frac{1}{2}\sqrt{\frac{9}{10}}\lambda(R^+ + 4xR)$
	$f_{0+}^{(-)}$	$-\sqrt{\frac{2}{15}}\lambda C^-$	$-\frac{1}{2}\sqrt{\frac{2}{15}}\lambda C^-$	$\frac{1}{2}\sqrt{\frac{2}{15}}\lambda C^-$
	$f_{0-}^{(-)}$	$\sqrt{\frac{2}{15}}\lambda C^-$	$\frac{1}{2}\sqrt{\frac{2}{15}}\lambda C^-$	$-\frac{1}{2}\sqrt{\frac{2}{15}}\lambda C^-$
	$f_{0+}^{(+)}$	$-\sqrt{\frac{2}{15}}\lambda C^+$	$-\frac{1}{2}\sqrt{\frac{2}{15}}\lambda C^+$	$\frac{1}{2}\sqrt{\frac{2}{15}}\lambda C^+$
	$f_{0-}^{(+)}$	$\sqrt{\frac{2}{15}}\lambda C^+$	$\frac{1}{2}\sqrt{\frac{2}{15}}\lambda C^+$	$-\frac{1}{2}\sqrt{\frac{2}{15}}\lambda C^+$
$D_{33}(1700)$	f_{-3}	$-\sqrt{\frac{9}{2}}T^-$	$\sqrt{\frac{9}{2}}(T^- + 2xT)$	
	f_{-1}	$-\sqrt{\frac{3}{2}}T^- - \frac{1}{\sqrt{3}}\lambda R^-$	$\sqrt{\frac{3}{2}}(T^- + 2xT) + \sqrt{\frac{1}{3}}\lambda(R^- + 2xR)$	
	f_{+1}	$-\sqrt{\frac{3}{2}}T^+ - \frac{1}{\sqrt{3}}\lambda R^+$	$\sqrt{\frac{3}{2}}(T^+ + 2xT) - \sqrt{\frac{1}{3}}\lambda(R^+ + 2xR$	
	f_{+3}	$-\sqrt{\frac{9}{2}}T^+$	$\sqrt{\frac{9}{2}}(T^+ + 2xT)$	$n = p$
	$f_{0+}^{(-)}$	$\sqrt{3}\lambda S^- - \sqrt{\frac{1}{3}}\lambda C^-$	$-\sqrt{3}\lambda S^-(1-2x) + \frac{1}{\sqrt{3}}\lambda C^-$	
	$f_{0-}^{(-)}$	$\sqrt{3}\lambda S^- + \sqrt{\frac{1}{3}}\lambda C^-$	$-\sqrt{3}\lambda S^-(1-2x) - \frac{1}{\sqrt{3}}\lambda C^-$	
	$f_{0+}^{(+)}$	$\sqrt{3}\lambda S^+ - \sqrt{\frac{1}{3}}\lambda C^+$	$-\sqrt{3}\lambda S^+(1-2x) + \frac{1}{\sqrt{3}}\lambda C^+$	

Table G.2 Production amplitudes for charged and neutral current weak interaction from Reference [7] .

Resonance	Helicity	Weak CC	Weak NC (p)	Weak NC (n)
	$f_{0-}^{(+)}$	$\sqrt{3}\lambda S^+ + \sqrt{\frac{1}{3}}\lambda C^+$	$-\sqrt{3}\lambda S^+(1-2x) - \frac{1}{\sqrt{3}}\lambda C^+$	
$P_{11}(1710)$	f_{-1}	$\sqrt{\frac{2}{3}}\lambda^2 R^-$	$\sqrt{\frac{1}{6}}(R^- + 2x(\frac{3}{2})R)$	$-\sqrt{\frac{1}{6}}(R^- + 2x(\frac{3}{2})R)$
	f_{+1}	$\sqrt{\frac{2}{3}}\lambda^2 R^+$	$\sqrt{\frac{1}{6}}(R^+ + 2x(\frac{3}{2})R)$	$-\sqrt{\frac{1}{6}}(R^+ + 2x(\frac{3}{2})R)$
	$f_{0+}^{(-)}$	$\sqrt{\frac{3}{2}}\lambda^2 S^- + \sqrt{\frac{3}{2}}\lambda(\lambda C^- - 2B^-)$	$\sqrt{\frac{3}{8}}\lambda^2 S^-(1-2x) + \sqrt{\frac{1}{6}}\lambda(\lambda C^- - 2B^-)$	$-\sqrt{\frac{3}{8}}\lambda^2 S^-(1-2x) - \sqrt{\frac{1}{6}}\lambda(\lambda C^- - 2B^-)$
	$f_{0-}^{(-)}$	$\sqrt{\frac{3}{2}}\lambda^2 S^- + \sqrt{\frac{3}{2}}\lambda(\lambda C^- - 2B^-)$	$\sqrt{\frac{3}{8}}\lambda^2 S^-(1-2x) - \sqrt{\frac{1}{6}}\lambda(\lambda C^- - 2B^-)$	$-\sqrt{\frac{3}{8}}\lambda^2 S^-(1-2x) + \sqrt{\frac{1}{6}}\lambda(\lambda C^- - 2B^-)$
	$f_{0+}^{(+)}$	$\sqrt{\frac{3}{2}}\lambda^2 S^+ + \sqrt{\frac{3}{2}}\lambda(\lambda C^+ - 2B^+)$	$\sqrt{\frac{3}{8}}\lambda^2 S^+(1-2x) + \sqrt{\frac{1}{6}}\lambda(\lambda C^+ - 2B^+)$	$-\sqrt{\frac{3}{8}}\lambda^2 S^-(1-2x) - \sqrt{\frac{1}{6}}\lambda(\lambda C^+ - 2B^+)$
	$f_{0+}^{(+)}$	$\sqrt{\frac{3}{2}}\lambda^2 S^+ + \sqrt{\frac{3}{2}}\lambda(\lambda C^+ - 2B^+)$	$\sqrt{\frac{3}{8}}\lambda^2 S^+(1-2x) - \sqrt{\frac{1}{6}}\lambda(\lambda C^+ - 2B^+)$	$-\sqrt{\frac{3}{8}}\lambda^2 S^-(1-2x) + \sqrt{\frac{1}{6}}\lambda(\lambda C^+ - 2B^+)$
$P_{13}(1720)$	f_{-3}	$\sqrt{\frac{9}{10}}\lambda T^-$	$\sqrt{\frac{9}{40}}\lambda(T^- + 4xT)$	$-\sqrt{\frac{9}{40}}\lambda T^-$
	f_{-1}	$-\sqrt{\frac{27}{10}}\lambda T^- - \sqrt{\frac{3}{5}}\lambda^2 R^-$	$-\sqrt{\frac{27}{40}}\lambda(T^- + 4xT) - \sqrt{\frac{5}{12}}\lambda^2(R^- + 2x(\frac{6}{5})R$	$\sqrt{\frac{27}{40}}\lambda^2 T^- + \sqrt{\frac{5}{12}}\lambda^2(R^- + 2x(\frac{4}{5})R$
	f_{+1}	$\sqrt{\frac{27}{10}}\lambda T^+ + \sqrt{\frac{3}{5}}\lambda^2 R^+$	$\sqrt{\frac{27}{40}}\lambda(T^+ + 4xT) + \sqrt{\frac{5}{12}}\lambda^2(R^+ + 2x(\frac{6}{5})R$	$-\sqrt{\frac{27}{40}}\lambda^2 T^+ - \sqrt{\frac{5}{12}}\lambda^2(R^+ + 2x(\frac{4}{5})R$
	f_{+3}	$-\sqrt{\frac{9}{10}}\lambda T^+$	$-\sqrt{\frac{9}{40}}\lambda(T^+ + 4xT)$	$\sqrt{\frac{9}{40}}\lambda T^+$
	$f_{0+}^{(-)}$	$-\sqrt{\frac{3}{5}}\lambda^2 S^- - \sqrt{\frac{5}{3}}\lambda(\lambda C^- - 5B^-)$	$-\sqrt{\frac{3}{20}}\lambda^2 S^-(1-4x) - \sqrt{\frac{5}{12}}\lambda(\lambda C^- - 5B^-)$	$\sqrt{\frac{3}{20}}\lambda^2 S^-(1-4x) + \sqrt{\frac{5}{12}}\lambda(\lambda C^- - 5B^-)$
	$f_{0-}^{(-)}$	$\sqrt{\frac{3}{5}}\lambda^2 S^- - \sqrt{\frac{5}{3}}\lambda(\lambda C^- - 5B^-)$	$\sqrt{\frac{3}{20}}\lambda^2 S^-(1-4x) - \sqrt{\frac{5}{12}}\lambda(\lambda C^- - 5B^-)$	$-\sqrt{\frac{3}{20}}\lambda^2 S^-(1-4x) + \sqrt{\frac{5}{12}}\lambda(\lambda C^- - 5B^-)$
	$f_{0+}^{(+)}$	$-\sqrt{\frac{3}{5}}\lambda^2 S^+ - \sqrt{\frac{5}{3}}\lambda(\lambda C^+ - 5B^+)$	$-\sqrt{\frac{3}{20}}\lambda^2 S^+(1-4x) - \sqrt{\frac{5}{12}}\lambda(\lambda C^+ - 5B^+)$	$\sqrt{\frac{3}{20}}\lambda^2 S^+(1-4x) + \sqrt{\frac{5}{12}}\lambda(\lambda C^+ - 5B^+)$
	$f_{0-}^{(+)}$	$\sqrt{\frac{3}{5}}\lambda^2 S^+ - \sqrt{\frac{5}{3}}\lambda(\lambda C^+ - 5B^+)$	$\sqrt{\frac{3}{20}}\lambda^2 S^+(1-4x) - \sqrt{\frac{5}{12}}\lambda(\lambda C^+ - 5B^+)$	$-\sqrt{\frac{3}{20}}\lambda^2 S^+(1-4x) + \sqrt{\frac{5}{12}}\lambda(\lambda C^+ - 5B^+)$
$F_{35}(1905)$	f_{-3}	$-\sqrt{\frac{18}{35}}\lambda^2 R^-$	$\sqrt{\frac{18}{35}}\lambda^2(R^- + 2xR)$	
	f_{-1}	$-\sqrt{\frac{1}{35}}\lambda^2 R^-$	$\sqrt{\frac{1}{35}}\lambda^2(R^- + 2xR)$	
	f_{+1}	$-\sqrt{\frac{1}{35}}\lambda^2 R^+$	$\sqrt{\frac{1}{35}}\lambda^2(R^+ + 2xR)$	
	f_{+3}	$-\sqrt{\frac{18}{35}}\lambda^2 R^+$	$\sqrt{\frac{18}{35}}\lambda^2(R^+ + 2xR)$	$n = p$

Table G.2 Production amplitudes for charged and neutral current weak interaction from Reference [7]   .

Resonance	Helicity	Weak CC	Weak NC (p)	Weak NC (n)
	$f_{0+}^{(-)}$	$\sqrt{\frac{4}{35}}\lambda^2 C^-$	$-\sqrt{\frac{4}{35}}\lambda^2 C^-$	
	$f_{0-}^{(-)}$	$-\sqrt{\frac{4}{35}}\lambda^2 C^-$	$\sqrt{\frac{4}{35}}\lambda^2 C^-$	
	$f_{0+}^{(+)}$	$\sqrt{\frac{4}{35}}\lambda^2 C^+$	$-\sqrt{\frac{4}{35}}\lambda^2 C^+$	
	$f_{0-}^{(+)}$	$-\sqrt{\frac{4}{35}}\lambda^2 C^+$	$\sqrt{\frac{4}{35}}\lambda^2 C^+$	
$P_{31}(1910)$	f_{-1}	$\sqrt{\frac{1}{15}}\lambda^2 R^-$	$\sqrt{\frac{1}{15}}\lambda^2 (R^- + 2xR)$	
	f_{+1}	$\sqrt{\frac{1}{15}}\lambda^2 R^+$	$-\sqrt{\frac{1}{15}}\lambda^2 (R^+ + 2xR)$	$n = p$
	$f_{0+}^{(-)}$	$-\sqrt{\frac{4}{15}}\lambda(\lambda C^- - 5B^-)$	$\sqrt{\frac{4}{15}}\lambda(\lambda C^- - 5B^-)$	
	$f_{0-}^{(-)}$	$\sqrt{\frac{4}{15}}\lambda(\lambda C^- - 5B^-)$	$-\sqrt{\frac{4}{15}}\lambda(\lambda C^- - 5B^-)$	
	$f_{0+}^{(+)}$	$-\sqrt{\frac{4}{15}}\lambda(\lambda C^+ - 5B^+)$	$\sqrt{\frac{4}{15}}\lambda(\lambda C^+ - 5B^+)$	
	$f_{0-}^{(+)}$	$\sqrt{\frac{4}{15}}\lambda(\lambda C^+ - 5B^+)$	$-\sqrt{\frac{4}{15}}\lambda(\lambda C^+ - 5B^+)$	
$P_{33}(1920)$	f_{-3}	$\sqrt{\frac{1}{5}}\lambda^2 R^-$	$-\sqrt{\frac{1}{5}}\lambda^2 (R^- + 2xR)$	
	f_{-1}	$-\sqrt{\frac{1}{15}}\lambda^2 R^-$	$\sqrt{\frac{1}{15}}\lambda^2 (R^- + 2xR)$	
	f_{+1}	$\sqrt{\frac{1}{15}}\lambda^2 R^+$	$-\sqrt{\frac{1}{15}}\lambda^2 (R^+ + 2xR)$	
	f_{+3}	$-\sqrt{\frac{1}{5}}\lambda^2 R^+$	$\sqrt{\frac{1}{5}}\lambda^2 (R^+ + 2xR)$	$n = p$
	$f_{0+}^{(-)}$	$\sqrt{\frac{4}{15}}\lambda(\lambda C^- - 5B^-)$	$-\sqrt{\frac{4}{15}}\lambda(\lambda C^- - 5B^-)$	
	$f_{0-}^{(-)}$	$\sqrt{\frac{4}{15}}\lambda(\lambda C^- - 5B^-)$	$-\sqrt{\frac{4}{15}}\lambda(\lambda C^- - 5B^-)$	
	$f_{0+}^{(+)}$	$\sqrt{\frac{4}{15}}\lambda(\lambda C^+ - 5B^+)$	$-\sqrt{\frac{4}{15}}\lambda(\lambda C^+ - 5B^+)$	
	$f_{0-}^{(+)}$	$\sqrt{\frac{4}{15}}\lambda(\lambda C^+ - 5B^+)$	$-\sqrt{\frac{4}{15}}\lambda(\lambda C^+ - 5B^+)$	
$F_{37}(1950)$	f_{-3}	$\sqrt{\frac{2}{7}}\lambda^2 R^-$	$-\sqrt{\frac{2}{7}}\lambda^2 (R^- + 2xR)$	

Table G.2 Production amplitudes for charged and neutral current weak interaction from Reference [7]   .

Resonance	Helicity	Weak CC	Weak NC (p)	Weak NC (n)
	f_{-1}	$\sqrt{\frac{6}{35}}\lambda^2 R^-$	$-\sqrt{\frac{6}{35}}\lambda^2(R^- + 2xR)$	
	f_{+1}	$-\sqrt{\frac{6}{35}}\lambda^2 R^+$	$\sqrt{\frac{6}{35}}\lambda^2(R^+ + 2xR)$	
	f_{+3}	$-\sqrt{\frac{2}{7}}\lambda^2 R^+$	$\sqrt{\frac{2}{7}}\lambda^2(R^+ + 2xR)$	$n = p$
	$f_{0+}^{(-)}$	$-2\sqrt{\frac{6}{35}}\lambda^2 C^-$	$2\sqrt{\frac{6}{35}}\lambda^2 C^-$	
	$f_{0-}^{(-)}$	$-2\sqrt{\frac{6}{35}}\lambda^2 C^-$	$2\sqrt{\frac{6}{35}}\lambda^2 C^-$	
	$f_{0+}^{(+)}$	$-2\sqrt{\frac{6}{35}}\lambda^2 C^+$	$2\sqrt{\frac{6}{35}}\lambda^2 C^+$	
	$f_{0-}^{(+)}$	$-2\sqrt{\frac{6}{35}}\lambda^2 C^+$	$2\sqrt{\frac{6}{35}}\lambda^2 C^+$	

189

Appendix H

Conservation of vector current for nonresonant interaction

The conservation of vector current (CVC) in HNV model [10] is preserved if:

$$k^\mu J_\mu^V = 0 \tag{H.0}$$

for the vector current of the five diagrams:

$$k^\mu (J_\mu^V)^{NP} + k^\mu (J_\mu^V)^{CNP} + k^\mu (J_\mu^V)^{PF} + k^\mu (J_\mu^V)^{CT} + k^\mu (J_\mu^V)^{PP} = 0 \tag{H.0}$$

where PP diagram has only the axial current $(J_\mu^V)^{PP} = 0$. For simplicity we will drop the overall $\frac{g_A}{\sqrt{2}f_\pi}$ factor. Using Equation 4.47 we have:

$$k^\mu J_\mu^{NP} = C^{NP} \frac{1}{s - M^2} \, \bar{u}(p_2) \, \slashed{q} \, \gamma_5 (\slashed{p}_1 + \slashed{k} + M) k^\mu F_\mu^V \, u(p_1), \tag{H.1}$$

where

$$
\begin{aligned}
k^\mu (F^V)_\mu &= 2 \left[F_1^V(k^2) \, \slashed{k} - \mu_V \frac{F_2^V(k^2)}{2M} k^\mu [\gamma_\mu, k^\nu \gamma_\nu] \right] \\
&= 2 \left[F_1^V(k^2) \, \slashed{k} - \mu_V \frac{F_2^V(k^2)}{2M} k^\mu k^\nu \sigma_{\mu\nu} \right].
\end{aligned}
\tag{H.1}
$$

where the second term is zero. Therefore:

$$
\begin{aligned}
k^\mu J_\mu^{NP} &= C^{NP}\frac{1}{s-M^2}\,\bar{u}(p_2)\ \slashed{q}(\slashed{p}_1+\slashed{k}-M)(2\,\slashed{k}F_1^V(k^2))\,\gamma_5\,u(p_1)\\
&= 2C^{NP}F_1^V(k^2)\frac{1}{k^2+2p_1k}\,\bar{u}(p_2)\ \slashed{q}(\slashed{p}_1+\slashed{k}-M)\,\slashed{k}\,\gamma_5\,u(p_1)\\
&= 2C^{NP}F_1^V(k^2)\frac{1}{k^2+2p_1k}\,\bar{u}(p_2)\ \slashed{q}(k^2+\slashed{p}_1\slashed{k}+\slashed{k}\,\slashed{p}_1)\,\gamma_5\,u(p_1)\\
&= 2C^{NP}F_1^V(k^2)\,\bar{u}(p_2)\ \slashed{q}\gamma_5\,u(p_1)
\end{aligned}
\tag{H.-1}
$$

$$
\begin{aligned}
k^\mu J_\mu^{CNP} &= C^{CNP}\frac{1}{u-M^2}\,\bar{u}(p_2)(2\,\slashed{k}F_1^V(k^2))\,(\slashed{p}_2-\slashed{k}+M)\,\slashed{q}\gamma_5\,u(p_1)\\
&= 2C^{CNP}F_1^V(k^2)\,\frac{1}{k^2-2kp_2}\,\bar{u}(p_2)\ \slashed{k}(\slashed{p}_2-\slashed{k}+M)\,\slashed{q}\gamma_5\,u(p_1)\\
&= -2C^{CNP}F_1^V(k^2)\,\frac{1}{k^2-2kp_2}\,\bar{u}(p_2)\,(k^2-\slashed{p}_2\slashed{k}-\slashed{k}\,\slashed{p}_2)\,\slashed{q}\gamma_5\,u(p_1)\\
&= -2C^{CNP}F_1^V(k^2)\,\bar{u}(p_2)\ \slashed{q}\gamma_5\,u(p_1)
\end{aligned}
\tag{H.-3}
$$

$$
\begin{aligned}
k^\mu J_\mu^{PF} &= C^{PF}F_{PF}(k^2)\,\frac{1}{k^2-2qk}\,\bar{u}(p_2)\,\gamma_5\,[2qk-k^2]2M\,u(p_1)\\
&= -C^{PF}F_{PF}(k^2)\,\bar{u}(p_2)\,2M\gamma_5\,u(p_1)
\end{aligned}
\tag{H.-3}
$$

$$
k^\mu (J_\mu^V)^{CT} = C^{CT}F_{CT}^V(k^2)\,\bar{u}(p_2)\ \slashed{k}\gamma_5\,u(p_1),
\tag{H.-3}
$$

Therefore H for $\nu p \to \mu p \pi^+$ channel ($C^{NP}=0$, $C^{CNP}=C^{PF}=C^{CT}=1$) will be:

$$
\begin{aligned}
k^\mu J_\mu^V &= \bar{u}(p_2)\,[-2F_V(k^2)\,\slashed{q}-2MF_{PF}+F_{CT}\,\slashed{k}]\gamma_5\,u(p_1)\\
&= \bar{u}(p_2)\,[-2F_V(k^2)\,\slashed{q}-(\slashed{p}_2-\slashed{p}_1)F_{PF}+F_{CT}\,\slashed{k}]\gamma_5\,u(p_1)
\end{aligned}
\tag{H.-3}
$$

If $2F_1(k^2)=F_{PF}(k^2)=F_{CT}(k^2)=F(k^2)$:

$$
k^\mu J_\mu^V = F(k^2)\bar{u}(p_2)\,[-\slashed{q}-\slashed{p}_2+\slashed{p}_1+\slashed{k}]\gamma_5\,u(p_1)=0
\tag{H.-2}
$$

Similarly Therefore H for $\nu n \to \mu n \pi^+$ channel ($C^{NP} = 1$, $C^{CNP} = 0$, $C^{PF} = C^{CT} = -1$) will be:

$$
\begin{aligned}
k^\mu J_\mu^V &= \bar{u}(p_2)\,[2F_V(k^2)\,\slashed{q} + 2MF_{PF} - F_{CT}\,\slashed{k}]\gamma_5\,u(p_1) \\
&= \bar{u}(p_2)\,[2F_V(k^2)\,\slashed{q} + (\slashed{p}_2 - \slashed{p}_1)F_{PF} - F_{CT}\,\slashed{k}]\gamma_5\,u(p_1)
\end{aligned}
$$

(H.-3)

where it is zero if $2F_1(k^2) = F_{PF}(k^2) = F_{CT}(k^2) = F(k^2)$.

If we multiply an extra form-factor to one the diagram we have to multiply it to the rest of diagrams. It is clear from Equations H.-2, H.-2, H.-1.

Appendix I

Fitting M_A and C_A^5

In subsection 5.2.1, we presented our fitting result on one data set i.e. ANL data [38] for $d\sigma/dQ^2$ in *Delta*-region, and then we show very good agreement with other data only with one data set fitting. Here we show fitting results for different data sets with and without background.

1. only $\nu p \to \mu p \pi^+$ channel and with three data set Here we add more data sets i.e.

   - ANL $d\sigma/dQ^2$ in *Delta*-region

   - ANL total cross-section with no invariant mass cut. Reanalysed data is from Reference [54].

   - BNL total cross-section with no invariant mass cut. Reanalysed data is from Reference [54].

   Here is the fitting result using the full MK-model:

   $$M_A = 0.687 \pm 0.052 \text{ GeV} , \qquad C_5^A = 1.043 \pm 0.104 \text{ GeV} \qquad \text{(I.0)}$$

   and the correlation matrix (Table I.1) shows that parameters are strongly anticorrelated. The minimum of reduced χ^2 is 0.72. The fitting result is very similar to what we got

   Table I.1 Correlation Matrix

	M_A	C_5^A
M_A	1	-0.96
C_5^A	-0.96	1

   in subsection 5.2.1 with only one data set.

2. all CC channels and with seven data set Here we add more data sets i.e.

- ANL $d\sigma/dQ^2$ in *Delta*-region

- ANL and BNL total cross-section of $\nu p \to \mu p \pi^+$ channel with no invariant mass cut. Reanalysed data is from Reference [54].

- ANL and BNL total cross-section of $\nu n \to \mu n \pi^+$ channel with no invariant mass cut. Reanalysed data is from Reference [55].

- ANL and BNL total cross-section of $\nu n \to \mu p \pi^0$ channel with no invariant mass cut. Reanalysed data is from Reference [55].

Here is the fitting result using the full MK-model:

$$M_A = 0.628 \pm 0.042 \text{ GeV} , \qquad C_5^A = 1.03 \pm 0.097 \text{ GeV} \qquad (I.0)$$

and the correlation matrix (Table I.2) shows that parameters are strongly anticorrelated. The minimum of reduced χ^2 is 2.75. If we turn off the nonresonant contribution we

Table I.2 Correlation Matrix

	M_A	C_5^A
M_A	1	-0.938
C_5^A	-0.938	1

will get:

$$M_A = 0.756 \pm 0.038 \text{ GeV} , \qquad C_5^A = 1.219 \pm 0.073 \text{ GeV} \qquad (I.0)$$

and the correlation matrix (Table I.3) shows that parameters are strongly anticorrelated. and the minimum of reduced χ^2 is 4.11.

Table I.3 Correlation Matrix

	M_A	C_5^A
M_A	1	-0.947
C_5^A	-0.947	1

Appendix J

NEUT prediction on nucleon targets

Here we show the NEUT comparison for two samples $CC1\pi^+$ and $CC1\pi^-$ on nucleon target to compare them with results on subsection 6.4.2. $CC1\pi^+$ sample on nucleon is actually the summation of two $\nu p \rightarrow \mu p \pi^+$ and $\nu n \rightarrow \mu n \pi^+$ channels that we showed them on subsection 6.4.1.

$CC1\pi^-$ sample on nucleon is actually the summation of two $\bar{\nu} p \rightarrow \mu^+ p \pi^-$ and $\bar{\nu} n \rightarrow \mu^+ n \pi^-$ channels that we showed them on subsection 6.4.1.
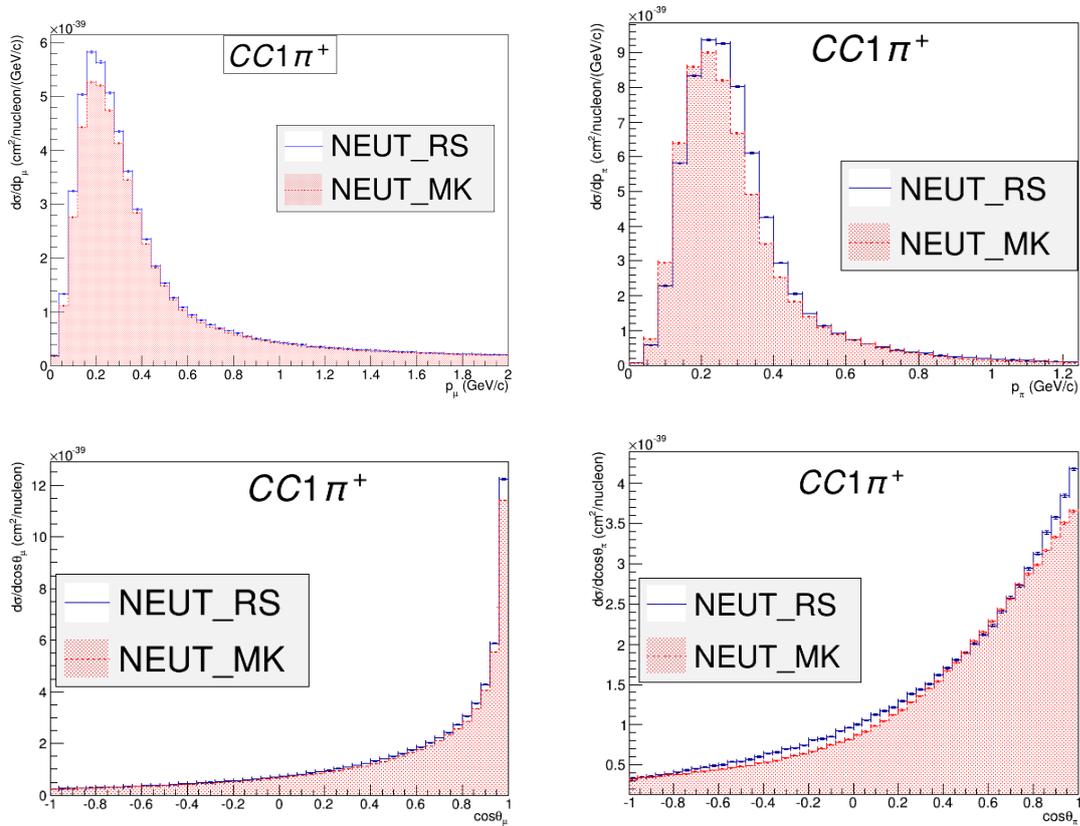
Fig. J.1 differential cross-section on free nucleon for CC1π^+ sample, as functions of lepton kinematics (left plots) and hadron kinematic (right plots) as it is predicted by NEUT for RS model (blue) and the new model (red).
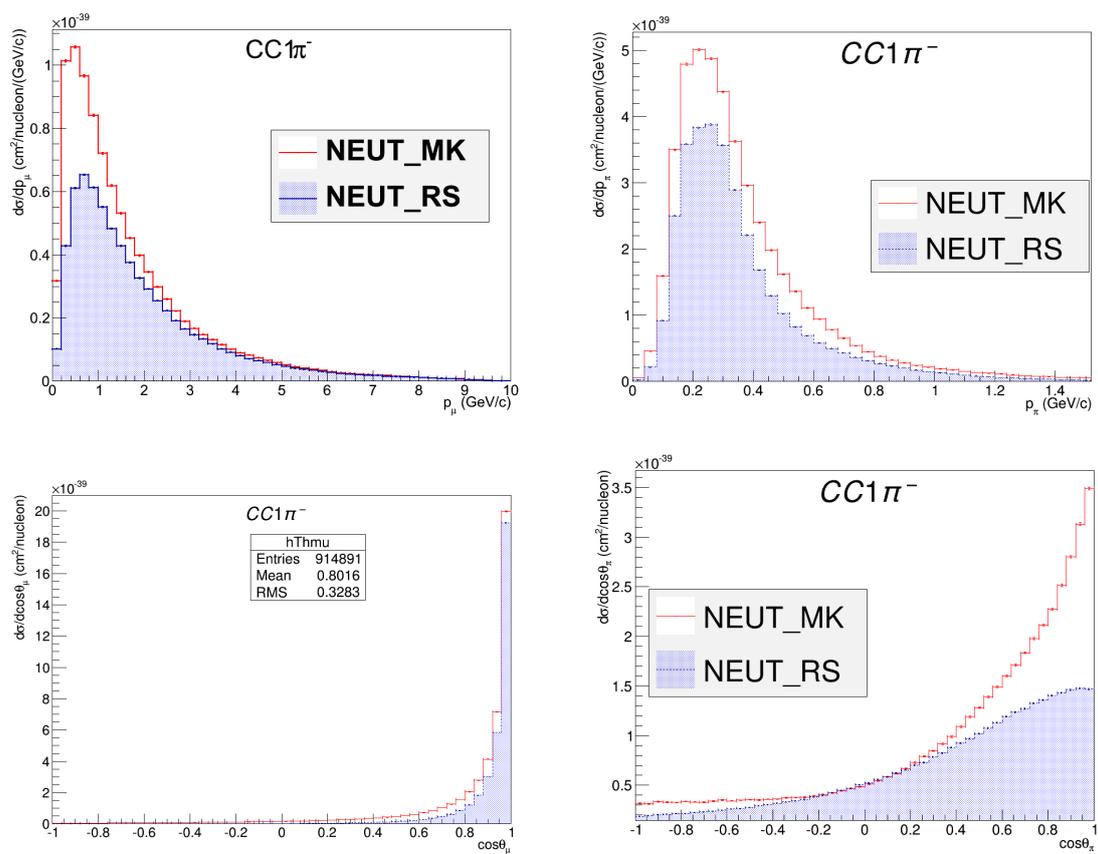
Fig. J.2 differential cross-section on free nucleon for CC1π^- sample, as a functions of lepton kinematics (left plots) and hadron kinematic (right plots) as it is predicted by NEUT for RS model (blue) and the new model (red).

References

[1] K. Abe *et al.* [T2K Collaboration], "Measurements of neutrino oscillation in appearance and disappearance channels by the T2K experiment with 6.6×10^{20} protons on target," Phys. Rev. D **91** (2015) no.7, 072010 doi:10.1103/PhysRevD.91.072010 [arXiv:1502.01550 [hep-ex]].

[2] G. L. Fogli and G. Nardulli, "A New Approach to the Charged Current Induced Weak One Pion Production," Nucl. Phys. B **160** (1979) 116. doi:10.1016/0550-3213(79)90233-5

[3] C. Barbero, G. Lopez Castro and A. Mariano, "Single pion production in CC nu/mu N scattering within a consistent effective Born approximation," Phys. Lett. B **664** (2008) 70. doi:10.1016/j.physletb.2008.05.011

[4] T. Sato, D. Uno and T. S. H. Lee, "Dynamical model of weak pion production reactions," Phys. Rev. C **67** (2003) 065201 doi:10.1103/PhysRevC.67.065201 [nucl-th/0303050].

[5] R. P. Feynman, M. Kislinger and F. Ravndal, "Current matrix elements from a relativistic quark model," Phys. Rev. D **3** (1971) 2706.

[6] F. Ravndal, "Weak production of nuclear resonances in a relativistic quark model," Nuovo Cim. A **18** (1973) 385. doi:10.1007/BF02722789

[7] D. Rein and L. M. Sehgal, "Neutrino Excitation of Baryon Resonances and Single Pion Production," Annals Phys. **133** (1981) 79.

[8] S. L. Adler, "Photoproduction, electroproduction and weak single pion production in the (3,3) resonance region," Annals Phys. **50** (1968) 189.

[9] D. Rein, "Angular Distribution in Neutrino Induced Single Pion Production Processes," Z. Phys. C **35** (1987) 43.

[10] E. Hernandez *et al.*, "Weak Pion Production off the Nucleon," Phys. Rev. D **76** (2007) 033005 doi:10.1103/PhysRevD.76.033005 [hep-ph/0701149].

[11] M. Gell-Mann and M. Levy, "The axial vector current in beta decay," Nuovo Cim. **16** (1960) 705. doi:10.1007/BF02859738

[12] K. S. Kuzmin *et al.*, "Lepton polarization in neutrino nucleon interactions," Mod. Phys. Lett. A **19** (2004) 2815 [hep-ph/0312107].

[13] C. Berger and L. M. Sehgal, "Lepton mass effects in single pion production by neutrinos," Phys. Rev. D **76** (2007) 113004 [arXiv:0709.4378 [hep-ph]].

[14] K. M. Graczyk and J. T. Sobczyk, "Lepton mass effects in weak charged current single pion production," Phys. Rev. D **77** (2008) 053003 [arXiv:0709.4634 [hep-ph]].

[15] M. Jacob and G. C. Wick, "On the general theory of collisions for particles with spin," Annals Phys. **7** (1959) 404 [Annals Phys. **281** (2000) 774].

[16] K. Gottfried and J. D. Jackson, "On the Connection between production mechanism and decay of resonances at high-energies," Nuovo Cim. **33** (1964) 309.

[17] K. M. Graczyk and J. T. Sobczyk, "Form Factors in the Quark Resonance Model," Phys. Rev. D **77** (2008) 053001 [arXiv:0707.3561 [hep-ph]].

[18] K. M. Graczyk *et al.*, "Electroweak form factors of the $\Delta(1232)$ resonance," Phys. Rev. D **90** (2014) no.9, 093001 doi:10.1103/PhysRevD.90.093001 [arXiv:1407.5445 [hep-ph]].

[19] S. Galster, H. Klein, J. Moritz, K. H. Schmidt, D. Wegener and J. Bleckwenn, "Elastic electron-deuteron scattering and the electric neutron form factor at four-momentum transfers $5\text{fm}^{-2} < q^2 < 14\text{fm}^{-2}$," Nucl. Phys. B **32** (1971) 221. doi:10.1016/0550-3213(71)90068-X doi:10.1103/PhysRevLett.41.1008

[20] S. Boyd, S. Dytman, E. Hernandez, J. Sobczyk and R. Tacik, "Comparison of models of neutrino-nucleus interactions," AIP Conf. Proc. **1189** (2009) 60. doi:10.1063/1.3274191

[21] T. Leitner, L. Alvarez-Ruso and U. Mosel, "Charged current neutrino nucleus interactions at intermediate energies," Phys. Rev. C **73** (2006) 065502 doi:10.1103/PhysRevC.73.065502 [nucl-th/0601103].

[22] T. J. Leitner, "Neutrino-nucleus interactions in a coupled-channel hadronic transport model,"

[23] C. H. Llewellyn Smith, "Neutrino Reactions at Accelerator Energies," Phys. Rept. **3** (1972) 261. doi:10.1016/0370-1573(72)90010-5

[24] L. A. Ahrens *et al.*, "Precise Determination of Sin**2-θ^-w From Measurements of the Differential Cross-sections for $\nu_\mu p \to \nu_\mu p$ and $\bar{\nu}_\mu p \to \bar{\nu}_\mu p$," Phys. Rev. Lett. **56** (1986) 1107 Erratum: [Phys. Rev. Lett. **56** (1986) 1883]. doi:10.1103/PhysRevLett.56.1107

[25] M. Glück, E. Reya and A. Vogt, Eur. Phys. J. C **5** (1998) 461 doi:10.1007/s100529800978, 10.1007/s100520050289 [hep-ph/9806404].

[26] A. Bodek and U. K. Yang, [hep-ex/0308007].

[27] E. J. Moniz, I. Sick, R. R. Whitney, J. R. Ficenec, R. D. Kephart and W. P. Trower, "Nuclear Fermi momenta from quasielastic electron scattering," Phys. Rev. Lett. **26** (1971) 445. doi:10.1103/PhysRevLett.26.445

[28] O. Benhar and A. Fabrocini, "Two nucleon spectral function in infinite nuclear matter," Phys. Rev. C **62** (2000) 034304 doi:10.1103/PhysRevC.62.034304 [nucl-th/9909014].

[29] S. Boyd, S. Dytman, E. Hernandez, J. Sobczyk and R. Tacik, "Comparison of models of neutrino-nucleus interactions," AIP Conf. Proc. **1189** (2009) 60. doi:10.1063/1.3274191

[30] T. Sjostrand, S. Mrenna and P. Z. Skands, "PYTHIA 6.4 Physics and Manual," JHEP **0605** (2006) 026 doi:10.1088/1126-6708/2006/05/026 [hep-ph/0603175].

[31] D. Rein and L. M. Sehgal, "Coherent pi0 Production in Neutrino Reactions," Nucl. Phys. B **223** (1983) 29. doi:10.1016/0550-3213(83)90090-1

[32] D. Rein and L. M. Sehgal, "PCAC and the Deficit of Forward Muons in pi+ Production by Neutrinos," Phys. Lett. B **657** (2007) 207 doi:10.1016/j.physletb.2007.10.025 [hep-ph/0606185].

[33] A. Higuera *et al.* [MINERvA Collaboration], "Measurement of Coherent Production of $\pi^{\pm}$ in Neutrino and Antineutrino Beams on Carbon from E_ν of 1.5 to 20 GeV," Phys. Rev. Lett. **113** (2014) no.26, 261802 doi:10.1103/PhysRevLett.113.261802 [arXiv:1409.3835 [hep-ex]].

[34] K. Hiraide *et al.* [SciBooNE Collaboration], "Search for Charged Current Coherent Pion Production on Carbon in a Few-GeV Neutrino Beam," Phys. Rev. D **78** (2008) 112004 doi:10.1103/PhysRevD.78.112004 [arXiv:0811.0369 [hep-ex]].

[35] M. Hasegawa *et al.* [K2K Collaboration], "Search for coherent charged pion production in neutrino-carbon interactions," Phys. Rev. Lett. **95** (2005) 252301 doi:10.1103/PhysRevLett.95.252301 [hep-ex/0506008].

[36] R. Acciarri *et al.* [ArgoNeuT Collaboration], "First Measurement of Neutrino and Antineutrino Coherent Charged Pion Production on Argon," Phys. Rev. Lett. **113** (2014) no.26, 261801 Erratum: [Phys. Rev. Lett. **114** (2015) no.3, 039901] doi:10.1103/PhysRevLett.113.261801, 10.1103/PhysRevLett.114.039901 [arXiv:1408.0598 [hep-ex]].

[37] R. Wittman, R. Davidson and N. C. Mukhopadhyay, "Watson's Theorem and Resonant Pion Photoproduction Amplitude in the Δ Channel," Phys. Lett. **142B** (1984) 336. doi:10.1016/0370-2693(84)91335-2

[38] G. M. Radecky *et al.*, Phys. Rev. D **25** (1982) 1161 [Phys. Rev. D **26** (1982) 3297].

[39] T. Kitagaki *et al.*, "Charged Current Exclusive Pion Production in Neutrino Deuterium Interactions," Phys. Rev. D **34** (1986) 2554.

[40] D. Allasia *et al.*, "Investigation of exclusive channels in neutrino / anti-neutrino deuteron charged current interactions," Nucl. Phys. B **343** (1990) 285. doi:10.1016/0550-3213(90)90472-P

[41] J. Bell *et al.*, "Cross-section Measurements for the Reactions Neutrino $p \to \mu^- \pi^+ p$ and Neutrino $p \to \mu^- K^+ p$ at High-energies," Phys. Rev. Lett. **41** (1978) 1008.

[42] H. J. Grabosch *et al.* [SKAT Collaboration], "Cross-section Measurements of Single Pion Production in Charged Current Neutrino and Anti-neutrino Interactions," Z. Phys. C **41** (1989) 527. doi:10.1007/BF01564697

[43] M. Derrick *et al.*, "Study of the Reaction Neutrino $N \to$ Neutrino $p\pi^-$," Phys. Lett. **92B** (1980) 363 Erratum: [Phys. Lett. **95B** (1980) 461]. doi:10.1016/0370-2693(80)90283-X, 10.1016/0370-2693(80)90191-4

[44] M. Derrick *et al.*, "Study of Single Pion Production by Weak Neutral Currents in Low-energy Neutrino *d* Interactions," Phys. Rev. D **23** (1981) 569. doi:10.1103/PhysRevD.23.569

[45] J. A. Formaggio and G. P. Zeller, "From eV to EeV: Neutrino Cross Sections Across Energy Scales," Rev. Mod. Phys. **84** (2012) 1307 doi:10.1103/RevModPhys.84.1307 [arXiv:1305.7513 [hep-ex]].

[46] W. Krenz *et al.* [Gargamelle Neutrino Propane and Aachen-Brussels-CERN-Ecole Poly-Orsay-Padua Collaborations], "Experimental Study of Exclusive One Pion Production in All Neutrino Induced Neutral Current Channels," Nucl. Phys. B **135** (1978) 45. doi:10.1016/0550-3213(78)90213-4

[47] H. Faissner *et al.*, "Observation of Neutrino and Anti-neutrino Induced Coherent Neutral Pion Production Off ^{27}Al," Phys. Lett. **125B** (1983) 230. doi:10.1016/0370-2693(83)91274-1

[48] T. Bolognese, J. P. Engel, J. L. Guyonnet and J. L. Riester, "Single Pion Production in Anti-neutrino Induced Charged Current Interactions," Phys. Lett. **81B** (1979) 393. doi:10.1016/0370-2693(79)90361-7

[49] S. Barlag, "Quasielastic Interactions And One Pion Production By Neutrinos And Anti-neutrinos On A Deuterium Target," INIS-mf-9455.

[50] S. J. Barish *et al.*, "Study of Neutrino Interactions in Hydrogen and Deuterium. 1. Description of the Experiment and Study of the Reaction Neutrino d –> mu- p p(s)," Phys. Rev. D **16** (1977) 3103.

[51] N. J. Baker *et al.*, "Quasielastic Neutrino Scattering: A Measurement of the Weak Nucleon Axial Vector Form-Factor," Phys. Rev. D **23** (1981) 2499.

[52] K. M. Graczyk, D. Kielczewska, P. Przewlocki and J. T. Sobczyk, "C_5^A axial form factor from bubble chamber experiments," Phys. Rev. D **80** (2009) 093001 doi:10.1103/PhysRevD.80.093001 [arXiv:0908.2175 [hep-ph]].

[53] C. Wilkinson, "Constraining neutrino interaction uncertainties for oscillation experiments,"

[54] C. Wilkinson *et al.*, "Reanalysis of bubble chamber measurements of muon-neutrino induced single pion production," Phys. Rev. D **90** (2014) 11, 112017 [arXiv:1411.4482 [hep-ex]].

[55] P. Rodrigues, C. Wilkinson and K. McFarland, "Constraining the GENIE model of neutrino-induced single pion production using reanalyzed bubble chamber data," Eur. Phys. J. C **76** (2016) no.8, 474 doi:10.1140/epjc/s10052-016-4314-3 [arXiv:1601.01888 [hep-ex]].

[56] Y. Hayato, "A neutrino interaction simulation program library NEUT," Acta Phys. Polon. B **40** (2009) 2477.

[57] C. Andreopoulos *et al.*, "The GENIE Neutrino Monte Carlo Generator," Nucl. Instrum. Meth. A **614** (2010) 87 doi:10.1016/j.nima.2009.12.009 [arXiv:0905.2517 [hep-ph]].

[58] S. Dytman, Acta Phys. Polon. B **40** (2009) 2445.

[59] F. Sánchez, "Possibility of measuring Adler angles in charged current single pion neutrino-nucleus interactions," Phys. Rev. D **93** (2016) no.9, 093015 doi:10.1103/PhysRevD.93.093015 [arXiv:1511.00501 [hep-ex]].

[60] K. Abe *et al.* [T2K Collaboration], "T2K neutrino flux prediction," Phys. Rev. D **87** (2013) no.1, 012001 Addendum: [Phys. Rev. D **87** (2013) no.1, 019902] doi:10.1103/PhysRevD.87.012001, 10.1103/PhysRevD.87.019902 [arXiv:1211.0469 [hep-ex]].

[61] J. T. Sobczyk and J. Żmuda, "Investigation of recent weak single-pion production data," Phys. Rev. C **91** (2015) no.4, 045501 doi:10.1103/PhysRevC.91.045501 [arXiv:1410.7788 [nucl-th]].

[62] A. A. Aguilar-Arevalo *et al.* [MiniBooNE Collaboration], "Measurement of Neutrino-Induced Charged-Current Charged Pion Production Cross Sections on Mineral Oil at $E_\nu \sim 1$ GeV," Phys. Rev. D **83** (2011) 052007 doi:10.1103/PhysRevD.83.052007 [arXiv:1011.3572 [hep-ex]].

[63] K. Abe *et al.* [T2K Collaboration], "The T2K Experiment," Nucl. Instrum. Meth. A **659** (2011) 106 doi:10.1016/j.nima.2011.06.067 [arXiv:1106.1238 [physics.ins-det]].

[64] Y. Fukuda *et al.* [Super-Kamiokande Collaboration], "The Super-Kamiokande detector," Nucl. Instrum. Meth. A **501** (2003) 418. doi:10.1016/S0168-9002(03)00425-X

[65] P. A. Amaudruz *et al.* [T2K ND280 FGD Collaboration], "The T2K Fine-Grained Detectors," Nucl. Instrum. Meth. A **696** (2012) 1 doi:10.1016/j.nima.2012.08.020 [arXiv:1204.3666 [physics.ins-det]].

[66] N. Abgrall *et al.* [T2K ND280 TPC Collaboration], "Time Projection Chambers for the T2K Near Detectors," Nucl. Instrum. Meth. A **637** (2011) 25 doi:10.1016/j.nima.2011.02.036 [arXiv:1012.0865 [physics.ins-det]].

[67] S. Assylbekov *et al.*, "The T2K ND280 Off-Axis Pi-Zero Detector," Nucl. Instrum. Meth. A **686** (2012) 48 doi:10.1016/j.nima.2012.05.028 [arXiv:1111.5030 [physics.ins-det]].

[68] D. Allan *et al.* [T2K UK Collaboration], "The Electromagnetic Calorimeter for the T2K Near Detector ND280," JINST **8** (2013) P10019 doi:10.1088/1748-0221/8/10/P10019 [arXiv:1308.3445 [physics.ins-det]].

[69] S. Aoki *et al.*, "The T2K Side Muon Range Detector (SMRD)," Nucl. Instrum. Meth. A **698** (2013) 135 doi:10.1016/j.nima.2012.10.001 [arXiv:1206.3553 [physics.ins-det]].

[70] K. Abe *et al.* [T2K Collaboration], "First measurement of the muon neutrino charged current single pion production cross section on water with the T2K near detector," Phys. Rev. D **95** (2017) no.1, 012010 doi:10.1103/PhysRevD.95.012010 [arXiv:1605.07964 [hep-ex]].

[71] L. Aliaga *et al.* [MINERvA Collaboration], "Design, Calibration, and Performance of the MINERvA Detector," Nucl. Instrum. Meth. A **743** (2014) 130 doi:10.1016/j.nima.2013.12.053 [arXiv:1305.5199 [physics.ins-det]].

[72] S. E. Kopp, "The NuMI neutrino beam at Fermilab," physics/0508001.

[73] D. G. Michael *et al.* [MINOS Collaboration], "The Magnetized steel and scintillator calorimeters of the MINOS experiment," Nucl. Instrum. Meth. A **596** (2008) 190 doi:10.1016/j.nima.2008.08.003 [arXiv:0805.3170 [physics.ins-det]].

[74] J. Devan *et al.* [MINERvA Collaboration], "Measurements of the Inclusive Neutrino and Antineutrino Charged Current Cross Sections in MINERvA Using the Low-ν Flux Method," Phys. Rev. D **94** (2016) no.11, 112007 doi:10.1103/PhysRevD.94.112007 [arXiv:1610.04746 [hep-ex]].

[75] C. L. McGivern *et al.* [MINERvA Collaboration], "Cross sections for ν_μ and $\bar{\nu}_\mu$ induced pion production on hydrocarbon in the few-GeV region using MINERvA," Phys. Rev. D **94** (2016) no.5, 052005 doi:10.1103/PhysRevD.94.052005 [arXiv:1606.07127 [hep-ex]].

[76] A. A. Aguilar-Arevalo *et al.* [MiniBooNE Collaboration], "The MiniBooNE Detector," Nucl. Instrum. Meth. A **599** (2009) 28 doi:10.1016/j.nima.2008.10.028 [arXiv:0806.4201 [hep-ex]].

[77] A. A. Aguilar-Arevalo *et al.* [MiniBooNE Collaboration], Phys. Rev. D **83** (2011) 052009 doi:10.1103/PhysRevD.83.052009 [arXiv:1010.3264 [hep-ex]].

[78] F. Capozzi, E. Lisi, A. Marrone, D. Montanino and A. Palazzo, "Neutrino masses and mixings: Status of known and unknown 3ν parameters," Nucl. Phys. B **908** (2016) 218 doi:10.1016/j.nuclphysb.2016.02.016 [arXiv:1601.07777 [hep-ph]].

[79] Y. Fukuda *et al.* [Super-Kamiokande Collaboration], "Evidence for oscillation of atmospheric neutrinos," Phys. Rev. Lett. **81** (1998) 1562 doi:10.1103/PhysRevLett.81.1562 [hep-ex/9807003].

[80] Q. R. Ahmad *et al.* [SNO Collaboration], "Measurement of the rate of $\nu_e + d \to p + p + e^-$ interactions produced by ^8B solar neutrinos at the Sudbury Neutrino Observatory," Phys. Rev. Lett. **87** (2001) 071301 doi:10.1103/PhysRevLett.87.071301 [nucl-ex/0106015].

[81] M. Antonello *et al.* [MicroBooNE and LAr1-ND and ICARUS-WA104 Collaborations], "A Proposal for a Three Detector Short-Baseline Neutrino Oscillation Program in the Fermilab Booster Neutrino Beam," arXiv:1503.01520 [physics.ins-det].

[82] K. Kodama *et al.* [DONUT Collaboration], "Observation of tau neutrino interactions," Phys. Lett. B **504** (2001) 218 doi:10.1016/S0370-2693(01)00307-0 [hep-ex/0012035].

[83] A. A. Aguilar-Arevalo *et al.* [MiniBooNE Collaboration], Phys. Rev. D **79** (2009) 072002 doi:10.1103/PhysRevD.79.072002 [arXiv:0806.1449 [hep-ex]].

[84] P. Stowell *et al.*, "NUISANCE: a neutrino cross-section generator tuning and comparison framework," JINST **12** (2017) no.01, P01016 doi:10.1088/1748-0221/12/01/P01016 [arXiv:1612.07393 [hep-ex]].

[85] C. Wilkinson *et al.*, "Testing charged current quasi-elastic and multinucleon interaction models in the NEUT neutrino interaction generator with published datasets from the MiniBooNE and MINERνA experiments," Phys. Rev. D **93** (2016) no.7, 072010 doi:10.1103/PhysRevD.93.072010 [arXiv:1601.05592 [hep-ex]].

[86] O. Altinok *et al.* [MINERvA Collaboration], "Measurement of ν_μ charged-current single π^0 production on hydrocarbon in the few-GeV region using MINERvA," arXiv:1708.03723 [hep-ex].